Protein Scaffolds for Cell Culture

Ana Isabel Machado Roque

Thesis submitted in partial fulfilment of the requirements of the regulations for the degree of Doctor of Philosophy

Newcastle University

Faculty of Medical Sciences

Institute of Cell and Molecular Biosciences

September 2012

Acknowledgments

I would like to express my thanks to Professor Jeremy Lakey for his guidance and support at all stages of the work.

My thanks go further to Professor Robin Harris and Dr Andrei Soliakov for their precious help on TEM experiments. My thanks also go to Dr Egor Zindy from COEBP, Manchester University, for his excellent help and work on cell data analysis.

Many thanks to all colleagues of the group, Yan Huang, Nat Wanatchaporn, Hannah Alfonsa (It was very nice to meet you girls!), Dr Christopher Johnson, Dr Helen Ridley, Dr David Chalton and Daria Stroukova for their help and for the good working atmosphere!

I would like to thank Dr Mark Birch, Dr Siôn Philips, Dr Deepan Shah for their good advices and also thank to Dr. Dale Athey and my sponsors: to the Medical Research Council (MRC) and Orla Proteins and Technologies.

Also, I warmly thank my parents and my brother for their continuous support and for always believe in me!

Abstract

We report here the design, purification and structural characterization of a new protein scaffold for cell culture. Prior studies in our group revealed the structure of the bacterial protein Caf1 to be flexible protein nanofibres, up to 1.5 μm. The existing Cafl expression system was cumbersome and difficult to mutate, we have now produced a system containing the *caf* operon which allows for the incorporation of specific peptide motifs. The small peptide, RGDS from fibronectin was inserted into 5 different surface loops of Caf1. The Caf1 mutants were expressed and purified and a structural characterization by biophysical methods was conducted. This revealed permissive sites into which new motifs can be inserted. The characterised proteins were sterilised and used to coat 96 well plates for cell culture. In this study we used mammalian cell lines such as 3T3 fibroblasts, PC12 neuronal cells and primary osteoblasts to understand how they behave in the presence of this biomaterial, in particular the formation of focal adhesions, changes in cytoskeleton rearrangement and nuclear and cell morphology. The controlled engineering of sites within the polymer allowed us to study their implication in cell attachment, survival and proliferation. Our preliminary results have shown that cells interact poorly with the unmodified protein e.g. without any motif associated. This reveals that the polymer is inert and does not influence cell growth by itself. In contrast, the incorporation of RGDS, can invert the scenario of cell growth; promoting cell attachment, survival and proliferation. In a second stage of the project we designed a separate compatible plasmid encoding *caf1* gene and used it with the previous plasmid to co-express hybrid Caf1 polymers. The long fibres can also be cross-linked with a non-toxic and non-immunogenic chemical compound – NHS-PEG. Thus a protein hydrogel composed of interchangeable folding units which can be used to incorporate different cell interacting peptide motifs. It is robust and, in the unmodified state highly protease resistant. Future studies will elucidate the versatility and potentiality for this peptide hydrogel in stem cell differentiation.

Table of contents

List of Figures

Page

List of Tables

List of Graphs

List of Abbreviations

GAGs	Glycosaminoglycans
ECM	Extracellular matrix
FN	Fibronectin
CollV	Collagen IV
NP	Non-protein (surfaces non-coated)
RGD	Arg-Gly-Asp
RGDS	Arg-Gly-Asp-Ser
RGES	Arg-Gly-Glu-Ser
WT	Wild-Type
PHSRN	Pro-His-Ser-Arg-Asn
FHRRIKA	Phe-His-Arg-Arg-Ile-Lys-Ala
IDAP	Ile-Asp-Ala-Pro
LDV	Leu-Asp-Val

HA	Hydroxyapatite
IKVAV	Ile-Lys-Val-Ala-Val
YIGSR	Tyr-Ile-Gly-Ser-Arg
PGs	Proteoglycans
FAK	Focal adhesion kinase
2D	Two dimensional
3D	Three dimensional
hMSCs	human mesenchymal stem cells
SAMs	self-assembled monolayers
PDMS	Poly-dimethylsiloxane
OmpA	Outer membrane protein A
tmOmpA	Transmenbrane beta-barrel of the monomeric outer membrane protein A
$OmpA_{TM}$-ECM peptides/ PEG-thiol/gold	ECM peptides were introduced into the transmembrane beta-barrel of the monomeric outer membrane protein ($OmpA_{TM}$). $OmpA_{TM}$ proteins were allowed to self-assemble on the surface PEG-thiol molecules self-assemble onto the gold surface filling gaps between the attached $OmpA_{TM}$ proteins
$OmpA_{TM}$-FLAG tag/ PEG-thiol/gold	FLAG-tag (N-DYKDDDDK-C) was introduced into the transmembrane beta-barrel of the monomeric outer membrane protein ($OmpA_{TM}$). $OmpA_{TM}$ proteins were allowed to self-assemble on the surface. PEG-thiol molecules self-assemble onto the gold surface filling gaps between the attached $OmpA_{TM}$ proteins
PEG-thiol	11-mercapto-1-triethyleneglycolundecane
IPTG	Isopropyl β-D-1-thiogalactopyranoside

BMP	Bone Morphogenetic Proteins
PC-12	cell line derived from a pheochromocytoma of the rat adrenal medulla
NGF	Nerve growth factor
PEG	poly(ethylene glycol)
CTS	chitosan-phosphate salt
β-TGF	transforming growth factor beta
EHS	Englebreth-Holm-Swarm
EAK-16	n-AEAEAKAKAEAEAKAK-c
4-PEG-Ace	4-arm PEG acetylene
NHS	N-hydroxyl succinimide
AA-NHS	acrylic acid
Acr-PEG-NHS	acryloyl-PEG-NHS
RGD (RGD-MA	mono-acrylamidoyl
RGD-PEGMA	RGD-PEG monoacrylate
PLA	poly lactic acid
PGA	polyglycolic acid
Caf1	Capsule-like antigen, fraction 1
Y. pestis	*Yersinia pestis*
CU pathway	chaperone/usher pathway
E. coli	*Escherichia coli*
DSE	donor-strand exchange
DSC	donor strand complementation

DsbA ,(B), (C)	Disulfide oxidoreductase A, (B), (C)
EDTA	Ethylenediamine tetraacetic acid
DAPI	4',6-diamidino-2-phenylindole
TRITC	Tetramethyl Rhodamine Isothiocyanate
DTT	Dithiothreitol
SDS	sodium dodecyl sulphate
IPTG	Isopropyl β-D-1-thiogalactopyranoside
X-Gal	5-bromo-4-chloro-indolyl-β-D-galactopyranoside
TCEP	Tris(2-carboxy-ethyl)phosphine hydrochloride
PBS	Phosphate buffered saline
SEM	Scanning electron microscopy
ESEM	Environmental scanning electron microscopy
'3T3' Fibroblasts	"3-day transfer, inoculum 3 x 10^5 cells"
PC-12	Pheochromocytoma cells
RPMI	Roswell Park Memorial Institute
SOC medium	super optimal broth with catabolite repression medium
PMF	Peptide Mass Fingerprinting
TEM	Transmission Electron Microscopy
CD	Circular Dichroism
DSC	Differential scanning calorimetry
FPLC	Fast Protein Liquid Chromatography
DMEM	Dulbecco's Modified Eagle Medium

COEBP	Centre of Excellence in Biopharmaceuticals
ANOVA	one-way analysis of variance
DTSSP	Dithiobis[sulfosuccinimidylpropionate]
NHS-PEG-NHS	O,O′-Bis [2-(N-Succinimidyl-succinylamino)ethyl]polyethylene glycol
4-arm PEG-NHS	4-arm PEG- Succinimidyl Carboxy Methyl ester
ACMA	School of Chemical Engineering and Advanced Materials
PCR	Polymerase chain reaction
Cyclo (RGDfC)	Cyclo (-Arg - Gly - Asp - D - Phe - Cys)
ALP	alkaline phosphatise
Calcein AM	(3',6'-Di (O-acetyl) -4',5'-bis [N,N-bis (carboxymethyl) aminomethyl] fluorescein tetraacetoxymethyl ester
GF-AFC	glycylphenylalanyl- aminofluorocoumarin
bis-AAF-R110	bis-alanylalanyl-phenylalanyl-rhodamine 110
6His-tag	Six-Histidine-tag

1. Chapter One: Introduction

1.1. Background of the problem

Research focus on cell behaviour, tissue engineering and regenerative medicine often involves cells cultured *in vitro* on flat plastic flasks. The cells cultured in this manner, i.e. in a two dimensional (2D) cell culture system present a flat shaped morphology. In contrast, cells within three dimensional (3D) cell culture matrices assume different morphologies as happens in their natural *in vivo* environment. Using 3D cell culture systems, researchers are discovering other cellular responses and patterns of gene expression that are more similar to the results obtained from *in vivo* studies.

Biotechnology companies produce an array of natural and synthetic extracellular matrices. The natural ECM matrices are derived from animal or plants and therefore are physiologically similar to the *in vivo* cell environment in terms of bioactivity with encapsulated cells and degradability. However there is a risk of pathogen transmission or immunogenic responses, the properties of these matrices are difficult to control and modify independently leading to a high variability in the results. Examples of these natural ECM matrices are: collagen, laminin, basement membrane extracted from mouse tumor, alginate and fibrin.

On the other hand, synthetic ECM matrices need to be engineered with bioactive ligands in order to interact biologically with cells leading to cell fate processes such as proliferation, migration and differentiation. Limitations associated with pathogen transmission, immunogenicity and the need for highly purified substrates can be overcome using synthetic ECM matrices such as Poly-ethylen glycol (PEG) modified forms, Hyaluronic acid (HA) modified forms, Poly(lactic-co-glycolic acid) (PLGA) or self-assembling protein hydrogels.

Many studies in this complex field have investigated different scaffold sources with specific properties, including biocompatibility, appropriate mechanical strength, interconnectivity and porosity or even the design of materials which combine all these remarkable properties an attempt to create new biomaterials. Hydrogels, for example due to their water content have a degree of flexibility very similar to natural tissue. They are currently used in tissue engineering as scaffolds containing human cells to repair tissue or to coat the wells of plates for cell culture.

The challenge to recreate model microenvironments for cell culture which more closely mimic the *in vivo* situation to more effectively support cell biological activities, such as cell differentiation, during *in vitro* culture and also reduce its complexity motivated us to construct a 3D system for cell culture. In this study we use Caf1 protein in a polymeric form whose structure resembles fibronectin (we intend therefore to insert fibronectin motifs, for example RGDS and PHSRN which together enhance cell adhesion); it has a low immunogenicity decreasing the risk of an immunogenic response or pathogen transmission); is resistant to proteases (when the study require non-degradable scaffolds; however we can also promote degradability if necessary by inserting specific cleavage sites) and it is water soluble which can allow us to form a hydrogel. The Caf1 polymers at high concentrations form a jelly-like material that is also soluble in water. We therefore used amine-reactive *N*-hydroxysuccinimide crosslinkers to chemically link the Caf1 polymers to form a hydrophilic three-dimensional cross-linked network of polymer chains that is hydrophilic i.e., can expand in water.

Through a 2D cell microarray system we have searched for most important combinations of motifs responsible for rat pheochromocytoma PC12 cell line adhesion, proliferation and differentiation. These results will be important for 3D cell culture studies as we can insert these peptides into the new protein scaffolds by site-directed mutagenesis and investigate the behaviour of different cell lines.

1.2. *In vivo* cell environment

All animal tissues are formed by an insoluble scaffold known as extracellular matrix (ECM). The ECM is composed of proteins such as fibronectin, collagens, laminin and elastin embedded in a hydrated gelatinous network of the polysaccharide chains of glycosaminoglycans (GAGs) and proteoglycans. These not only provide a supporting structure for various cell types but also largely influence their physiological behaviour (Kleinman *et al*., 1987).

The proteins of the ECM can be classified into structural (i.e., collagen and elastin) and adhesive (i.e., fibronectin and laminin) types (Alberts *et al.*, 2002).

Fibronectin (FN) is a major glycoprotein component of the plasma membrane matrix and has a linear arrangement of about thirty domains (**Figure 1.1**) (Mao and Schwarzbauer, 2005). The cell-adhesive (cell-binding) domain of FN has been the most extensively studied region which consists of repeating units approximately 90 amino acid residues in length, termed FN type III repeats (Aota *et al.*, 1994) which includes peptide ligands that mediate the adhesion, spreading and migration of cells and affect differentiation (Giancotti *et al.*, 1986). An important discovery by Pierschbacher and Ruoslahti (1984) was that the tripeptide Arg-Gly-Asp (RGD) is the principal adhesive ligand (Pierschbacher and Ruoslahti, 1984).This small peptide, which is located in the 10th type III domain of FN (FN10), binds integrin receptors including α5β1 and αIIbβ3 (See later). Its discovery was followed by the identification of several additional ligands that influence cell adhesion. Feng et al., have shown that Pro-His-Ser-Arg-Asn (PHSRN) mediates cell attachment in a manner analogous to RGD and that the two peptides bind competitively to cell surface integrin receptors (Feng and Mrksich, 2004), while this peptide remains the best understood ligand in FN, a substantial effort has addressed the discovery and functional characterization of additional ligands that play roles in cell adhesion (Eisenberg *et al*., 2009). -Phe-His-Arg-Arg-Ile-Lys-Ala- (-FHRRIKA-) binds to heparan sulphate transmembrane proteoglycans. It was found that the FHRRIKA and RGD peptide combinations did not enhance mesenchymal stem cell (MSC) attachment to hydroxyapatite (HA), relative to RGD alone, although a slight amount of spreading was caused by FHRRIKA (Sawyer *et al.*, 2007). HepII/IIICS is a smaller region of fibronectin. HepII is the major proteoglycan-binding domain of FN while the IIICS (type III connecting segment or V region) is a α4β1-binding region that can be alternatively spliced, giving rise to five variants in the human molecule (Mould and Humphries, 1991). The 25-mer CS1 peptide dominates the activity of the HepII/IIICS region and contains the tripeptide Leu-Asp-Val (LDV) as its minimal active site. The Ile-Asp-Ala-Pro (IDAP) motif is a LDV-like sequence in the fibronectin HepII peptide H1 and has been identified as a functional integrin-binding site (Clements *et al*., 1994).

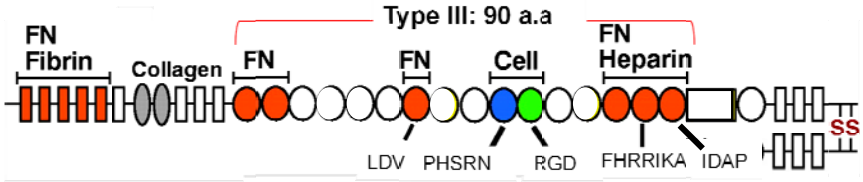

Figure 1.1 – Functional domains and major functional recognition sites of fibronectin. The fibronectin molecule is composed of three structural motifs: FnI represented by rectangles, FnII represented by ovals, FnIII represented by circles. The FnIII is the most well-known and is 90 amino acids in length. Through two chain disulfide bonds at the C-terminus, one molecule of fibronectin can be associated to another fibronectin molecule forming a dimer. The binding sites for fibronectin (FN), fibrin, collagen, cell and heparin are indicated as well as the sequences of amino acids responsible for that binding (Wierzbicka-Patynowski and Schwarzbauer, 2003).

Collagen (**Figure 1.2**) is the main component of mammalian connective tissue, accounting for approximately 30% of human body protein. The most abundant form is type I collagen, found in high concentrations in many tissues such as tendon, skin and bone (Pavlin *et al.*, 1992). Because of its abundance and its unique physical and biological properties, type I collagen has been used extensively in the formulation of biomedical materials (Nguyen *et al.*, 2003). Bhatnagar described the ability of the -GTPGPQGIAGQRGVV- peptide, from collagen I, to promote attachment of human dermal fibroblasts to anorganic bovine bone mineral (Bhatnagar *et al.*, 1999). The most predominant component of basement membranes is Type IV collagen. Type IV collagen not only forms the main structural frame of all basement membranes, but also serves as scaffolding for the binding of other basement membrane components. Type IV collagen has the ability to promote the adhesion and motility of various normal and transformed cell types (Floquet *et al.*, 2004; Han *et al.*, 2010).

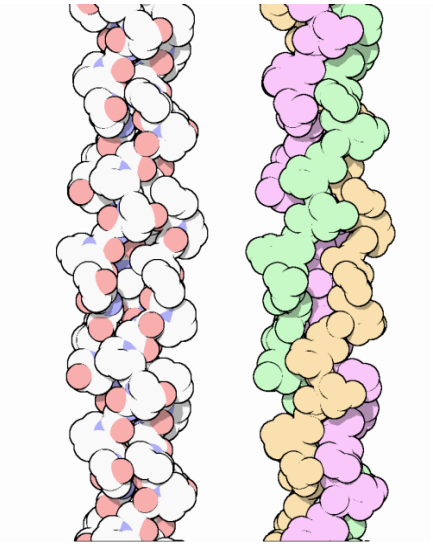

Figure 1.2 – Collagen structure. Image shows part of the segment of the whole collagen structure which is a triple helix formed by three intertwined chains containing around 20 amino acids. In the entire collagen molecule each chain comprises over 1400 amino acids. Collagen structure has a characteristic amino acid arrangement characterised by a repeat sequence of three amino acids in which the third is always a glycine. The glycine is a small amino acid and thus fits very well inside the helix contrary to proline, also present in the chain, whose structure bends becoming more difficult to fit in classic globular proteins. A modified form of proline, hydroxyproline is also found in the chain (David Goodsell & RCSB PDB-101 Molecule of the month April 2000).

Laminin is a large glycoprotein and the main component of the basal lamina. It consists of three polypeptide chains in a cross-shaped structure (Alberts *et al.*, 2002) (**Figure 1.3**). These chains have been cloned and sequenced, and biologically active sites responsible for cell binding have been identified using both proteolytic fragments and synthetic peptides (Iwamoto *et al.*, 1987). One active site for cell adhesion is located above the carboxyl globule on the long arm of the laminin A chain (residues 2091-2108) and contains the amino acid sequence Ile-Lys-Val-Ala-Val (IKVAV) which promotes angiogenesis, cell spreading, neurite outgrowth, and lung colonization by B16F10 melanoma (Kleinman *et al.*, 1987). Another peptide Tyr-Ile-Gly-Ser-Arg (*YIGSR*), from the cysteine-rich domain III on the β1 chain (residues 929-933), has been shown to promote cell attachment and migration, and to inhibit angiogenesis and melanoma lung colonization by binding to the 32/67-kDa laminin-binding protein that functions as its receptor (Bresalier *et al.*, 1995).

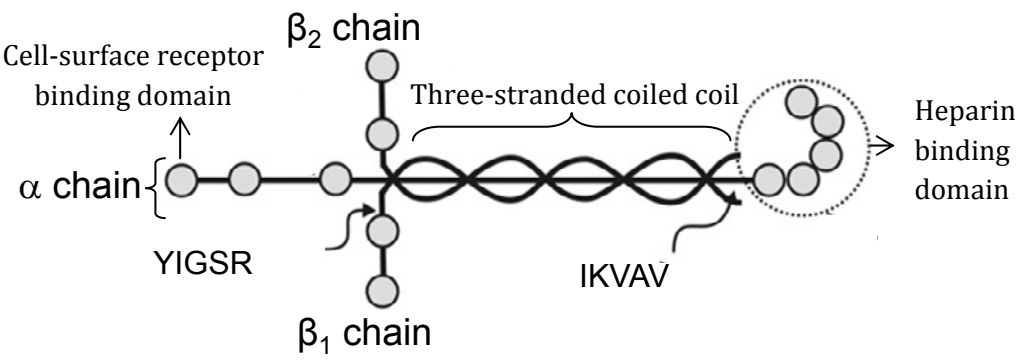

Figure 1.3 – Laminin structure presenting well-known functional domains. (Modified from (Dalton and Mey, 2009)). The structure of laminin is composed of three large polypeptides α, β1 and β2 chains linked by disulphide bonds in a cross-linked way. Part of the long arm is formed by a three stranded coiled coil. Laminin contains several functional domains at the ends of the alpha chain for cell- , heparin- and also for integrin-binding such as YIGSR and IKVAV motifs (Alberts *et al*., 2002).

Elastin is a protein in connective tissue consisting of elastic fibres composed of elastin molecules which form a cross-linked network providing enough elasticity for the fibres to stretch and relax upon deformation (Kielty *et al.*, 2002). These cross-linked structures are formed by covalent bond interactions of lysine residues between single elastin molecules and can influence biochemically and mechanically the cell behaviour. Cells surrounded by this microenvironment can convert mechanical signals into biochemical signals due to the direct interaction of the ECM with the cytoskeleton via cell-surface receptors (Lutolf and Hubbell, 2005).

ECM proteins are embedded in highly negatively charged, polysaccharide-rich, gelatinous substances formed by glycans, including glycosaminoglycans (GAGs) and proteoglycans (PGs) (Zhu, 2010).

Glycosaminoglycans (GAGs) are macromolecular hydrophilic, unbranched and negatively charged polysaccharide chains forming rigid and highly extended conformations. Their negatively charged polysaccharide chains attract counterions inducing an osmotic effect and enable the matrix to retain large volumes of water (Alberts *et al*., 2002). The most important groups of GAGs are keratin sulphate, chondroitin sulphate, and heparin sulphate which are sulphated, covalently linked to protein via linker proteins, synthesized intracellularly and released via exocytosis.

Another GAG member is hyaluronic acid. Hyaluronic acid is unsulphated, not covalently linked to proteins, can be released directly from the cell surface by an enzyme complex embedded in the plasma membrane, and free of sugar groups (Gandhi and Mancera, 2008).

Proteoglycans (PGs) are heavily glycosylated proteins with a high sugar content. The proteoglycan unit consists of a core protein to which one or more GAG chains are covalently attached which enable them to form gels of varying charge density and porosity and also function as filters to regulate the molecular diffusion of molecules and cells. Due to their structure and chemical organization, proteoglycans can mediate cell adhesion, regulate the secretion of growth factors, activate the secretion of proteases, and inhibit proteolytic enzymes involved in the assembly and degradation of ECM components (Alberts *et al*., 2002).

Cells express several cell surface adhesion receptors; including integrins, syndecans and other proteoglycans, cadherins and cell adhesion molecules. Among these cell surface receptors, the integrin family of transmembrane heterodimeric receptors is the most extensively studied and has a central role in controlling, for instance, cell adhesion to extracellular matrix (ECM) proteins (Hynes, 2002). Cell adhesion plays a critical role in many cellular functions, from migration and proliferation to apoptosis (Chen *et al.*, 2003).

Integrins consist of non-covalently-associated heterodimers, α and β subunits which are typical type-1 transmembrane proteins with the amino terminus outside and a single transmembrane domain that connects to a carboxy-terminal cytoplasmic tail (Shattil *et al.*, 2010). The external amino terminus (integrin extracellular domain) binds to specific amino acid sequences, such as the arginine-glycine-aspartic acid (RGD) recognition motif present in many extracellular matrix proteins, including fibronectin, bone sialoprotein, and osteopontin (Pierschbacher and Ruoslahti, 1984; Sastry and Burridge, 2000; Geiger *et al.*, 2001).

Upon ligand-binding, integrins undergo conformational changes that activate their short cytoplasmic tails and consequently their association with the actin cytoskeleton. The interaction between integrin cytoplasmic tails and the actin cytoskeleton is mediated by

other structural and signalling proteins which together form dynamic macromolecular complexes designated focal adhesions. Burridge and colleagues discovered several of these cytosolic proteins at high concentrations in the focal adhesions. Among them, **vinculin** (Geiger, 1979; Burridge and Feramisco, 1980), which also binds to filamentous actin (F-actin) directly and it is considered to be the universal marker for focal adhesions; **talin** (Burridge and Connell, 1983), which promotes the transition of the integrins from an inactive to an active state by binding to their cytoplasmic domain through its 'head domain' and to F-actin:vinculin through its 'tail domain' and finally **α-actinin** (Youssoufian and Kwiatkowski, 1990), which is an actin crosslinking protein (**Figure 1.4**).

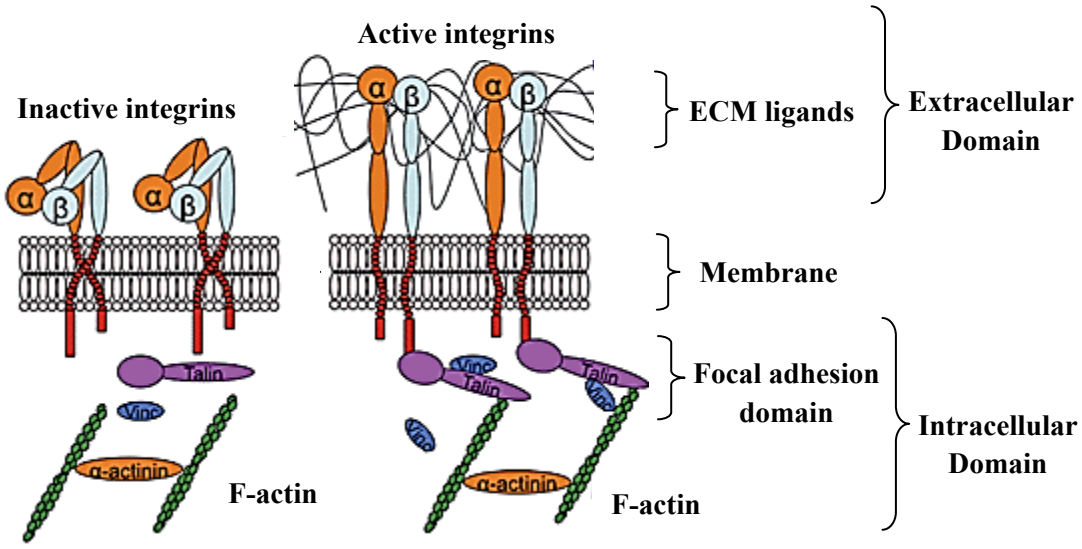

Figure 1.4 - Biogenesis of focal adhesions. The integrins that are not bound to the extracellular matrix (ECM) ligands are present on the cell surface in an inactive conformation (**Inactive integrins**), which is characterized by 'bent' extracellular domains that hide the ECM-binding pocket. This conformation is stabilized by interactions between integrin transmembrane domains and membrane-proximal extracellular domains. When talin is recruited to the plasma membrane it binds to the cytoplasmic tail of β-integrins. This interaction separates the cytoplasmic domains and induces the integrins to adopt the 'primed' conformation (**Active integrins**). The integrin extracellular domains extend and reveal the ligand-binding site, allowing the integrin to bind specific ECM ligands. The separated integrin cytoplasmic domains and talin form a platform for the recruitment of other focal-adhesion proteins such as vinculin (vinc) and α-actin. These proteins form together the focal adhesions (Legate *et al.*, 2006 ; Honarmandi *et al.*, 2011). Consequently cell spreading and flattening promote the progressive maturation of the focal adhesions (Chen *et al.*, 2003).

The network of protein interactions and cellular components composing the focal adhesion complex in mammalian cells has been intensely studied and globally organized into a structure termed the *integrin adhesome* which includes, at the moment, around 180 protein–protein interaction nodes (Zaidel-Bar *et al.*, 2007).

Some studies in which focal adhesion proteins such as vinculin or focal adhesion kinase (FAK - involved in cellular adhesion and spreading signalling pathways) were knocked out, resulted in cells that fail to spread normally (Chen *et al*., 2003).

The actin cytoskeleton is a highly dynamic network that rapidly changes shape and organization in response to stimuli and cell cycle progression. It is composed of actin polymers and a large variety of associated proteins. An important determinant of the cellular shape and motility is the orientational distribution of actin filaments within a cell (Rao *et al.*, 1990) The functions of the actin cytoskeleton is to mediate a variety of essential biological functions in all eukaryotic cells, including intra- and extra-cellular movement and structural support (Chen *et al*., 2003).

The cell shape is probably the most obvious indicator and regulator of physical effects on cell function due to at least two reasons: first, cells have their unique morphology, for example chondrocytes are small and round, myoblasts are medium-sized and spindle-like, and osteoblasts are large and polygonal. Secondly, the variation in gene expression leading to matrix synthesis or expression of surface markers is often associated with the changes in cellular morphology (Freytes *et al.*, 2009).

1.3. *In vitro* cell environment

Many cells in culture adhere and spread on a surface in order to survive, proliferate and function (Mrksich, 2009). Previous studies have shown that cell attachment and spreading is related to gene expression and protein production, implying a cell shape-based regulation of cellular function (Li *et al.*, 2008).

Many efforts have been made to re-create the complex interactions observed *in vivo* between cell-cell and cell-ECM components to produce *in vitro* models that mimic the cells environment. Research focused on cell behaviour, tissue engineering and regenerative medicine has led to the development of synthetic biomaterials (Pariente *et al*., 2002). Although some of these problems can be overcome using recombinant proteins, their biological activities are compromised by a lack of control over the conformation and orientation of proteins at the surface. A greater control over the properties of such biological materials and cell responses was attained when synthetic analogues became available (Lutolf and Hubbell, 2005).

Consequently, many studies in this complex field have investigated different scaffold sources with specific properties, mainly appropriate mechanical strength, interconnectivity and porosity in an attempt to create new functional biomaterials. On

the other hand, other studies have focused on defining the most suitable cell type for, among other purposes, biomedical applications (Dado and Levenberg, 2009).

Cell culture systems

Organs and biological tissues are composed of living cells organized within structural and functional complex 3D extracellular matrices (Vogel and Baneyx, 2003). Therefore, differences in shape, functional activities, molecular composition of focal adhesion and signalling pathways between cells cultured in 2D and 3D cell culture systems have been described (Corbett *et al.*, 1996; Cukierman *et al.*, 2001).

The cells growing in 3D matrices present diverse shapes between them whereas in 2D planar surfaces the cells have in general a more uniform shape within the cell population. Many functional activities, such as proliferation or migration, are enhanced in 3D matrices compared to 2D surfaces. Most noteworthy are the differences in the molecular composition of the focal adhesion formed due to cell-ECM protein interactions. In a study conducted by Zamir et al. (2000) they found that interactions between human foreskin fibroblast and fibronectin lead to 3D matrix adhesions which contain large quantities of $\alpha_5\beta_1$ integrins but do not show co-localization with β_3 integrins, whereas the interaction between cells and ECM on 2D surfaces results in a formation of focal adhesions rich in $\alpha_v\beta_3$ integrins and co-localized $\alpha_5\beta_1$ integrins (Zamir *et al.*, 2000). In addition, $\alpha_5\beta_1$ integrins in 3D matrix adhesions co-localise with the cytoplasmic proteins paxillin and vinculin whereas in 2D focal adhesions the β_3 integrins co-localised with the same cytoplasmic proteins. Furthermore, in 3D focal adhesion the protein FAK is not phosphorylated but it is in 2D focal adhesions. This result indicates that in these two cell culture systems, cell function is regulated by different signalling pathways (Vogel and Baneyx, 2003).

Moreover, in 2D culture systems, cells experience the homogenous concentration of nutrients, growth factors, and cytokines present in the media with the section of the membrane that contacts the surrounding media (Ashe and Briscoe, 2006).

Two-dimensional cell culture systems confine cells to a planar environment and restricts the more-complex morphologies observed *in vivo*. For example, 2D culture polarizes cells such that only a segment of the cell's membrane can interact with the ECM and neighbouring cells, while the rest of the cell is exposed to the culture media

which leads to unnatural, polarized integrin binding and mechanotransduction, which both affect intracellular signalling and phenotypic fate (Zhang *et al.*, 2005a). This effect is not observed in 3D culture systems, since cells are encapsulated within 3D matrices (Badylak *et al.*, 2009).

Despite the differences between these two cell culture systems, both have been useful in many studies to understand more about cell-ECM environment interaction. In particular, 2D experiments have given rise to important findings in the dynamic relationship between cell function and interactions with the cellular microenvironment. For instance, Engler and co-workers demonstrated that the differentiation of human mesenchymal stem cells (hMSCs) is dependent on the mechanical stiffness of the 2D culture platform (Engler *et al.*, 2006). Moreover, Ingber described that the degree to which a cell is mechanically distended on a 2D scaffold influences relative growth and apoptotic rates (Ingber, 2006). Thus, experiments with these 2D cell culture systems have provided the base for our initial understanding of the complex biological phenomena, including molecular biology, stem cell differentiation and tissue morphogenesis (Tibbitt and Anseth, 2009).

Over the past few decades, tissue engineers and cell biologists have begun to develop material systems to culture mammalian cells within 3D ECM mimics to circumvent the limitations posed by traditional 2D cell culture.

Types of scaffolds

The idea that cellular scaffolds can be used exclusively as passive vehicles with which to study the relationship between gene expression and cell function has become outdated. Nowadays, it is evident that the cellular microenvironment contributes to the spatially and temporally complex signals that direct cell phenotype (Nakamura *et al.*, 2008).

A brief description of some examples of common scaffolds which provide support for cell growth, differentiation and organization is described below.

A) Self-assembled monolayers on surfaces

The interaction of cells with self-assembled monolayers (SAMs) of different components was first studied by Mrksich and Whitesides. The main motivation to create different classes of SAMs, (e.g. alkanethiolates on gold and alkylsiloxanes on hydroxylated surfaces) was to overcome problems associated with adsorption of proteins to the surfaces. Among them, changes in orientation and conformation, denaturation and loss of activity which have implications on the cell attachment to these surfaces. Thus, cell attachment depends on the nature of the adsorbed layer of protein (Mrksich and Whitesides, 1996). SAMs of alkanethiolates binding on gold surfaces occurs through their thiol groups allowing the formation of dense monolayers of long-chain alkanethiols containing a terminal group (X) which will determine the surface properties. These SAMs are very stable in contact with air, water or ethanol for long periods and therefore, have been used in cell culture. SAMs of alkylsiloxanes are formed by the interaction of a solution of alkyltrichlorosilane (or alkyltriethoxysilane) with hydroxylated surfaces such as the native oxide of glass or silicon. Both the conformation and binding of alkylsilanes to surface hydroxyl groups is not as well understood as for the gold-thiol interaction. However, it is well known that the surface properties can be controlled by controlling the terminal function group of the alkylsilanes (Mrksich and Whitesides, 1996).

Proteins in solution can be immobilised to SAMs by covalent coupling. A variety of surface chemistries have been used based on disulfide bonds and amide formation (Hickman *et al.*, 1994). In order to avoid the denaturation of the proteins after their immobilization, proteins can be coupled to "inert materials" such as polyethylene glycol that can support protein immobilization and stabilization, which is important for the correct presentation of the functional groups in cell culture (Wang *et al*., 1993).

Since then many studies of peptides and other surface chemistries have been carried out (Li *et al.*, 2012). One of these techniques is micro-contact printing in which biomolecules, for example ECM proteins, are adsorbed to a fabricated material such as a stamp of poly-dimethylsiloxane (PDMS) which is an inexpensive silicone elastomer compatible for cell culture, and then printed onto a culture substrate allowing different cell behaviour studies depending on the geometry, feature shape and nano- or micro-scale dimensions left by the stamp (Whitesides *et al.*, 2001). An example of the

application of this method is in cell proliferation studies, using a single island or groups of closely spaced dots (protein arrays) containing ECM proteins which can constrain or promote cell spreading, respectively. Using these approaches to pattern substrates onto culture surfaces it has allowed us to understand that the cell shape or area can regulate apoptosis and proliferation (Chen *et al.*, 1997).

In other cases proteins can be specifically engineered to bind onto a variety of different surfaces using various different chemistries (Terrettaz *et al.*, 2002). For gold surfaces, molecules can be immobilised using thiol chemistry (Dubois and Nuzzo, 1992) The sulphur atom in thiol alkanes will form strong gold-thiolate bonds with the gold. The monolayer that is formed is strong, stable and orientated (Bain *et al.*, 1989). Thiol bearing cysteine residues can be introduced into strategic locations in proteins using conventional molecular biology techniques (Chaffey *et al*., 2008). A single cysteine in the protein will bond the protein to the gold surface in a specific orientation (Brun *et al*., 2008).

An example of a system for stable self-assembly of proteins on surfaces is presented below.

Outer membrane protein A (OmpA) from *Escherichia coli* is a monomeric porin with an N-terminal 8-stranded β-barrel transmembrane domain and a soluble *C*-terminal periplasmic binding domain (Sugawara and Nikaido, 1992). It has a very stable beta barrel structure (Tamm *et al.*, 2001). The core protein transmembrane region is easily refolded from bacterial inclusion bodies (Shah *et al*., 2007).

The transmembrane domain of OmpA (tmOmpA) can be immobilised to gold surfaces through a cysteine residue that has been inserted at the N-terminus of tmOmpA. This protein has four external loops able to accept inserts either short sequences of amino acids from ECM proteins or larger proteins domains (**Figure 1.5**) (Shah *et al*., 2007) or also IgG-binding proteins (Shah *et al*., 2007; Brun *et al*., 2011).

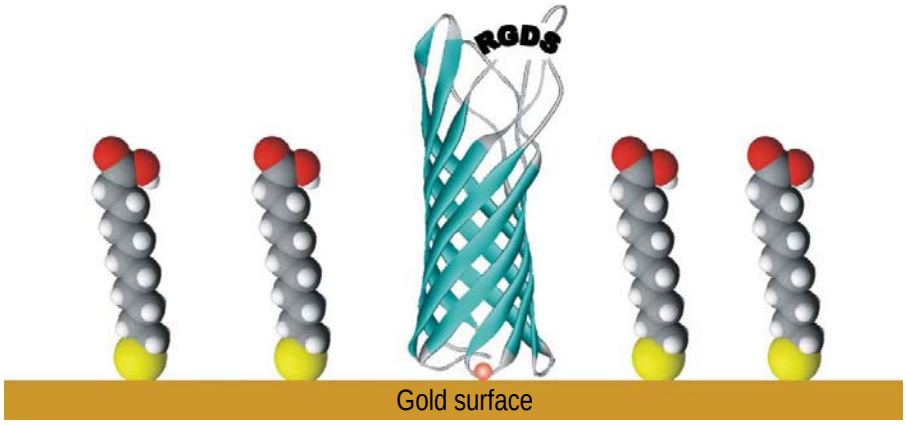

Figure 1.5 – Cartoon representation of tmOmpA scaffold presenting the RGDS motif from fibronectin assembled on gold surface surrounded by thiol-alkane (*11-mercaptoundecanoic acid* molecules). RGDS motif was inserted in a constrained loop of OmpA beta-barrels orientated in order to be completely exposed at the surface for cell recognition. Binding of tmOmpA to the gold surface and orientation of the motifs are achieved by the insertion of a single cysteine residue (in red). The space between protein molecules was filled with thiol-alkane molecules which were able to assemble to the gold surface through their terminal sulphur atom (yellow). For cell adhesion studies PEG-thiol (Triethylene glycol mono-11-mercaptoundecyl ether) was used (Cooke *et al.*, 2008).

The tmOmpA-ECM scaffolds are also known as Orla technology since it is commercialised by Orla Protein technologies Ltd. **Figure 1.6** illustrates the main steps of this technology.

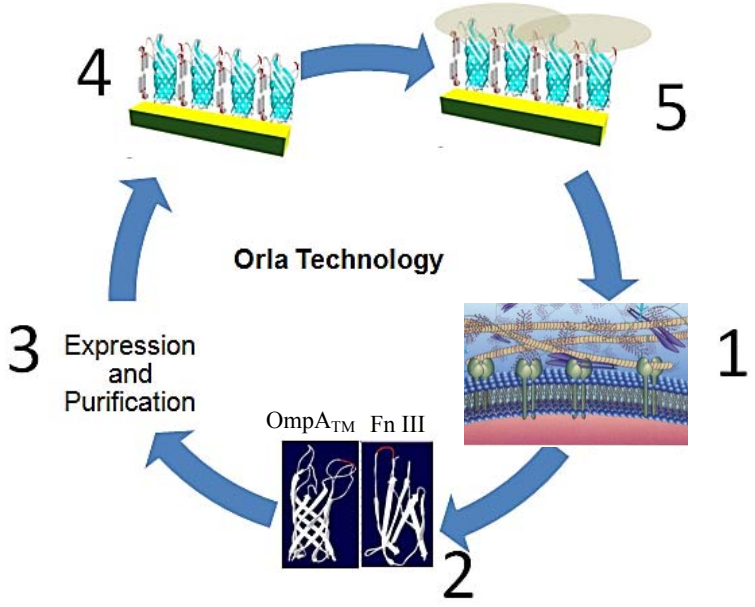

Figure 1.6 – The RGDS peptide as a simple model system to demonstrate the Orla protein technology for cell culture. 1- *In vivo* cells are in contact with extracellular matrix. **2 -** RGDS peptide from fibronectin was introduced into the transmembrane beta-barrel of the monomeric outer membrane protein A (tmOmpA) from *E. coli* by primer directed PCR insertion (RGDS in red). The 3D Structure of the tenth type III module of fibronectin (Fn III) and the 3D structure of the Orla scaffold protein modelled with RGDS on Loop1. **3 -** Protein expression and purification – for more details see the section 2.1. **4 -** Self-assembly of monolayers on cell culture surfaces. **5 -** Attachment of cells to patterned RGDS surfaces.

Cooke et al. (2008) have shown that self-assembled monolayers of tmOmpA molecules can be used as scaffolds to present motifs from collagen I, collagen IV, fibronectin and laminin in a controlled manner to enhance the adherence of PC12 cells to glass surfaces. These results resembled the effect of the corresponding whole molecules on this cell line (Cooke *et al*., 2008).

In another study Cooke and co-workers examined tmOmpA presenting ECM motifs of collagen, fibronectin, and laminin and found that it influenced the formation of neurites by differentiating PC12 cells. The effect of these peptide sequences was also tested on the development of adult neural stem/progenitor cells and the study revealed that collagen I and fibronectin induced the formation of beta-III-tubulin positive cells, whereas collagen IV reduced such differentiation (Cooke *et al.*, 2010).

Other studies using engineered proteins, a bacterial protein TolAIII was engineered to contain a cysteine in a C-terminal hydrophobic helix, allowing chemisorption to gold surfaces. The helix was termed a "switch-tag" (ST) since it was composed of 12 amino acids that form a water soluble coil which switches to a hydrophobic helix in the presence of alkane thiols (Chaffey *et al*., 2008). The TolAIII protein was modified to include bioactive motifs from bone morphogenetic protein-2 (BMP-2) and osteopontin. They showed that osteoblasts responded specifically to soluble recombinant BMP2 and Tol-BMP-ST, when added to osteoblast cell culture media, by the activation of the TGF-beta/Smad signalling pathway. However when TolA BMP-2 and osteopontin motifs were immobilised through the ST, in the absence of other osteogenic components, these scaffolds supported osteoblast differentiation *in vitro* over 28 days (Mitchell *et al.*, 2010). Moreover, printed on gold surfaces using soft lithography, the proteins provided adhesion sites for the cells, cell growth control and even signals for differentiation in the form of bone formation. In one case, mesenchymal stem cells differentiated into osteoblasts in response to an engineered protein with a BMP motif (Mitchell *et al*., 2010).

B) Hydrogels

Hydrogels provide a highly swollen three-dimensional environment similar to soft tissues and therefore have been utilised in a wide range of biomedical applications, among them implants for tissue engineering, scaffolds or carriers for drugs (Billiet *et al.*, 2012).

Over the past few decades a variety of natural and synthetic polymers were used to prepare hydrogels for cell culture (Lee and Mooney, 2001). Natural polymers are usually biocompatible, biodegradable and bioactive, having an important role in cell adhesion and biological signalling. However, they present batch-to-batch variability, limited sources, can lead to immunogenic responses and reduce control over the material structure and properties (Tibbitt and Anseth, 2009). Examples of natural polymers are: (1) polysaccharides such as chitosan (Bhattarai *et al.*, 2010) and hyaluronic acid (Tan *et al.*, 2009), (2) Proteins such as gelatin (Welz and Ofner, 1992) and mixtures such as matrigel (Kleinman and Martin, 2005). Synthetic polymers present controllable degradation rates and mechanical strengths but do not possess biological

cues for cell adhesion, proliferation or differentiation and tissue regeneration (Slaughter *et al.*, 2009). Examples of synthetic polymers are: polypeptides and poly(ethylene glycol) (PEG) (Veronese, 2001).

Natural polymers

Chitosan-based hydrogel

Chitosan is a linear polysaccharide composed of β-(1,4)-linked D-glucosamine and *N*-acetyl-D-glucosamine units. Its structure is similar to glycosaminoglycans and thus has low toxicity, an excellent biocompatibilty and can be degraded *in vivo* by lysozyme and chitosanase enzymes (Liu *et al.*, 2009). Chitosan-based hydrogels can be applied in a form of injectable gel for drug discovery and used for regenerative medicine of several tissues for example, bone (Nair *et al.*, 2011), cartilage (Ruel-Gariepy *et al.*, 2004), nerve (Chenite *et al.*, 2000) and also for brain cancer treatment (Kim *et al.*, 2010).

Cho and co-workers prepared a chitosan-phosphate salt (CTS) hydrogel using β-Glycerol phosphate disodium salt (GP) which can induce a sol-gel transition in chitosan solution at physiological pH and temperature. *In vitro*, encapsulating a mixture of chondrocytes and β-transforming growth factor β into this hydrogel allowed the delivery of this osteogenic mixture for normal cartilage regeneration over three weeks (Cho *et al.*, 2005). These CTS/GP hydrogels are developed by BioSyntech Inc. (Laval, Quebec, Canada).

Hyaluronic acid

Hyaluronic acid (HA) is a linear polysaccharide consisting of alternating units of β-1,4-D-glucuronic acid and β-1,3-N-acetyl-D-glucosamine connected by glycosidic bonds. Chemically it is a non-sulphated glycosaminoglycan (Toole *et al.*, 1989) and is a major component of the natural extracellular matrix of mammalian connective tissues (Bodnár *et al.*, 2009).

It has an important role in many biological processes such as in the organization of the extracellular matrix, in tissue hydration, in joint lubrication, maintaining the

integrity of connective tissues and facilitating wound healing (Zhao *et al*., 2012). Due to its hydrophilic and viscoelastic properties it is currently used in clinical applications for example visco-supplementation and visco-surgery. It has been injected into the joint to increase lubrication and thus treat arthritis or under the skin for tissue augmentation or even in eye surgery (Goa and Benfield, 1994).

The excellent results obtained using HA to recapitulate and modulate tissue regeneration processes reinforced its acceptance as an important component of artificial matrices (Allison and Grande-Allen, 2006). However, in its native form, HA is soluble in water forming viscous solutions with poor biochemical properties which result in its quick degradation and metabolisation. Thus, it is convenient to modify and cross-link HA to control its physical and chemical properties e.g. to control degradation or metabolism (Lapcik *et al.*, 1998).

Choh and colleagues reported the synthesis of disulfide-cross-linked hyaluronic acid hydrogels using a thiol-disulfide exchange reaction, for protein delivery and cell encapsulation (Choh *et al.*, 2011). They demonstrated that encapsulation of several types of cells including fibroblasts, endothelial cells, and mesenchymal stem cells in these type of hydrogels resulted in a high cell viability, during and after encapsulation, up to 7 days in culture. However, poor cell adhesion was observed since these hydrogels do not contain cell-adhesive peptides (Choh *et al*., 2011).

Gelatin

Gelatin is a derivative of collagen and is formed by breaking the natural triple-helix structure of collagen into single-strand molecules (Lee and Mooney, 2001). Gelatin hydrogels are very often used as delivery systems for growth factors such as, for example, vascular endothelial growth factor *(*VEGF) which promotes lymphangiogenesis or bone morphogenetic protein 2 (BMP-2) (Chen *et al.*, 2007) and transforming growth factor beta (β-TGF) for bone regeneration (Huang *et al.*, 2011). Chondrocytes were encapsulated in gelatin hydrogels with poly(N-isopropylacrylamide)-grafted gelatin that formed a hydrogel at 37 ºC and to high levels of collagen and sulphate glycosaminoglycans over 12 weeks of culture (Ibusuki *et al.*, 2003).

Matrigel

Matrigel is a soluble and sterile extract of basement membrane proteins derived from a mouse tumour. This type of tumour was named Englebreth-Holm-Swarm (EHS) because it was discovered by J. Englebreth-Holm of Denmark and it was maintained and characterised by Richard Swarm (Kleinman and Martin, 2005). The EHS tumour is also known as EHS extract, reconstituted basement membrane and later Matrigel (Kleinman and Martin, 2005).

Since 1972 the components of this tumour matrix were investigated and it was found that it is composed mainly of collagen (Smith *et al.*, 1975) namely collagen IV (Timpl *et al*., 1979), the large glycoprotein laminin (Timpl *et al.*, 1979), a large heparan sulphate-containing proteoglycan designated perlecan (Hassell *et al.*, 1980) matrix metalloproteinases-2 (Liotta *et al.*, 1979) and growth factors (Vukicevic *et al.*, 1992). In terms of structure, sites were found where collagen IV, laminin and perlecan bind to one (Laurie *et al.*, 1986) and form a supramolecular complex (Grant *et al.*, 1989). These studies showed that this matrix resembled basement membrane found in many animal tissues, thus it was tested is ability to be used as a substrate for cell culture (Kleinman and Martin, 2005).

Afterwards, Kleinman et al. described a method to extract the EHS tumour, and purify the sterilised extracellular matrix to be able to use it in cell culture studies. Importantly, Kleinman suggested that to produce a sterile solution, five millilitres of chloroform per litre could be added to the extract inside a dialysis bag and then release the chloroform by dialysis (Kleinman *et al.*, 1986b) This final product was named Matrigel by John Hassell and it can be stored as a frozen solution (10-15 mg/ml) (Hassell *et al*., 1980).

The applicability of Matrigel for cell culture was examined, and for that the matrigel frozen solution was thawed overnight at 4 ºC; at 24-37 ºC it gels in 30 minutes. After this, cells can be plated on top of the gelled material or even mixed with matrix prior to gelling at temperatures closer to 37 ºC (Kleinman and Martin, 2005).

It was found that Matrigel can promote the differentiation of several different cell lines. Some of these cell lines and primary lines do not proliferate but differentiate once in contact with this matrix (Kleinman and Martin, 2005). Chondrocytes growing in Matrigel form cartilaginous nodules on the surface of the matrix (Bradham *et al.*, 1995). Moreover, human embryonic stem cells can be cultured on Matrigel containing mouse

fibroblast-conditioned medium (Xu *et al.*, 2001). Thus, matrigel has been shown to be an optimal matrix for the culture of stem cells because of its ability to maintain self-renewal and pluripotency. However it is still poorly understood how matrigel helps stem cells to maintain their undifferentiated state. Hughes *et al.* suggested that it will be challenging to replace Matrigel in a variety of cell culture and experimental assays due to its complexity (Hughes *et al.*, 2010).

Matrigel is commercialised by BD Biosciences, Mississauga, Canada.

Synthetic polymers

Polypeptides

Many peptides sequences self-assemble into nanofibre hydrogel networks by hydrogen bonding or hydrophobic interactions or even stereo specific-interactions between the specific amino acid building blocks (Holmes, 2002). Two examples of these peptides contain structural motifs including β-hairpins (Haines *et al.*, 2005) and amphiphilic sequences (Zhang *et al.*, 2005b) which allow the self-assembly of biomaterials *in situ* in response to, for example, temperature, pH, ionic strength under mild conditions (Chung and Park, 2009).

Polyalanine-poloxamine-polyalanine block polymers that can form hydrogels sensitive to the temperature due to the strengthening of the β-sheet and the dehydration of the poloxamers block when the temperature is increased. These hydrogels were successfully used to promote chondrocyte proliferation and differentiation (Choi *et al.*, 2010).

The first molecule of the ionic class of amphiphilic self-assembling peptides was the EAK-16 which is composed of 16 amino acid peptide (n-AEAEAKAKAEAEAKAK-c), where n- and c- refer to the N- and C-termini of the peptides, respectively. Oligopeptides were blocked on both C- and N- termini (Zhang *et al*., 1992). EAK-16 was modified to design other self-assembling peptides, the RAD16 (n-RARADADARARADADA-c). Oligopeptides were blocked on both C- and N-termini, substituting the positively charged lysines by arginines and negatively charged glutamic acids by aspartic acids (Zhang *et al.*, 1995). The amino acid sequence

containing only RAD motif resembled the integrin receptor-binding site RGD (Zhang *et al.*, 1993).

These peptides are composed of L-amino acids and therefore their degradation will yield normal amino acids that can be easily degraded by the body and are biocompatible with many cell types (Zhang *et al*., 1995). Moreover, due to their primary sequences composed of alternating hydrophilic and hydrophobic side-chains these peptides present a high solubility in pure water and a stable β-sheet structure (Zhang *et al.*, 1993; Zhang *et al.*, 1994). The RAD16 hydrogels can form well-ordered nanofibres (1000-fold smaller than synthetic polymer microfibres) *in situ* in the presence of salt solutions or physiological pH media due to intra- or inter-molecular electrostatic interactions or salt-induced disruption (Zhang *et al.*, 2005b).

The self-assembled peptide RAD16 can either incorporate growth factors or functional motifs such as sequences to promote cell adhesion and differentiation. Cells can be fully embedded in the 3-D functionalised self-assembling peptides. In one study peptide scaffolds alone without addition of soluble growth factors enhanced survival of the neural stem cells and promoted differentiation of these cells towards neural and glial phenotypes (Gelain *et al.*, 2006).

The results obtained for cell adhesion and differentiation using RAD16 peptides were similar to the ones using Matrigel. However, designer self-assembling peptides RAD16 hydrogels have the advantages of containing only synthetic and pure components and a completely defined composition (Gelain *et al*., 2006).

RAD16 hydrogel was used to encapsulate neonatal cardiomyocytes that were subsequently injected into the myocardium. As result of this study, high cell viability was observed and cells were also able to recruit neighbouring endogenous cells into the hydrogel (Branco and Schneider, 2009). These self-assembled peptides are also known as BD™ PuraMatrix™ Peptide Hydrogel commercialized by BD biosciences.

Other self-assembling matrices including peptide amphiphile, nanofibre matrices and coiled coil structures (Boyle and Woolfson, 2011).

PEG hydrogels

On the other hand, hydrogels for cell culture can also be formed of purely non-natural and hydrophilic polymers such as poly(ethylene glycol) (PEG) which has a low immunogenicity and toxicity, resistance to protein adsorption, good biocompatibility

and the ability to form porous scaffolds. Nevertheless, it presents some disadvantages when used as scaffold for cell culture; PEG is neither cell adhesive nor biodegradable (Alcantar *et al.*, 2000).

PEG can be linear or branched with multi-arm or star structures. The functional end groups can be the same (symmetric) or different (asymmetric), which makes it versatile for hydrogel formation or for conjugating with biomolecules (Zhu, 2010). PEG hydrogels have been shown to maintain the viability of encapsulated cells and allow for ECM deposition as they degrade, demonstrating that synthetic gels can function as 3-D cell culture platforms even without integrin-binding ligands (Dutta and Dutta, 2009).

Different cross-linking methods can be used to introduce bioactivity into poly (ethylene glycol) (PEG) hydrogels including **photo-copolymerization** in which the properties of the polymers can be modified when exposed to UV light (Peppas *et al.*, 1999), **Click chemistry** which, by joining small modular units, can be used to enhance swelling capacities and improve mechanical properties of the hydrogel (Polizzotti *et al.*, 2008) **post-grafting** allows the formation of PEG hydrogels followed by grafting peptides (or proteins) on the hydrogel surface (Zhu, 2010).

West and co-workers formed PEG hydrogel containing growth factors such as basic fibroblast growth factor (bFGF) (DeLong *et al.*, 2005), tumour growth factor (*TGF)* (Mann *et al.*, 2001) which were acrylated by conjugating with Acr-PEG-NHS, followed by **photo-copolymerization**. They showed that the covalently tethered growth factors were able to maintain mitogenic activity and also to enhance fibroblast proliferation and migration (West and Hubbell, 1999).

Yang et al. synthesized a cell-adhesive PEG hydrogel by **Click chemistry** between 4-arm PEG acetylene (4-PEG-Ace) and RGD diazide (RGD-$2N_3$). The gelation time ranged from 2 to 30 min, depending on catalyst, temperature and precursor concentration. They demonstrated that PEG hydrogels with the incorporation of RGD peptides improved primary human dermal fibroblasts cell attachment and greater cell proliferation, compared with the control hydrogels without RGD (Yang *et al.*, 2004).

Hern and Hubbell synthesised a mono-acrylated RGD with or without PEG spacers by functionalizing the N-terminal amines of RGD peptides with N-hydroxyl succinimide (NHS) ester of acrylic acid (AA-NHS) and acryloyl-PEG-NHS (Acr-PEG-NHS, Mw 3400) to produce mono-acrylamidoyl RGD (RGD-MA) and RGD-PEG monoacrylate (RGD-PEGMA), respectively (Hern and Hubbell, 1998). The RGD-MA or RGD-PEGMA monomers were incorporated into the Polyethylene (glycol) diacrylate

(PEGDA) which is a synthetic, hydrophilic material which forms hydrogels in the presence of photoinitiator and UV light in a process called photopolymerization. The final result is a cell-adhesive hydrogel (Hern and Hubbell, 1998). They investigated *in vitro* the application of these PEG hydrogels containing various RGD densities on human foreskin fibroblasts spreading for 24 h and found that cell spreading was specifically mediated by hydrogels composed of PEG spacer (MW 3400) containing the immobilised RGD peptides while PEGDA hydrogels with RGD-MA without a PEG spacer mediated cell spreading non-specifically (Hern and Hubbell, 1998).

Moreover, PEG hydrogels have been engineered with linear, hydrophilic and biodegradable polymers such as polylactic acid (PLA) and polyglycolic acid (PGA) that can promote their biodegradability however this type of degradation is not cell-mediated (Athanasiou *et al.*, 1998). The appropriate method to include biodegradability on PEG hydrogels is to develop the proteolytic degradation mechanisms present in the ECM, incorporating enzyme-sensitive peptide sequences such as fibrin-derived YK↓NRD and VR↓N (↓ indicating the cleavage site). These have been used to make plasmin-sensitive PEG hydrogels (Jo *et al.*, 2010); peptides like collagen-derived GPQG↓IAGQ make MMP-sensitive PEG hydrogels (Kraehenbuehl *et al.*, 2008); sensitive peptides, such as AAPV↓RGGG and AAAAAAA also have been used for proteolytic modification of PEG hydrogels (Salinas and Anseth, 2008) ; PE↓NFF is one of the major peptide sequences at the MMP-13 cleavage site of aggrecan, a cartilage ECM component (Salinas and Anseth, 2008). Anseth and co-workers incorporated a cysteine-containing bifunctional peptide (CPENFFRGD) containing the RGD motif for cell adhesion and the cleavage sequence for MMP13, the PENFF, into the PEG hydrogels using the thiol-acrylate photopolymerization. These hydrogels promote the differentiation of human mesenchymal stem cells (hMSCs) (Salinas and Anseth, 2008).

It is very important in tissue regeneration to control the degradation rate of scaffolds since a rapid degradation of the scaffold compared with the tissue regeneration will not allow the convenient cell growth while the slow degradation of the scaffold compared with the tissue regeneration will impede the progression of cell growth and differentiation thus impeding tissue regeneration (Zhu, 2010).

As the field moves forward, the need for matrices that combine the benefits of natural and synthetic hydrogels is becoming more apparent, along with the need to identify the essential biophysical and biochemical signals to incorporate in these synthetic extracellular matrices (ECM) analogues (Tibbitt and Anseth, 2009). While

natural scaffolds are more efficient to promote cell adherence, synthetic scaffolds are able to control cell mechanical properties and their degradation rate (Dado and Levenberg, 2009).

1.4. Caf1 from *Yersinia pestis*

Most gram-negative pathogens express fibrous adhesive virulence molecules that mediate targeting to the site of infection. Adhesive organelles are large multimeric protein complexes, often in two common forms: the rod-like fibres (called fimbriae or pili) and flexible fibres (called fibrillae or atypical non-pilus adhesins) (Knight *et al.*, 2000; Zavialov *et al.*, 2002). Type 1 pili are produced by uropathogenic *Escherichia coli* (*E. coli*) and are responsible for attachment, invasion, and formation of biofilms in the bladder (Wright *et al.*, 2007) whereas P pili are produced by pyelonephritic strains of *E. coli* and are involved in the colonization of the kidney (Roberts *et al*., 1994).

Capsule-like antigen, fraction 1 (Caf1) belongs to the group of atypical non-pilus adhesins and is synthesized in large quantities by *Yersinia pestis* (*Y. pestis*) forming a proteinaceous capsule which is highly immunoprotective allowing escape of the bacterium from phagocytosis (Williams, 1972; Du *et al.*, 2002).

Yersinia pestis is the causative agent of bubonic and pneumonic plague. The bubonic plague is an infection of the lymph nodes, which become swollen and tender forming a bubo whereas the pneumonic plague is a lung infection that occurs via the respiratory tract resulting in the production of highly infectious bloody sputum (Titball and Williamson, 2001).

Another protein secreted by *Y. pestis*, this time under low calcium growth conditions at 37 ºC is V antigen which is mediated by Lcr plasmids (called pCD in *Y. pestis*) (Straley and Bowmer, 1986).

V antigen was detected on the surface of the bacterium which confirms that it may form part of a complex mechanism used to translocate the bacterial toxins (protein effectors) across the plasma membrane of eukaryotic cells called the injectisome or type III secretion system (Cornelis, 2006). Mutants of *Y. pestis* which do not produce V antigen are not capable of delivering protein effectors into the eukaryotic host cell (Straley and Bowmer, 1986).

It was demonstrated that Caf1 and V antigens can promote low protective immune responses when used individually while the combination of these proteins had

an increasing protective effect when used to immunise mice against plague (Titball and Williamson, 2001). Better results were obtained using Alhydrogel adjuvant to bind the antigens strongly, enhancing their persistence at the injection site and also delivering them to dendritic cells (Soliakov *et al.*, 2010). Therefore, the Caf1 proteinaceous capsule together with V antigen is the basis for development of new generation of plague vaccines (Titball and Williamson, 2001). Thus Caf1 is poorly immunogenic by itself and is tolerated by the human body (Titball and Williamson, 2001).

The majority of *Yersinia pestis* strains contain the 110 kb pFra plasmid, which encodes the *caf* operon. The *caf* operon comprises four genes, encoding for the capsule subunit – Caf1 (Galyov *et al.*, 1990), the chaperone-like protein – Caf1M (Galyov *et al.*, 1991), the outer membrane usher protein – Caf1A (Karlyshev *et al.*, 1992b) and the trans-regulator – Caf1R (Karlyshev *et al.*, 1992b). These genes mediate the formation of Caf1 capsule in *Yersinia pestis* at temperatures above 35-37 ºC. A similar capsule forms on the surface of *Escherichia coli* cells in which the corresponding *Y. pestis* operon is expressed (Galyov *et al.*, 1990).

Originally, the cosmid p153, carrying a segment of about 40 kb in size of the plasmid pFra, was used for transformation of *E. coli* and Caf1 production. Other subclones of the cosmid p153 were made. However, only the plasmids carrying the four genes of *caf* operon have mediated a high level of the Caf1 expression (Galyov *et al*., 1991).

Caf1 subunits are synthesised as pre-proteins in the cytoplasm and transported across the inner membrane via the SEC machinery (YEG). In the *Escherichia coli* expression system, a signal peptide is generally required for the secretion of proteins through the inner membrane into the periplasm (Liu *et al.*, 2006). The potential Caf1 signal peptide sequence contains 21 amino acids and it has been identified as: MKKISSVIAIALFGTIATANA. The signal peptide is cleaved off during transport across the inner membrane which leads to secretion of Caf1 protein of 149 residues into the *Y. pestis* periplasm. However, the presence of a signal peptide alone does not ensure efficient protein secretion (Galyov *et al*., 1990).

The general chaperone/usher (CU) pathway allows the assembly of a major class of adhesive fibres on the outer membrane of a large group of Gram-negative bacteria

(Sauer *et al.*, 2004). Our knowledge regarding the assembly of adhesive fibres mediated by the chaperone/usher systems derives from studies of uropathogenic *E. coli* P pili and type 1 pili assembly (Knight *et al.*, 2000).

The chaperone/usher systems can be divided into two subfamilies, FGS and FGL (Hung *et al.*, 1996; Zavialvo *et al.*, 2005).

The FGS (possessing a short sequence between F1 β-strand and G1 β-strand) chaperone/usher systems are used for assembly of rod-like organelles such as P pilus and type 1 pili in *E. coli*. Whereas FGL (possessing a long sequence between F1 β-strand and G1 β-strand) chaperone/usher systems can mediate the assembly of thin flexible fibres or afimbrial organelles such as *Yersinia pestis* Caf1 capsular antigen, Salmonella Saf1 and *E. coli* Afa/Dr adhesins (Knight *et al.*, 2000). Although the FGL system is less well understood compared with the FGS system, the best known model for FGL system studies is the *Yersinia pestis* F1 capsular antigen (Knight *et al*., 2000).

The crystal structures of the type 1 pilus FimC:FimH chaperone-adhesion complex and the P pilus PapD:PapK chaperone-adapter subunit complex have revealed that both, pilus subunits and chaperones, have a common non-canonical immunoglobulin (Ig)-like fold which is characterised by the absence of its C-terminal β-strand creating a deep hydrophobic cleft on the surface of the subunit (Choudhury D, 1999 ; Sauer *et al.*, 2000).

This characteristic of chaperone-subunit complex also extends to for the Caf1M:Caf1 complex (**Figure 1.7**) (Zavialov *et al.*, 2003).

After translocation of the newly synthesised Caf1 subunit across the inner membrane into the periplasm, the chaperone binds to the Caf1 domain by donating its G1 β-strand to complete the Caf1 subunit Ig-like fold in order to create polymers of stable monomers joined by non-covalent links in a process called **donor strand complementation (DSC)** (**Figure 1.8**) (Zavialov *et al.*, 2005).

A recent study conducted by Yu and co-workers (Yu *et al.*, 2012) has shown that the folding of Caf1M and Caf1 Ig domains is a fast first-order process, since Caf1M can rapidly bind an early folding intermediate of Caf1 and mediate its partial folding due to a large hydrophobic effect and extensive main-chain hydrogen bonding. However the folding of Caf1 subunit Ig modules into the fibre conformation is a slow second-order process due to the presence of a less hydrophobic, tighter and thus less dynamic environment between the Caf1 subunits (Yu *et al*., 2012).

For Caf1 fibre assembly to proceed, the G1 donor strand of the chaperone has to leave the acceptor cleft of the Caf1 subunit so that the cleft can receive the N-terminal donor-strand extension of an incoming Caf1 subunit to complement the incomplete Ig fold of the previously assembled Caf1 subunit in the growing Caf1 fibre. The process of exchanging donor strands in the acceptor cleft is called **donor-strand exchange (DSE)** (Knight *et al.*, 2000; Zavialov *et al.*, 2002).

DSE produces a very stable interaction; subunit oligomers resist dissociation by SDS at room temperature allowing the construction of a very large and robust fibre (Sauer *et al*., 2000).

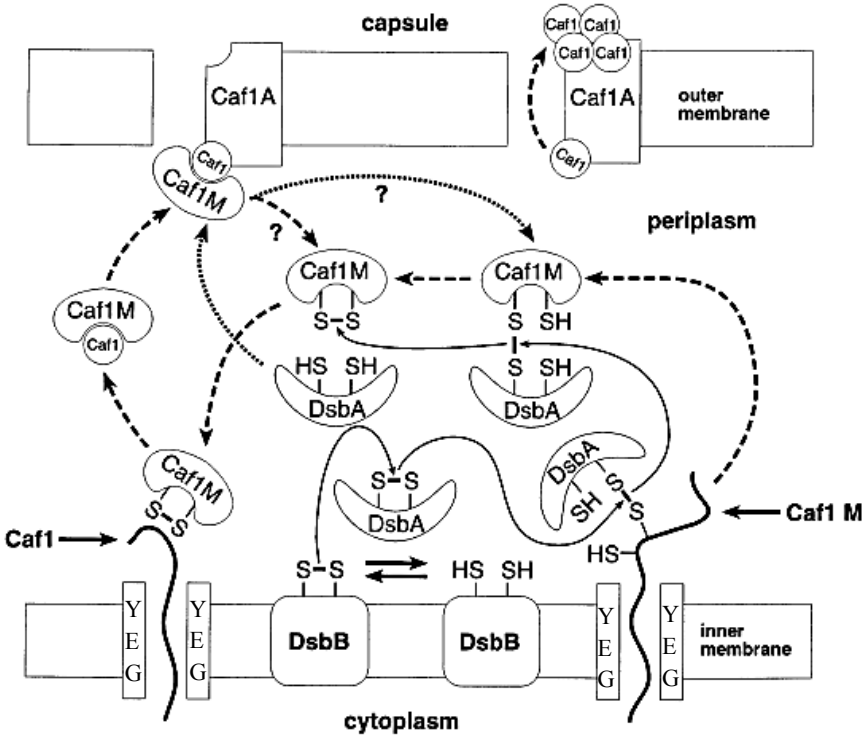

Figure 1.7 - Representation of Caf1 fibre assembly. The chaperone, Caf1M and the capsular subunit, Caf1 are secreted into the periplasm in an unfolded reduced state. The DsbA protein binds the unfolded chain of Caf1M, and rapidly transfers its disulphide to the folding protein. Reduced DsbA is re-oxidized by DsbB, an integral membrane protein. The folded and oxidized Caf1M binds the unfolded chain of Caf1, helping in the folding and preventing non-productive aggregation in the periplasm. The Caf1:Caf1M complex interacts with the outer-membrane usher Caf1A. Caf1M is released as the Caf1 subunits assemble at the cell surface to form the Caf1 capsule. The stimulation for the dissociation of Caf1M is unknown, but one hypothesis involves the reduction of Caf1M by, for example, DsbA or DsbC (as indicated by dotted arrow), with formation of a competitive Caf1M: DsbA (C) complex, resulting in the release of the reduced form of Caf1M which could then re-enter the cycle following re-oxidation. The direction of disulphide transfer is shown by the solid arrows, and changes in Caf1M by the dashed arrows (Zavyalov *et al.*, 1997).

The assembly is independent of the proton motive force and cellular energy in the form of ATP (Jacob-Dubuisson *et al.*, 1994). It was suggested for the P pilus of the FGS family that binding energy provided by interactions between pilus subunits in the helical rod leads to export (Jacob-Dubuisson *et al.*, 1994; Thanassi *et al.*, 1998).

Zavialov et al. reported a conformational change involving the entire hydrophobic core of Caf1 protein which can explain the mechanism in which periplasmic chaperones mediated the folding and polymerization of Caf1 subunits in the absence of cellular energy (Zavialov *et al.*, 2003). In this model (Zavialov *et al.*, 2003) the periplasmic chaperone binds to Caf1 subunit inducing the formation of a high-energy folding intermediate of Caf1 subunit. This conformational change of Caf1 subunit allows the chaperone to preserve folding energy that can contribute to Caf1 subunit assembly. The release of the Caf1 subunit from the chaperone: subunit complex allows folding to be completed and leads to fibre formation (Zavialov *et al.*, 2003).

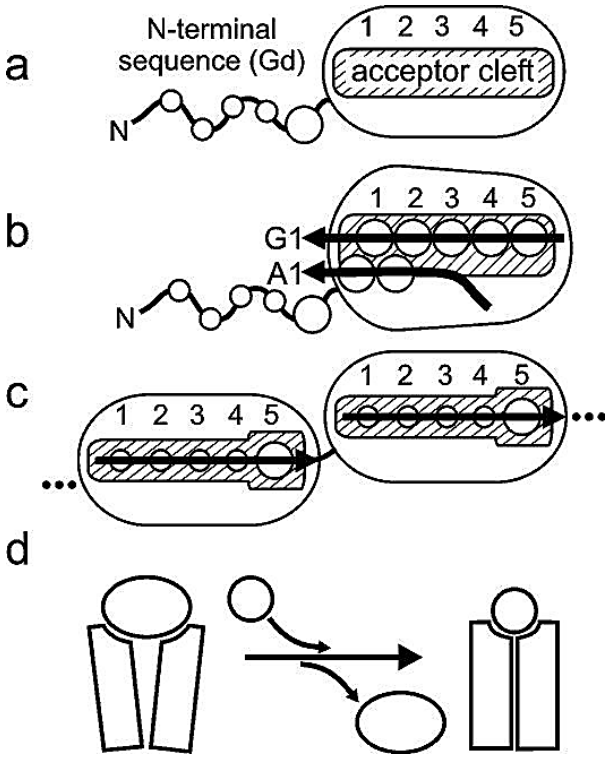

Figure 1.8 – Caf1 assembly mechanism. (a) The free Caf1 subunit contains a hydrophobic acceptor cleft with five sub-sites for the insertion of five side chains of a donor strand. The Caf1 N-terminal donor strand segment is unstructured. **(b)** The chaperone strands, A_1 and G_1 interact with Caf1 subunit edge strands to form a super-barrel. Large G_1 and A_1, partially, donor residues insert into the acceptor cleft between the two sheets of the subunit β-sandwich such that the super-barrel acquires a fused hydrophobic core. **(c)** The Caf1 subunits form Ig-like fibre modules by insertion of the N-terminal G_d donor strand of one subunit into the hydrophobic acceptor cleft of a neighbouring subunit. **(d)** Once Caf1 subunit is released from Caf1M and incorporated into the fibre, the two sheets of the subunit β-sandwich move together to form a close packed subunit hydrophobic core (Zavialov *et al.*, 2005).

The crystal structure of ternary Caf1M:Caf1:$Caf1_N$ complex in which $Caf1_N$ has its N-terminal strand removed which prevents polymer formation and stabilises the

ternary complex, was solved to 2.2 Å resolution and revealed that the polypeptide chain of Caf1 was organised in a six-stranded, two-layer β-sandwich. In this ternary complex the Caf1 N-terminal extension adopts a β-strand conformation which interacts with the hydrophobic cleft of $Caf1_N$, which completes the hydrophobic core of $Caf1_N$. The interactions between Caf1 and $Caf1_N$ were used to create the linear fibre model (Soliakov *et al*., 2010) (**Figure 1.9 - A**).

The monomeric unit of Caf1 has a molecular mass of 15.5 kDa but formation of a large molecular mass complex (in excess of 3 MDa) is possible with fibre formation (Andrews *et al.*, 1996; Miller *et al.*, 1998).

The Caf1 oligomers can be separated using gel electrophoresis as a distinctive pattern of bands with molecular masses ranging from 20 to > 500 kDa (Habig *et al.*, 1971; Soliakov *et al.*, 2010).

Re-association of Caf1, previously heat denatured in 7 M urea or 1% (w/v) SDS, created dimers and tetramers leading to the bilayer model for the quaternary structure of Caf1 (Soliakov *et al*., 2010). While the free Caf1 subunit is only slightly stable (Zavialov *et al.*, 2005) the capsule is extremely stable and remains intact in 0.5% (w/v) SDS at 75 ºC, and is resistant to proteolysis by trypsin or proteinase K (Perry and Fetherston, 2007). Caf1 subunits form aggregates under physiological conditions (Galyov *et al*., 1990; Karlyshev *et al*., 1992).

Soliakov and co-workers (Soliakov *et al*., 2010) showed by electron microscopy that Caf1 antigen forms flexible polymers up to 1.5 microns long, which may contain more than 250 monomers with total molecular masses of about 4 MDa (**Figure 1.9 - B**).

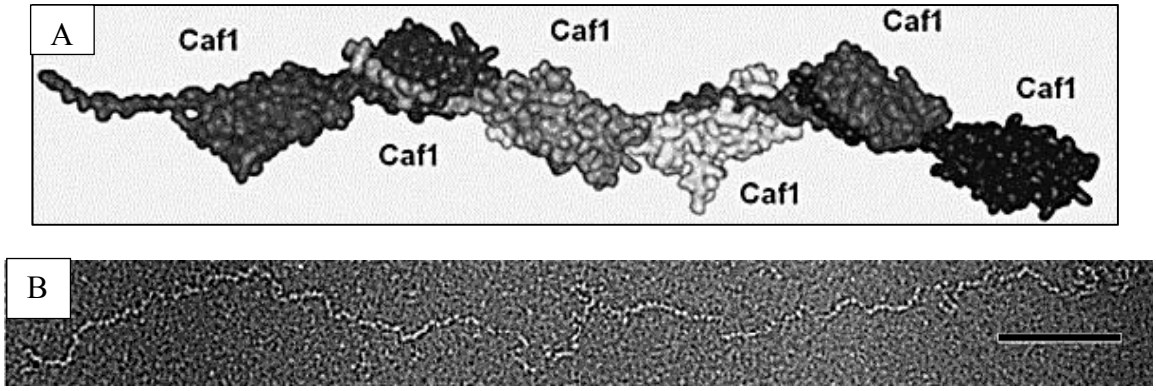

Figure 1.9 – Linear polymeric form of Caf1 protein from *Yersinia pestis*. (A) Model for a Caf1 fibre assembly was generated based on crystal structure of ternary Caf1M:Caf1:$Caf1_N$ complex and assuming the same orientation between the successive Caf1 subunits. **(B)** Caf1 as a long and linear polymer negatively stained observed by Transmission electron microscopy (Soliakov *et al*., 2010). Scale bar indicates 100 nm.

Production and purification of Caf1 protein from *Yersinia pestis* cells is a time consuming procedure. Instead, use of recombinant *Escherichia coli* for the production of Caf1 was reported (Baker *et al.*, 1952 ; Simpson *et al.*, 1990 ; Andrews *et al.*, 1996; Miller *et al.*, 1998). Expression of Caf1 is usually associated with the appearance of a white diffuse layer above a centrifuged cell pellet. This is termed the flocculent layer.

Baker and co-workers (Baker *et al*., 1952) extracted Caf1 with a solution of toluene-saturated sodium chloride from acetone-dried *Y. pestis* grown on agar plates. The antigen was partially purified by differential ammonium sulphate precipitations, which yielded two Caf1-containing fractions: one of the fractions consists of protein and carbohydrate, whereas the other fraction is composed entirely of Caf1 protein.

Miller and co-workers (Miller *et al*., 1998) used a recombinant low-copy plasmid pAH34L, which contains the *caf* operon. Caf1 protein expression was high and the flocculent layer was saturated with 50% of ammonium sulphate, dialysed and loaded in size-exclusion chromatography column.

Holtzman and co-workers subcloned the *caf* operon into the medium copy-number plasmid pBR322-Kanamycin. The fermentation was conducted in a rich medium containing soy protein extract and glycerol as carbon source to a high cell density – 60 OD_{600} and a high molecular weight oligomers of Caf1 were purified to > 90% by ultra-filtration tangential flow cartridges (pore sizes of 300 and 100 kDa) followed by 33% saturation ammonium sulphate precipitation and then Superdex-200

size exclusion chromatography (Holtzman *et al.*, 2006). Finally it is of interest for the possible use of Caf1 in 3D cell culture matrices that its Ig-subunit structure closely resembles that of fibronectin III.

Aims

The main aims of this project are:

- The synthesis, production and biophysical characterization of a new cell culture system using the long polymer Caf1.
- Site-directed mutagenesis to insert RGDS and RGES motifs into the Caf1 polymer to promote or inhibit cell adhesion, respectively.
- Improve an established 2D system using tmOmpA by the development of an arraying method and demonstrated it effectiveness of the ECM inserted peptides.
- Study of mammalian cell adhesion, shape and number of focal adhesions using Caf1 as a protein scaffold for cell culture by immunofluorescence and scanning electron microscopy.
- Produce a Caf1 hydrogel by the cross-linking of Caf1 polymer and three different NHS-cross-linkers in order to obtain hydrogels with distinct physical and mechanical properties.
- Construct an over-expression Caf1 system to produce hybrid Caf1 polymers (for example - Caf1:Caf1RGDS) exported by this system.

2. Chapter Two: Material and Methods

Introduction

This chapter describes the procedures followed in completing the experiments discussed in chapters 3-5 and provides a set of instructions for anyone wishing to replicate or carry similar studies in the future. It is divided into two parts: Part A and B. Part A corresponds to a study performed to understand the effect of small peptides from large molecules on mammalian cell adhesion and proliferation using an existing 2D cell culture system from Orla Protein Technologies Ltd. Part B corresponds to an initial study performed to develop a new cell culture system with specific properties which could lead to a 3D cell culture system in the future.

Suppliers

All chemicals and reagents were obtained from either Sigma-Aldrich (UK); http://www.sigmaaldrich.com or Invitrogen (UK); http://www.invitrogen.com unless otherwise stated. The Precision plus protein molecular weight standard was purchased from Bio-Rad Laboratories (UK*)* Ltd; http://www.bio-rad.com/.

Part A: Use an existing 2D cell culture system

In this study, we have used an existing methodology which enables the stable self-assembly of proteins on surfaces (Shah *et al*., 2007). The system described here uses the transmembrane domain of outer membrane protein A (tmOmpA) from *E. coli*. The beta-barrel structure of OmpA makes the protein ideal for forming engineered scaffolds. Thus, the protein can be immobilised to gold surfaces in an orientated manner through gold-sulphur bonds via an engineered cysteine at the N-terminus of tmOmpA (Shah *et al*., 2007). The strong reactivity between the sulphur atoms from the thiol group of the cysteine with the gold, results in the protein covalently bound to the gold surface. The protein binds to the gold in an oriented way forming a self-assembled monolayer (SAM). We took advantage of the fact that tmOmpA has four external loops where we can insert either short sequences of amino acids from ECM proteins or larger proteins domains and thus study the biological effects of these motifs on cell morphology (**Figure 2.1**).

2.1. Protein engineering, expression, purification and refolding

The protein engineering, expression, purification and refolding was performed by Shah et al., (2007). Briefly, oligonucleotides encoding ECM peptides with flanking regions complementary to tmOmpA were designed and synthesised (Sigma Genosys; http://www.sigmaaldrich.com/Brands/Sigma_Genosys.html).

The oligonucleotides were ligated into the gene encoding the modified tmOmpA domain scaffold in a way that the motif was within outer loop-1 of tmOmpA. All constructs thus possess a His tag and a cysteine residue at the N-terminus (**Figure 2.1**). Then different plasmids (Shah *et al*., 2007) with motifs were constructed as shown in **Table 2.1.** As a negative control we used the parental tmOmpA which does not contain any cell interaction peptides.

The protein expression was conducted in three baffled flasks of 2L each containing 750 ml of Lysogeny broth (LB) media with 100 µg/ml ampicillin; these were inoculated with 5 ml from a 50 ml overnight culture of BL21. The cultures were incubated at 37 ºC with 180 rpm shaking until their optical density had reached 0.6 at 600 nm. The protein expression was induced with 1 mM final concentration of IPTG (Isopropyl β-D-1-thiogalactopyranoside) added to each flask. BL21 cells were harvested by centrifugation at 3600 x g for 20 min at 4 ºC in a Mistral 3000i centrifuge (MSE, UK). The protein formed inclusion bodies, which were isolated by disrupting the cells in BugBuster® Protein Extraction Reagent (Novagen) containing lysozyme to a final concentration of 200 µg/ml and 1 µl (25 units) of benzonase nuclease (per ml BugBuster reagent). The inclusion bodies were washed three times in a detergent solution (1:10 dilution of BugBuster) and solubilised in 8 M urea, 20 mM sodium phosphate pH 7.6, 500 mM sodium chloride and 20 mM imidazole.

Contaminants were removed by a two-step purification step. The purification of tmOmpA based proteins was performed by 5 ml Histrap^{TM} HP column from GE Healthcare with a step elution of 250 mM imidazole. After that selected fractions containing the desired proteins were purified on a 1 ml QFF HiTrap anion exchange column from GE Healthcare in 30 mM ethanolamine buffer at pH 9.5 with elution in the same buffer plus 80 mM NaCl to complete the purification.

The proteins were refolded from the urea denatured state by a slow dilution (approximately 200 µl of urea solubilised stock protein per hour) into refold buffer [consisting of 50 mM Tris–HCl pH 8, 1 mM DTT, 0.1 mM EDTA and 1 % (w:v) n-

octylglucopyranoside]. When the dilution was complete the protein was left for at least 48 h at 37°C to refold. Before use the protein was passed down a PD10 column (GE Healthcare) and eluted in fresh refold buffer (Shah *et al*., 2007).

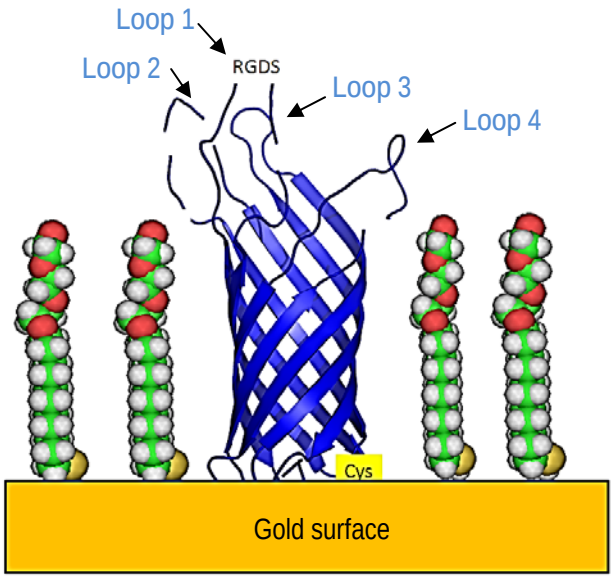

MHHHHHHSSCAPKDNTWYTGAKLGWSQYHDTGFINNNGPTHENQLGAGAFGGYQVNPY 58
VGFEMGYDWLGRMPYKGSVENGAYKAQGVQLTAKLGYPITDDLDIYTRLGGMVWRADTK 117
SNVYGKNHDTGVSPVFAGGVEYAITPEIATRLEYQWTNNIGDAHTIGTRPDNGMLSLGVSYR 179
FGQGEAAPVVAPAPAPA 196

Figure 2.1 – Cartoon representation of tmOmpA assembled on gold surface surrounded by PEG-thiol molecules [Protein Data Bank (PDB) ID code 1BXW (Pautsch *et al*., 1998); http://www.pymol.org]; four loops (indicated by the arrows). The gaps in the X-ray model of the tmOmpA loops are due its high flexibility. On loop 1 of the tmOmpA we inserted the tetra-peptide RGDS. At the N-terminus of tmOmpA was a single inserted cysteine residue which allows the protein to bind to the gold surface. The space between protein molecules was filled with PEG-thiol molecules which were able to assemble to the gold surface through their thiol groups. The protein and PEG-thiol molecules interact via hydrophobic and van der Waals forces. Below the tmOmpA cartoon is represented tmOmpA amino acid sequence. A unique cysteine mutation is indicated in yellow; the sequence -GFINNNGPT- correspond to the first loop, -KGSVEN- correspond to the second loop, -SNVYG- correspond to loop 3 and -NIGDAHTIGTRP- sequence correspond to loop 4.

Table 2.1 – Biomimetic substrates, peptides of interest and the ECM molecule from which they are derived.

Type of source	Peptides from ECM proteins	ECM proteins source
Orla 1	RGDS 1 (inserted in loop 1)	Fibronectin
Orla 2	RGDS 2 (inserted in Loop 2)	Fibronectin
Orla 31	GTPGPQGIAGQRGVV	Collagen I
Orla 32	MNYYSNS	Collagen IV
Orla 34	PHSRN	Fibronectin
Orla 35	RGDS + PHSRN	Fibronectin
Orla 36	YIGSR	Laminin
Orla 37	IKVAV + YIGSR	Laminin
Orla 62	FHRRIKA	Fibronectin
Orla 95	LDVP	Fibronectin
Orla 96	IDAP	Fibronectin
Orla 97	LDVP + RGDS + PHSRN	Fibronectin

Preparation of peptide-modified surfaces

Borosilicate glass coverslips (2 cm diameter) were covered with gold (25 nm thick layer). The gold surfaces were cleaned in 2% Hellmanex (Hellma, UK) for 20 min at room temperature (RT) and then they were passivated by incubation with 1 ml of 1% (v:v in MilliQ H20) solution of 2-mercaptoethanol (Fisher, UK) for 15 min at RT.

The thiol group on the *β*-carbon bonds to the gold surface. This leaves the hydroxyl groups exposed creating a hydrophilic surface. This allows for more specific orientation of the protein when binding to the gold surface as the amount of hydrophobic interactions between the outside of the *β*-barrel structure of the scaffold protein and the gold surface are reduced (Brun *et al*., 2008). The surfaces were washed with 2 ml of MilliQ H_2O five times, each time for 5 min at RT. Before the protein is incubated on the surface the thiol group in the protein was reduced to enable specific bonding to the gold surface. This was done using the reducing agent Tris(2-carboxy-

ethyl)phosphine hydrochloride (TCEP) to a final concentration of 5 mM. TCEP is the preferred reducing agent because unlike dithiothreitol (DTT) and 2-mercaptoethanol, TCEP will not compete with the protein during assembly by binding to the gold surface (Brun *et al*., 2008).

The gold coverslip is coated with 1 ml of protein solution at a concentration of 5 μM. The protein was applied to the gold coverslips in two 1 h incubations at room temperature. The surface is washed with 1 ml of 1% (w:v in distilled water) solution of sodium dodecyl sulphate (SDS) for 5 min at RT. The SDS will remove any protein that is non-specifically bound to the gold surface. The surfaces were washed with 2 ml of MilliQ H_2O 5 times, each time for 5 min at RT, in between each protein application.

After the protein assembly the gaps between the immobilised protein molecules were filled in by overnight incubation with PEG-thiol (11-mercapto-1-triethyleneglycolundecane, HSC11-EG3) (ProChimia Surfaces, Sopot, Poland) at RT. PEG-thiol was diluted to a final concentration of 0.5 mM in absolute ethanol. Before incubation on the gold surface the PEG-thiol was incubated at RT with a final concentration of 5 mM TCEP. At the end of the incubation in PEG-thiol the gold surface is once again washed with a 1% (w:v in distilled water) SDS solution to remove any non-specifically bound PEG-thiol. The surfaces were washed with 2 ml of MilliQ H_20 five times, each time for 5 min at RT (**Figure 2.2**).

The coverslips were dried under air. Control surfaces with PEG-thiol only or tmOmpA/PEG-thiol were also prepared. Before proceeding to cell culture, the coverslips were sterilised by immersion in 3 ml 70% ethanol for 15 min followed by five washes with 5 ml sterile phosphate buffered saline (PBS) (Cambrex).

For the formation of microspots of TmOmpA-Flag epitope on gold surfaces, 5 μL of tmOmpA- FLAG tag (N-DYKDDDDK-C) protein at a concentration of 5 μM was applied to each well of the Press-to-Seal™ silicone isolator with adhesive (24 wells and 2.5 mm diameter) that was attached to a gold surface previously washed and prepared as described above. After protein assembly on gold surface, the silicone isolator was removed and the entire surface filled in with PEG-thiol molecules for 1 h at RT as mentioned before.

Direct visualization of the protein assembly on the surface, was possible using tmOmpA-FLAG tag (N-DYKDDDDK-C). Anti-FLAG monoclonal antibody conjugated with alkaline phosphatase was diluted 1:100 in TBS buffer (50 mM Tris-

HCl, pH 7.4, 150 mM NaCl) and added to the pre-assembled layer in the gold surface. The antibody was incubated for 1h incubation at RT.

The surfaces were washed with 2 ml of TBS buffer (50 mM Tris-HCl, pH 7.4, 150 mM NaCl, 0.05 % Tween 20) five times, each time for 5 min at RT, to remove any unbound antibody and then stained with 1 ml of NBT/BCIP solution, BCIP (5-Bromo-4-Chloro-3'-Indolyphosphate p-Toluidine Salt) and NBT (Nitro-Blue Tetrazolium Chloride) yield an intense, insoluble dark precipitate when reacted with alkaline phosphatase.

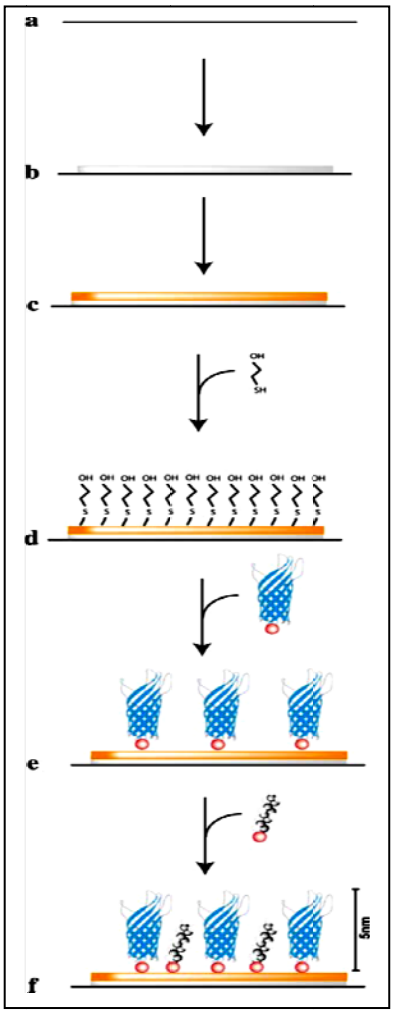

Figure 2.2 – Self-assembled protein monolayers. a – The borosilicate glass coverslips were cleaned with 70% ethanol to remove any residues; **b –** coverslips were coated with titanium to facilitate the attachment of gold layer; **c –** a layer of gold was sputtered coated onto the surface performed by Dr. Siôn Phillips at INEX at Newcastle University; **d –** the surface was passivated by addition of beta-mercaptoethanol in order to promote the attachment of tmOmpA proteins; **e -** tmOmpA proteins were allowed to self-assemble on the surface and attach via the unique cysteine residue (in red); **f –** Thioalkane molecules self-assemble onto the gold surface filling gaps between the attached tmOmpA proteins forming an intact molecular monolayer (Cooke *et al*., 2008).

Cell culture and maintenance

PC-12 cells were purchased from American Type Culture Collection (ATCC; http://www.lgcpromochematcc.com) and maintained as previously described (Greene and Tischler, 1976). Briefly, stock cultures were grown on cell culture plasticware

(VWR; http://uk.vwr.com) pre-coated with a 0.1% solution of collagen IV (in 0.25% glacial acetic acid) (Fisher Scientific, UK) in RPMI (Roswell Park Memorial Institute) 1640 medium supplemented with 10% heat-inactivated fetal bovine serum, 20 units/ml of penicillin/streptomycin. Cultures were maintained under standard conditions at 37 ºC in a humidified 5% CO_2 incubator. The medium was changed three times a week and cells passaged as required using 0.05% trypsin-ethylenediamine tetraacetic acid (EDTA) (1x) solution containing phenol red (Invitrogen, UK), as standard.

Attachment of cells to peptide-modified surfaces

PC-12 cells growing on 80 cm^2 cell culture polystyrene sterile flasks with filter cap (Thermo Scientific Nunc, UK) (cell passage number 42) were incubated in 2 ml of 0.05% trypsin-EDTA (1x) solution, containing phenol red, for detachment. Cells were counted using a hemocytometer. We added $1x10^5$ cells, in Roswell Park Memorial Institute (RPMI) 1640 medium without serum, per well of a 6-well culture plate (Nunclon^{TM}△Surface, UK) containing coverslips coated with tmOmpA engineered with different motifs of fibronectin, collagen IV and laminin (**Table 2.1**). The cells were maintained at 37 ºC, 5% CO_2 in an incubator for 24 h. After 24 h cultures were washed once with 2 ml sterile phosphate buffered saline (PBS) pH 7.4. Three independent experiments with two replicates each were performed.

Proliferation of cells on peptide-modified surfaces

The same protocol for cell attachment was followed, however after 24 h cultures were washed once with 1ml RPMI 1640 medium without serum and followed by 3 ml per coverslip of RPMI 1640 medium supplemented with 10% heat-inactivated fetal bovine serum, 20 units per ml of penicillin/streptomycin. Cells were maintained at 37 ºC, 5% CO_2 in an incubator for another 24 h. Three independent experiments with two replicates each were performed.

Immunocytochemistry

The cells were washed with 2 ml PBS pH 7.4 and fixed using 4% paraformaldehyde in PBS pH 7.4 for 30 min, and then washed twice with PBS. The

cells were stained with DAPI (1 μg/ml) diluted in PBS pH 7.4 for 15 min and then washed four times with PBS, 5 min per wash. The cells were permeabilized in 0.1% Triton X-100 in PBS for 1 minute and then incubated in Rhodamine-phalloidin diluted 1:1000 in PBS pH 7.4 for 15 min and washed four times with PBS, 5 min per wash.

Fluorescence Microscopy

Cells were visualized using an inverted fluorescence microscope (Leica lX81). The images were captured by a Leica DFC295 camera. Ten random fields of view using 10x objective lens were imaged for each surface tested. Total magnification 100x. Experiments were repeated in triplicate.

Statistical Analysis

Data sets were compared using one-way analysis of variance (ANOVA). Followed by Tukey's test for multiple comparisons with the significance level set at $\alpha = 0.05$. All data reported are means ± standard error.

Part B: Development of a new cell culture system

The system described here uses the Caf1 polymer from *Y. pestis*. The *caf* operon was cloned into a vector and used to transform an *E. coli* strain. Caf1 is known to be a β-structure protein composed of many monomers forming long and flexible fibres, which makes the protein ideal for forming engineered scaffolds (Soliakov *et al*., 2010). In addition, we took advantage of the fact that Caf1 monomeric form has five external loops where we can insert short sequences of amino acids from ECM proteins and thus study the biological effects of these motifs in cell morphology.

Recombinant capsular antigen fraction 1 (Caf1) was provided by Avecia Biologics Ltd, UK and used in this study as a control. The Caf1 protein was supplied at a concentration of ~ 1 mg/ml in 0.5 mM phosphate buffer pH 7.4, 150 mM NaCl.

Caf1 protein was expressed extracellularly using *Escherichia coli* strain BL21 (DE3)/pGEMCaf1 and purified using size exclusion chromatography.

2.2. Analysis of suitable sites for mutation in polymeric Caf1

Subcloning of Caf1, expression and purification

The oligonucleotide primer pair (**Table 2.2**) were designed to amplify the entire *caf* operon (about 5.2 Kb in size; GenBank, accession number AY450847) from the plasmid pAH34L vector (**Table 2.3**). The *caf* operon was amplified by PCR (**Table 2.4**) using the KOD HOT START DNA polymerase (Novagen, UK) which generates blunt-ended fragments.

Primers were synthesised by Eurofins MWG operon, Germany.

Table 2.2 – Oligonucleotide primers for PCR amplification of *caf* operon using the pAH34L plasmid as a template.

Primer	Nucleotide sequence (5′ to 3′)
F1 Forward	ATAAATCGGTTCAGTGGCCTCAACGCTGTG
F1 Reverse	GGTTAGGCTCAAAGTAGGATAATTC

Table 2.3 – Vectors used in this study.

Vectors	Gene bank accession number of the vector	Reference/Company
pAH34L-Kan	X61996	Miller *et al*., 1998
pGEM-T Easy-Amp	-	Promega, UK
pET3a-Amp	-	Novagen, UK
pBAD33-Cm	-	Guzman *et al*., 1995
pSMART-LC-Kan	AF532106	Lucigen, USA
pSMART-HC-Amp	AF399742	Lucigen, USA

Table 2.4 - *caf* operon amplification by PCR using a Thermo Hybaid PCR Express thermal Cycler (UK).

Polymerase chain Reaction (PCR)			
	Number of cycles	**Temperature (ºC)**	**Time**
Polymerase activation	1	95	1 min
Denaturation	30	95	20 s
Annealing		55	10 s
Extension		70	5 min

Agarose Gel Electrophoresis for DNA separation and purification

The PCR product obtained by amplifying the *caf* operon from pAH34L was loaded onto a 0.7% agarose gel stained with ethidium bromide (0.5 μg/ml). DNA was visualised on the trans-illuminator (UV light with a wavelength of 254 nm) (Gel-Doc, Bio-Rad, UK). The PCR product of oligonucleotides which corresponds to the *caf* operon was excised from the agarose gel using a sterile scalpel blade. The extracted DNA band was purified with QIAquick gel extraction kit and QIAquick PCR purification kit (Qiagen, UK) following the manufacturer's instructions.

Restriction digests

Reactions using *Hin*dIII, *Bam*HI and *Eco*RI (Promega, UK) restriction enzymes were conducted in a total volume per preparation of 20 μl containing 2 μl of 5x restriction enzyme reaction Buffer (Promega, UK), 5 μl of DNA sample, 12 μl nuclease-free water and 1 μl restriction enzyme. For the control tube, all components referred above were added except the restriction enzymes. All components were mixed gently and spun for 2 seconds in a microcentrifuge. The tubes were immediately incubated at 37 ºC for 45 min.

Subcloning of caf operon using pSMART-HC-Amp and pSMART–LC-Kan vectors

Both, pSMART-HC-Amp and pSMART-LC-Kan vectors (**Table 2.3**) were obtained from (Lucigen, USA). The copy number of pSMART-HC is similar to pUC19, about 300-500 copies per cell. The copy number of pSMART-LC is similar to pBR322, about 15-30 copies per cell. The pSMART vectors are pre-digested, with blunt, dephosphorylated ends. The small size of the pSMART vectors (1.7-2.0 Kb) could facilitate subcloning and mutagenesis experiments of the large insert DNA. After DNA purification the PCR product must be treated with T4 polynucleotide kinase (10 U) (NEB, UK) to add 5´-phosphates to oligonucleotides in order to allow subsequent ligation. In the cloneSmart ligation reaction, the pre-processed pSMART vector is ligated with blunt, phosphorylated insert (200 ng of insert). The positive control used was the lambda/HcII insert (500 ng) and the negative control without insert was also performed following the manufacturer's instructions and recommendations for the ligation (Lucigen, US). Transformants of 10G *E. coli* chemically competent cells [F- mcrA D(*mrr-hsd*RMS-*mcr*BC) Φ80*dlacZ*△M15 △*lac*X74 *end*A1 *rec*A1*ara*D139 △(*ara*, *leu*)7697 *gal*U *gal*K *rps*L *nup*Gλ- *ton*A] (Lucigen, USA) containing the new recombinant plasmid, were selected on LB agar plates containing the appropriate antibiotic for either pSMART HC-Amp and LC-Kan. The plates were incubated overnight at 37 ºC. Afterwards, improvements to subclone the *caf* operon were made such as increasing the incubation time to 24 h at 4 ºC.

Subcloning of caf operon was conducted using pGEM-T Easy

The pGEM®-T Easy Vector (**Table 2.3**) was obtained from Promega, UK. The vector contains T7 and SP6 RNA Polymerase promoters flanking a multiple cloning site (MCS) within the α-peptide coding region of the enzyme β-galactosidase. Insertional inactivation of the α-peptide allows recombinant clones to be directly identified by blue/white screening on indicator plates using X-gal (Maniatis *et al.*, 1982). The T7 Promoter Primer (the sequence is: 5´TAATACGACTCACTATAGGG3´) or the pUC/M13 Forward Primer (the sequence is:5´CCCAGTCACGACGTTGTAAAACG3´) can be used to sequence ssDNA produced by the pGEM®-T Easy Vectors.

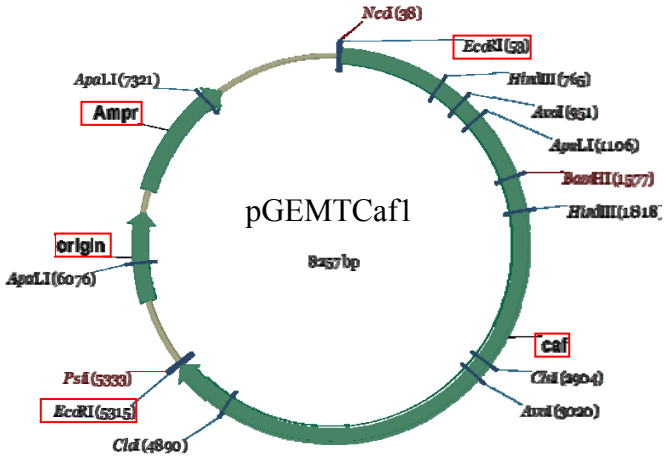

Figure 2.3 – Genetic map of pGEMCaf1. The main components in the vector are inserted into red boxes. The *caf* operon with its own promoter region and ribosomal binding site was inserted into the pGEM-T Easy vector and named pGEMTCaf1; ori (origin of replication), pMB1; restriction sites: *EcoRI*.

A-tailing procedure

The reactions were prepared by mixing 5 µL of purified PCR fragment, 1 µL *Taq* DNA polymerase 10x reaction buffer with $MgCl_2$ and dATP to a final concentration of 0.2 mM, 5 units of *Taq* DNA polymerase and nuclease-free water to a final reaction volume of 10 µL. The reactions were incubated at 70 ºC for 25 min.

Ligation with pGEM-T Easy

To construct the pGEMCaf1 plasmid including Caf1 with its original promoter region (**Figure 2.3**) a reaction mixture was prepared in 0.5 ml microcentrifuge tubes containing 5 µl of 2x rapid ligation buffer with ATP for T4 DNA ligase high enzyme activity (included in the Promega kit), 1 µl of T4 DNA ligase (3 Weiss units/ µl), 1 µl pGEM-T Easy vector from Promega (50 ng), 2 µl of A-tailed PCR product (50 ng) (the molar ratio of PCR product: vector used was 1:2) and nuclease-free water to a final volume of 10 µl. The control reactions were prepared as mentioned above adding 1 µl control insert DNA (4 ng) (included in the Promega kit) or 1 µL nuclease-free water instead of the PCR product. All reactions were mixed by pipetting and incubated for 24 h at 4 ºC. The ligation reaction was stopped by heat-denaturation at 65 ºC for 10 min.

Transformation using the pGEMCaf1 ligation reaction

Lysogeny broth (LB) plates (Miller's LB Broth high salt and granulated) were prepared by dissolving 25 g in 1 L of distilled water and 15 g/L agar was added. LB-agar was sterilized by autoclaving for 15 min (Melford Laboratories, UK). For each ligation reaction LB-agar were prepared and supplemented with 100 µg/ml ampicillin, 0.5mM IPTG (Isopropyl β-D-1-thiogalactopyranoside) and 80µg/ml X-Gal (5-bromo-4-chloro-indolyl-β-D-galactopyranoside).

The 0.5 ml microcentrifuge tubes containing the ligation reactions were centrifuged to collect the contents at the bottom and 2 µl of each ligation reaction were added to a sterile (12 × 75 mm) polypropylene Falcon round-bottom tubes (BD Biosciences) on ice. Frozen XL10 Gold chemically competent *E. coli* cells were removed from storage and place in an ice bath until just thawed (about 5 min). The cells were mixed by gently flicking the tube and 45 µl of cells were transferred into each sterile (12 × 75 mm) polypropylene Falcon round-bottom tubes (BD Biosciences) containing the ligation reactions. The Falcon tubes were left on ice for 30 min. The XL10 gold chemically competent *E. coli* cells were heat-shocked by placing them at 42ºC water bath for 30 seconds and returned to ice for 2 min. Pre-warmed super optimal broth with catabolite repression (SOC) medium (allows bacteria to adapt quickly to a preferred or rapidly metabolisable carbon and energy source first), 950 µL was added to the cells in the tubes. The tubes were incubated at 37 ºC in a rotating wheel at 225 rpm for 1 hour. Transformed cells (100 µL) were plated onto LB plates containing ampicillin/IPTG/X-Gal prepared above. The plates were incubated overnight at 37 ºC.

Table 2.5 – Bacterial strains used in this study.

***E. coli* strains**	**Genotype**	**Resistance**	**Supplier**
DH5α	F- Φ80*lac*Z△M15 △(*lac*ZYA-*arg*F)U169 *deo*R *rec*A1 *end*A1 *hsd*R17(rk-, mk+) *pho*A *sup*E44 *thi*-1 *gyr*A96 *rel*A1λ$^-$	None	Invitrogen, UK
Mach 1	ΔrecA1398 endA1 tonA Φ80ΔlacM15 ΔlacX74 hsdR(r_K^- m_K^+)	None	Invitrogen, UK
BL21 (DE3)	*E. coli* B F$^-$ *dcm ompT hsdS*(r_B^- m_B^-) *gal* λ(DE3)	None	Invitrogen, UK
XL10 Gold	endA1 glnV44 recA1 thi-1 gyrA96 relA1 lac Hte Δ(mcrA)183 Δ(mcrCB-hsdSMR-mrr)173 tet^R F'[proAB $lacI^qZ$ΔM15 Tn10(Tet^R Amy Tn5(Kan^R)]	Tetracyclin and Kanamycin	Stratagene, UK
TOP 10	F- mcrA Δ(mrr-hsdRMS-mcrBC) φ80lacZΔM15 ΔlacX74 nupG recA1 araD139 Δ(ara-leu)7697 galE15 galK16 rpsL(Str^R) endA1 λ$^-$	None	Invitrogen, UK
10G	F$^-$ *mcr*A Δ(*mrr-hsd*RMS-*mcr*BC) *end*A1 *rec*A1 Φ 80d*lac*Z Δ M15 Δ *lac*X74 *ara*D139 Δ (*ara,leu*)7697 *gal*U *gal*K *rps*L (StrR) *nup*G λ *ton*A	None	Lucigen, US

Gene sequencing

A single colony was picked from each successful transformation and introduced into a tube containing 2% agar in LB medium and sent for sequencing. Gene sequencing was carried out by Beckman Coulter Genomics - Formerly Agencourt Bioscience and Cogenics, UK using the pUC/M13 Forward Primer or pUC/M13 Reverse Primer.

Glycerol stock preparations of the pGEMCaf1 plasmid

Small-scale plasmid DNA purification was conducted using the QIAGEN plasmid DNA purification kit and transformed into DH5α chemical *E. coli* competent cells. Briefly, DH5α chemical *E. coli* competent cells were heat-shocked by placing them at 42 ºC water bath for 30 seconds and returned to ice for 2 min. Pre-warmed super optimal broth with catabolite repression (SOC) medium, 950 µL was added to the

cells in the tubes. The tubes were incubated at 37 ºC with 225 rpm for 1 hour. Transformed cells, 100 µL were plated on LB plates containing ampicillin/IPTG/X-Gal prepared above. The plates were incubated overnight at 37 ºC.

A single colony was picked from the freshly streaked selective plate and inoculated in 5 ml LB containing 100 µg of ampicillin and culture at 37°C for 5–6 h with vigorous shaking (approx. 300 rpm). The bacterial cells were centrifuged at 6,000 x *g* for 15 min at 4°C. An autoclaved 60% glycerol solution was added to the centrifuged bacteria (volume ratio was 1:1). An aliquot of 100 µl of the glycerol/bacterial solution was added to a 1.5 ml Eppendorf type tube and stored at –80ºC.

Site-directed mutations using the pGEMCaf1

The mutagenic primers are presented on **Table 2.6.** Mutagenic primers to insert RGDS and RGES peptides into Caf1 (mutations are underlined) were designed and analysed by Oligoanalyser version 3.1 software. Mutations within the *Caf1* gene were created in pGEMCaf1 by PCR using *Pfu* polymerase (Stratagene) (**Table 2.7**) as described in the Quikchange XL Stratagene manual. Stratagene's QuikChange XL site-directed mutagenesis kit is derived from the QuikChange XL site-directed mutagenesis method. The XL version of the kit is specialized for efficient mutagenesis of large or difficult-to-mutagenize plasmid templates since it contains components specifically designed for more efficient DNA replication of large plasmids such as the case of the designated QuikSolution™ reagent and to ensure the highest transformation efficiencies possible for bacterial transformation using the XL10-Gold ultra competent cells. The transformation efficiency of XL10-Gold cells is 5-fold higher than the transformation efficiency of XL1-Blue cells employed in the original QuikChange kit. Moreover, XL10-Gold cells contain the Hte phenotype, which increases the transformation efficiency of larger DNA plasmids (Greener *et al.*, 1997).

Table 2.6 – Mutagenic oligonucleotide primers for site directed-mutagenesis using the pGEMCaf1 as template.

Primer	Nucleotide sequence (5′ to 3′)
DS**RGDS**FD Forward (Caf1RGDS L1)	ATTGGCAAGGATTCTAGAGGTGATTCCTTTGATATCTCTCCTAAG
DS**RGDS**FD Reverse (Caf1RGDS L1)	CTTAGGAGAGATATCAAAGGAATCACCTCTAGAATCCTTGCCAAT
DA**RGDS**PM Forward (Caf1RGDS L2)	TAACTTTACAGATGCCAGGGGTGATAGCCCCATGTACTTAACAT
DA**RGDS**PM Reverse (Caf1RGDS L2)	ATGTTAAGTACATGGGGCTATCACCCCTGGCATCTGTAAAGTTA
EN**RGDS**VV Forward (Caf1RGDS L3)	ACGGTGAGAACCTTCGTGGGGATTCCGTCGTCTTGGCTAC
EN**RGDS**VVReverse (Caf1RGDS L3)	GTAGCCAAGACGACGGAATCCCCACGAAGGTTCTCACCGT
IG**RGDS**GN Forward (Caf1RGDS L4)	CTCCAATTACAATTGGTCGTGGTGACTCTGGAAACATCGATAC
IG**RGDS**GN Reverse (Caf1RGDS L4)	GTATCGATGTTTCCAGAGTCACCACGACCAATTGTAATTGGAG
TS**RGDS**NH Forward (Caf1RGDS L5)	ACTTAACATTTACTTCTCGAGGAGATTCAAACCACCAATTCACTAC
TS**RGDS**NH Reverse (Caf1RGDS L5)	GTAGTGAATTGGTGGTTTGAATCTCCTCGAGAAGTAAATGTTAAGT
G35C Forward (Caf1G35C L4)	ACAATTATGGACAATTGTAACATCGATACAGAA
G35C Reverse (Caf1G35C L4)	TTCTGTATCGATGTTACAATTGTCCATAATTGT
G79C Forward (Caf1G79C L5)	ACATTTACTTCTCAGGATTGTAATAACCACCAATTCACT
G79C Reverse (Caf1G79C L5)	AGTGAATTGGTGGTTATTACAATCCTGAGAAGTAAATGT
R94C Forward (Caf1R94C L1)	ATTGGCAAGGATTCTTGTGATTTTGATATCTCT
R94C Reverse (Caf1R94C L1)	AGAGATATCAAAATCACAAGAATCCTTGCCAAT
TS**RGES**NH Forward (Caf1RGES L5)	ACTTAACATTTACTTCTCGAGGAGAATCAAACCACCAATTCA
TS**RGES**NH Reverse (Caf1RGES L5)	GTAGTGAATTGGTGGTTTGATTCTCCTCGAGAAGTAAATGTTAAGT

Quikchange XL Site-directed mutagenesis (Stratagene, UK) method was used to prepare the control reaction and sample reactions as indicated below (**Table 2.7**). All

the components were included in the Quikchange XL site-directed mutagenesis kit with the exception of the dsDNA template (pAH34L plasmid encoding *caf* operon).

Table 2.7 – PCR Reaction components.

Components	**Volume (µL)**
10x reaction buffer with $MgSO_4$ (200mM Tris-HCl (pH 8.8 at 25 °C), 100mM KCl, 100mM $(NH_4)_2SO_4$, 20mM $MgSO_4$, 1.0% Triton X-100 and 1mg/ml nuclease-free BSA)	5
dsDNA template 10 ng/µl (pAH34L plasmid encoding *caf* operon)	2
Forward primer (1 pmole/µl)	1.25
Reverse primer (1 pmole/µl)	1.25
dNTP mixture (200 µM)	1
Quick solution	3
Nuclease-free sterile water	36.5
PfuUltra High Fidelity DNA polymerase (2.5 U/µL)	1
Total volume	50

Each reaction used the cycling parameters outlined in **Table 2.8.**

Table 2.8 – Cycling parameters for the Quikchange XL method.

Segment	**Cycles**	**Temperature (ºC)**	**Time**
Polymerase activation	1	95	1 min
Denaturation	18	95	50 s
Annealing		60	50 s
Extension		68	8.5 min

The amplification products were digested with 1 µL *DpnI* enzyme (10 U/µL), provided with the site directed-mutagenesis Quikchange XL kit, for 1 hour at 37 ºC to digest the parental (i.e., the non-mutated and methylated) supercoiled dsDNA.

XL10 Gold chemically ultracompetent *E.coli* cells (Stratagene, UK) were transformed as described above using two microliters of DpnI-treated DNA. The reactions were incubated at 37 ºC for 1 hour with shaking at 225-250 rpm and 100 µl of each transformation reaction was plated on LB plates containing ampicillin/IPTG/X-Gal and incubated overnight at 37 ºC.

A single colony was picked from each successful transformation and sent to sequencing to be analysed by Agencourt Bioscience and Cogenics (UK) as described above, using pUC/M13 Reverse Primer.

Bacterial strains and fermentation

The plasmid DNA from (DH5α/ pGEMCaf1-WT, DH5α/ pGEMCaf1-RGDS Loop 1, DH5α/ pGEMCaf1-RGDS Loop 2, DH5α/ pGEMCaf1- RGDS Loop 3, DH5α/ pGEMCaf1-RGDS Loop 4, DH5α/ pGEMCaf1-Loop 5) was used to transform the BL21/(DE3) chemically competent *E. coli* cells.

Small-scale protein expression and characterization

The LB broth supplemented with 100 μg/ml of ampicillin was used for culturing *E. coli* BL21(DE3) containing the plasmids pGEMCaf1, pGEMCaf1 RGDS L1, pGEMCaf1 RGDS L2, pGEMCaf1 RGDS L3, pGEMCaf1 RGDS L4, pGEMCaf1 RGDS L5 and as a negative control pUC19; 250 ml flasks containing 50 ml of growth medium were inoculated with a single colony from a freshly spread plate of transformed BL21(DE3) and incubated at 37 ºC with 180 rpm shaking for 4 h. After this incubation time, the optical density at 600 nm was measured and a measured volume of each preparation was inoculated into glass test tubes containing 5 ml of LB broth, 100 μg/ml of ampicillin to achieve the same optical density (0.2 at 600 nm). These were incubated at 180 rpm for 16 h at 37 ºC. The following day, the bacterial cell culture was transferred to a 15 ml Falcon tube under aseptic conditions. The Falcon tubes were centrifuged at 3000 rpm for 15 min at 4 ºC. Pictures of all Falcon tubes were taken using a camera. The sizes of the pellet and flocculent layer were immediately measured using a ruler. Excess of LB media, (approximately 4 ml) was carefully taken out of each Falcon tube using a pipette. The flocculent layer, with the remaining LB, was carefully separated from the cell pellet. The cell pellet was resuspended in 1 ml of LB. Twenty microliters of each sample was taken and Novex® Tricine SDS sample buffer (2X) was added to each sample. Samples were heated at 95 ºC for 5 min and loaded onto a Tricine-SDS-PAGE gel (Schaegger, 2006). The molecular weight marker used was the Precision Plus. The gels were run for approximately 4 h at 200 V (constant voltage). One of the gels was stained with Coomassie Brilliant Blue and the other gel was used to perform a western blot as follows: the nitrocellulose membrane (BA85 Protran, 0.45 μm, 7 x 8.5 cm) from Whatman was cut to gel size and wetted in Towbin transfer buffer, Tween-Tris-buffered saline (TTBS) pH 8.5 (25mM Tris, 192 mM glycine, 20% methanol, pH 8.3). Protein bands were transferred from SDS-PAGE to nitrocelluolose

membrane using the Trans-Blot Semi-Dry cell (Bio-RAD). For that a gel sandwich was prepared as follows: a pre-wet extra thick blot paper (7 x 8.4 cm) (BIO-RAD) was embedded in TTBS pH 8.5 and placed on anode metal plate, then a pre-wet nitrocellulose membrane was placed on top of it, followed by the equilibrated SDS-PAGE and finally the pre-wet filter paper embedded in TTBS pH 8.5. The blot was run at 15V for 30 min. The nitrocellulose membrane was placed in TTBS pH 8.5 + 5% skimmed dry milk on a gel shaker for 30 min at room temperature. This blocks all areas of nitrocellulose membrane that do not have any protein bound to it. The membrane was rinsed in TTBS. The membrane was incubated with mouse anti-Caf1 monoclonal antibody (YPF19) from Thermo scientific (UK) diluted 1:500 with TTBS and incubated overnight at 4 ºC. The membrane was rinsed three times, each time for 5 min in TTBS at room temperature. The membrane was incubated with secondary antibody; goat anti-mouse IgG, horseradish peroxidase conjugate diluted 1:1000 in TTBS for 45 min at room temperature. The membrane was rinsed three times, each time for 5 min in TTBS at room temperature. Bound antibody was detected using 4CN (4-chloro-1-naphthol) substrate. The resulting blot was scanned and then analysed by the ImageJ software in order to quantify the bands presented on the blot. Three independent experiments with two replicates each were carried out.

Large-scale protein expression

One litre and half of LB containing 2 drops of anti-foam, was autoclaved in the fermentor´s glass vessel (Minifor) and left to cool down for one day. The overnight cultures were prepared as follows: two 250 ml flasks, each containing 50 ml of LB media with 100 μg/ml of ampicillin were inoculated with a single colony of *E. coli* BL21(DE3)/pGEMCaf1 from a freshly spread plate. The cultures were incubated at 37 ºC with 180 rpm shaking for 16 h. The temperature and the initial agitation of the fermentor containing the LB media were set to 37 ºC and 400 rpm, respectively. The overnight cultures in 15 ml Falcon tubes (BD Bioscience) were centrifuged at 3000 rpm for 10 min at 4 ºC. The supernatant containing β-lactamase was discarded and the pellet was resuspended in 5 ml of sterile LB media. This part of the *work* was done close to *the Bunsen burner* flame. To the 1.5 L of LB media in the fermentor´s vessel, 10 ml of 60% Glycerol, 1 ml of 0.5 M $MgSO_4$, 100 μg/ml of ampicillin and 5 ml of overnight

culture were added. The fermentation was started and the bacterial cells left to grow for approximately 8 h until its optical density had reached 10 at 600 nm.

Sub-Cellular fractionations

The overnight cultures were prepared as follows: two 250 ml flasks, each containing 50 ml of LB media with 100 μg/ml of ampicillin were inoculated with a single colony of *E. coli* BL21(DE3)/pGEMCaf1WT, RGDS L1, L2, L3, L4, L5 and RGES L5 from a freshly spread plates. The cultures were incubated at 37 ºC with 180 rpm shaking for 16 h. The overnight cultures in 15 ml Falcon tubes (BD Bioscience) were centrifuged at 3000 rpm for 10 min at 4 ºC.

Cell pellets from 50 ml of culture were washed twice in PBS and resuspended in 10 ml of cold spheroplast buffer (50 mM Tris, pH 8.0, 18% (w/v) sucrose, 1 mM $CaCl_2$, 0.5 mM EDTA and 0.5 μg/ml lysozyme). After 20 min incubation on ice, the cells were spun at 10,000 rpm, using the JA-20 rotor, fixed angle (Beckman) for 15 min at 4 °C.

The supernatant (periplasmic fraction) was stored at -20 ºC. The pellet was resuspended in 5 ml of TE buffer (50 mM Tris, pH 8.0, 2.5 mM EDTA) buffer and sonicated for 5 min. The lysate was centrifuged at 10,000 rpm for 4 min at 4 ºC. The pellet, mainly containing unbroken cells was resuspended in 500 μl of SDS lysis buffer. The supernatant was centrifuged at 15,000 x g for 40 min at 4 ºC and the supernatant (cytoplasmic fraction) was stored at -20 ºC. The pellet was resuspended in 3 ml of TE buffer with 2% sarkosyl (N-lauryl-sarkosine), incubated at 25 ºC for 20 min and ultracentrifuged at 50,000 rpm, using a fixed angle 50 Ti rotor, (Beckman) for 40 min at 4 ºC. The supernatant (inner membrane fraction) was collected and stored at -20 ºC and the pellet was resuspended in 500 μl SDS lysis buffer (outer membrane fraction). The sub-cellular fractions were run on SDS-PAGE and western blotted as described in the "Small-scale protein expression and characterization" section.

Analysis of Caf1 cysteine mutants

E. coli BL21(DE3)/pGEMCaf1G79C L5, BL21(DE3)/pGEMCaf1G35C L4, BL21(DE3)/pGEMCaf1R94C L1 cells were grown in 50 ml of LB media as described in the "Small-scale protein expression and characterization" section.

Cell pellets from 50 ml of culture were washed twice in PBS and resuspended in an equal volume of cold spheroplast buffer (50 mM Tris, pH 8.0, 18% sucrose, 1 mM Cacl2, 0.5 mM EDTA and 0.5 μg/ml lysosyme). After 20 min incubation on ice, the cells were spun at 10,000 rpm for 15 min at 4 °C. The supernatant (periplasmic fraction) was stored at -20 ºC. The Caf1 pellet of each mutant was resuspended in 1 ml of LB media. For each Caf1 cysteine mutant, 10 μl of cell pellet, resuspended in LB media, and supernatant were heated in the presence of SDS-sample buffer at 95 ºC for 5 min. The periplasmic fractions were made in duplicate, for each Caf1 mutant sample and in one of the tubes was added 1 mM of DTT. In both of the tubes containing the periplasmic fraction SDS-sample buffer was added and the samples were heated at 95 ºC for 5 min. Samples were loaded onto a precast 4-20% gradient polyacrylamide electrophoresis gel (Invitrogen, UK) and western blotted as in the "Small-scale protein expression and characterization" section.

Analysis of ammonium sulphate fractionation

E. coli BL21(DE3)/pGEMCaf1WT cells were grown in 50 ml of LB media as described before. Cell culture was centrifuged at 14000 x g for 45 min at 4 ºC. The supernatant was discarded and the cell pellet and flocculent layer were resuspended in 100 ml phosphate-buffered saline (PBS) pH 7.6 and incubated with gentle rolling at room temperature for 30 min. The resuspension was centrifuged at 14000 x g for 30 min and the supernatant was divided into four groups and each group of 100 ml sample was adjusted to 25, 30, 40 and 50% ammonium sulphate saturation, using solid ammonium sulphate. After stirring for 1 h, the fractionate was centrifuged at 14000 x g for 30 min at 4 ºC. The ammonium sulphate pellet was resuspended in PBS pH 7.6 and a 20 μl aliquot of each supernatant and ammonium sulphate pellet preparation was heated in the presence of SDS-sample buffer (2x) at 95 ºC for 5 min. The samples were loaded onto a 12% SDS-PAGE (Laemmli, 1970) and stained with Coomassie Brilliant Blue.

Purification of Caf1 proteins

After fermentation in the 1.5 L fermentor, *E. coli* BL21 (DE3)/ pGEMCaf1 cultures were centrifuged at 14000 x g, using JA-20 rotor (Beckman) for 45 min at 4 ºC.

The cell pellet and flocculent layer were resuspended in 100 ml PBS pH 7.6 and incubated with gentle rolling at room temperature for 30 min. The resuspension was centrifuged at 14000 x g for 30 min and the supernatant was adjusted to 30% ammonium sulphate saturation. After stirring for 1 h, the fractionate was centrifuged at 14000 x g for 30 min at 4 ºC. The ammonium sulphate pellet was resuspended in PBS pH 7.6 and dialysed against 5 L of the same buffer at 4 ºC, overnight.

The dialysed crude extract was centrifuged at 27000 x g to remove insoluble material. Aliquots of 1 ml of the dialysed extract were applied to an FPLC Superdex 200 column that had been previously equilibrated with 50 mM PBS pH 7.6. The Caf1 proteins were eluted with the same buffer at a constant flow rate of 1 ml/min. Peak fractions were collected and analysed for Caf1 by SDS-PAGE and western blotting in the "Small-scale protein expression and characterization" section.

Protein Concentration determination

Protein concentrations in solution were measured using UV-1800 UV Visible spectrophotometer (Shimadzu, Japan) with 1 cm path length quartz cuvette (Hellma, GmbH and Co., Germany). The protein levels were monitored at 280 nm. The concentration of proteins in solution was calculated according to the Beer-Lambert Law:

$A = \varepsilon . c . l$, when

A is the absorbance at 280 nm, ε is the molar extinction coefficient, c is the molar concentration and l is the path length (Ingle and Crouch, 1988).

The molar extinction coefficients and molecular weights of proteins used in this work are shown on **Table 2.9**.

Table 2.9 – Protein parameters such as molar extinction coefficient, molecular weight and number of amino acids are presented.

Protein	Extinction coefficient (M^{-1} cm^{-1})*	Molecular weight (g mol^{-1})*	Number of amino acid residues
Caf1	5960	15563.2	149
Caf1 RGDS L1	5960	15707.3	151
Caf1 RGDS L2	5960	15735.4	150
Caf1 RGDS L3	5960	15592.2	149
Caf1 RGDS L4	5960	15675.3	151
Caf1 RGDS L5	5960	15564.2	149
Caf1 RGES L5	5960	15578.2	149
Caf1 G35C L4	5960	15609.3	149
Caf1 G79C L5	5960	15609.3	149
Caf1 R94C L1	5960	15510.1	149

* The extinction coefficients and molecular weight were calculated from the protein amino acid sequences using the ProtParam tool at http://www.expasy.ch/tools/protparam.html

Preparation of Caf1 oligomers

Ten µL of Caf1 in 50 mM phosphate buffer pH 7.6 at a concentration of 0.3 mg/ml per 1.5 ml Eppendorf tube was added. Samples were boiled at 95 ºC for 0, 45 sec and 5 min. Each sample was placed on ice immediately. After all samples were ready, 10 µL of SDS sample buffer (2x) was added to each sample. Samples were loaded in a 12% SDS-PAGE gel.

Mass spectrometry

Protein samples were sent to "Pinnacle – Proteomics and Biological Mass spectrometry at Newcastle University" to confirm the identity of the protein studied using Peptide Mass Fingerprinting (PMF) procedure. Samples were analysed on a Voyager Maldi and data were analysed by Mascot program.

Transmission Electron Microscopy (TEM)

Protein samples and the negatively stained specimens were prepared as described (Harris, 1997; Soliakov *et al.*, 2010).

Briefly Caf1-WT, Caf1-RGDS L5 and Caf1-RGES L5 protein samples were prepared in distilled water to a final concentration of 50 μg/ml. Ten microliters of sample droplet was applied to an electron microscope grid (400 meshes) with thin carbon support film for 10–20 s and drained using a filter paper. Buffer and salts were washed three times using 20 μl droplets of water each time (Harris, 1997). The remaining protein adsorbed onto the carbon film was negatively stained by adding a 20 μl droplet of 2% uranyl acetate solution. The excess of uranyl acetate stain was drained with a filter paper and the grid was allowed to air dry. The negatively stained specimens were studied in a Philips CM100 transmission electron microscope operated at 100 kV. Electron micrographs were recorded and saved as TIFF format. The general magnification used was ×130 000. Image analysis was conducted by Jmicrovision 1.2.5 (Roduit, 1997). Fifty-two images of each specimen (Caf1-WT, Caf1-RGDS L5, Caf1-RGES L5) were analysed. The toolbox of the Jmicrovision 1.2.5 allowed drawing a line along the Caf1 fibres, which give us the value of the length in pixels. The length of each fibre was determined in pixels and converted by using the following equation (Soliakov *et al*., 2010):

$$nanometers = \frac{\text{pixel length (obtained)} \times scale\ bar\ length\ (nm)}{\text{pixel length of the scale bar}}$$

The fibre lengths obtained were used to construct a box charts by OriginPro version 8 software. Using the SPSS version 19 software, the one-way analysis of variance (ANOVA) was conducted. Followed by multiple comparisons with the significance level set at $\alpha = 0.05$. All data reported are means ± standard error.

Circular Dichroism Far –UV, Far-UV thermal analysis and Near U.V

Circular dichroism Far-UV and Near-UV measurements of Caf1 were conducted using JASCO-810 spectropolarimeter (Jasco, Japan). Far-UV thermal denaturation circular dichroism measurements were performed using JASCO with Peltier temperature controller capable of varying temperature over 20-95 ºC range (Jasco, Japan)

For Far-UV CD, Caf1 samples were diluted to approximately 0.5 mg/ml in 50 mM phosphate buffer, pH 7.2 and a 0.5 mm-path-length round cuvette (Hellma, GmbH & Co., Germany) was used. CD spectra were recorded at a scanning speed of 20 nm min $^{-1}$ with 10 accumulative scans at 20 ºC using Spectra Manager software, version 1.53 (Jasco).

For Far-UV thermal analysis, Caf1 samples were diluted to approximately 0.1 mg/ml in 50 mM phosphate buffer, pH 7.2 and analysed in a 1-mm quartz-Suprasil rectangular capped cuvette (Hellma, GmbH & Co., Germany) at 202 nm over a gradient of increasing temperature (1 ºC/min). The CD spectra changed very little between 5 and 30 ºC; thus 30 ºC was used in the normalization procedure as fully folded, and 95 ºC was normalized as fully unfolded. The thermal melt data were processed using Spectra Manger software, version 1.53 (JASCO). Data were normalised using the following equation:

$$Xnew = \frac{X - Xmin}{\mathrm{Xmax} - \mathrm{Xmin}}$$

X is the value obtained for the Caf1 fraction folded, Xmin is the minimum value obtained for the Caf1 folded fraction, Xmax is the maximum value for the Caf1 folded fraction.

For Near-UV, Caf1 samples were diluted to approximately 0.5 mg/ml in 50 mM phosphate buffer, pH 7.2 and a 1cm-path-length cuvette (Hellma, GmbH & Co., Germany)

Processing of spectra included subtracting the buffer spectrum from the sample spectrum and converting concentration dependent units of [mdeg] into standard units of $\Delta\varepsilon$ (M^{-1} cm^{-1}); mean residue and molar protein concentration were used in far-UV and

near-UV CD calculations respectively. The mean residue weight (MRW) is given by the following equation:

$$MRW = \frac{Protein\ molecular\ weight\ (kDa)}{\text{Number of amino acid residues per molecule}}$$

Differential scanning calorimetry (DSC)

Differential scanning calorimetry measurements were performed using a VP-DSC microcalorimeter (MicroCal, UK) (Cell volume of 0.52 ml). All samples were de-gassed for 5 min in a ThermoVac unit (MicroCal, UK) prior to analysis. Caf1 samples were scanned with a scan rate of 1 ºC/min, and a filtering period of 16 seconds with 0.30 mg/ml of protein in the sample cell and an appropriate buffer in the reference cell. The DSC data were processed in the MicroCal Origin software V.8. Processing of data included subtracting reference scans from sample scans and adjusting the baseline.

Fast Protein Liquid Chromatography (FPLC) analysis

Aliquots of 5 ml were loaded onto an FPLC Superdex 200 gel filtration column GE healthcare pre-equilibrated with PBS pH 7.6 at a flow rate of 1 ml/min.

Molecular weight markers were loaded to determine the approximate molecular weight of Caf1 samples. These included carbonic anhydrase from bovine erythrocytes (29 kDa); Albumin, bovine serum (66 kDa); Alcohol dehydrogenase from yeast (150 kDa); β-Amylase from sweet potato (200 kDa); Aproferritin from horse spleen (443 kDa); Thyroglobulin, bovine (669 kDa). The void volume of the column was determined using Blue dextran (2,000 kDa).

2.3. Studies to Investigate the Mammalian Cell Responses to Biomimetic Protein Scaffolds

Preparation of surfaces coated with Caf1 proteins

The protein used in this study was Caf1-RGDS. Caf1-WT and Caf1-RGES were used as negative control peptides. Fibronectin, collagen IV were used as positive control peptides. Non-coating wells were also used as controls. Proteins were diluted in PBS pH

7.4 to obtain the desired concentration of 50 μg/ml. In the class II cabinet the protein solutions were filtered using a Nalgene 0.22 μm syringe filter. Fifty μl of protein solution were pipetted into each well of a 96-well plate using a multi-channel pipette. The plates were sealed with Parafilm and placed on the rocking platform at 4 ºC, overnight. The remaining protein solution was aspirated from the wells of the plates and each well was washed once with PBS pH 7.4. The PBS was removed just prior to adding the cells to prevent the proteins from drying out.

Cell Culture

The rat pheocytochrome cell line PC-12 and mouse 3T3 Fibroblasts were obtained from ATCC (American Type Culture Collection), and were preserved in Roswell Park Memorial Institute (RPMI)-1640 medium and Dulbecco's Modified Eagle Medium (DMEM) supplemented with 20% fetal bovine serum. The rat primary osteoblast cell line was kindly provided by Dr. Mark Birch, and was grown in DMEM supplemented with 10% fetal bovine serum, 50 μg/ml streptomycin and 50 U/ml penicillin. Cells were used between passage 3 and 6 in the case of rat primary osteoblast cells; and passage 27 and 31 in the case of PC12 cell and passage 155 in the case of 3T3 Fibroblasts. Cells were incubated at 37 °C in a 5% CO_2 environment.

Attachment of cells to surfaces coated with peptides

Cells were harvested using 0.05% trypsin-Ethylenediamine tetraacetic acid (EDTA) (1x) solution containing phenol red for detachment and centrifuged at 1000 rpm for 5 min. The cell pellet was resuspended in PBS pH 7.4 without calcium and magnesium and centrifuged at 1000 rpm for 5 min. This wash step was repeated once again in order to remove completely the serum. The washed cell pellet was resuspended in the cell culture medium. Cells were counted using a hemocytometer. Cell suspension was diluted in cell culture medium to a final concentration of $2.5x10^5$cells/ml. One hundred μL of prepared cells suspension was added to each well of 96-well plates. The plate was placed in the incubator at 37 ºC, 5% CO_2 for 4 h. After 4 h of incubation the cells which did not attach were carefully aspirated from the wells of the plates and 100 μl of cell culture medium containing serum was added to each well. The plates for 4 h cell culture adhesion study were reserved for the next procedure described on section 2.3. After changing the cell culture medium, the plates were placed in the incubator for

24 h at 37 ºC, 5% CO_2. Three independent experiments with two replicates each were carried out.

Proliferation of cells on surfaces coated with peptides

The same procedure described in the "Attachment of cells to surfaces coated with peptides" section was applied for the proliferation of cells on surfaces coated with peptides with the difference being that the total incubation time was 48 h. Three independent experiments with two replicates each were carried out.

Calcein AM Assay of cultures grown on peptide-modified surfaces

Cell attachment was conducted exactly as described above. This assay was performed for the same incubation times: 4, 24 and 48 h. At the end of each incubation time, the cell culture medium was carefully removed and each well of the 96-well plates (4ti-0221 - black, clear bottom, sterile, tissue culture treated) (4titude, UK) was washed once with 100 µl of PBS pH 7.4.

One Hundred µL of 1 µM calcein-AM solution in PBS pH 7.4 with calcium and magnesium was added to each well. The plates were incubated for 30 min and the fluorescence was measured at an excitation wavelength of 485 nm and an emission wavelength of 520 nm using the BMG FLUOstar OPTIMA. To correct the background, the mean value for the background insert wells was determined and subtracted from each remaining value. Three independent experiments with two replicates each were carried out.

Scanning electron microscopy

Glass round coverslips (12 mm diameter) were washed with 1% Hellmanex for 10 min and rinsed three times in *Milli-Q* water (18.2 MΩ) prepared by a *Milli-Q* Plus system (Millipore, Bedford, USA). The coverslips were placed in a Falcon tube containing absolute ethanol until needed. In the fume hood, prior to adding the proteins the coverslips were placed into 4 well-plates (Nunc), the plates were labelled with the name of the proteins. The protein solutions in PBS were filtered as mentioned above and 500 µl of each protein solution was applied to the corresponding well of the plate.

The plates were placed on a rocking platform at 4 ºC, overnight. The protocol described above was used for cell harvesting and attachment. With only one modification, the number of cells added to each well was adjusted according to the area of the wells. For this experiment 5×10^4 cells/ml were added into the wells of the plates. After 24 h incubation, the medium was aspirated and the cell culture carefully washed once with PBS pH 7.4. The samples were fixed in 2% glutaraldehyde in PBS pH 7.4 at room temperature for 30 min. After fixation, the fixative was aspirated into a waste container for disposal. The samples were washed twice for 2 min in 1 ml PBS pH 7.4 to remove excess fixative, and the waste liquid was discarded. For the dehydration process, 1 ml of 25% ethanol was added into each well and incubated for 15 min at room temperature. The ethanol was aspirated and discarded. The last step was repeated using increasing concentrations of ethanol: 50 %, 75 %, 100 % and finally absolute ethanol. Once in absolute ethanol, the drying process was conducted using a Baltec Critical Point dryer. The sample was mounted on an aluminium stub with carbon discs.

The samples were coated with 15 nm of gold using a Polaron SEM coating unit (Electron Microscopy Research Services). The gold coating increases the sample's conductivity and consequently improves image quality. The samples were then ready for imaging using a conventional Cambridge Stereoscan 360 scanning electron microscope.

Immunocytochemistry

Immunocytochemistry was performed on 96-well plates (4ti-0221) (4titute, UK). All the volumes mentioned below are referred to volume per well of the 96-well plate. Cultured cells were fixed with 4% paraformaldehyde in PBS pH 7.4 for 20 min at room temperature and washed twice with 100 µl of PBS pH 7.4 containing 0.05% Tween-20.

Cells were permeabilised with 100 µl of 0.1% Triton X-100 in 1x PBS for 5 min at room temperature. Then, they were washed twice with 100 µl of PBS pH 7.4 containing 0.05% Tween-20. A volume of 100µl of blocking solution - 1% BSA in PBS pH 7.4 was applied for 30 min at room temperature. The mouse primary monoclonal antibody (Anti-Vinculin) (ab18058, Abcam, UK) was diluted 1:100 in blocking solution and incubated for 1 hour at room temperature. Each well was washed three times (5 min each) with 1x PBS containing 0.05% Tween-20. The anti-mouse secondary antibody

(FITC-conjugated) (Abcam) was diluted 1:100 in PBS pH 7.4 just before use. For double labelling Rhodamine-conjugated Phalloidin was diluted 1:500 in PBS pH 7.4 and incubated simultaneously with the secondary antibody for 45 min at room temperature. Each well was washed three times (5 min each) with 1x PBS containing 0.05% Tween-20. Following this washing step, nuclei counterstaining were performed by incubating cells with DAPI diluted 1:1000 in 1x PBS for 5 min at room temperature, followed by washing cells three times (5 min each) with 1x PBS containing 0.05% Tween-20. Cells were covered with 100 µl of PBS pH 7.4 prior to visualization to prevent cells from drying out. The plates were scanned using the Cellomics ArrayScan VTI image reader at the Centre of Excellence in Biopharmaceuticals (COEBP) by Dr. Egor Zindy.

Competitive Assays using the soluble CycloRGDfc peptide

Cells were harvested using 0.05% trypsin-EDTA (1x) solution containing phenol red for detachment and centrifuged in 15 ml Falcon tube (BD Biosciences) at 1000 rpm for 5 min. The cell pellet was resuspended in PBS pH 7.4 without calcium and magnesium and centrifuged at 1000 rpm for 5 min. This wash step was repeated once again in order to completely remove the serum. The washed cell pellet was re-suspended in a suitable cell culture medium. Cell suspension was diluted in cell culture medium to a final concentration of $2.5x10^6$ cells/ml.

Cells were incubated with CycloRGDfc peptides (ANASPEC, U.S supplied by Cambridge Biosciences, UK) at a final concentration of 7 µM for 1 hour at 37 ºC. One hundred µL of treated cell suspension was added to each well of 96-well plates (4ti-0221- 4titute, UK) coated with Caf1 proteins and positive controls: fibronectin and collagen IV. As a negative control some wells of the plate were not coated, as described in the "Preparation of surfaces coated with Caf1 proteins" section. The plate was placed in an incubator at 37 ºC, 5% CO_2 for 4, 24 and 48 h.

Quantitation of cell shape and cell-ECM contact areas (cell focal adhesions).

Image processing was conducted by the Arrayscan software – Cellomics® Morphology Explorer BioApplication V3 version. This bio-application can record multiple parameters simultaneously down to individual tracked cells at 37 ºC. In this

study the morphological parameters used were the following: "Object counts", to determine the cell number; "object area and shape", to determine the cell area and shape; "morphology of discrete objects" such as spots or fibres to determine the number and area of cell focal adhesions. The images were analysed by Arrayscan software (Thermo-fisher) at the Centre of Excellence in Biopharmaceuticals (COEBP) by Dr. Egor Zindy.

Statistical analysis

Statistical analyses including principal component analysis were performed using SPSS (version 19 for Windows). A one-way analysis of variance (ANOVA) was used to analyze the number of cells which adhere on different surfaces. Followed by multiple comparisons with the significance level set at $\alpha = 0.05$. All data reported are means ± standard error.

2.4. Advanced Use of Caf1 Polymer

Co-expression of Caf1 using the vector pBAD33 and pAH34L

The pBAD33 vector (Guzman *et al.*, 1995) (**Table 2.3**) was the kind gift of Florian Szardenings from Kenn Gerdes' laboratory Newcastle UK. The pBAD33 plasmid was sent to GeneArt and the *Caf1* gene (528 bp in size; GenBank, accession number AY450847) was synthesised and cloned into pBAD33 vector between *KpnI* and *XbaI* restriction sites; followed by two stop codons. This created a plasmid suitable for future gene synthesis mutagenesis by GeneArt. The pAH34L containing the *caf* operon was created by Miller et al. 1998 (**Figure 2.4**).

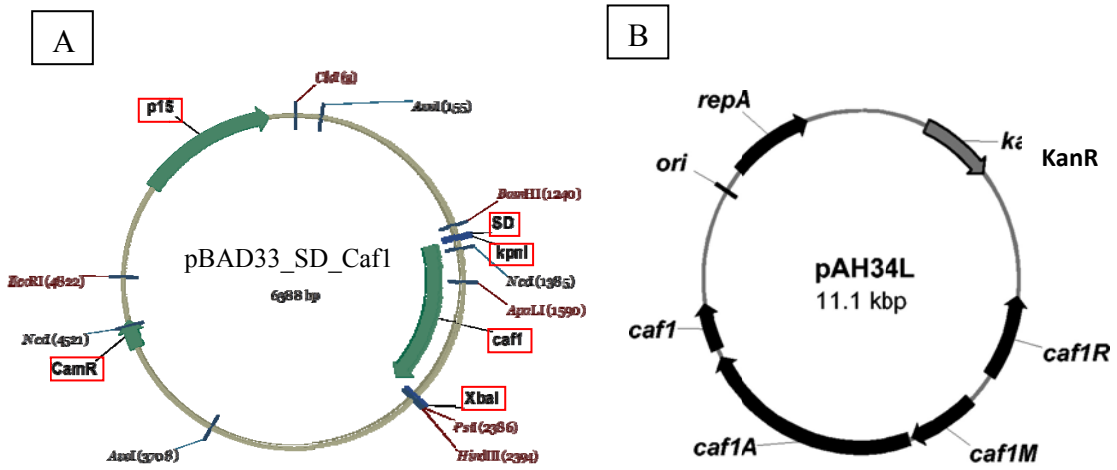

Figure 2.4 – Genetic map of pBAD33_SD_Caf1 and pAH34L. (A) pBAD33_SD_Caf1 vector map. The main components in these vectors are inserted into red boxes. P15, origin of replication; CamR, Chloramphenicol resistance gene; SD, Shine-Dalgarno sequence; restriction sites: kpnI and XbaI; Caf1, *Caf1* gene. **(B) pAH34L (Miller *et al.*, 1998) vector map**. pBR322, origin of replication; KanR, Kanamycin resistance gene; *caf* operon composed of: *Caf1R, Caf1M, Caf1A* and *Caf1* genes, with its own promoter region and ribosomal binding site was inserted into the pAHL vector called pAH34L vector.

As the pBAD33 does not contain a ribosomal binding site (Shine-Dalgarno sequence), a six-base consensus sequence, AGGAGG was inserted 8 base pairs upstream of the start codon AUG using the set of primers presented in **Table 2.10** in a Quikchange site-directed mutagenesis reaction (**Table 2.11 and 2.12**) The resulting plasmid was named pBAD33-SD.

Table 2.10 – Oligonucleotide primers to introduce a Shine-Dalgarno sequence into the pBAD33 vector.

Primer	Nucleotide sequence (5′ to 3′)
pBAD33_SD Forward	GGGCTAGCGAATAGGAGGTCGGTACCATGAAAAAAATCAGC
pBAD33_SD Reverse	GCTGATTTTTTTCATGGTACCGACCTCCTATTCGCTAGCCC

Quikchange site-directed mutagenesis reaction (Stratagene, UK) method was used to prepare the control reaction and sample reactions as indicated below (**Table 2.11**). All the components were from the Quikchange site-directed mutagenesis kit with the exception of the ds DNA template (pBAD33 plasmid encoding *Caf1* gene).

Table 2.11 – PCR Reaction setup.

Components	**Volume (µL)**
10x reaction buffer with $MgSO_4$ provided (200mM Tris-HCl (pH 8.8 at 25 °C), 100mM KCl,100mM $(NH_4)_2SO_4$, 20mM $MgSO_4$, 1.0% Triton X-100 and 1mg/ml nuclease-free BSA)	5
ds DNA template 10 ng/µl (pBAD33 plasmid encoding *Caf1* gene)	2
Forward primer (1 pmole/µl)	1.25
Reverse primer (1 pmole/µl)	1.25
dNTP mixture provided (200 µM)	1
Quik solution	3
Nuclease-free water	36.5
*pfu*Turbo DNA polymerase (2.50 U/µL)	1
Total volume	50

Each reaction was performed using the cycling parameters outlined in **Table 2.12.**

Table 2.12 – Cycling parameters for the Quikchange site-directed mutagenesis (Stratagene, UK).

Segment	**Cycles**	**Temperature (ºC)**	**Time**
Polymerase activation	1	95	1 min
Denature	18	95	50 s
Annealing		60	50 s
Extension		68	8.5 min

Mach1-T1^R chemically competent cells (see on **Table 2.5**) were transformed as described before. For one transformant from each construct, the complete sequence of the mutated Caf1 was confirmed (Beckman Coulter Genomics - Formerly Agencourt Bioscience and Cogenics, UK).

Plasmid DNA and Bacterial strains

Top10 chemically competent *E. coli* were transformed with the plasmid DNA of pBAD33_SD_Caf1 (pBAD33 containing the Shine–Dalgarno sequence (SD) and *Caf1 gene*) (Cm^R; low-copy plasmid; pACYC184-origin of replication) obtained from GeneArt or pAH34L (Kan^R; low-copy plasmid; ColE1-origin of replication) and both pBAD33_SD_Caf1 (Cm^R) + pAH34L (Kan^R) (**Table 2.3**). Transformed cells were grown on L-agar plates supplemented with 20 μg/ml of chloramphenicol, 100 μg/ml of ampicillin and both antibiotics, 20 μg/ml of chloramphenicol and100 μg/ml of ampicillin, respectively.

Small-scale Caf1 protein co-expression

LB broth supplemented with 100 μg/ml of ampicillin or 20 μg/ml of chloramphenicol antibiotics or both was used for culturing *E. coli* TOP10/pBAD33_SD_Caf1, *E. coli* TOP10/pAH34L and *E. coli* TOP10/pBAD33_SD_Caf1 + pAH34L, respectively. Two groups with three glass test tubes each containing 10 ml of LB broth media with the suitable antibiotics and in the presence or absence of 0.2% of D-glucose, were incubated at 37 ºC with 180 rpm shaking until their optical density had reached 0.5-0.6 at 600 nm. Then, 0.002-2 % of L-arabinose was added to the respective tubes. The following day, the bacterial cell culture was transferred to a 15 ml Falcon tube in aseptic conditions. The cultures were centrifuged and analysed by SDS-PAGE and western blot as described before. This experiment was performed in triplicate.

Co-expression of Caf1 mutants using the vector pBAD33 and pAH34L

The *Caf1*gene (528 bp in size; GenBank, accession number AY450847) mutants were synthesised by GeneArt (**Table 2.13**) and cloned into pBAD33 vector between *KpnI* and *XbaI* restriction sites; followed by two stop codons.

Small-scale of Caf1 mutants co-expression

LB broth supplemented with 100 μg/ml of ampicillin or 20 μg/ml of chloramphenicol antibiotics and with both 100 μg/ml of ampicillin and 20 μg/ml of chloramphenicol antibiotics were used to culture *E. coli* TOP10/pBAD33_SD_Caf1mutants, *E. coli* TOP10/pAH34L and *E. coli* TOP10/pBAD33_SD_Caf1mutants + pAH34L, respectively. Two groups with three glass test tubes each containing 10 ml of LB broth media with the required antibiotics were incubated at 37 ºC with 180 rpm shaking until their optical density had reached 0.5-0.6 at 600 nm. After measuring the optical density, 0.2 % of L-arabinose was added in the respective tubes. The following day, the bacterial cell culture was transferred to a 15 ml Falcon tube in aseptic conditions. The cultures were centrifuged and prepared to be analysed by SDS-PAGE and western blot was performed as described in the "Small-scale protein expression and characterization" section. This experiment was made in triplicate.

Table 2.13 – The Caf1 amino acid sequences of genes synthesised by GeneArt in pBAD33.

Caf1	Amino acid sequence
Caf1-6His NT	MKKISSVIAIALFGTIATANAASSHHHHHHDLTASTTATATLVEPARIT LTYKEGAPITIMDNGNIDTELLVGTLTLGGYKTGTTSTSVNFTDAAGD PMYLTFTSQDGNNHQFTTKVIGKDSRDFDISPKVNGENLVGDDVVLA TGSQDFFVRSIGSKGGKLAAGKYTDAVTVTVSNQ
Caf1-6His CT	MKKISSVIAIALFGTIATANAADLTASTTATATLVEPARITLTYKEGAPI TIMDNGNIDTELLVGTLTLGGYKTGTTSTSVNFTDAAGDPMYLTFTSQ DGNNHQFTTKVIGKDSRDFDISPKVNGENLVGDDVVLATGSQDFFVR SIGSKGGKLAAGKYTDAVTVTVSNDGGGSHHHHHH
Caf1-6His NT + Spacer linking peptide	MKKISSVIAIALFGTIATANAASSHHHHHHGGGGSGGGGSDLTASTTA TATLVEPARITLTYKEGAPITIMDNGNIDTELLVGTLTLGGYKTGTTST SVNFTDAAGDPMYLTFTSQDGNNHQFTTKVIGKDSRDFDISPKVNGE NLVGDDVVLATGSQDFFVRSIGSKGGKLAAGKYTDAVTVTVSNQ
Caf1-PHSRN (DSRD) Loop1	MKKISSVIAIALFGTIATANAADLTASTTATATLVEPARITLTYKEGAPI TIMDNGNIDTELLVGTLTLGGYKTGTTSTSVNFTDAAGDPMYLTFTSQ DGNNHQFTTKVIGKPHSRNGGDISPKVNGENLVGDDVVLATGSQDFF VRSIGSKGGKLAAGKYTDAVTVTVSNQ
Caf1_PHSRN (NLVGD) Loop 3	MKKISSVIAIALFGTIATANAADLTASTTATATLVEPARITLTYKEGAPI TIMDNGNIDTELLVGTLTLGGYKTGTTSTSVNFTDAAGDPMYLTFTSQ DGNNHQFTTKVIGKDSRDFDISPKVNGEPHSRNDVVLATGSQDFFVRS IGSKGGKLAAGKYTDAVTVTVSNQ
Caf1_FLAG epitope NT	MKKISSVIAIALFGTIATANAADYKDDDDKDLTASTTATATLVEPARIT LTYKEGAPITIMDNGNIDTELLVGTLTLGGYKTGTTSTSVNFTDAAGD PMYLTFTSQDGNNHQFTTKVIGKDSRDFDISPKVNGENLVGDDVVLA TGSQDFFVRSIGSKGGKLAAGKYTDAVTVTVSNQ
Caf1_Cys NT	MKKISSVIAIALFGTIATANAACDLTASTTATATLVEPARITLTYKEGA PITIMDNGNIDTELLVGTLTLGGYKTGTTSTSVNFTDAAGDPMYLTFTS QDGNNHQFTTKVIGKDSRDFDISPKVNGENLVGDDVVLATGSQDFFV RSIGSKGGKLAAGKYTDAVTVTVSNQ
Caf1_G35C Loop 4	MKKISSVIAIALFGTIATANAADLTASTTATATLVEPARITLTYKEGAPI TIMDNCNIDTELLVGTLTLGGYKTGTTSTSVNFTDAAGDPMYLTFTSQ DGNNHQFTTKVIGKDSRDFDISPKVNGENLVGDDVVLATGSQDFFVR SIGSKGGKLAAGKYTDAVTVTVSNQ
Caf1_Q106C Loop 2	MKKISSVIAIALFGTIATANAADLTASTTATATLVEPARITLTYKEGAPI TIMDNGNIDTELLVGTLTLGGYKTGTTSTSVNFTDAAGDPMYLTFTSC DGNNHQFTTKVIGKDSRDFDISPKVNGENLVGDDVVLATGSQDFFVR SIGSKGGKLAAGKYTDAVTVTVSNQ
Caf1_PENFF-NT	MKKISSVIAIALFGTIATANAAPENFFDLTASTTATATLVEPARITLTYK EGAPITIMDNGNIDTELLVGTLTLGGYKTGTTSTSVNFTDAAGDPMYL TFTSQDGNNHQFTTKVIGKDSRDFDISPKVNGENLVGDDVVLATGSQ DFFVRSIGSKGGKLAAGKYTDAVTVTVSNQ

Preparation of Caf1 hydrogel

The Caf1 protein sample used for the preparation of hydrogels was supplied by Avecia at a concentration of ~ 1 mg/ml in 0.5 mM phosphate buffer, 150 mM NaCl, pH 7.4. The Caf1 protein sample was concentrated in Ultra 15 ml Filters for Protein Purification and Concentration (Merck Millipore) using 10-minute spins at 3000 rpm, 4 ºC to a final concentration of 60 mg/ml (in a final volume of 1 ml). The final concentration of Caf1 in the concentrated sample was measured using a UV-1800 UV visible spectrophotometer (Shimadzu, Japan) with 1 cm path length quartz cuvette (Caf1 extinction coefficient = 5960 M^{-1} cm^{-1}) (Hellma, GmbH and Co., Germany). For this, the sample was diluted 1:1000 in water and the Caf1 concentration determined as mentioned above. The Caf1 protein sample at 60 mg/ml was stored at 4 ºC as a stock solution.

Three cross-linkers were chosen based on their different spacer arms: **(1)** a linear homobifunctional and short spacer arm – 3,3′-Dithiobis[sulfosuccinimidylpropionate] (DTSSP) *(*M.W. 608.51; Spacer arm ~ 12.0 Å) (Fisher Scientific, UK); **(2)** a linear homobifunctional and long spacer arm – O,O′-Bis [2-(N-Succinimidyl-succinylamino)ethyl]polyethylene glycol (NHS-PEG-NHS) (M.W. 10000, Spacer arm ~ 197 Å) (Sigma-Aldrich, UK); **(3)** a long spacer – 4-arm PEG- Succinimidyl Carboxy Methyl ester (4-arm PEG-NHS) (M.W. 20000, Spacer arm ~ 394 Å) (Creative PEGWorks, USA).

The DTSSP, NHS-PEG-NHS and 4-arm PEG-NHS solutions were prepared by dissolving 30 mg of each cross-linker in 1 ml of Milli-Q water. The solution was mixed carefully by vortexing. The Caf1 solution at 60 mg/ml was then cross-linked with various volumes of each cross-linker at 30 mg/ml for final concentrations of 30 mg/ml of Caf1 and 3, 6, 9 and 15 mg/ml of DTSSP, NHS-PEG-NHS and 4-arm PEG-NHS.

The 4-arm PEG-NHS solutions were also prepared by dissolving 2 mg of 4-arm PEG-NHS in 1 ml of Milli-Q water. The Caf1 solution at 60 mg/ml was also cross-linked with various volumes of 4-arm PEG-NHS cross-linker at 2 mg/ml for final concentrations of 10 mg/ml of Caf1 and 1, 10, 100, 500 and 1000 µg /ml of 4-arm PEG-NHS.

Gelation time

The different solutions containing Caf1 protein and different concentrations of cross-linkers reacted in 12 mm x 75 mm round glass test tubes. The glass test tubes containing the solutions were mixed using the vortex mixer in intervals of 1 minute at room temperature. The gelation rate of Caf1 protein cross-linked with the different cross-linkers was monitored under sealed conditions for a total reaction time of 30 min.

During the 30 min the tubes were slightly inverted to observe if the solution slid along the walls of the tube. If this was the case it was considered that the sample did not lose its fluidity (it remained in a liquid state). When tubes were inverted and the solution stopped sliding along the walls it was considered that it had reached the gelation time and thus lost its fluidity. The gelation time was then recorded. If the solution did not pass from a liquid state to a gel state within 30 min at room temperature the gelation time was not determined (N.D). The reaction was stopped by adding quenching buffer to a final concentration of 20 mM Tris pH 7.6.

Degree of cross-linking by SDS-PAGE gel

Ten microliters of each sample were taken and 2x SDS sample buffer were added to each Caf1 protein cross-linked sample. Samples were heated at 95 ºC for 5 min and loaded onto a 4-20% gradient gel. The molecular weight marker used was the Precision plus Protein. The gels were scanned and analysed by Image J version 1.46 to determine the relative density of non-cross-linked and cross-linked Caf1. The experiment was performed in triplicate.

Gel swelling

The solutions containing Caf1 protein and different concentrations of cross-linkers were reacted as above in 12 mm x 75 mm round glass test tubes. The glass test tubes containing the solutions were mixed for 10 seconds at room temperature and immediately, using a pipette, 40 µl drops of each cross-linked solution were placed into a sterile plastic Petri dish (90mm diameter x 13mm deep). After 30 min the reaction was stopped by adding quenching buffer to a final concentration of 20 mM Tris pH 7.6. The water was evaporated from the samples at room temperature for 16 h. After this time,

the initial diameters (D_0) of the dehydrated Caf1 hydrogel drops in the Petri dishes were measured with a ruler and the values recorded. One millilitre of PBS pH 7.4 was added to each dehydrated Caf1 hydrogel drop in the Petri dish and incubated for 18 h at 37 ºC. The excess of PBS was carefully absorbed by using a filter paper (0.45 μm). The final diameter (D_t) of the hydrated Caf1 hydrogel drops was measured.

The following equation was used to determine the diameter change,

$$\text{Diameter change} = \frac{(\text{Dt} - \text{D0})}{\text{D0}} \text{ x100\%}$$

Cytotoxicity and Viability assay

The different solutions containing Caf1 protein and different concentrations of cross-linkers were mixed for 10 seconds at room temperature and, using a pipette, 10 μl of the reaction were immediately transferred to a single well in a 96-well polystyrene plate (Corning, UK) and left to react for 30 min. Caf1 hydrogels were incubated with 1 ml of DMEM medium for 4 h before adding the cells. Rat primary osteoblasts were used to test cell viability and cytotoxicity on the Caf1 hydrogels. Cells were plated at a density of 20,000 per well in Dulbecco´s modified eagles medium and the plate was incubated at 37 ºC, 5% CO_2 for 16 h. The viability/cytotoxicity reagents containing both GF-AFC substrate and bis-AAF-R110 substrate (Promega, UK) mixture were added to the wells of the 96-well plate. The plate containing the cells was incubated at 37 ºC for 2 h. The fluorescence was measured at the following two wavelength sets: 400 nm excitation and 505 nm emission for viability and 485 nm excitation and 520 nm emission for cytotoxicity on a BMG FLUOstar OPTIMA plate reader.

TEM for Caf1 hydrogels

The Caf1 hydrogels were prepared as mentioned above followed by the gelation as described above. To observe the Caf1 hydrogels by TEM, the samples were diluted in distilled water to a final concentration of 50 μg/ml. Protein samples, Caf1 hydrogels cross-linked with 4-arm PEG-NHS at different concentrations of cross-linker and controls such as cpCaf1 (Chalton *et al*., 2006) cross-linked with 4-arm PEG-NHS, 4-arm PEG-NHS and negatively stained specimens were prepared as described (Harris, 1997). The images obtained were analysed by Jmicrovision version 1.2.5 (Roduit, 1997).

SEM for Caf1 hydrogels

Scanning electron microscopy (SEM) was conducted to analyse the morphologies of Caf1 hydrogels. The different solutions containing Caf1 protein mixed with different concentrations of cross-linkers were mixed for 10 seconds at room temperature and, using a pipette, 40 μl of Caf1 hydrogel solution were immediately transferred to a well within a 4-well polystyrene plate containing a clean 12 mm glass coverslip in the bottom. The gelation was conducted for 30 min at room temperature and then the reaction was stopped by adding quenching buffer to a final concentration of 20 mM Tris pH 7.6. One millilitre of PBS pH 7.4 was added in each well containing the Caf1 hydrogels. The plates were incubated at 37 ºC for 18 h. The excess of PBS was absorbed using a filter paper (0.45 μm) and the Caf1 hydrogels were fixed with 2% glutaraldehyde in PBS pH 7.4, dehydrated and gold-coating as mentioned before.

SEM analysis of Caf1 freeze dried hydrogels after gelation were also conducted. After gelation as mentioned above, the Caf1 hydrogels were swelled in PBS at 37 ºC for 2 h, quickly frozen in liquid nitrogen and stored at -20 ºC. After 16 h, hydrogels were freeze-dried in a VirTis Freeze Dryer under vacuum at -50 ºC for 6 h (Freezone 4.5, Labconco, US). Then, the Caf1 hydrogels were immediately placed inside a glass vacuum desiccator until the subsequent mounting and gold coating procedure. During this the freeze-dried hydrogels were fractured to reveal their interior, mounted onto aluminium stubs with double-sided carbon tape, and sputtercoated with gold by the

Electron Microscopy unit services in Newcastle University. The morphology of the hydrogels was examined using the scanning electron microscopy at 8 kV.

Environmental scanning electron microscopy (ESEM) for Caf1 hydrogel

A few trial experiments to image Caf1 hydrogel morphology in its natural state were conducted by ESEM using a XL30 ESEM-FEG microscope (FEI Company Hillsboro, OR), equipped with Peltier elements to control the sample temperature. This service was performed by Dr Pauline Carrick at the School of Chemical Engineering and Advanced Materials (ACMA), Herschel Building, Newcastle University. A small piece of hydrogel was inserted into the microscope chamber and the pressure and temperature were set to 4.6 torr and 1 ºC, respectively, to provide a relative humidity of 100%, using the wet mode. Images were recorded with an accelerating voltage of 10-15 kV.

SEM for mammalian cell attached on Caf1 hydrogel

Mammalian cell adhesion to the Caf1 hydrogels was assessed by SEM. After preparing the gels as mentioned above, Caf1 hydrogels were incubated with 1 ml of DMEM medium for 4 h before adding the cells. Rat primary osteoblasts and mouse 3T3 fibroblasts were plated at a density of 50,000 cells per well in 1 ml of DMEM (containing 20 units/ml of penicillin/streptomycin but without serum) on Caf1 hydrogels and control wells (polystyrene tissue culture treated wells). The plates were placed in the incubator at 37 ºC, 5% CO_2 for 16 h. The medium containing the cells which did not adhere to the Caf1 hydrogels was carefully removed. The procedure for fixation, dehydration and gold coating was performed as mentioned above.

3. Chapter Three: Analysis of Mutation Sites for Caf1 in a Polymeric Form

3.1. Introduction

The structure and function of the capsule-like antigen fraction 1 (Caf1) protein has been introduced in Chapter 1. Caf1 is expressed by *Yersinia pestis* at temperatures of 35-37 ºC producing a gelatinous antiphagocytic capsule which covers the bacterial surface (McIntyre *et al.*, 2004). However, Caf1 is not expressed at temperatures of 26ºC and below as, for example, in the flea gut. The Caf1 capsule is composed of high-molecular weight polymers formed by DSE from a sequence of single Caf1 protein subunits of approximately 15.6 kDa and can grow to extend to twice the diameter of the bacterial cell (Galyov *et al.*, 1990). The capsule is soluble in water being easily detached from the bacterial cell surface and very stable and resistant to proteolysis by trypsin or proteinase K (Zavialov *et al.*, 2005).

Considering some Caf1 characteristics such as resistance to proteolysis (e.g. trypsin), stability, low toxicity and a structure that resembles fibronectin structure, our aim was to investigate the potentiality of Caf1 as a scaffold for cell culture. Nevertheless to achieve this we needed to insert cell adhesion and interaction sites by mutagenesis.

Caf1 was initially cloned and expressed by Miller and co-workers (Miller *et al.*, 1998) from *E. coli* containing the recombinant low-copy plasmid pAH34L, which contains *caf* operon. This plasmid pAH34L was revealed to be an efficient system for Caf1 protein expression. However we found it was not possible to mutate Caf1 in this plasmid, maybe due to its total size (around 11 Kbp) and the lack of convenient restriction sites. For these reasons this plasmid was not suitable for mutagenesis. This study thus initially presents the cloning of *caf* operon into a plasmid used for site-directed mutagenesis.

Expression and mutagenesis of a long fibrous protein from a large plasmid presents some clear difficulties. The large plasmid size is partially due to the 5 Kb operon required to secrete the fully formed fibres form the bacterial surface. Thus, for the correct expression of *Caf1* gene, encoding the Caf1 protein (Galyov *et al.*, 1990) the

participation of three other genes is absolutely necessary: *Caf1m*, *Caf1a* and *Caf1r* encoding the Caf1M protein (molecular periplasmic chaperone of Caf1) (Galyov *et al.*, 1991), Caf1A protein ("anchoring" Caf1 on the surface of the bacteria) (Karlyshev *et al.*, 1992b) and Caf1R protein (transcription regulator) (Karlyshev *et al.*, 1992b) respectively. The four genes form the *caf* operon (Karlyshev *et al.*, 1992b).

The fibrous structure produced by the expression system places particular constraints upon the mutagenesis and purification. Several studies have revealed that there are regions in Caf1 subunit critical for it proper folding and assembly.

The most important regions are in the C-terminus and N-terminus of Caf1. Caf1 is secreted from the cytoplasm to the periplasm through the SEC mechanism in the inner membrane. The proper folding of Caf1 subunits is provided by the interaction between the C-terminus of the Caf1 subunit and the chaperone, Caf1M. The Caf1 subunits are unstable due to its incomplete immunoglobulin-like β-sandwich fold lacking the last C-terminal (G) β-strand and exposing a hydrophobic core which can be complemented by the Caf1M chaperone G1 β-strand. The Caf1:Caf1M complex in the periplasm proceeds to the outer membrane where Caf1 subunits interact with the usher, Caf1A which mediates the export of Caf1 fibres to the outside the bacterial cell. The next Caf1 subunit is transported by another Caf1M just like the previous Caf1 subunit, now linked to the usher, and bound to the Caf1:Caf1A complex through its N-terminus which substitutes the Caf1M chaperone G1 β-strand (Zavyalov *et al.*, 1997). Zavialov and co-workers demonstrated that deletion and point mutagenesis in the N-terminus of Caf1, containing the β-strand motif of alternating hydrophobic and hydrophilic residues essential for polymerization *in vitro,* blocked the assembly of Caf1 subunits into Caf1 fibres (Zavialov *et al.*, 2002). This finding was later supported by the structure of Caf1M-Caf1-Caf1 ternary complex (Zavialov *et al.*, 2003; Zavialov *et al.*, 2005). However, there is a gap in the literature of studies showing the effect of mutations in Caf1 loops on Caf1 secretion and assembly.

To purify Caf1, several studies were conducted which took advantage of the fact that Caf1 is exported to the outside of the bacterial cells. Among them, Miller et al. cultured bacterial cells containing pAH34L encoding the *caf* operon at 37 ºC for 19 h, centrifuged the bacterial cell culture and noticed the presence of a layer on top of the cell pellet called the flocculent layer which contain large amounts of Caf1. The flocculent layer was gently washed in PBS and centrifuged to remove remaining cell

pellet. Then solid ammonium sulphate was added to the supernatant to take the solution to 50% saturation at room temperature followed by centrifugation and the resulting pellet was resuspended in PBS pH 7.6. A final purification step was conducted by size exclusion chromatography (Miller *et al.*, 1998).

Yersinia can benefit from *caf* operon expression via the production of the anti-phagocytic Caf1 capsule at temperatures above 37 ºC (Protsenko *et al.*, 1983). The expression of *Caf1* needs to be regulated with an inducible promoter (in case of *Yersinia caf* operon this is the PCaf1M) which determines what levels of expression of *Caf1* should be transcribed in order to balance between the advantages of Caf1 for *Yersinia* such as the use of Caf1 capsule to assist in infection (Thanassi *et al.*, 1998) and the disadvantage of Caf1 that could function as a protective antigen (Meyer *et al.*, 1974) if large amounts of capsular protein is exposed to the mammalian immune system. An efficient strategy adopted by the pathogen was placing the *caf* operon expression under the tight control of a temperature-sensitive promoter (Galyov *et al*, 1990), in this way the Caf1 and others virulence determinants are only expressed at mammalian body temperature which limits the phagocytosis (Du *et al*., 2002).

Recent findings reinforced the vulnerability of *caf* operon of *Yersinia pestis* (Cao *et al.*, 2012). Cao et al. investigated the effects of overexpression of *caf* operon in wild-type *Salmonella enterica* serovar Typhimurium since it has been shown previously that *caf* operon is functional in *Salmonella* (Yang *et al.*, 2007) thus it is possible to use *Salmonella enterica* serovar Typhimurium strains to analyse *Yersinia* virulence factors. The reason why they did not use *Yersinia pestis* is due to its high pathogenicity and therefore its manipulation can only be conducted in a Biosafety level 3 facility which presents limitations for the work. In this study, PCaf1M in the *Yersinia* native *caf* operon was replaced with a potent constitutive promoter, which increased Caf1 protein yield by 18.8- to 35.2-fold. Their results showed that *Salmonella* was heavily attenuated *in vitro* and *in vivo* through the overexpression of the *caf* operon using the potent constitutive promoter while the expression of the *caf* operon under the regulation of its native promoter almost did not influence the Salmonellae virulence (Cao *et al*., 2012).

Zaviolov et al. showed that the Caf1M chaperone/Caf1A usher pathway responsible for Caf1 assembly could facilitate the secretion of full-length heterologous proteins fused to the Caf1 subunit in *Escherichia coli*. One of the proteins studied was

the human Interleukin 1β which was inserted between the Caf1 signal peptide and the mature Caf1 subunit. Due to the Caf1 signal peptide this heterologous protein crossed the inner membrane to the periplasm where the Caf1M bound specifically to the free C-terminus of the Caf1 subunit inducing the folding of Caf1 and the dissociation of the Caf1 chimera from the inner membrane to the periplasm. Although they suggested that in the presence of Caf1M, the chaperone and Caf1A, the outer membrane protein, the human Interleukin 1β: Caf1 heterologous protein could be detected at the cell surface of *E. coli* no results were shown in this study (Zavialov *et al.*, 2001) or elsewhere.

The Caf1 WT and Caf1 mutants produced in this study were characterised by circular dichroism, differential scanning calorimetry and transmission electron microscopy. A brief description of each of these techniques is provided below.

Circular dichroism (CD) has become a valuable structural technique for measuring proteins or other chiral molecules via the absorption of the left and right circularly polarised light in the ultraviolet spectrum (Kelly *et al.*, 2005). This differential absorption produces a series of absorption bands that can vary in intensity and wavelength. These absorption bands correspond to transition of electrons from the ground state to the excited state that happens due to absorption of light energy. In proteins, the light energy is absorbed by amine bonds of the polypeptide backbone, disulphide bonds of cysteine residues and side chains of aromatic residues. Absorption of light energy by peptide bonds occurs in the far-ultraviolet between 180 nm and 250 nm and involves two types of electronic transitions, the $n \rightarrow \pi^*$ transitions and $\pi \rightarrow \pi^*$ transitions. These electronic transitions are sensitive to the polypeptide backbone conformation and allow us to measure the secondary structure content of the proteins (Fasman, 1996).

Circular dichoism can also be used to study the tertiary structure of proteins. Measurements of the tertiary structure is possible due to sensitivity of $\pi \rightarrow \pi^*$ electronic transitions of side chains of aromatic residues to the local environment. These electronic transitions absorb light energy mainly in the near-ultraviolet between 250 nm and 320 nm, producing for each protein a unique tertiary structure spectrum. In the near ultraviolet circular dichroism, the molar extinction coefficient is based on protein

molarity due the variable contribution of the principal chromophores, the side chains of aromatic residues (Kelly *et al.*, 2005).

Differential scanning calorimetry (DSC) is a thermo-analytical technique, which can provide information about the thermal changes in a biological sample over a defined range of temperature under constant pressure (Dean, 1995). The biological sample and the reference (an appropriate buffer) are introduced in different calorimeter cells and heated at a constant rate, usually at temperatures between 25 and 110 ºC. Both, the sample and the reference are maintained at approximately the same temperature during the experiment **(**Dean, 1995). The sample and reference are scanned and the difference in the quantity of heat necessary to increase the temperature of the sample and buffer are measured as a function of temperature. The result is presented as thermograms, which show the relation between the heat capacity of the sample and the temperature. From the analysis of the thermograms we can obtain the melting temperature and calorimetric enthalpy. For proteins, melting temperature is defined as the temperature at which 50% of the protein molecules are unfolded (Cooper *et al.*, 2000).

Transmission electron microscope (TEM) can be operated by the same basic principles of the light microscope. However, the main source of illumination is a beam of electrons of a very short wavelength instead of light; what allows a resolution much higher than the light microscope. The high magnifications make it a useful instrument to study cells in detail or other materials to the order of a few angstroms (10^{-10} m) (Robinson, 1986; Ruska, 1987).

The beam of electrons is emitted from a tungsten filament at the top of a cylindrical column of approximately 2 meters high and they pass through a vacuum in the column of the microscope. The TEM uses electromagnetic lenses to focus the beam of electrons, which then pass through the specimen under study (Ruska, 1986). At the bottom of the microscope the unscattered electrons hit a fluorescent screen that gives rise to a "shadow image" of the specimen with its different parts displayed in varied darkness according to their density (Ruska, 1986). For this study, the specimen is negatively stained with solutions of heavy metal salts that form an amorphous electron dense layer when air-dried. The specimen which is embedded in such layers scatters

fewer electrons compared to the stain and stands out from the background due to the contrast. The most common negative stains are the uranyl acetate and ammonium molybdate (Harris, 1997). Before applying the samples on carbon films, these need to become more reactive, thus the surface of carbon films is bombarded by ions and the surface cleaned from impurities by a process designated glow-discharge (Harris, 1997). Transmission electron microscopy allowed us to investigate the quaternary structure of Caf1 mutant protein.

3.2. Results

Subcloning of caf operon into a vector suitable for mutagenesis

The amplification of *E. coli* plasmid pAH34L (Miller *et al*, 1998) (about 11 Kbp in size), which includes the *Yersinia pestis caf* operon, by PCR created a product of approximately 5.2 Kb in size (**Figure 3.1-A**), using the "Caf1 pair" of primers (see material and methods, **Table 2.2**) and an ultra-high-fidelity KOD DNA Polymerase which allows a very low error rate due to its unique proofreading capacity, high specificity and increased read length (Mizuguchi *et al.*, 1999), to check that this was the correct product, it was digested with *Hin*dIII and *Bam*HI restriction enzymes which cut the *caf* operon and *Eco*RI which does not cut *caf* operon (**Figure 3.1-B**).

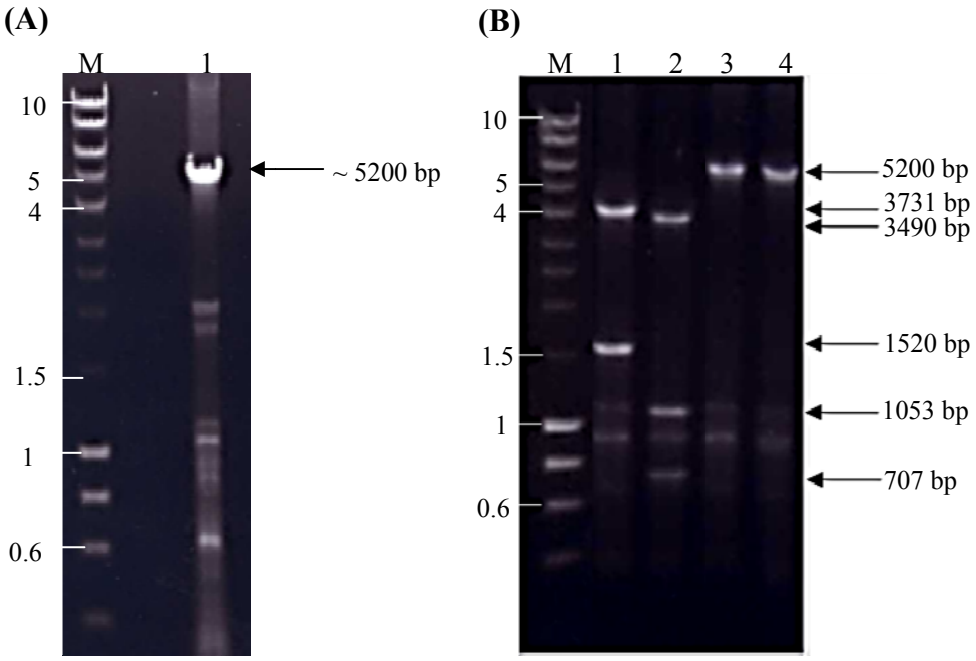

Figure 3.1 – PCR amplification of *caf* operon using pAH34L vector as a template and restriction digest of PCR product. (A) PCR amplification. **M**, molecular size markers (Kb); **lane 1**, *caf* operon. (**B)** Restriction digestion of PCR product. **M**, molecular size markers (Kb); **lane 1**, *caf* operon digested with *Bam*HI restriction enzyme showed two bands of 3731 bp and 1520 bp; **lane 2**, *caf* operon digested with *Hin*dIII showed three bands of 3490 bp and 1053 bp and 707 bp; **lane 3**, *caf* operon digested with *Eco*RI showed a single band of 5200 bp due to the absence of the specific *Eco*RI restriction site; **lane 4**, *caf* operon non-digested showed a single band of 5200 bp.

After confirmation that the PCR product obtained was the *caf* operon by restriction analysis, the *DNA* fragment of the expected size (~ 5 Kb) was purified from the 0.7% agarose gel using QIAGEN Gel Extraction kit.

The identity and integrity of the DNA fragment was confirmed by restriction analysis with *Hin*dIII and *Bam*HI restriction enzymes which cut the *caf* operon and *Eco*RI which does not cut *caf* operon (**Figure 3.2**)

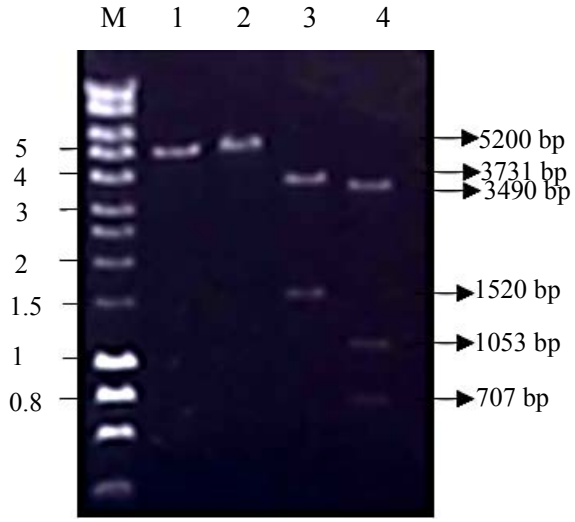

Figure 3.2 – Analysis of the *caf* operon cloned into the pGEM-T Easy vector. Restriction digestion of PCR product. **M**, molecular size markers (Kb); **lane 1**, *caf* operon non-digested; **lane 2**, *caf* operon digested with *Eco*RI showed a single band of 5200 bp due to the absence of the specific *Eco*RI restriction site; **lane 3**, *caf* operon digested with *Bam*HI resctriction enzyme showed two bands of 3731 bp and 1520 bp; **lane 4**, *caf* operon digested with *Hin*dIII showed three bands of 3490 bp, 1053 bp and 707 bp.

After restriction analyses were performed to confirm the identity of the PCR product the purified PCR product was subcloned into a new vector.

Initially, we attempted to subclone the *caf* operon into pSMART–HC-Amp and pSMART–LC-Kan vectors (Lucigen, USA). The copy number of pSMART-HC is

similar to pUC19, about 300-500 copies per cell. The copy number of pSMART-LC is similar to pBR322, about 15-30 copies per cell.

The pSMART vectors were pre-digested, with blunt, dephosphorylated ends. The small size of the pSMART vectors (1.7-2.0 Kb) could facilitate subcloning and mutagenesis experiments of the large insert DNA.

After DNA purification the PCR product must be treated with *T4* polynucleotide *kinase* (10 U) (NEB, UK) to add 5´-phosphates to oligonucleotides in order to allow subsequent ligation. In the cloneSmart ligation reaction, the pre-processed pSMART vector is ligated with blunt, phosphorylated insert.

The positive control used was the lambda/HcII insert and the negative control without insert was also performed. Transformants of 10G *E. coli* chemically competent cells containing the new recombinant plasmid were selected on LB agar plates containing the appropriate antibiotic for either pSMART HC-Amp and LC-Kan. The plates were incubated overnight at 37 ºC.

Then, several colonies from the plates were used to perform minipreparation of plasmid DNA (using the Qiagen kit). The plasmid DNA was digested with *Eco*RI restriction enzyme to release the insert. All clones screened were empty i.e. only a single band was observed, on the 0.7% agarose gel, with around 2 Kb which are the size of the vectors. The results obtained are presented in **Figure 3.3.**

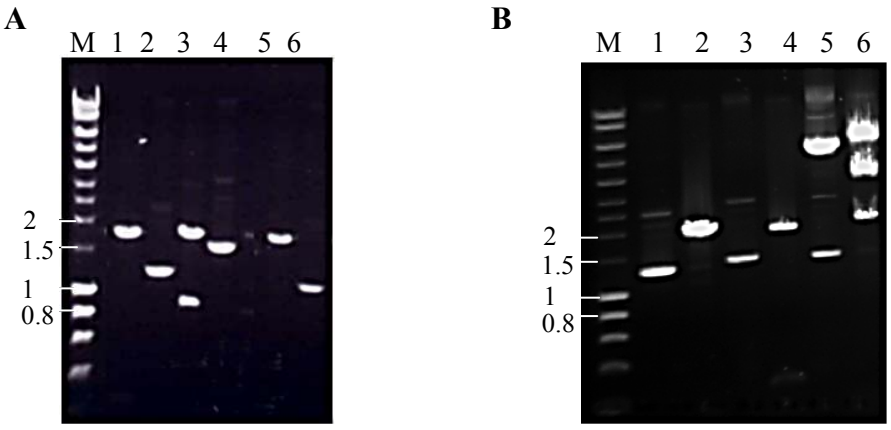

Figure 3.3 – Restriction digestion of pSMART vectors. M, molecular size markers (Kb), **A) pSMART–HC-AMP**. **Lane 1,** pSMART–HC-AMP with no insert (negative control) digested with *Eco*RI showed a band of 1.8 kb. **Lane 2,** pSMART–HC-AMP with no insert (negative control) non-digested showed a band of 1.3 kb. **Lane 3,** pSMART–HC-AMP with lambda/HcII insert (positive control) digested with *Eco*RI showed two bands of 1.8 kb and 0.6 Kb. **Lane 4,** pSMART–HC-AMP with lambda/HcII insert (positive control) non-digested showed a single band of 1.3 Kb. **Lane 5,** pSMART–HC-AMP with insert digested with *Eco*RI showed a single of 1.8 kb. **Lane 6,** pSMART–HC-AMP non- digested showed a single of 1.3 kb. **B) pSMART–LC-Kan**. **Lane 1,** pSMART–LC-Kan with no insert (negative control) non-digested showed a band of 1.3 kb. **Lane 2,** pSMART–LC-Kan with no insert (negative control) digested with *Eco*RI showed a band of 1.8 kb. **Lane 3,** pSMART–LC-Kan non-digested showed a single of 1.3 kb **Lane 4,** pSMART–LC-Kan with insert digested with *Eco*RI showed a single of 1.8 kb. **Lane 5,** pSMART–LC-Kan with lambda/HcII insert (positive control) non-digested showed a single band of 1.3 Kb. **Lane 6,** pSMART–LC-Kan with lambda/HcII insert (positive control) digested with *Eco*RI showed two bands of 1.8 kb and 0.6 Kb.

A second attempt to subclone the *caf* operon was conducted using pGEM-T Easy (Promega, UK). The PCR product was generated by a proofreading enzyme – KOD HOT START DNA polymerase (Novagen, UK) which produces blunt ends. This PCR product with blunt ends can only be ligated into the pGEM-T Easy vector if they are first tailed with dATP using *Taq* DNA Polymerase which adds a single nucleotide, generally adenine, to the 3′-ends of amplified PCR products. The pGEM-T Easy linearized vector contain single 3′terminal thymidines (T's) at each end which

complement the A overhang added by the polymerase (Kobs, 1996). This process is designed by A-tailing. Thus, after DNA purification the PCR product was prepared for ligation into the pGEM-T Easy using the A-tailing procedure. XL10 gold chemically competent *E. coli* cells were transformed with the ligation reaction and four of the transformants obtained were sent for sequencing (see below).

In parallel to sequencing, restrictions analysis was performed using E*co*RI restriction enzyme, which has two restriction sites in the pGEM-T Easy plasmid and able to release the insert, this showed two bands: one band with approximately 3 Kb which might correspond to the vector and the second band above 5 Kb which might correspond to the insert (**Figure 3.4**).

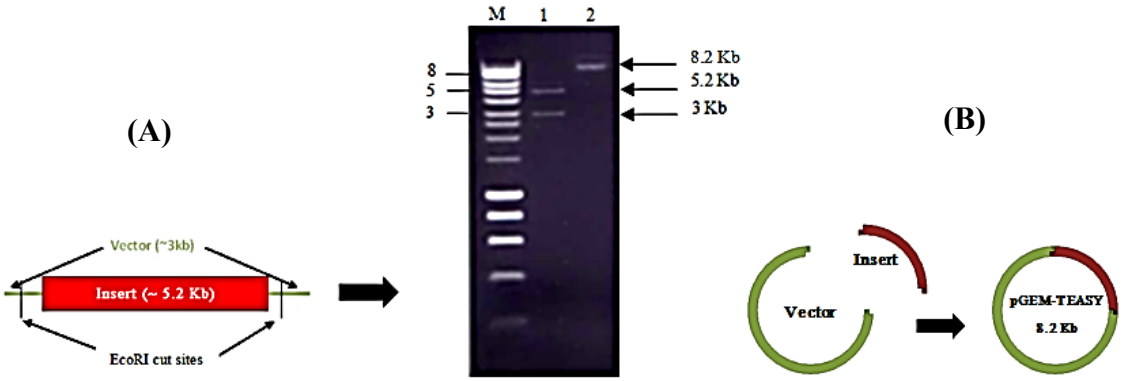

Figure 3.4 – Restriction digestion of pGEMCaf1. Gel electrophoresis shows **M**, molecular size markers (Kb); **lane 1**, pGEMCaf1 digested with *Eco*RI showing two bands of 5 Kb and 3 Kb; **lane 2**, pGEMCaf1 non-digested showed a single band of approximately 8 Kb. **(A)** Diagram shows *caf* operon insert (~ 5 Kb), pGEM-T Easy vector (3 Kb) and E*co*RI cut sites; **(B)** Diagram shows *caf* operon insert (5.2 Kb), pGEM-T Easy vector (3 Kb) and, after ligation, the resulting plasmid of 8.2 Kb.

Results provided by gene sequencing has shown that the amino acid sequence of the *caf* operon cloned into pGEM-T Easy (**Figure 3.5**) was identical to the previously reported sequence from *Yersinia pestis* strain 482 plasmid pMT1 encoding the *caf* operon, complete sequence (GenBank accession number, AY450847).

(A) **(B)**

Figure 3.5 – Sequencing results of the pGEMCaf1. (A) Image showing the start of the *caf* operon with *cafr* gene. **(B)** Image showing the end of the *caf* operon with *Caf1* gene. The translation sequence was obtained using the Expasy tool (http://expasy.org/tools/dna.html). Universal primers such as T7 Promoter Primer (***5***'-AAT TCT AAT ACG ACT CAC TAT AGG -3') or the pUC/M13 Forward Primer (***5***'-GTA AAA CGA CGG CCA GTG -3') were used to sequence DNA produced by the pGEM-T Easy vector. Legend: 1 – Part of the sequence of pGEM-T Easy; 2 – Nucleotide and amino acid sequence of the *Caf1r* and Caf1R, respectively; 3 - Nucleotide and amino acid sequence of the *Caf1* and Caf1, respectively.

The plasmid DNA of each construct was used to transform the BL21(DE3) chemically competent *E. coli* cells. A single colony of transformed BL21(DE3) was inoculated in 50 ml of LB media supplemented with 100 µg/ml of ampicillin and incubated at 37 ºC with 180 rpm shaking for 16 h. The bacterial cell culture in a 15 ml Falcon tube was centrifuged at 3000 rpm for 15 min at 4 ºC and the supernatant discarded. A flocculent layer was observed on surface of cells and removed carefully using a pipette. The flocculent layer was homogenised in SDS-sample buffer and loaded on a 12% SDS-PAGE. From the results of SDS-PAGE an approximately 15 kDa band was observed and a western blotting was employed to confirm if the band corresponds to Caf1 by using a monoclonal anti-Caf1 antibody (**Figure 3.6**).

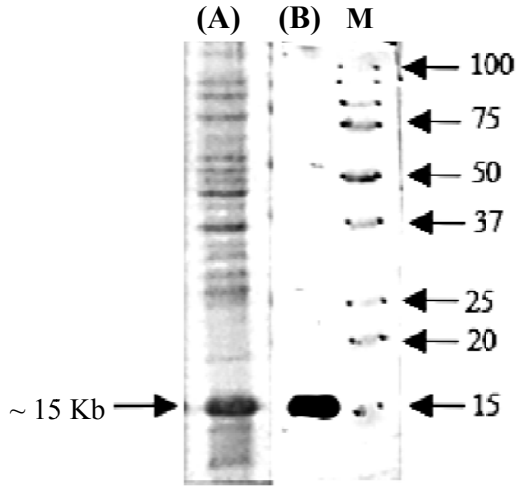

Figure 3.6 – Analysis of Caf1 expression. One of the gels was **(A)** stained with Coomassie blue R250 and the other gel **(B)** used to perform a western blot. **M**, molecular weight marker proteins (molecular mass x 10^3 kDa arrowed). **(A)** 12% SDS-PAGE. Sample analysed (10 μL) was prepared from overnight bacterial cell culture *Escherichia coli* (pGEMCaf1) grown at 37 ºC. The whole cells sample was heated at 95 ºC for 5 minutes and an equal volume of SDS-sample buffer was added to each sample before loading the samples on 12% SDS-PAGE. **(B)** Western blotting using a mouse monoclonal anti-Caf1 antibody. The resulting *blot* was probed for Caf1 with mouse anti-Caf1 monoclonal antibody and then developed with HRP goat anti-mouse antibody colour development solution with 4CN (4-chloro-1-naphthol).

In order to confirm the identity of the band of approximately 15 kDa on the 12% SDS-PAGE, the band was excised from the gel and sent for mass spectrometry. Results obtained confirmed that the band of approximately of 15 kDa is Caf1 (**Figure 3.7**).

(A)

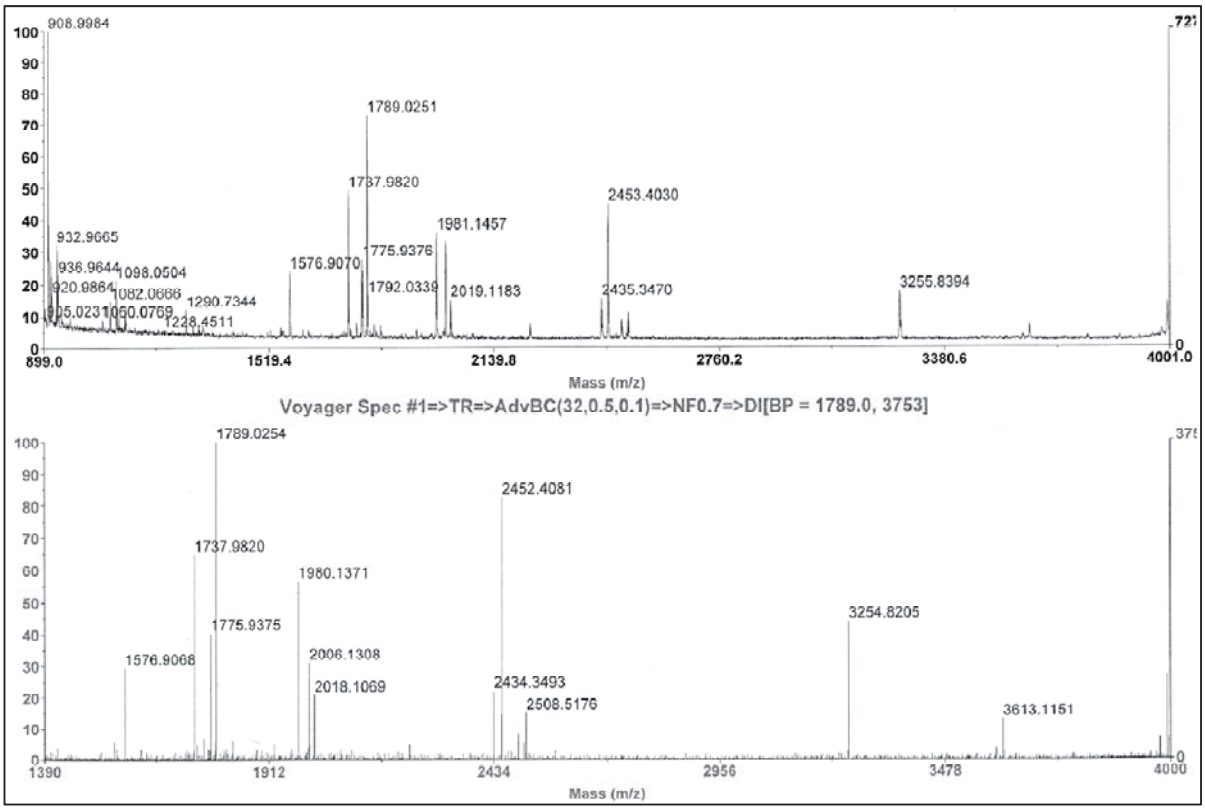

(B)

<u>MKKISSVIAIALFGTIATANA</u>ADLTASTTATATLVEPARITLTYKEGAPITIMDNG
NIDTELLVGTLTLGGYKTGTTSTSVNFTDAAGDPMYLTFTSQDGNNHQFTTKVI
GKDSRDFDISPKVNGENLVGDDVVLATGSQDFFVRSIGSKGGKLAAGKYTDAV
TVTVSNQ

Figure 3.7 – The peptide mass fingerprinting of Caf1. (A) Spectral masses (in mass per charge unit, *m*/*z*) of Caf1 obtained by MALDI-TOF mass spectrometry. MALDI-TOF analysis of the tryptic digests of this protein excised from SDS-PAGE confirmed that this protein is Caf1 of *Yersinia pestis* (Mascot score of 71 and sequence coverage of 50%, for the 17.8 kDa protein). **(B)** Caf1 amino acid sequence, the signal peptide of Caf1 is underlined (the signal peptide is not present in the mature Caf1 protein).

Site-directed mutagenesis in Caf1 loops

The mutations were modelled into the loops of the Caf1 subunit using PyMOL and the published coordinates for the *Caf1$_N$:Caf1M:Caf1* complex (PDB file: 1Z9S) Caf1$_N$ has the N terminal beta-strand deleted; this allowed a stable ternary complex to be prepared (**Figure 3.8**).

(A)

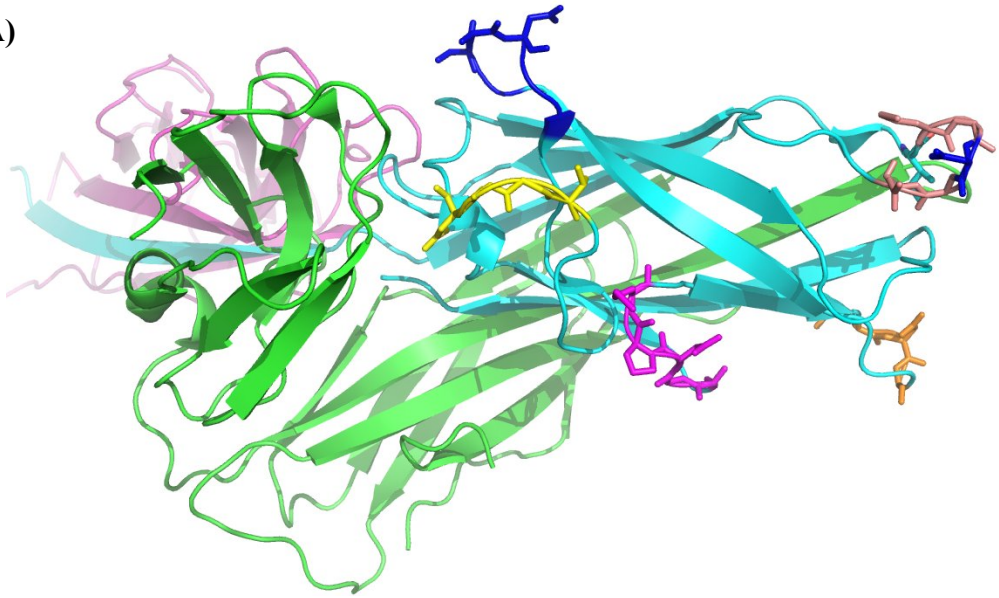

(B)

ADLTASTTATATLVEPARITLTYKEGAPITIMDNGNIDTELLVGTLTLGGYKTGT
TSTSVNFTDAAGDPMYLTFTSQDGNNHQFTTKVIGKDSRDFDISPKVNGENLV
GDDVVLATGSQDFFVRSIGSKGGKLAAGKYTDAVTVTVSNQ

Figure 3.8 – *Caf1$_N$:Caf1M:Caf1* complex (PDB file: 1Z9S). (A) This image was generated using *PyMOL software (http://www.pymol.org)*. The chaperone, Caf1M is represented in green and the Caf1 fibre is represented in blue. The Caf1 loops are represented as follows: ***Loop 1 –*** *"...DSRDFD..."*; ***Loop 2 –*** *"...AGDP..."*; ***Loop 3 –*** *"...VGDD..."*; ***Loop 4 –*** *"...MDNG..."*; ***Loop 5 –*** *"...QDGNN..."*. **(B)** Caf1 amino acid sequence shows the loops of Caf1 subunit (they are highlighted in salmon, pink, orange, dark blue and yellow) were the sites chosen to incorporate the mutations.

After performing site-directed mutagenesis as described in chapter 2, colonies from successful transformation were sent for sequencing. Results obtained from gene

sequencing confirmed the expected new sequences which are shown below (**Figure 3.9** and **3.10**).

(A) Caf1 RGDS L1

ADLTASTTATATLVEPARITLTYKEGAPITIMDNGNIDTELLVGTLTLGGYKTGTTSTSVNFTDAA
GDPMYLTFTSQDGNNHQFTTKVIGKDS**RGDS**FDISPKVNGENLVGDDVVLATGSQDFFVRSIGS
KGGKLAAGKYTDAVTVTVSNQ

(B) Caf1 RGDS L2

ADLTASTTATATLVEPARITLTYKEGAPITIMDNGNIDTELLVGTLTLGGYKTGTTSTSVNFTDA**R**
GDSPMYLTFTSQDGNNHQFTTKVIGKDSRDFDISPKVNGENLVGDDVVLATGSQDFFVRSIGSK
GGKLAAGKYTDAVTVTVSNQ

(C) Caf1 RGDS L3

ADLTASTTATATLVEPARITLTYKEGAPITIMDNGNIDTELLVGTLTLGGYKTGTTSTSVNFTDAA
GDPMYLTFTSQDGNNHQFTTKVIGKDSRDFDISPKVNGENL**RGDS**VVLATGSQDFFVRSIGSKG
GKLAAGKYTDAVTVTVSNQ

(D) Caf1 RGDS L4

ADLTASTTATATLVEPARITLTYKEGAPITIG**RGDS**GNIDTELLVGTLTLGGYKTGTTSTSVNFTD
AAGDPMYLTFTSQDGNNHQFTTKVIGKDSRDFDISPKVNGENLVGDDVVLATGSQDFFVRSIGS
KGGKLAAGKYTDAVTVTVSNQ

(E) Caf1 RGDS L5

ADLTASTTATATLVEPARITLTYKEGAPITIMDNGNIDTELLVGTLTLGGYKTGTTSTSVNFTDAA
GDPMYLTFTS**RGDS**NHQFTTKVIGKDSRDFDISPKVNGENLVGDDVVLATGSQDFFVRSIGSKG
GKLAAGKYTDAVTVTVSNQ

(F) Caf1 RGES L5

ADLTASTTATATLVEPARITLTYKEGAPITIMDNGNIDTELLVGTLTLGGYKTGTTSTSVNFTDAA
GDPMYLTFTS**RGES**NHQFTTKVIGKDSRDFDISPKVNGENLVGDDVVLATGSQDFFVRSIGSKGG
KLAAGKYTDAVTVTVSNQ

Figure 3.9 – Protein sequences of Caf1 RGDS and RGES mutants.

(G) Caf1 G35C L4

ADLTASTTATATLVEPARITLTYKEGAPITIMDNCNIDTELLVGTLTLGGYKTGTTSTSVNFTDAA
GDPMYLTFTSQDGNNHQFTTKVIGKDSRDFDISPKVNGENLVGDDVVLATGSQDFFVRSIGSKG
GKLAAGKYTDAVTVTVSNQ

(H) Caf1 G79C L5

ADLTASTTATATLVEPARITLTYKEGAPITIMDNGNIDTELLVGTLTLGGYKTGTTSTSVNFTDAA
GDPMYLTFTSQDCNNHQFTTKVIGKDSRDFDISPKVNGENLVGDDVVLATGSQDFFVRSIGSKG
GKLAAGKYTDAVTVTVSNQ

(I) Caf1 R94C L1

ADLTASTTATATLVEPARITLTYKEGAPITIMDNGNIDTELLVGTLTLGGYKTGTTSTSVNFTDAA
GDPMYLTFTSQDGNNHQFTTKVIGKDSCDFDISPKVNGENLVGDDVVLATGSQDFFVRSIGSKG
GKLAAGKYTDAVTVTVSNQ

Figure 3.10 – Protein sequences of Caf1 cysteine mutants.

After the confirmation by sequencing of the successful insertion of the mutations in Caf1 WT, we proceeded to the expression of Caf1 WT and its mutants. Our first attempt was to express these constructs in a small-scale bacterial culture.

In addition the following mutations were attempted several times but no successful transformants were generated following QuikChange; the residues QDGNN in Caf1 substituted by PHSRN motif (from fibronectin), YIGSR (from laminin) and the PNEEF (MMP-cleavage site).

Expression of Caf1 WT and Caf1 mutants

a) Small-scale Caf1 protein expression

After 16 hrs of protein expression and following centrifugation a flocculent layer was visible in some of the preparations. This flocculent layer was previously observed by Miller and coworkers (Miller *et al*., 1998). The flocculent layer was clearly visible in the preparations of the pGEMCaf1 WT, pGEMCaf1 RGDS L1, pGEMCaf1 RGDS L3, pGEMCaf1 RGDS L4 and pGEMCaf1RGDS L5. No visible flocculent layer was

visible on pGEMCaf1 RGDS L2 and on the negative control pUC19. An interesting observation was the small size of the cell pellet in preparations which presented a large flocculent layer (**Figure 3.11**).

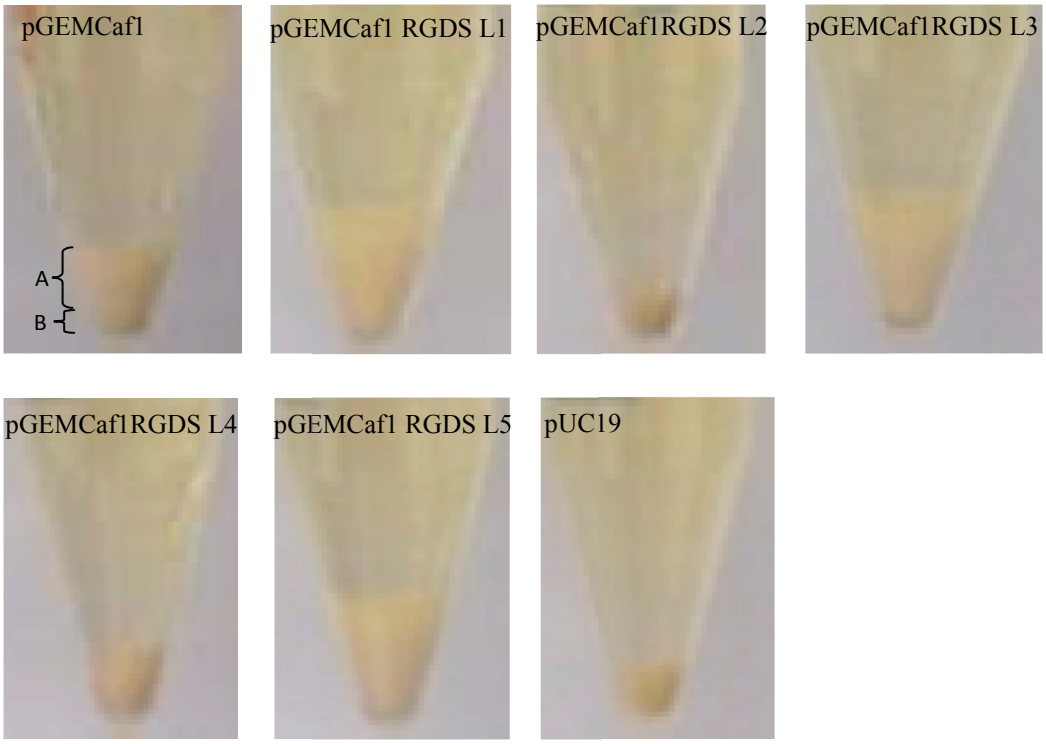

Figure 3.11 – Analysis of the expression of Caf1 WT and Caf1 RGDS mutants. (**A)** Flocculent layer. (**B)** Cell pellet.

The graph below (**Graph 3.1**) illustrates the relationship between the size of the flocculent layer and the relative density of Caf1 protein on each sample. Quantification of Caf1 was performed by analysis of the bands on the western blot by densitometry (**Figure 3.12**). The quantity of Caf1 in the cell pellet measurements measured by densitometry was very similar for all preparations except for the pGEMCaf1 RGDS L2 and pUC19. The pGEMCaf1 RGDS L2 encodes a *caf* operon with a mutation on *Caf1* gene; however no expression of Caf1, inside the bacterial cells, was observed. The pUC19 does not encode the *caf* operon and thus no band was expected on the western blot probed with mouse monoclonal anti-Caf1 antibody. The content of Caf1 inside the bacterial cells was revealed to be variable. The mutants pGEMCaf1 RGDS L4 and pGEMCaf1 RGDS L5 presented large amounts of intracellular Caf1. The size of the

flocculent layer was slightly larger on pGEMCaf1 WT and pGEMCaf1 RGDS L5 than on the other Caf1 mutants. However, the quantity of Caf1 detected in the flocculent layer of the pGEMCaf1WT was lower than in the flocculent layer of the pGEMCaf1 RGDS L5. Although the size of the flocculent layer was higher in the pGEMCaf1 RGDS L1 than in pGEMCaf1 RGDS L3, the quantity of Caf1 present in the flocculent layer of these two mutants was similar. Even though the pGEMCaf1 RGDS L4 presented the smallest size of the flocculent layer, the quantity of Caf1 in the flocculent layer was one of the highest.

Graph 3.1 - Relation between the size of flocculent layer or the cell pellet of Caf1 and the total Caf1 density from densitometry of western blots.

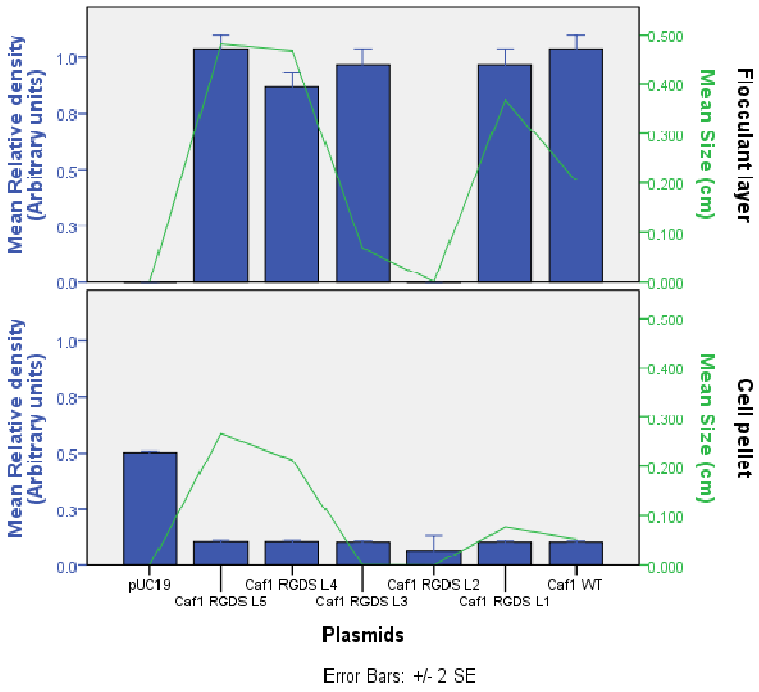

The flocculent layer and the cell pellet were separated by aspirating the flocculent layer carefully using a Gilson P1000 Pipetteman. These two fractions were loaded in the 18% Tris-tricine gel used for resolving low molecular weight proteins and *higher resolution* of smaller peptides (**Figure 3.12**).

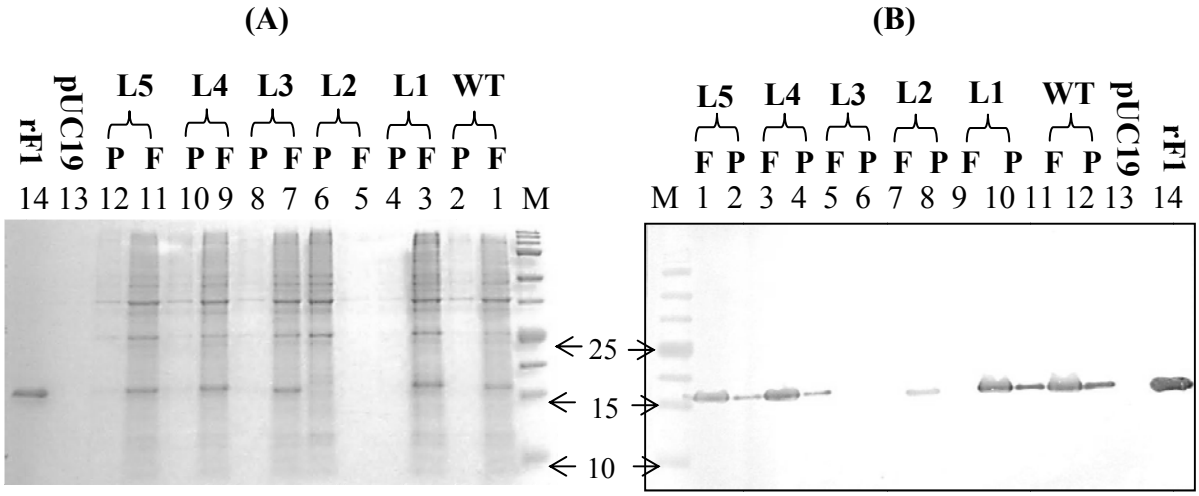

Figure 3.12 – Analysis of Caf1 WT and Caf1 mutants. (A) 18 % Tris-tricine gel of the cell pellet and flocculent layer**.** Caf1 samples in SDS-sample buffer were heated at 95 ºC for 5 minutes. **(B)** Western blotting of the cell pellet and flocculent layer using mouse monoclonal anti-Caf1 antibody. Caf1 samples in SDS-sample buffer were heated at 95 ºC for 5 minutes. **M**, contained molecular weight marker proteins (molecular mass x10^3 kDa arrowed)**; lane 1,** Caf1WT present in the flocculent layer (F)**; lane 2,** Caf1 WT present in the cell pellet (P); **lane 3**, Caf1 RGDS L1present in the flocculent layer (F); **lane 4**, Caf1 RGDS L1 present in the cell pellet (P); **lane 5**, Caf1 RGDS L2 present in the flocculent layer (F); **lane 6**, Caf1 RGDS L2 present in the cell pellet (P); **lane 7**, Caf1 RGDS L3 present in the flocculent layer (F); **lane 8**, Caf1 RGDS L3 present in the cell pellet (P); **lane 9**, Caf1 RGDS L4 present in the flocculent layer (F); **lane 10**, Caf1 RGDS L4 present in the cell pellet (P); **lane 11**, Caf1 RGDS L5 present in the flocculent layer (F); **lane 12**, Caf1 RGDS L5 present in the cell pellet (P); **lane 13**, PUC19 present in the supernatant (absence of flocculent layer), **lane 14**, rF1 standard (purified by Avecia).

a) Sub cellular location of Caf1

Fractionation of sub-cellular proteins enables Caf1 protein localization assessment. BL21(DE3) cells containing plasmid pGEMCaf1 were cultured at 37 ºC with 180 rpm shaking for 16 hrs. Then, the cell culture was centrifuged and the supernatant was decanted and kept at 4 ºC for further analysis. The cell pellet was used in a stepwise process for separation and extraction of periplasmic and cytoplasmic fractions, and

inner and outer membrane fractions. The spheroplast buffer (lysis buffer) containing 18% sucrose, $CaCl_2$ and lysozyme was added to the cell pellet. The sucrose increases osmolarity and stabilizes integrity of membranes and the lysozyme damages the bacterial cell wall realising the periplasmic fraction. The localization of Caf1 WT, Caf1 RGDS mutants and RGES L5 mutant was examined. **Table 3.1** showed that a low quantity of Caf1 WT was found in cytoplasmic and inner membrane fractions and a slightly higher relative density was presented in the outer membrane and periplasmic fractions. Interestingly, it seems that most of the Caf1 WT was expressed to outside the cells, thus into the supernatant and only a small quantity was presented in the flocculent layer. Caf1 RGDS L1 is present in large quantities in the flocculent layer, periplasmic fraction and outer membrane fraction. Only a small quantity of Caf1 RGDS L1 was secreted to outside the cells. No Caf1 RGDS L2 was detected in any cellular fraction and the relative density of Caf1 RGDS L4 determined in all cellular fractions was very low. Caf1 RGDS L3 was found mainly in the supernatant. The expression of Caf1 RGDS L5 and Caf1 RGES L5 revealed large amounts of Caf1 distributed in different cellular fractions but mainly present in the flocculent layer. The western blots used to quantify Caf1 in the different sub-cellular fractions by imageJ are presented below (**Figure 3.13**).

Table 3.1 – Caf1 protein quantification in the sub cellular fractions by densitometry.

Caf1	% Relative density of Caf1 in sub cellular fractions (mean of density reading ± S.E)					
	Supernatant	Flocculant layer	Periplasmic fraction	Cytoplasmic fraction	Inner membrane fraction	Outer membrane fraction
WT	65% (0,98±0,002)	12% (0,19±0,01)	10% (0,15±0,004)	1% (0,01±0,0012)	3% (0,05±0,002)	9% (0,13±0,008)
RGDS L1	81% 0,27±0,015	31% 0,99±0,005	21% 0,69±0,008	3% 0,11±0,006	8% 0,25±0,004	29% 0,93±0,03
RGDS L2	0	0	0	0	0	0
RGDS L3	89% 0,75±0,034	2% 0,015±0,002	1% 0,01±0,0004	0	2% 0,02±0,001	6% 0,05±0,004
RGDS L4	31% 0,047±0,001	0	26% 0,04±0,004	4% 0,006±0,0005	13% 0,02±0,002	26% 0,04±0,001
RGDS L5	29% 0,91±0,02	25% 0,77±0,03	31% 0,96±0,004	3% 0,091±0,004	11% 0,35±0,005	0.8% 0,026±0,01
RGES L5	15% 0,48±0,03	26% 0,8±0,03	29% 0,89±0,008	5% 0,16±0,04	12% 0,37±0,010	13% 0,41±0,008

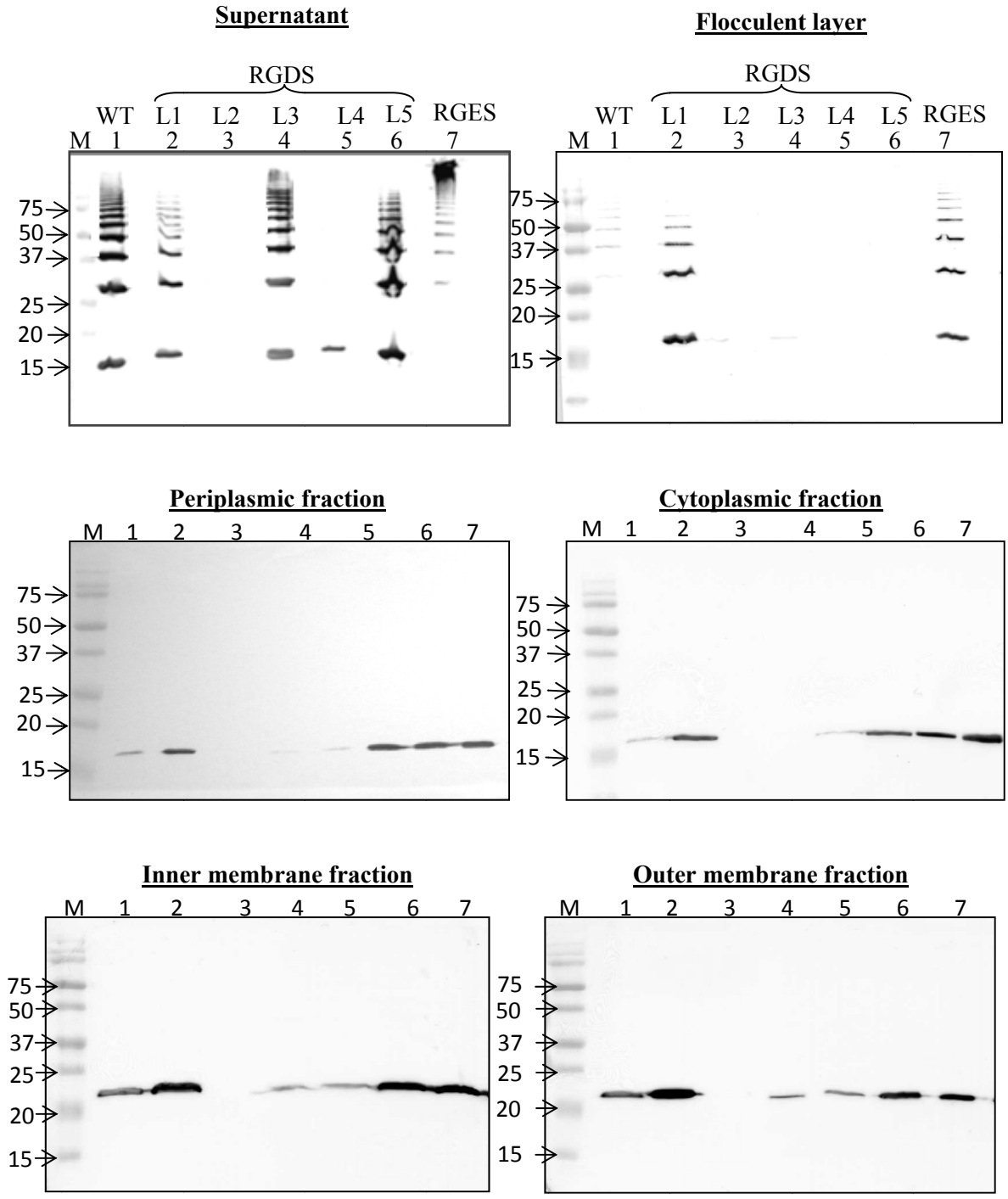

Figure 3.13 – Western blots of sub-cellular fractions containing Caf1 WT and Caf1 RGDS mutants were detected by the monoclonal anti-Caf1 antibody. Caf1 protein samples from the supernatant and flocculent layer were heated in SDS-sample buffer, at 95 ºC for 45 seconds. Caf1 protein samples from the periplasmic, cytoplasmic, inner membrane and outer membrane fractions were heated in SDS-sample buffer at 95 ºC for 5 minutes. **M**, molecular weight marker proteins (molecular mass x 10^3 kDa arrowed); **lane 1**, Caf1 WT; **lane 2**, Caf1 RGDS L1; **lane 3**, Caf1 RGDS L2; **lane 4**, Caf1 RGDS L3; **lane 5**, Caf1 RGDS L4; **lane 6**, Caf1 RGDS L5; **lane 7**, Caf1 RGES L5.

Expression of BL21(DE3)/pGEMCaf1 encoding the *Caf1* gene mutated with a single cysteine residue did not produce a flocculent layer in any of the three Caf1 cysteine mutants (Caf1 G79C L5, Caf1 R94C L1, Caf1 G35C L4). The expression of Caf1 cysteine mutants was analysed by SDS-PAGE gradient gels *(*4-20*%)* and western blotting (**Figure 3.14**).

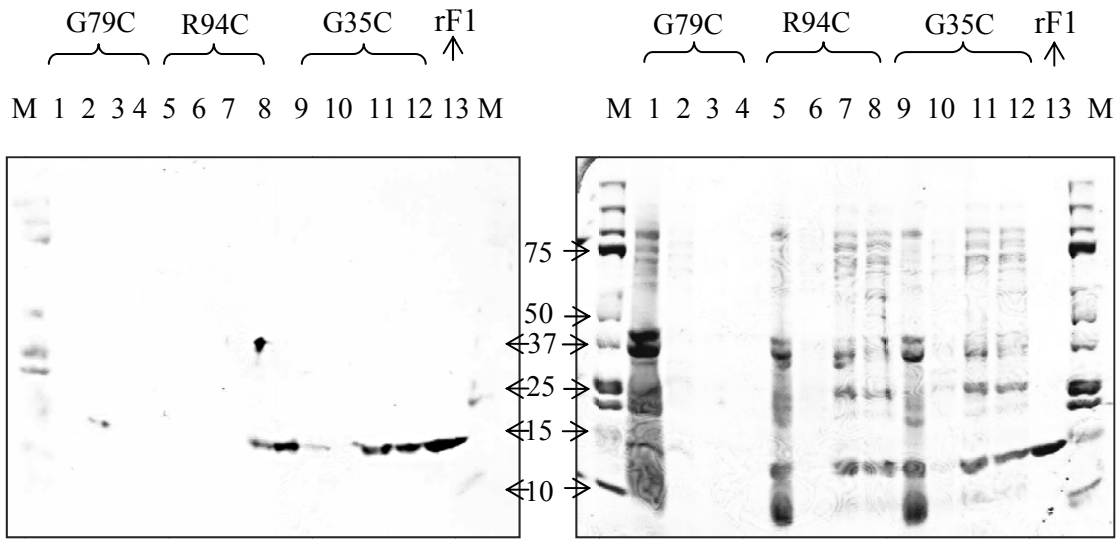

Figure 3.14 – Analysis of Caf1 cysteine mutants. Whole cells samples were heated at 100°C for 5 minutes in SDS sample buffer. Periplasmic fractions from *E. coli* BL21(DE3) expressing Caf1 cysteine mutants were heated at 95 ºC for 5 minutes in SDS-sample buffer with 1 mM dithiothreitol (DTT) or in the absence of DTT. **(A)** SDS-PAGE Gradient Gels *(*4-20*%).* **(B)** Western blotting using a mouse monoclonal anti-Caf1 antibody. **M**, contained molecular weight marker proteins (molecular mass x 10^3 kDa arrowed); **lane 1**, Caf1 G79C L5 present in the cell pellet; **lane 2**, Caf1 G79C L5 present in the supernatant; **lane 3**, Caf1 G79C L5 present in the periplasmic fraction; **lane 4**, Caf1 G79C L5 present in the periplasmic fraction in the presence of 1 mM of DTT; **lane 5**, Caf1 R94C L1 present in the cell pellet; **lane 6**, Caf1 R94C L1 present in the supernatant; **lane 7**, Caf1 R94C L1 present in the periplasmic fraction; **lane 8**, Caf1 R94C L1 present in the periplasmic fraction in the presence of 1 mM of DTT; **lane 9**, Caf1 G35C L4 present in the cell pellet; **lane 10**, Caf1 G35C L4 present in the supernatant; **lane 11**, Caf1 G35C L4 present in the periplasmic fraction; **lane 12**, Caf1 G35C L4 present in the periplasmic fraction in the presence of 1 mM of DTT; **lane 13**, rF1 standard (Avecia).

A small amount of Caf1 G79C L5 was detected in the supernatant (**Figure 3.14**). A different result was obtained for Caf1 R94C; this mutant was detected in the periplasmic fraction in the presence of 1 mM of DTT. Nevertheless, Caf1 G35C was detected in the cell pellet; a very small amount of Caf1 G35C was detected in the supernatant and in the periplasmic fraction in the presence and absence of DTT.

After analysing the distribution of Caf1 WT, Caf1 RGDS mutants and Caf1 RGES L5 mutant a large-scale bacterial culture was performed, followed by purification. The total yield of pure Caf1 proteins was determined by measuring optical density at 280 nm in a spectrophotometer (**Table 3.2**)

After large scale cell growth (1 L), the centrifugation of *E. coli* BL21(DE3)/pGEMCaf1 and some of the mutant's cultures resulted in the sedimentation of bacterial cells above which a layer of flocculated material was visible. This flocculated material was shown to contain Caf1. Additional Caf1 could be removed from the surface of the bacterial cells by gentle washing in PBS (Miller *et al*., 1997).

The SDS-PAGE (**Figure 3.15**) shows Caf1WT purification by 25%, 30%, 40% and 50% of ammonium sulphate fractionation. The results show that 25% ammonium sulphate do not precipitate Caf1 (**lane 5**) which remains in solution (**lane 1**). Using 30-50% of ammonium sulphate fractionation, almost the entire Caf1 protein content was precipitated (**lanes 6-8**) while some amounts of Caf1 protein and significant amounts of contaminating proteins remained in solution (**lanes 2-4**).

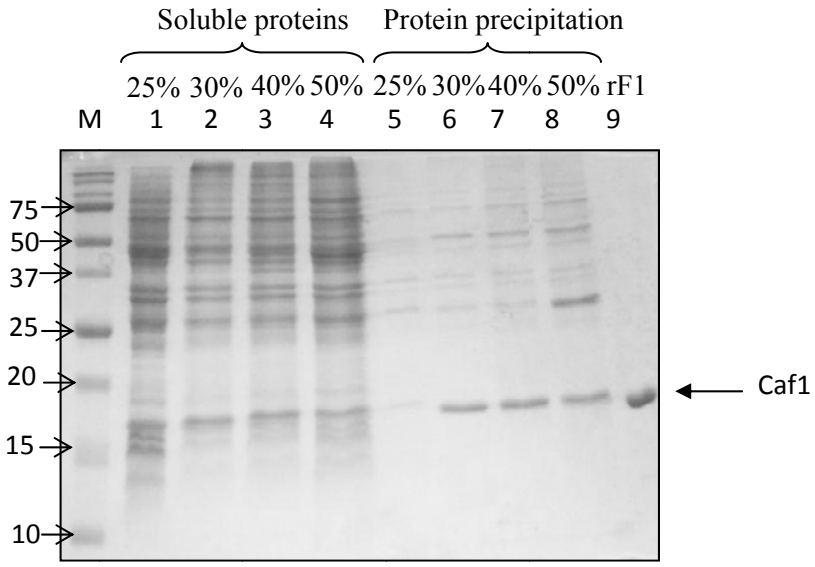

Figure 3.15 – Coomassie Brilliant Blue-stained 12% SDS-PAGE of Caf1 enriched by differential precipitation with ammonium sulphate. Caf1 samples in SDS-sample buffer were heated at 95 ºC for 5 minutes. **M**, molecular weight marker proteins (molecular mass x 10^3 kDa arrowed); **lane 1**, soluble protein remaining in the supernatant after 25% Ammonium sulphate treatment; **lane 2**, soluble protein remaining in the supernatant after 30% Ammonium sulphate treatment; **lane 3**, soluble protein remaining in the supernatant after 40% Ammonium sulphate treatment; **lane 4**, supernatant from 50% ammonium sulphate treatment of salt extract; **lane 5**, precipitate from 25% ammonium sulphate treatment of salt extract; **lane 6**, precipitate from 30% ammonium sulphate treatment of salt extract; **lane 7**, precipitate from 40% ammonium sulphate treatment of salt extract; **lane 8**, precipitate from 50% ammonium sulphate treatment of salt extract; **lane 9**, rF1 standard (Avecia).

FPLC Superdex 200 gel filtration chromatography column (maximum pressure: 3 MPa; flow rate: 1 mL/min; mobile phase: 50 mM PBS buffer pH 7.6; volume of sample injected: up to 1 mL) was used in this study to purify Caf1 WT and Caf1 mutants. Caf1 proteins were eluted in the void volume (V_0 = 47 mL) of the gel filtration column and the total volume was 113 ml (V_T = 113 ml). The data for standard protein markers for the gel filtration chromatography are presented in the **Table 3.2** and **Figure 3.16**. Caf1 proteins, WT and mutants form large molecules with very high molecular weight and are eluted in the void volume. For some, Caf1 proteins, more than one peak was detected.

Table 3.2 – Protein standards used for the calibration of Superdex-200 column and Caf1 proteins, supernatant (SUP) and flocculent layer (FL) loaded in the same column.

Protein	Molecular weight (MW) (kDa)	Log_{10} MW	V_e (mL)	Distribution coefficient (K_D) $K_D= (V_e-V_0)/(V_T-V_0)$
Carbonic Anhydrase	29	1.46	105	0.88
Albumin	66	1.82	98	0.77
Alcohol Dehydrogenase	150	2.18	94	0.71
Beta Amylase	200	2.30	92	0.68
Apoferritin	443	2.65	88	0.62
Thryroglobulin	669	2.82	82	0.53
Caf1 WT (SUP)	>700 >700	5.2 -5.2	43.34 49.26	(-0.055) 0.034
Caf1 RGDS L1(SUP)	>700	5.1	45.74	(-0.019)
Caf1 RGDS L2(SUP)	>700	-5.06	47.02	0.0003
Caf1 RGDS L3(SUP)	>700 >700	-5.2 - 5.5	50.06 53.90	0.046 0.10
Caf1 RGDS L4(SUP)	>700	5.10	46.22	(-0.012)
Caf1 RGDS L5(SUP)	>700 >700 >700	5.3 5.2 5.3	42.86 48.78 50.85	(- 0.060) 0.026 0.058
Caf1 RGES L5(SUP)	>700	-5.1	47,34	0,005
Caf1 WT (FL)	>700 >700	5.3 -5.3	43.18 50.38	(-0.058) 0.051
Caf1 RGDS L1(FL)	>700 >700	5.3 5.1	43.66 46.86	(-0.050) (-0.002)
Caf1 RGDS L2(FL)	>700	- 5.1	47.63	0.0095
Caf1 RGDS L3(FL)	>700	- 5.1	47.34	0.0051
Caf1 RGDS L4(FL)	>700	5.1	46.86	(-0.002)
Caf1 RGDS L5(FL)	>700	- 5.1	46.54	(0.0069)
Caf1 RGES L5(FL)	>700	-5.2	48.78	0.027

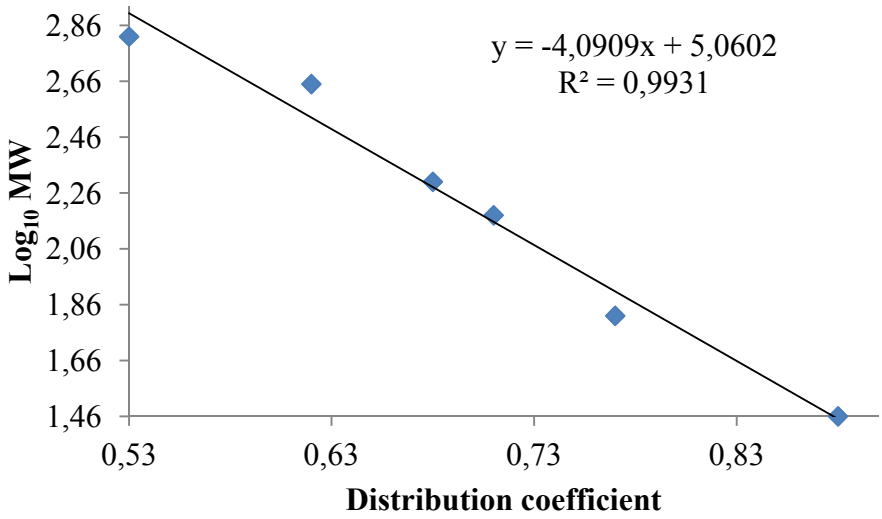

Figure 3.16 - Calibration curve for the Superdex 200 column.

Chromatograms (**Figure 3.17 and 3.18**) show the elution pattern for each sample and each fraction collected in the void volume (47 ml) was loaded on 12% SDS-PAGE (**Figure 3.19**). Analytical gel filtration chromatography (Superdex 200 column) was conducted on Caf1 samples obtained from the supernatant or the flocculent layer. The graphs below (**Figure 3.17 and 3.18**) revealed that Caf1 proteins both, WT and mutants were eluted as large molecules (> 700 kDa) in the void volume. The very high molecular weight of Caf1 proteins did not allow the determination of the size of Caf1 and thus the insertion of Caf1 in the calibration curve (**Figure 3.16**). According to the manufacturer (Sigma-Aldrich) Superdex-200 column has a fractionation range of 10-600 kDa since Caf1 WT proteins are much larger than 600 kDa was likely eluted in the void volume. Here we showed that the Caf1 mutants produced maintain the same high molecular weight that characterise the Caf1 protein. Comparing the chromatographic profiles of Caf1 proteins it is possible to observe that the majority of Caf1 protein produced was present in the supernatant. And in the flocculent layer the quantity of Caf1 proteins is in general much lower than in the supernatant. However, a large amount of Caf1 RGES L5 protein was obtained from the flocculent layer fraction and a smaller amount of this protein was obtained from the supernatant.

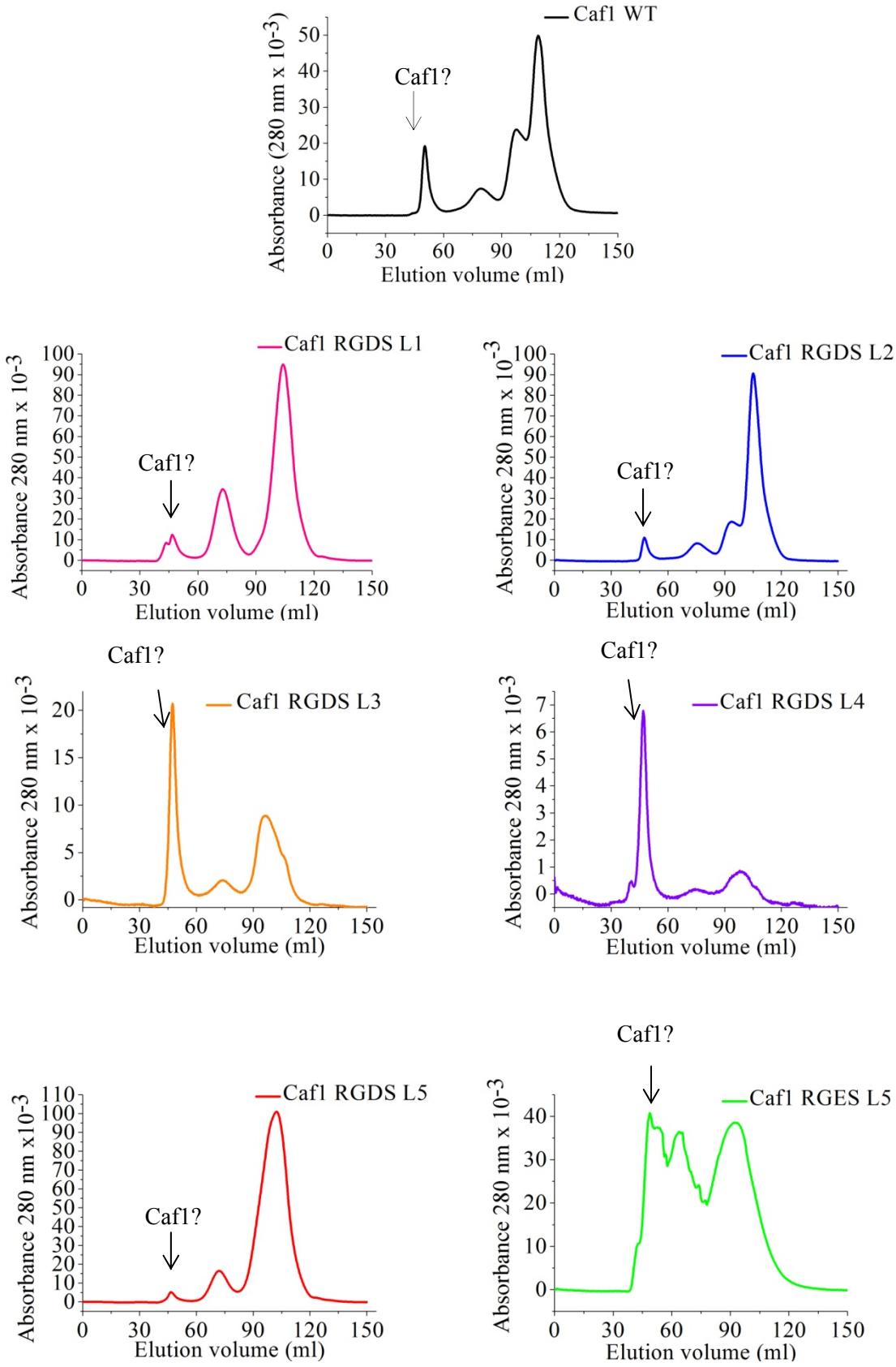

Figure 3.17 – Chromatographic profiles of Caf1 proteins present in the flocculent layer. The Caf1 fractions were applied to a Superdex 200 gel filtration FPLC column.

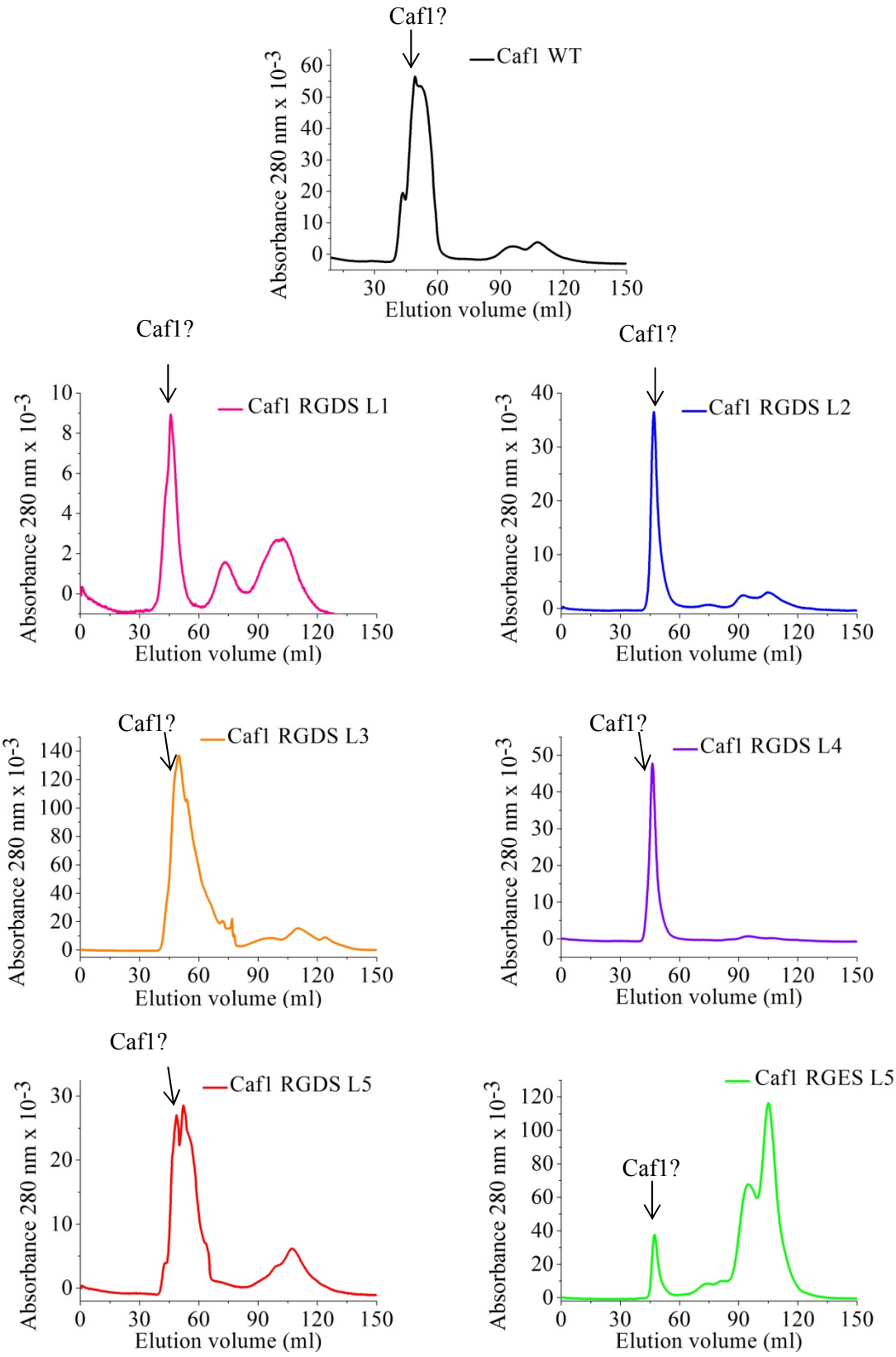

Figure 3.18 – Chromatographic profiles of Caf1 proteins present in the supernatant. The Caf1 fractions were applied to a Superdex 200 gel filtration FPLC column.

A 5 ml sample, containing void volume peak collected as the fraction from 45 to 60 ml was loaded onto a 12% SDS-PAGE (**Figure 3.19**).

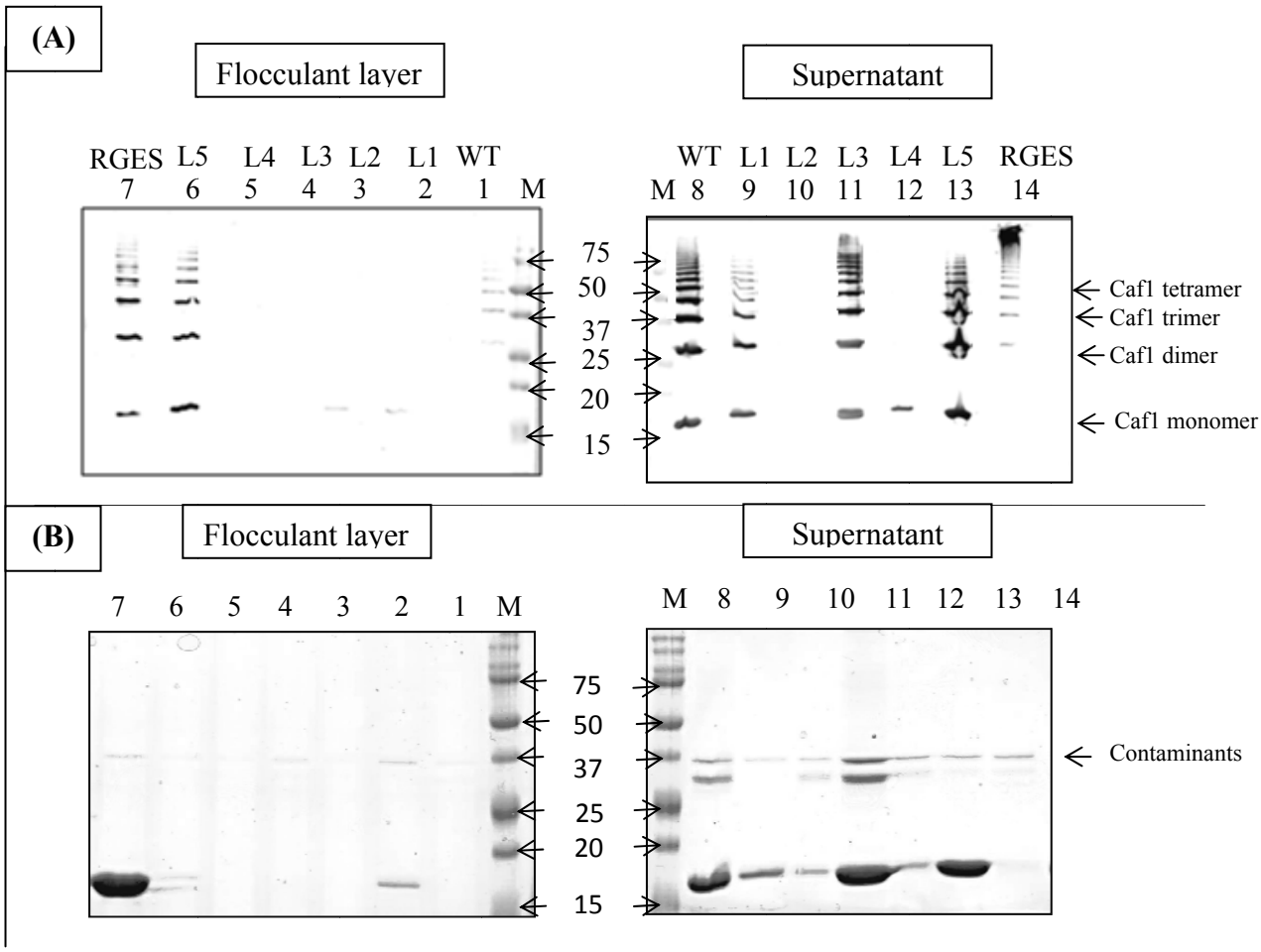

Figure 3.19 – Caf1 protein fractions from Superdex 200 gel filtration FPLC column. (**A)** Western blotting using a mouse monoclonal anti-Caf1 antibody. Caf1 samples in SDS-sample buffer were heated at 95 ºC for 45 seconds (**B)** Coomassie Blue-stained 12% gradient SDS-PAGE of Caf1 fraction. Caf1 samples in SDS-sample buffer were heated at 95 ºC for 5 minutes. **M**, molecular weight marker proteins (molecular mass x 10^3 kDa arrowed); **lane 1**, Caf1 WT present in the flocculent layer; **lane 2**, Caf1 RGDS L1 present in the flocculent layer; **lane 3**, Caf1 RGDS L2 present in the flocculent layer; **lane 4**, Caf1 RGDS L3 present in the flocculent layer; **lane 5**, Caf1 RGDS L4 present in the flocculent layer; **lane 6**, Caf1 RGDS L5 present in the flocculent layer; **lane 7**, Caf1 RGES L5 present in the flocculent layer; **lane 8**, Caf1 WT present in the supernatant; **lane 9**, Caf1 RGDS L1 present in the supernatant; **lane 10**, Caf1 RGDS L2 present in the supernatant; **lane 11**, Caf1 RGDS L3 present in the supernatant; **lane 12**, Caf1 RGDS L4 present in the supernatant; **lane 13**, Caf1 RGDS L5 present in the supernatant; **lane 14**, Caf1 RGES L5 present in the supernatant.

After size exclusion chromatography, the Caf1 protein fractions were analysed by SDS-PAGE and western blotting (**Figure 3.19-A and B**). From the western blotting analysis we could verify that Caf1 WT, Caf1 RGDS L1, Caf1 RGDS L3, Caf1 RGDS L5 and Caf1 RGES L5 formed polymers as shown by the ladder (**Figure 3.19-A**) From the analysis of the SDS-PAGE we could observe that there were other bands in addition to the Caf1 monomer present on the gel (**Figure 3.20-B**). This showed that the first purification was not enough. A second size exclusion purification was conducted in order to purify the Caf1 proteins. The result of the second Caf1 purification is shown in **Figure 3.21**. The Caf1 WT and Caf1 RGDS L5 gel bands were sent to mass spectrometry to confirm their identity (**Figure 3.20**).

(A)

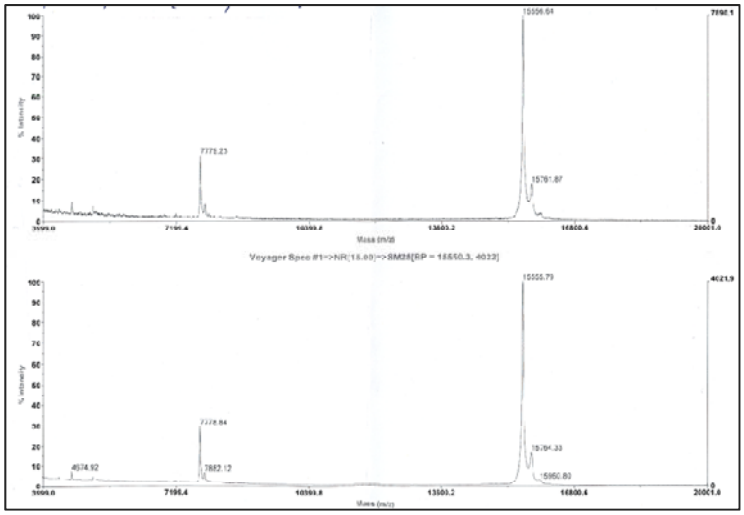

(B)

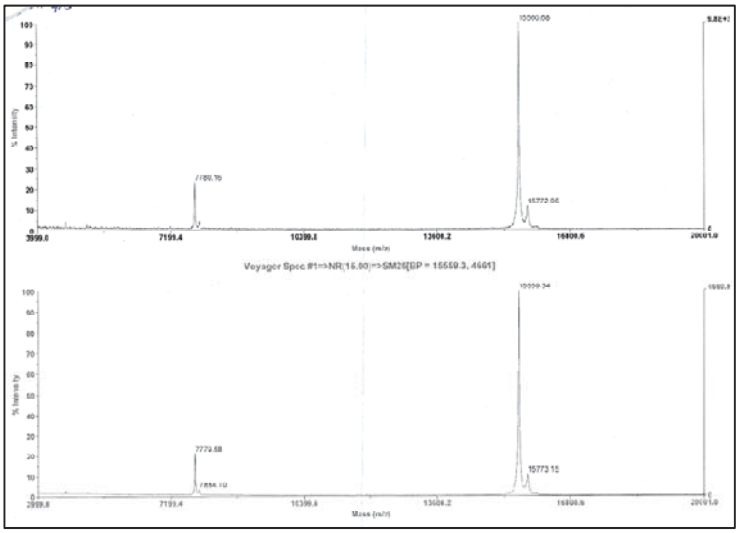

Figure 3.20 - The peptide mass fingerprinting of Caf1. (A) Spectral masses (in mass per charge unit, *m*/*z*) of Caf1 WT obtained by MALDI-TOF mass spectrometry **(B)** Spectral masses (in mass per charge unit, *m*/*z*) of Caf1 RGDS L5 obtained by MALDI-TOF mass spectrometry.

After a second purification procedure, the total Caf1 yield is presented in the **Table 3.3**. Observing the values obtained by the measurements using the spectrophotometer after purification it's evident that most Caf1 proteins are obtained from the supernatant.

Table 3.3 - Total yield of pure Caf1 from *E. coli* BL21 (DE3)/pGEMCaf1.

Source of Caf1	**F1 Yield (mg/liter)**
E.coli BL21(DE3)/pGEMCaf1 WT	
Layer	0.34
Supernatant	2.37
E.coli BL21(DE3)/pGEMCaf1 RGDS L1	
Layer	0.27
Supernatant	0.4
E.coli BL21(DE3)/pGEMCaf1 RGDS L2	
Layer	0.058
Supernatant	0.5
E.coli BL21(DE3)/pGEMCaf1 RGDS L3	
Layer	0.14
Supernatant	0.5
E.coli BL21(DE3)/pGEMCaf1 RGDS L4	
Layer	0.12
Supernatant	0.94
E.coli BL21(DE3)/pGEMCaf1 RGDS L5	
Layer	0.18
Supernatant	1.3
E.coli BL21(DE3)/pGEMCaf1 RGES L5	
Layer	2.8
Supernatant	0.56

The Caf1 WT, Caf1 RGDS L5 and Caf1 RGES L5 proteins were the most pure proteins obtained after size exclusion chromatography. The Caf1 samples were loaded

in the 18% Tris-tricine gels. One of the gels was stained with Coomassie Brilliant Blue and the other gel was probed for Caf1 using a mouse monoclonal anti-Caf1 antibody (**Figure 3.22**).

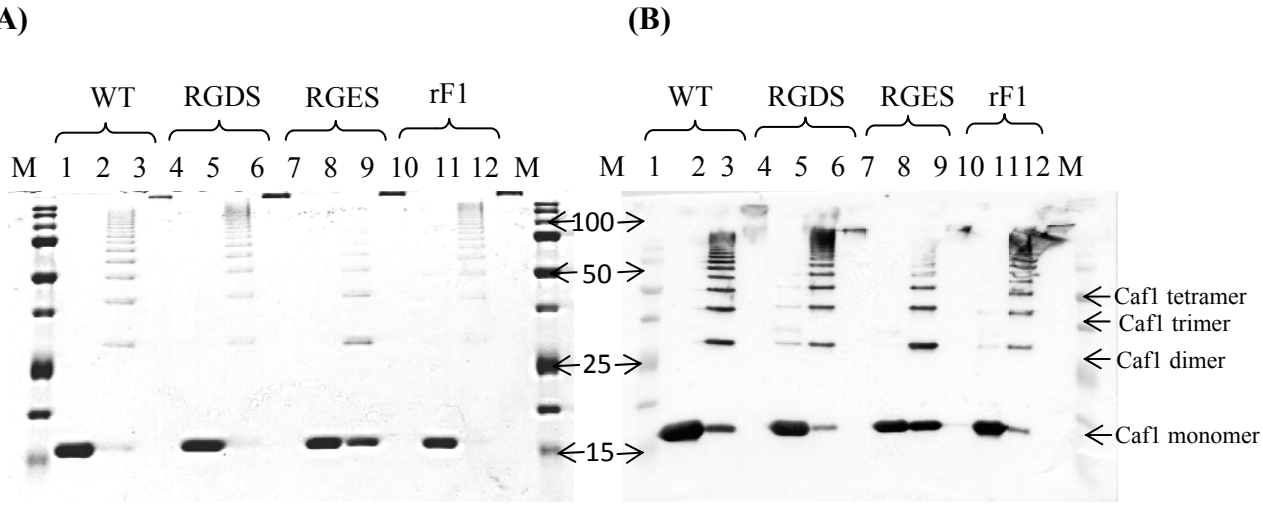

Figure 3.21 – Formation of Caf1 oligomers. (**A)** 18% Tris-tricine gel. (**B)** Western blotting using a mouse monoclonal anti-Caf1 antibody. The Caf1 WT, Caf1 RGDS L5 and Caf1 RGES L5 purified protein fractions were heated at 95 ºC for 45 seconds and 5 minutes. And a non-denature sample of each proteins were loaded as well. **M,** molecular mass marker proteins (molecular mass x 10^3 kDa arrowed); **lane 1**, contained Caf1 WT sample heated at 95 ºC for 5 min; **lane 2**, contained Caf1 WT sample heated at 95 ºC for 45 seconds; **lane 3,** contained Caf1 WT sample non-denatured; **lane 4,** contained Caf1 RGDS L5 heated at 95 ºC for 5 minutes; **lane 5,** contained Caf1 RGDS L5 heated at 95 ºC for 45 seconds; **lane 6,** contained Caf1 RGDS L5 non-denatured; **lane 7**, contained Caf1 RGES L5 heated at 95 ºC for 5 minutes; **lane 8**, contained Caf1 RGES heated at 95 ºC for 45 seconds; **lane 9**, contained Caf1 RGES non-denatured; **lane 10**, contained rF1 heated at 95 ºC for 5 minutes; **lane 11**, contained rF1 heated at 95 ºC for 45 seconds; **lane 12**, contained rF1 non-denatured.(Miller *et al.*, 1998)

The SDS-PAGE and the western blotting (**Figure 3.21**) results were similar for all Caf1 proteins and show that non-denatured proteins do not enter in the separation gel (band at the top of the gel) due to their high molecular weight in a polymeric form. Once the proteins were heated at 95 ºC for 45 sec the Caf1 subunits started to dissociate forming a ladder and after heating the proteins for 5 min in SDS sample buffer the dissociation of the Caf1 monomers was complete forming a single band of

approximately 15 kDa (in SDS the dissociation process of Caf1 is irreversible) (Miller *et al.*, 1998)

A structural characterization of the purified Caf1 proteins was conducted.

Structural characterisation of Caf1 WT, Caf1 RGDS L5 and Caf1 RGES L5 mutants by CD, DSC and TEM.

Circular Dichroism (CD)

Far-ultraviolet circular dichroism (Far-UV CD) spectra of Caf1 WT, Caf1 RGDS L5 and Caf1 RGES L5 are shown in **Figure 3.2**.

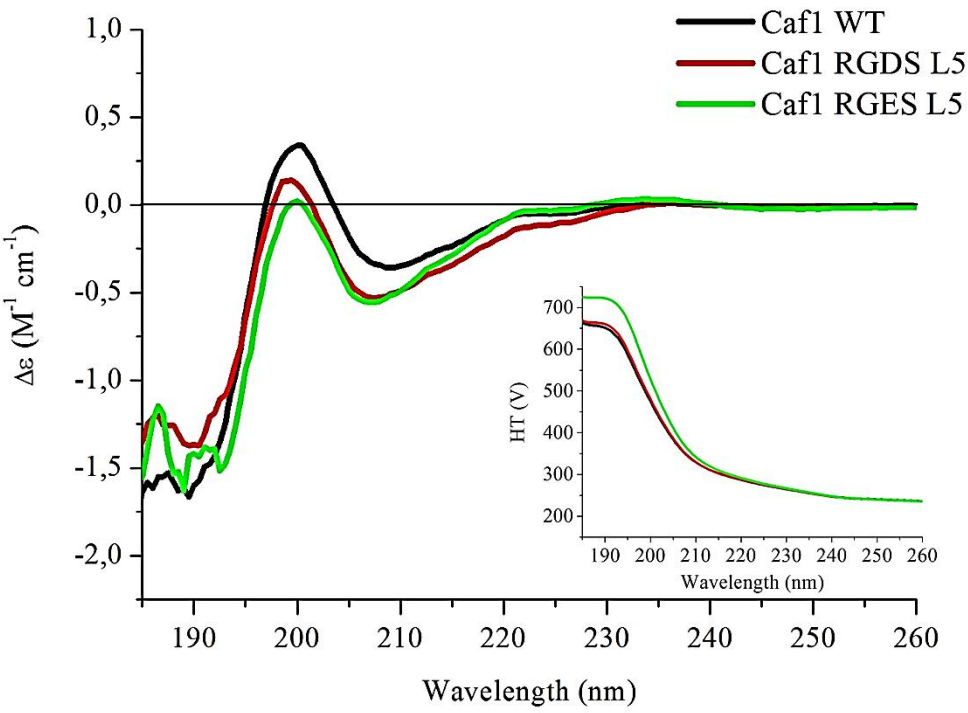

Figure 3.22 - Far-UV CD spectra of Caf1 WT, Caf1 RGDS and Caf1 RGES. Each curve represents the average of 10 accumulated spectra measured at a concentration of 0.5 mg/ml Caf1 (0.05 cm path length cell). The sample contained 50 mM sodium phosphate, pH 7.2. Each spectrum was corrected by subtraction of a comparable blank. The abscissa is in units Δε (M^{-1} cm^{-1}) where M is the molar concentration of amino acid residues. The inserted graph shows the high tension voltage on the photomultiplier for the Caf1 proteins (Miller *et al.*, 1998).

The Far-UV CD spectra of Caf1 WT presented a maximum positive peak at 200 nm and a maximum at 208 nm and negative region between 185 and 197 nm. Compared with Caf1 WT spectrum, the Caf1 RGDS L5 and Caf1 RGES L5 were similar in shape but differed in intensity. The inserted graph shows the high tension voltage which indicates that Caf1 WT and Caf1 RGDS L5 samples have similar concentrations. However, Caf1 RGES L5 has a higher absorbance between 180 and 200 nm, which could be due to the presence of some contaminants. Protein concentration was determined at 280 nm.

The near-ultraviolet circular dichroism (Near-UV CD) spectra of Caf1 WT, Caf1 RGDS L5 and Caf1 RGES L5 are represented in **Figure 3.23**.

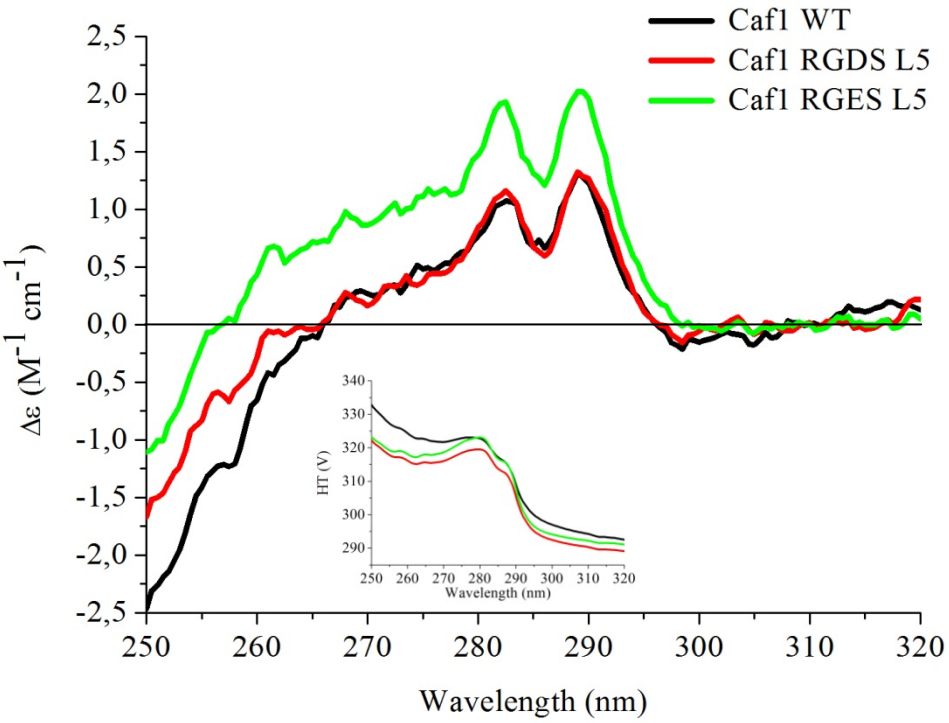

Figure 3.23 - Near-UV CD spectra of Caf1 WT, Caf1 RGDS and Caf1 RGES. Each curve represents the average of 10 accumulated spectra measured at a concentration of 0.5 mg/ml Caf1 (0.05 path length cell). The sample contained 50 mM sodium phosphate, pH 7.2. Each spectrum was corrected by subtraction of a comparable blank. The abscissa is in units Δε (M^{-1} cm^{-1}) where M is the molar concentration of amino acid residues (Chalton *et al.*, 2006).

The near-UV spectrum of Caf1 is characterised by two minor peaks at 262 and 269 nm and two major peaks at 283 nm and 290 nm. Both minor and major peaks are positive and well-spaced. The near-UV CD spectra of Caf1 WT, Caf1 RGDS L5 and Caf1 RGES L5 have identical peaks shape. However the spectrum of Caf1 RGES L5 shows a different intensity again possibly due to the presence of contaminants.

The thermal unfolding of Caf1 proteins was analysed by Far-UV circular dichroism (CD) (**Figure 3.24**) and differential scanning calorimetry (DSC) (**Figure 3.25**).

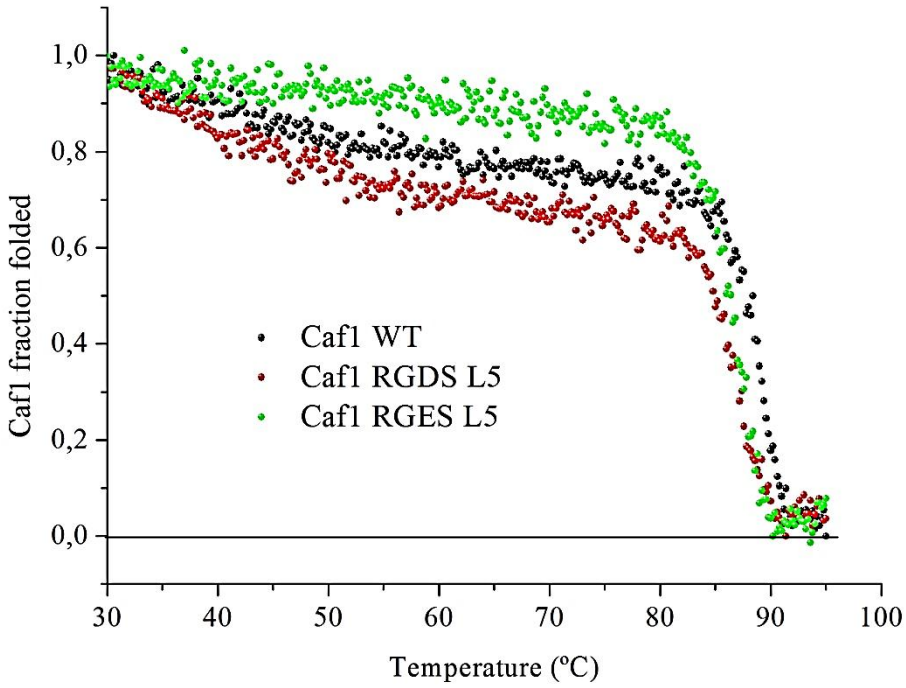

Figure 3.24 - Analysis of thermal unfolding profiles of Caf1 WT, Caf1 RGDS L5 and Caf1 RGES L5. The CD signal at 202 nm corresponds to the characteristic peak in the Far UV spectrum and is particularly sensitive to changes in the secondary structure of Caf1 proteins. Thermal far-UV CD analyses were measured at 202 nm by increasing the temperature from 25 ºC to 95 ºC at a constant rate of 1 ºC/min.

DSC was conducted at temperatures between 25ºC and 95 ºC at a constant heating rate of 1 ºC/min to determine the mid-point temperature of unfolding (Tm). **Figure 3.25** shows the DSC thermograms of Caf1 proteins.

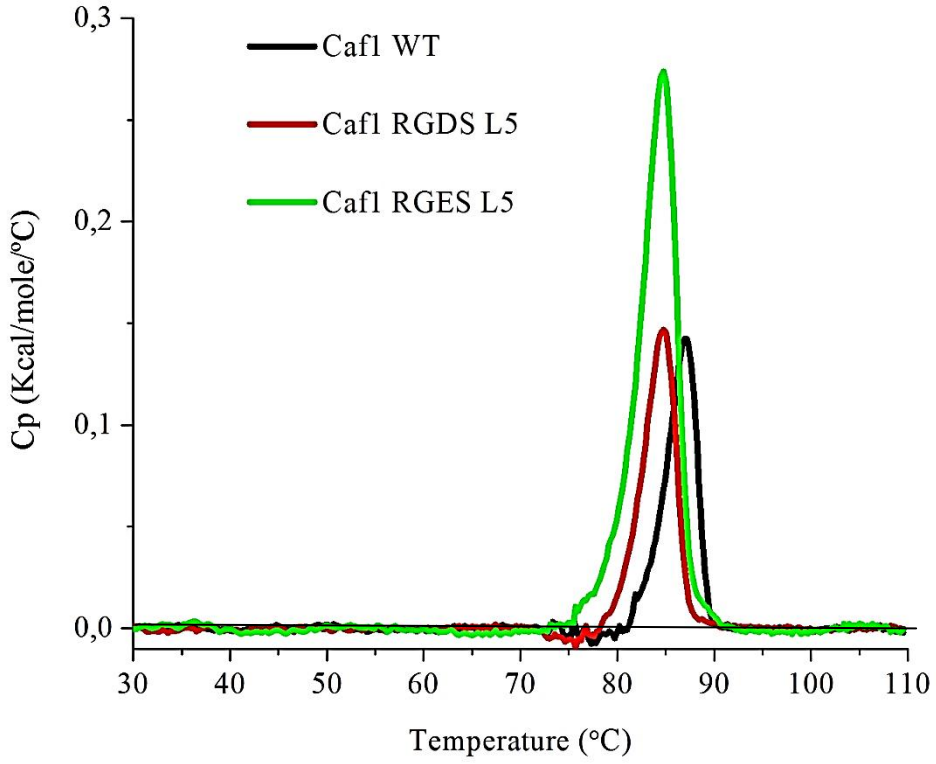

Figure 3.25 – Differential scanning calorimetry of Caf1 WT, Caf1 RGDS L5, Caf1 RGES L5. The thermal transitions of Caf1 proteins are represented by peaks. The apexes of the peak correspond to the melting temperature (Tm). The thermograms of Caf1 proteins were buffer corrected. The protein samples were diluted in 50 mM phosphate pH 7.2 to a final concentration of 0.3 mg/ml.

Differences in the measurements by CD and DSC revealed that the Caf1 RGES L5 sample might present some contaminants. The UV-visible spectrophotometer measurements between 240-320 nm show the spectrum of the Caf1 proteins used in this study, Caf1 WT and Caf1 RGDS L5 present similar curves however Caf1 RGES L5 shows a higher broad peak between 250 and 280 nm.

Table 3.4 – The thermal stability of Caf1 WT, Caf1 RGDS L5 and Caf1 RGES L5 was measured by CD and differential scanning calorimetry.

	DSC *Tm* (ºC)	CD *Tm* (ºC)
Caf1 WT	86	83
Caf1 RGDS L5	84	83
Caf1 RGES L5	83	81

Measured by CD, Caf1 WT and Caf1 RGDS L5 unfold with a transition temperature (T_m) of 83 °C compared to Caf1 RGES L5 at 81 °C. Data obtained by differential scanning calorimetry showed the T_m of 86 ºC for Caf1 WT, T_m of 84 ºC for Caf1 RGDS L5 and T_m of 83 ºC for Caf1 RGES L5.

The Caf1 WT, Caf1 RGDS L5 and Caf1 RGES L5 fibres were observed by transmission electron microscopy using the negative staining procedure (Harris, 1997 and Soliakov *et al*., 2010). In general the Caf1 proteins visualised were long and extremely flexible fibres as judged by their disorder on the grid (**Figure 3.26**).

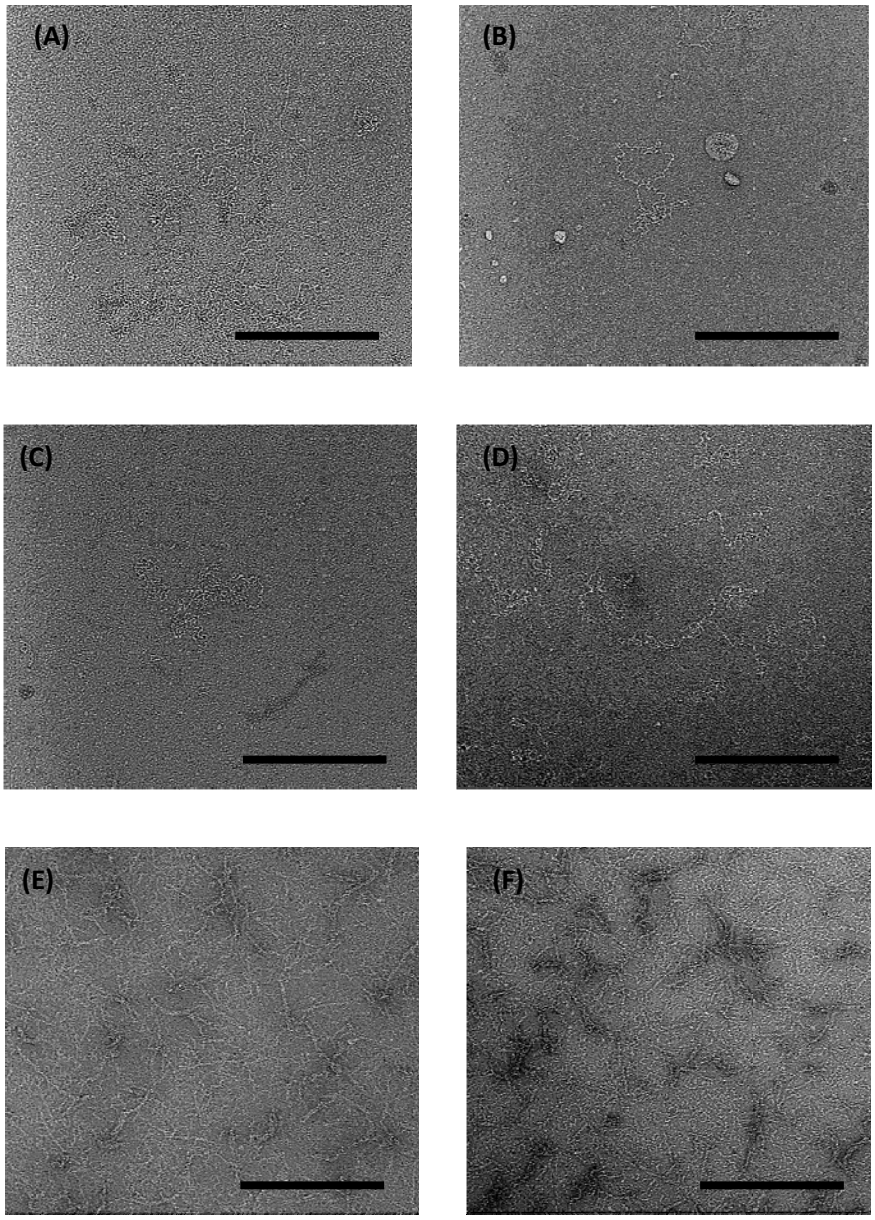

Figure 3.26 – Transmission electron microscopy of Caf1-WT, Caf1 RGDS L5, Caf1 RGES L5. The images show long flexible Caf1 polymers stained with 2% (w/v) uranyl acetate. The images were captured using the Philips CM100 transmission electron microscopy, operated at 100 kV and using a magnification of 130000 x. Scale bar indicates 100 nm in all scales. **(A)** and **(B)** Caf1 WT; **(C)** and **(D)** Caf1 RGDS L5; **(E)** and **(F)** Caf1 RGES L5.

The Caf1 WT, Caf1 RGDS L5 and Caf1 RGES L5 fibres length were analysed by Jmicrovision software version 1.2.5. (Roduit, 2007) using the analysis 1D toolbox. The length of the fibres were analysed following the procedure described in Soliakov *et al.*, 2010. Due to the high degree of aggregation of free Caf1 fibres it was not possible to

determine accurately the length distribution of Caf1 fibres, thus the Caf1 aggregates were disregarded in this analysis. The fibre lengths obtained were represented by box charts (**Figure 3.27**).

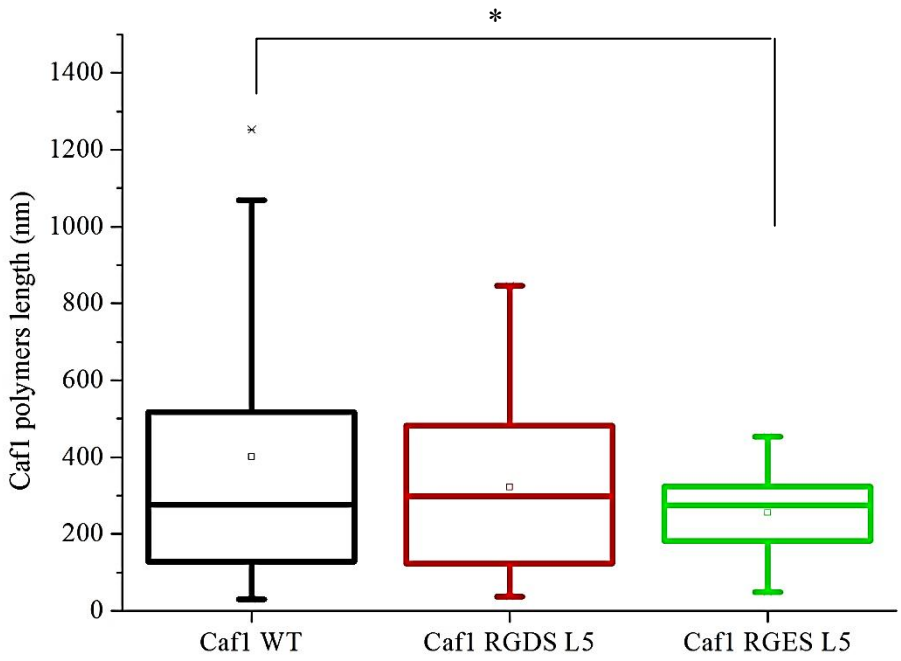

Figure 3.27 - Box charts of Caf1 WT, Caf1 RGDS L5, Caf1 RGES L5 polymers length. The box represents the interquartile range which contains 50% of the values. The whiskers are lines that extend from the box to the highest and lowest values. The line across the box indicates the median. Extreme values are indicated (+). Graphs were obtained using the OriginPro software version 8. Statistical significance was determine by One-way ANOVA analyses were conducted by SPSS version 19 (*) $p > 0.05$.

Figure 3.27 shows the mean of the fibre length determine for Caf1WT was 401 nm, for Caf1 RGDS L5 was 323 nm and for Caf1 RGES L5 was 257 nm.
The maximum fibre length determined for Caf1 WT was 1068 nm, for Caf1 RGDS L5 was 847 nm and for Caf1 RGES L5 was 448 nm.

The box charts of Caf1 proteins show that:

- 25% of the Caf1 WT fibres were longer than 518 nm.
- 25% of the Caf1 RGDS L5 fibres were longer than 464 nm.
- 25% of the Caf1 RGES L5 fibres were longer than344 nm.

- 50% of the Caf1 WT fibres were longer than 276 nm.
- 50% of the Caf1 RGDS L5 fibres were longer than 304 nm.
- 50% of the Caf1 RGES L5 fibres were longer than 282 nm.

- 25% of the Caf1 WT fibres were shorter than 142 nm.
- 25% of the Caf1 RGDS L5 fibres were shorter than 128 nm.
- 25% of the Caf1 RGES L5 fibres were shorter than 184 nm.

3.3. Discussion

The *caf* operon was successfully cloned into pGEMT-easy vector. The Caf1 was expressed and a flocculent layer containing Caf1 was observed.

In this study, a set of primers were designed to amplify the entire *caf* operon from pAH34L and a band corresponding to the size of *caf* operon (approximately 5 kb) was excised from the agarose gel, the DNA was purified and analysed by restriction analysis. Then, the ligation of the *caf* DNA insert into the vector was performed.

For this work, we chose pSMART vector (Lucigen) due to its small size, suitability for site-directed mutagenesis and to the absence of transcription in or out of the inserted DNA. However, all the attempts to clone *caf* operon into the pSMART vectors were unsuccessful. The reasons for the difficulty to clone are not well defined; one of the explanations could be the instability of the DNA sequence cloned, which was not supported by this vector. Therefore, we chose the pGEM-T Easy (Promega) to clone the *caf* operon and the expression of *Caf1* from the pGEMCaf1 vector was high. Although pGEM-T Easy vectors are not generally used for protein expression due to the lack of a ribosomal binding site and thus poor translation, the *caf* operon sequence includes a well conserved Shine-Dalgarno sequence, TAAGGAGGT located 7 bp before the initiation codon of *Caf1* gene. In addition, it contains a region upstream of the ribosome-binding site for *Caf1* gene has putative promoter sequences similar to the *E. coli* consensus sequences (Galyov *et al.*, 1991).

Results provided by gene sequencing have shown that the nucleotide sequence of the *Caf1* cloned into pGEM-T Easy was identical to the previously reported sequence from *Yersinia pestis* strain 482 plasmid pMT1 *caf* operon, complete sequence (GenBank accession number, AY450847). The identity and integrity of the DNA insert was also analysed by restriction analysis using the *Hin*dIII and *Bam*HI restriction enzymes which cut the *caf* operon, at 3490, 1053, 707 bp and 1520, 3731 bp, respectively (**Figure 3.1**). The *Eco*RI restriction enzyme does not cut the *caf* operon as indicated in the restriction map for the *Yersinia pestis caf* operon. The restriction analysis using E*co*RI restriction enzyme, which has two restriction sites in the pGEM-T Easy vector and able to release the insert, showed two bands: one band with about 3 Kb which is approximately the size of pGEM-T Easy vector and the second band slightly above 5 Kb which might correspond to the *caf* operon insert (**Figure 3.1**).

The expression of *Caf1* from its own temperature dependent promoter using the pGEMCaf1 plasmid, followed by centrifugation revealed the presence of a flocculent layer. Miller *et al*., 1998 observed this flocculent layer and found that it contained Caf1 protein. We subsequently isolated the flocculent layer and ran it on SDS-PAGE. The gels were either stained with Coomassie Brilliant Blue or probed for Caf1 using a monoclonal anti-Caf1 antibody. A significant band just above 15 kDa was observed. This band was excised from the Coomassie stained gel, destained and sent for mass spectrophotometry. Peptide Mass Fingerprinting (PMF) procedure was conducted in order to determine the masses of the peptide fragments, after enzymatic digestion (trypsin). The masses are searched using a database query tool (Mascot) that allows the identification of the protein with a high degree of statistical significance. A score of 71 and sequence coverage of 50% was obtained for F1 capsule antigen *Yersinia pestis* with a mass of 17.655 kDa. This result agreed well with previous studies which reported a predicted size of 17.0-17.6 kDa (Galyov *et al.*, 1990).

Small peptides were successfully inserted into Caf1 polymer.

The goal of this chapter was, for the first time, to mutate Caf1 fibres with small peptides from extracellular matrix proteins. The small size of the RGDS peptide and its well-known adhesion role on mammalian cells were the two main reasons to choose this motif to be inserted into the Caf1 loops. Also Caf1 resembles fibronectin domains that contain RGDS. From previous work on the Caf1 assembly/secretion pathway and also from Soliakov and co-workers (Soliakov *et al.*, 2010) studies on the tertiary and quaternary structure of Caf1, it was expected that mutations on Caf1 to obtain hybrid long fibres would be a demanding work. It was uncertain whether the usher would accept the changes.

The mutations were made using the $Caf1_N$:Caf1M:Caf1 complex as a model (PDB file: 1Z9S) and the PyMOL software (**Figure 3.8**). The RGDS motif was incorporated through the minimum number of deletions, substitutions and additions of peptides in order to not change the structure of Caf1. The decision to mutate the loops of Caf1 was made based on the higher accessibility of the RGDS motifs to the cells and also to avoid important sites of Caf1M:Caf1 and Caf1A:Caf1 interaction, such as the conservative Arg-20 in Caf1M together with the G1 β-strand of Caf1M anchor the C-

terminus of Caf1 subunit in a donor strand complementation interaction. Also, the N-terminal of Caf1 is associated with the self-assembly of Caf1 subunits.

Five Caf1 mutants with RGDS motifs (cell adhesive peptide), one mutant with a RGES motif (which is a cell non-adhesive peptide control) and three mutants with a single cysteine residue were constructed. The results obtained from DNA sequencing confirmed the insertion of the RGDS motif in each of the five Caf1 loops, and also the incorporation of the RGES in the loop five of Caf1 and the substitution of a single residue of Caf1 loops 1, 4 and 5 to a cysteine residue.

Caf1 does not have cysteine residues in its amino acid sequence. The incorporation of at least one cysteine into the Caf1 polymer might provide us the possibility to couple fluorophores for Caf1 detection, quantification and to cross-link the fibres.

Some of the Caf1 RGDS mutants and the single RGES mutant produced a flocculent layer containing Caf1 fibres. The mutants Caf1 RGDS L2, Caf1 G35C, Caf1 G79C, Caf1 G94C did not produce Caf1 polymers although monomeric protein was observed in the cytoplasm or periplasm.

It was an interesting result that not all mutants expressed Caf1 (**Figure 3.11**).This could give insights into the Caf1 polymerization process, since some of the mutations might prevent proper Caf1 assembly and secretion outside the cells. Extreme cases like the RGDS mutation in the loop 2 of Caf1 completely prevented the expression of Caf1 considering the result obtained by western blot. We should not disregard the possibility that Caf1 gene was expressed however it might be immediately degraded by cytoplasmic proteases (Derynck *et al.*, 1984). However, the expression of Caf1 RGDS L2 might be very low, a fact that could also justify the almost total absence of Caf1 RGDS L2 in the cytoplasm and consequently in other cellular fractions.

The levels of Caf1 expression varied considerably. Our initial assumption of a linear relation between the size of the flocculent layer and amount of Caf1 (relative density) presented in the flocculent layer was not observed. In contrast, the size of the flocculent layer was slightly higher on pGEMCaf1 WT and pGEMCaf1 RGDS L5. However, the quantity of Caf1 detected in the flocculent layer of the pGEMCaf1 WT was lower than in the flocculent layer of the pGEMCaf1 RGDS L5. This result agreed well with an initial *in vitro* study which suggested that the Caf1 capsule is released from

the cells (Englesberg *et al.*, 1954) more recently many other studies have shown the same result (Andrews *et al.*, 1996; Miller *et al.*, 1998).

For the mutants pGEMCaf1 RGDS L1 and pGEMCaf1 RGDS L3, although the size of the flocculent layer was similar the Caf1 content in the flocculent layer was different; the Caf1 RGDS L1 was presented in more quantity in the flocculent layer than Caf1 RGDS L3. This result might suggest that mutations in the loop 3 of Caf1 can have a more severe effect on Caf1 assembly.

Even though the pGEMCaf1 RGDS L4 presented the smallest size of the flocculent layer, the quantity of Caf1 detected in the flocculent layer was very high. This result was not consistent with the other fractions of Caf1 RGDS L4.

In order to understand better what could be behind the differences in the levels of the Caf1 expression sub cellular fractionation studies (**Table 3.1, Figure 3.13**) were conducted by cold osmotic shock. Since the assembly of Caf1, as described before, is a long process (i) starting in the cytoplasm with the expression of Caf1; (ii) secretion of Caf1 across the inner membrane through the Sec pathway to the periplasm; (iii) formation of the Caf1:Caf1M complex and (iv) finally the secretion of Caf1 through the outer membrane protein to the cell surface, the strategy here was to analyse the route of Caf1 from the cytoplasm to the outer membrane surface.

We found that most of the Caf1 WT was outside the cells, in the supernatant. Only a small quantity was present in the flocculent layer. This result is consistent with our previous result described above and is consistent in the small- and large-scale cell culture (Miller *et al*., 1998).The flocculent layer contains mainly Caf1 and cell debris/cell lysis including cell membranes and outer membrane proteins (Andrews *et al.*, 1996).

Caf1 RGDS L1 was present in large quantities in the flocculent layer, periplasmic fraction and outer membrane fraction. Only a small quantity of Caf1 RGDS L1 was secreted into the supernatant. It could be that this mutation prevents the correct binding of Caf1 subunits to the usher and therefore, prevents the translocation of the Caf1 RGDS L1 fibres through the outer membrane.

The Caf1 RGDS L2 was not detected in any cellular fraction and the relative density of Caf1 RGDS L4 determined in all cellular fractions was very low. These RGDS mutations in the loop 2 and 4 are close to the N-terminus which might affect the interaction between the Caf1 subunits and the usher. The Caf1 RGDS L3 was found mainly in the supernatant however bound to other proteins.

Runco and co-workers (Runco *et al.*, 2008) found that Caf1A outer membrane protein was only required for both assembly and secretion of Caf1 in *Y. pestis* but not required for Caf1 secretion in recombinant *E. coli* as also observed by Karlyshev and colleagues (Karlyshev *et al.*, 1992b). This was because the levels of Caf1 in the periplasm of *Y. pestis* decreased in the absence of Caf1A and the periplasmic Caf1 levels increased in *E. coli*. The assembly pathway of Caf1 in *E.coli* systems is not well understood. These investigators found that *Y. pestis* possesses a mechanism to sense and respond to the inappropriate accumulation of Caf1 subunits in the periplasm but *E. coli* does not. Thus, in *E. coli* in the absence of Caf1A the release of Caf1 fibres into the culture medium can occur in a non-specific way (Runco *et al.*, 2008).

An assumption that could be made regarding our results is that although Caf1A is present in *E. coli* system, as is the whole *caf* operon, the *E. coli* system does not have a regulatory mechanism to respond to either a high levels of *Caf1* gene expression using the pGEM-T Easy or the accumulation of Caf1 in the periplasm. The folding of Caf1 by the chaperone and the Caf1 fibre assembly can be more or less aggravated by the incorporation of mutations into Caf1.

The expression of Caf1 WT and Caf1 RGES L5 revealed large amounts of Caf1 distributed in different cellular fractions but mainly present in the flocculent layer. The expression of Caf1 cysteine mutants led to an absence of the flocculent layer. The results were confirmed by SDS-PAGE and western blotting using the monoclonal anti-Caf1 antibody. Caf1 G35C L4 and Caf1 R94C L1 Caf1 were not detected in the supernatant and periplasmic fraction of the bacterial cell. However, a low amount of Caf1 was present in the pellet of both mutants. This means that a small quantity of Caf1 is expressed in the cytoplasm and probably degraded by cytoplasmic proteases. Since we did not observe Caf1 cysteine mutants in the periplasm this fact could indicate that Caf1-Cysteine was degraded by periplasmic proteases. For Caf1 G79C L5 a small quantity of Caf1 in the supernatant and a considerable amount of Caf1 present in the periplasmic fraction was detected by western blot. As the Caf1 native structure does not have cysteine residue, the introduction of a cysteine residue in each monomer of Caf1 could lead to the formation of disulfide bridges between Caf1 subunits and Caf1M (which contains two conserved cysteine residues close to the putative binding pocket for the formation of functional Caf1M *in vivo* mediated by DsbA and B and the accumulation of Caf1 in the periplasm (Zavyalov *et al.*, 1997).

The expression and purification of Caf1 proteins need some improvements. About 3 mg/L of pure Caf1 WT protein was produced per litre of culture. Two of the Caf1 mutants, Caf1 RGDS L5 and RGES L5 were expressed and purified.

After analysing the distribution of Caf1 WT and RGDS mutants, a large-scale bacterial culture was performed, followed by purification. The total yield of pure Caf1 proteins was determined using the spectrophotometer (**Table 3.2**). The yield of Caf1 obtained in 1L of culture was low. These results suggested that either *caf* gene expression was unstable in the pGEM-T Easy vector or longer cell culture incubations need to be performed at lower temperatures (30-35 ºC). Further studies to explore the right conditions for Caf1expression in *E. coli* system need to be conducted. This Caf1 instability phenomenon has been seen by Simpson and co-workers (Simpson *et al.*, 1990). Although the yields of Caf1 were generally low, the yield for Caf1 WT was higher than the yields of Caf1 mutants. Among the Caf1 mutants, the yields of Caf1 RGDS L5 and RGES L5 were the highest of all mutants and the most pure. These results confirm that small mutations in loop 5 might have fewer effects on Caf1 assembly and secretion. Nevertheless, more structural studies must be done.

The SDS-PAGE shows that Caf1 WT purification by 25% of ammonium sulphate saturation leads to Caf1 in solution. This result was shown by Wang *et al*., 2008. And by 30% and 40% of ammonium sulphate fractionation, most of the Caf1 is precipitated without many contaminants. And by 50% of ammonium sulphate fractionation some contaminants are precipitated with Caf1.

The size exclusion chromatographic elution profile of Caf1 RGES L5 differs from the WT.

The polymer properties of Caf1 were used to obtain larger quantities of the antigen through gel filtration chromatography by selecting a resin that would allow the isolation of Caf1 in the void volume of the column while retaining the contaminating proteins. Caf1 from *E. coli* were applied to a Superdex-200 preparative gel filtration column. As shown by western blotting, fractions containing the bulk of the Caf1 were recovered consistently at the exclusion limit of the column, more than 700 kDa. While contaminating protein species, as well as minor amounts of Caf1, were present in pooled fractions from the retained volume.

Pure proteins, Caf1 WT, Caf1 RGDS L5 and Caf1 RGES L5 are very thermo-stable proteins forming high-molecular mass polymers.

Our results for the oligomerization are in according with the studies of Miller and co-workers (Miller *et al*., 1998) which have shown that Caf1 in an oligomeric form can be converted to the monomeric form by heating to 95 ºC in the presence of SDS which prevented the re-association of Caf1 monomers into oligomers. The disruption of hydrogen bonds and hydrophobic interactions prevents the oligomerisation of Caf1 (Miller *et al*., 1998). Soliakov and colleagues also found that incubation times between 90 and 105 seconds at 95 ºC promoted the formation of Caf1 oligomers, as a ladder of bands and this dissociation process tended to increase with longer incubation time. After three minutes only Caf1 trimers, dimers and monomers were observed on the SDS polycrylamide gel and after five minutes only the monomeric form of Caf1 was present on the gel (Soliakov *et al*., 2010).

The polymer to oligomer conversion of Caf1 WT, Caf1 RGDS L5 and RGES L5 was conducted by heating the samples at 95 ºC during 45 seconds followed by cooling the samples on ice to stop the Caf1 dissociation. The control was non-denatured and appears as a band at the top of the gradient gel and a sample of denatured Caf1, heated at 95 ºC for 5 minutes appears as a single band with a molecular weight approximately of 15 kDa which corresponds to the Caf1 monomer (as shown in **Figure 3.19**).

The melting temperature obtained for Caf1 WT, Caf1 RGDS L5 and Caf1 RGES L5 by Far-UV CD thermal analysis and DSC were similar and higher than 80 °C which is consistent with previous results (Soliakov *et al*., 2010). The results obtained in this study show that the Caf1 RGDS L5 and Caf1 RGES L5 are slightly less stable than Caf1 WT.

Caf1 WT secondary, tertiary and quaternary structures are similar to Caf1 RGDS L5 and RGES L5.

Analyses of secondary and tertiary structure were conducted by circular dichroism and show that CD spectrum of Caf1 WT, Caf1 RGDS L5 and Caf1 RGES L5 is not usual β-structure. This result supports the proposal by Karlyshev and co-workers (Karlyshev *et al.*, 1992a) that Caf1 had at least 50% β-sheet structure. More recently X-

ray crystallography of the structure of Caf1 has suggested that the protein adopts a tightly folded β-rich IgG fold (Zavialvo *et al.*, 2005).

The far-UV CD spectrum of Caf1 RGDS L5 is similar to the far-UV CD spectrum of Caf1WT. However exhibits a weaker CD signal around 200 nm. This difference in the signal intensity could be due to purity of the sample.

The spectra for near UV CD for the Caf1 WT, Caf1 RGDS L5 and RGES L5 show a general similar structure. The main structural characteristics revealed on the near UV CD spectrum previously (Miller *et al*., 1998; Chalton *et al*., 2006; Soliakov *et al*., 2010) such as the two minor at 262 and 269 nm and major peaks at 283 and 290 nm were observed in this study.

Transmission electron microscopy, using negative stain, revealed that Caf1 polymers (**Figure 3.26**) displayed various shapes, like twisted loops, multiple bends and turns along their length, revealing a highly flexible quaternary structure. Soliakov and co-workers (Soliakov *et al*., 2010) have shown that Caf1 is a highly flexible polymer which can even form 90º turns although long straight sections are also common. Analysis of Caf1 fibre was performed in the Jmicrovision software (Roduit, 2007). We determined the length of Caf1 WT, Caf1 RGDS L5, Caf1 RGES L5 fibres and the mean fibres length was 401, 323 and 257 nm, respectively. Although it was evident, by the box chart of Caf1 WT, that there was a great heterogeneity of Caf1 fibre length; from very short Caf1 fibres and mainly in a circular form (with 142 nm in length) up to very long Caf1 fibres in a more linear form with 1068 and 1290 nm in length (can be seen in **Figure 3.27**). Similar results for Caf1 WT fibre length were observed by Soliakov and colleagues (Soliakov *et al*., 2010) in which the Caf1 WT fibres length are variable and some linear fibres can reach the 1500 nm. In this study we found more groups of fibres and less long individual fibres. This observation, in some cases, compromised the correct determination of the fibre length and linked fibres were ignored. This could mean that longer fibres could be present in the samples but it was difficult to obtain precise measurements. The possible union between fibres is due to the donor strand exchange, which is the process of exchanging donor strands in the acceptor cleft, have been seen by Soliakov and co-workers. They also found that shorter polymers (between 100 and 200 nm in length) have a greater tendency to form closed loops due to either the lack of constraints in fibre flexibility or to the larger number of configurations that

decreased the probability of fibre ends meeting (Soliakov *et al*., 2010). It is possible that the large groups of fibres observed could be a single self-assembled Caf1 fibre. Regarding the Caf1 RGDS L5 and RGES L5 mutants the fibres length was slightly shorter and more homogeneous. This result can be explained by the reduced efficiency of the chaperone-usher system to assemble and secrete the Caf1 mutants.

4. Chapter Four: Studies to Investigate the Mammalian Cell Adhesion to Biomimetic Protein Scaffolds

4.1. Introduction

The extracellular matrix (ECM) provides a surface to which cells can adhere in order to survive, proliferate and function. Studies of cell behaviour, tissue engineering and regenerative medicine have led to the development of synthetic biomaterials such as recombinant ECM proteins and peptides (Badylak *et al.*, 2009).

This chapter seeks to study mammalian cell behaviour, in particular cell adhesion, using two different protein scaffolds which were functionalised through the insertion of ECM motifs to be used in cell culture. One of the protein scaffolds is tmOmpA (commercialised by Orla Protein Technologies) examined by others (Shah *et al.*, 2007 ; Cooke *et al.*, 2008 ; Cooke *et al.*, 2010) as a suitable scaffold for mammalian cell culture, promoting cell adhesion, proliferation and differentiation. The other protein scaffold is Caf1 (described in chapter 3). The application of Caf1 for mammalian cell adhesion will be investigated.

In this work we gave particular attention to cell adhesion which can occur in three phases: attachment, spreading and, finally, formation of focal adhesions and stress fibres (Murphy-Ullrich, 2001).

Cell attachment to ECM ligands is mediated by cell-expressed surface receptors – the integrins, which become active and increase their affinity for their ECM ligands with subsequent formation of actin microfilaments and cell spreading. When cells receive the appropriate signals from extracellular matrix they proceed to organize their cytoskeleton resulting in the formation of focal adhesions and actin-containing stress fibres. Focal adhesions contain structural and signalling proteins which can establish the connection between the terminus of actin and the ECM leading to mechanical and biochemical signals (Parsons *et al.*, 2010). Cell adhesion is essential for cell survival. If the ECM ligand-integrin interactions are disrupted, cells detached from the ECM undergo apoptotic cell death. This can occur naturally by a mechanism designated *anoikis* (from the Neolatin: ἀν- "without", οἰκ- "house", and -σις "trait or attribute" which leads to apo-pto-sis "the state of being without a home" (Frisch and Francis,

1994) to prevent cells to grow in inappropriate locations however some cells can adapt to new ECM conditions and adhere independently as the case of cancer cell (Guadamillas *et al.*, 2011). Cell survival requires both integrin signalling and cell shape namely extended spread morphology (Murphy-Ullrich, 2001) (**Figure 4.1**).

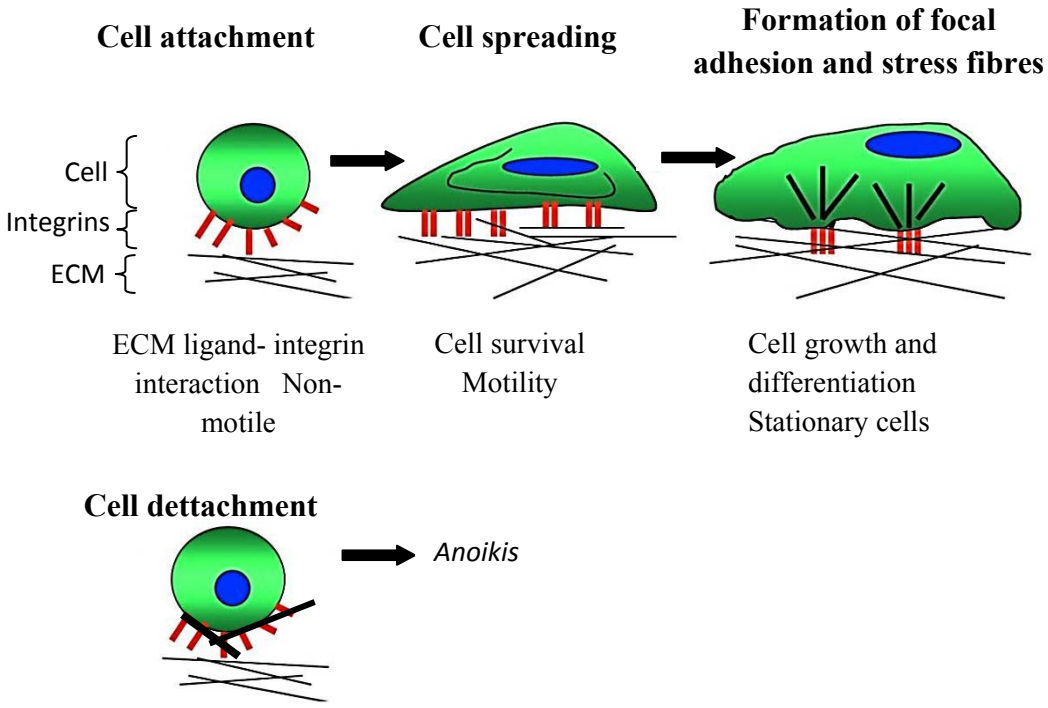

Figure 4.1 – Cell adhesion process comprising three main stages: cell attachment, spreading, and the formation of focal adhesions and stress fibres. Through the process the adhesive strength increases. Initially the cells attach to ECM ligands remaining in a non-motile state until the activation of integrins which triggers a signalling cascade between actin and ECM leading to cell spreading and survival which could imply some cell motility. In a final step the formation of mature focal adhesion and stress fibres occur promoting cell growth, differentiation and leading to cell stationary state (Modified from Murphy-Ullrich, 2001).

Whole ECM proteins are used as substrate to maintain cells in culture, for example type I collagen can be used as a thin film to culture endothelial cells, hepatocytes or other cell lines promoting cell attachment and proliferation (Orwin and Hubel, 2000). Type IV collagen is frequently used for PC-12 cells adhesion (Greene and Tischler, 1976). Furthermore fibronectin can improve cell adhesion through their well-known ligand, RGD that recognises $\alpha_5\beta_1$ or $\alpha_{IIb}\beta_3$ receptors and also proliferation of

fibroblasts, osteoblasts among others cell lines. Nevertheless, the use of these proteins, which are isolated from other organisms, is likely associated with high risk of infections and undesirable immune responses. Moreover, proteins can be proteolytic degraded after a certain time which implies their substitution for new proteins and unfeasible for long-term medical applications (Hersel *et al.*, 2003).

Model substrates that mimic the ECM can provide an alternative scaffold for cell culture or to understand the dynamic between cells and ECM. Among the ECM proteins, fibronectin is a predominant protein of the extracellular matrix which contains several sites for cell adhesion and interaction with other ECM proteins.

Previous studies using engineered proteins containing ECM binding-sites were adhered to flat gold surfaces through thiol chemistry. One of these proteins is the transmembrane domain of outer membrane protein A (tmOmpA) (from Orla Protein Technologies) which can be oriented and immobilised on gold surfaces by a single cysteine residue. This protein has four external loops suitable for the insertion of either short sequences of amino acids from ECM proteins or larger protein domains (Saha *et al*., 2007). The spaces between protein molecules were filled in using thioalkanes to stabilize the core of the protein (Saha *et al*., 2007), keeping the loops containing the ECM motifs exposed to the ligand-integrin receptors interaction, and also to avoid the non-specific protein adsorption on the surfaces (Athey *et al.*, 2005). Cooke et al. (2008) revealed that small peptides from ECM proteins incorporated into tmOmpA loops, e.g. fibronectin, collagen, laminin can mimic the effect of the whole proteins (Cooke *et al.*, 2008). In another study, Cooke et al. (2010) examined how the ECM peptides presented in tmOmpA scaffold can be used to regulate the growth of neurites from PC12 cells and also influence the growing of beta-III-tubulin (a neural marker) positive cells from primary neural stem/progenitor cells (NSPCs) and they found that PC-12 primed with nerve growth factor (NGF), responsible for the PC-12 cells differentiation and formation of neurites, when grown on surfaces coated with tmOmpA containing motifs from laminin, fibronectin, collagen I, and collagen IV, increased their neurite length while the cells on the control synthetic surface (only tmOmpA scaffold) did not. Moreover, motifs for collagen I and fibronectin PHSRN significantly induced the formation of beta-III-tubulin in adult NSPCs above control levels. Thus, ECM motifs presented on tmOmpA scaffold can promote the PC-12 and adult NSPCs differentiation (Cooke *et al.*, 2010).

In this chapter we expanded the studies mentioned above, using a range of different ECM peptides from fibronectin, laminin and collagen I and IV in order to reinforce the potentiality of tmOmpA scaffold as a cell culture system. The results from this study, together with other studies can provide insights to generate new bio-functional scaffolds. In chapter 3 we presented a new scaffold, Caf1 and in this chapter we aimed to investigate it applicability for mammalian cell adhesion. An interesting aspect is the fact that the structure of Caf1fibre is similar to the structure of fibronectin whole molecule.

Although pure Caf1 proteins have in theory low immunogenicity (Soliakov *et al*. 2010), we need to analysed the viability of the mammalian cells in the presence of Caf1 proteins in comparison with other proteins such as fibronectin and collagen.

The specificity of the cell adhesion on surfaces coated with proteins can be addressed by cell adhesion competitive assays using, for example RGD peptides. The small cyclic peptides are preferentially chosen since they are very stable and resistant to enzymatic degradation whereas the linear peptides present slow enzymatic degradation (Fields et al., 1998).

Here, competitive studies were conducted in the absence or presence of Cyclo (RGDfC) (- Arg - Gly - Asp - D - Phe - Cys), $\alpha_v\beta_3$ integrin binding cyclic RGD peptides (Prante *et al.*, 2007) which are polypeptide chains containing the amino and carboxyl termini linked together with a peptide bond that forms a circular chain and can also antagonize the pro-adhesive activities of other matrix proteins (Hersel *et al.*, 2003). They can bind strongly to the αvβ3 and avb5 integrins (Jeschke *et al.*, 2002). The αvβ3 integrin serves as a receptor for a variety of extracellular matrix proteins displaying the arginine-glycine-aspartic acid (RGD) tripeptide sequence (Xiao *et al.*, 2010). The conformation of cyclopeptides is controlled by variation of the ring size, amino acid chirality, N-methylation of peptide backbone, or introduction of constraining structural elements (Haubner *et al.*, 1996). Interestingly, soluble synthetic peptides containing the RGD motif do not mediate cell adhesion or migration, but inhibit the bioactivity of larger peptides containing the RGD peptides apparently by competition for receptor ligation (Akiyama and Yamada, 1985).

The characteristics of the mammalian cell lines used for this study are presented below.

Pheochromocytoma cells (PC-12) were obtained from a solid adrenal gland tumour passaged (pheochromocytoma) subcutaneously in New England Deaconess Hospital strain white rats (Greene and Tischler, 1976).

In growth medium, the PC-12 cells have a round or polygonal shape and tend to grow in small clumps (approximately 10 μm in size). The cells do not extend processes unless they are induced by the nerve growth factor protein (NGF). The apparent doubling time of the PC-12 cells is long at about 48 h. Cell growth is slightly less satisfactory when medium RPMI 1640 was replaced with Dulbecco's Modified Eagle's Medium and unsatisfactory when horse serum was omitted. The appropriate medium for this cell line is RPMI-1640 Medium with foetal bovine serum added to a final concentration of 5% (Greene and Tischler, 1976).

In cell culture flasks the PC-12 cells form floating clusters with few scattered lightly adhered cells. They can adhere in large number to surfaces coated with ECM proteins, namely on tissue culture plates coated with collagen, fibronectin and laminin (Levi *et al.*, 1983).

PC-12 cells express two β_1 integrins: $\alpha_1\beta_1$, and $\alpha_3\beta_1$, which together mediate PC-12 cells attachment on laminin and collagen I and IV (Tomaselli *et al.*, 1990).

This cell line has undergone approximately 70 generations since its isolation and has shown no major changes in cell growth characteristics, morphology, noradrenergic properties, or NGF sensitivity. The homogeneity and near-diploidy of the cell chromosome number suggest that the line will tend to remain genotypically and phenotypically stable *in vitro* for many generations (Kleinman *et al.*, 1982; Kleinman *et al.*, 1986a; Schwarz *et al.*, 1990).

3T3-Swiss albino Fibroblasts (3T3 cell line) was established by Todaro and Green in 1962 from disaggregated Swiss mouse embryos (Todaro and Green, 1963). Cell morphology of the early established lines was virtually indistinguishable from that of normal fibroblasts (approximately 15 μm in size). The 3T3 Fibroblast cell line was always plated at a relatively low cell density and there was little or no cell-to-cell contact prior to establishment. This cell line is sensitive to contact inhibition and ceases growing completely as the culture reaches confluence. Contact inhibition is a property of normal cells lost to some degree both by malignant and by most established cell lines. The cells became progressively more able to form multilayers and interlace with one another (Todaro and Green, 1963).

After being put into Dulbecco's Modified Eagle's Medium with 10% (v/v) bovine calf serum, the doubling time for these cells is approximately 18 h. The cells can attach and grow in plastic flasks without any ECM protein coating. They do not grow well on some types of glass surface (Todaro and Green, 1963).

Fibroblasts express a number of integrins, including α5β1 (the 'classical' fibronectin receptor) and αvβ3 (the 'vitronectin' receptor) (Gailit and Clark, 1996). It is now appreciated that these initial descriptors are not entirely accurate, as fibronectin is also a ligand for αvβ3, as well as for several other integrins (Felding-Habermann and Cheresh, 1993; Newham and Humphries, 1996; Horton, 1997).

Primary osteoblast cultures used in this study were obtained from the parietal bones of foetal rat calvaria (a kind gift of Dr. Mark Birch, Musculoskeletal Research Group, Newcastle University). Osteoblastic cells are large and polygonal (>15 μm in size). This cell line can grow in Dulbecco's Modified Eagle's Medium with 10% (v/v) bovine calf serum; the doubling time for these cultures is approximately 38 h (Wang *et al.*, 1999). The cells can either adhere or grow in plastic flasks or on surfaces coated with ECM proteins.

Osteoblasts and osteoprogenitor cells express multiple integrins; including α1β1, α2β1, α3β1, α4β1, α5β1, α6β1, α8β1, and αvβ3 that bind to numerous extracellular matrix components (Moursi *et al.*, 1997; Gronthos *et al.*, 2001).

The alkaline phosphatase (ALP) and von Kossa stains can be used on osteoblast cultures to examine the expression of ALP and the subsequent matrix mineralization that usually occur in 2 and 3 weeks after cell confluence, respectively (Krause *et al.*, 2000). Importantly, most synthetic materials do not support robust osteoblast activities, compared with natural matrices, and often result in poor cell differentiation and limited bone formation (Krause *et al.*, 2000; Stephansson *et al.*, 2002; Mitchell *et al.*, 2010).

A brief description of the assays and techniques used in this study is provided below.

Calcein AM assay is a tool to assess cell viability and/or cytotoxicity that uses Calcein AM (3',6'-Di (O-acetyl) -4',5'-bis [N,N-bis (carboxymethyl) aminomethyl] fluorescein tetraacetoxymethyl ester), which is a non-fluorescent, hydrophobic compound that can easily penetrates through the cell membrane of live cells due to its lipophilic

characteristics. Calcein AM is hydrolysed by intracellular esterases in the cytoplasm that cleave the ester bonds producing a hydrophilic, anionic and strongly fluorescent compound called Calcein that is well-retained in the cell cytoplasm (Lichtenfels *et al.*, 1994). Among other reagents, such as Carboxy-fluorescein diacetate or bis-carboxyethyl-carboxyfluorescein, Calcein-AM is the most appropriate fluorescent dye for staining viable cells because of its low cytotoxicity (Lichtenfels *et al*., 1994). It's well described that Calcein does not inhibit any cellular functions such as proliferation or chemotaxis of lymphocytes (Wang *et al.*, 1993). The excitation and emission wavelengths of calcein are 490 nm and 515 nm, respectively. Cells grown in black-walled plates can be stained and quantified in less than 2 h and the degree of fluorescence can be correlated with cell viability.

The Cellomics ArrayScan VTI reader is an automated instrument designed for bright field and fluorescence imaging in a controlled environment so that lagre numbers of growing cultures can be analysed robotically.

It is composed of a stage with a microplate insert, allowing processing (e.g. imaging dye combinations) of a 96-well plate in less than four minutes, Carl Zeiss scientific grade digital camera and integrated acquisition and analysis software. Some bio-applications are available to analyse translocations from nucleus to cytoplasm and cytoplasm to membrane, cell growth and motility or compartmental analysis (www.thermoscientific.com).

Scanning electron microscopy is one of the most versatile methods available for the examination and analysis of the structure; including surface topography/morphology, crystalline structure, and chemical composition of heterogeneous organic or inorganic materials on a nanometre to micrometre scale (Vernon-Parry, 2000).

For conventional SEM, the samples need to be electrically conductive and completely dry. This is due to the specimen chamber being at high vacuum. In order to achieve this, samples usually undergo chemical fixation to preserve and stabilise their structure. Standard SEM fixing solutions are glutaraldehyde or Karnovsky's fixative. In some SEM procedures the first fixation step can be followed by a second fixing in osmium tetroxide, which increases the bulk conductivity of the sample. Samples are subsequently dried using a critical point dryer, and finally sputter coated with gold to

further enhance their conductivity. They have to be coated with thin metallic coatings to avoid charging by the accumulation of electrons; here we generally use 15 nm of gold or another conductive material (platinum, osmium) using a Polaron SEM coating unit (Electron Microscopy Research Services, Newcastle University). When the samples are scanned, the electrons (derived from an electron beam thermionically emitted by an electron gun fitted with a metal filament, such as tungsten that can be heated for electron emission) interact with atoms located on the sample surface. The resulting scattering electrons are detected and processed, which leads to high-resolution images illustrating the samples' topography and composition. SEM micrographs appear three-dimensional because of the large depth of field of the SEM as well as the shadow relief effect of the secondary and backscattered electrons (McCann *et al.*, 1993). Three-dimensional images allow direct and high-resolution stereo viewing of surfaces. An analysis of the characteristic X-radiation emitted from samples can yield both qualitative and quantitative elemental information from an area 1 μm in diameter and 1 μm in depth under normal operating conditions (Goldstein and Michael, 2003).

4.2. Results

Our first aim was investigate the effect of small peptides, inserted into the loops of tmOmpA, on cell attachment and proliferation compared with the controls which are only tmOmpA/PEG-thiol/gold (no motifs) and PEG-thiol/gold alone (no protein added to the surface). A screening with 12 different tmOmpA-ECM peptides and 2 controls (tmOmpA and PEG-thiol) was performed (protein concentration of 5 μM). These 14 surfaces (made in triplicate) were used in cell culture for 24 h and 48 h. During the first 24 h we hypothesised that the cells would have enough time to either attach or not to the surfaces presenting different proteins. For that the cells were suspended in serum-free media to avoid non-specific attachment to other proteins from the serum. After 24 h these cells were fixed and stained and further observed by fluorescence microscopy (**Figure 4.2**). The number of cells adhered to the different surfaces was counted (**Figure 4.3**). During the counting of cells we verified that on the surfaces, cells presented at least 5 different shaped-types (**Figure 4.4**). For the next 24 h, we changed the media of the other set of surfaces, and added serum in order to allow cells to proliferate on the surfaces. After 48 h we proceeded to the fixation, staining and counting of cells as described above (**Figure 4.5**). We also observed differences on cell shape on different surfaces.

Increased cell attachment and proliferation on tmOmpA-ECM peptides/PEG-thiol/gold surfaces

Cell attachment on tmOmpA-ECM peptides/PEG-thiol/gold surfaces was determined by staining PC-12 cells with 4',6-diamidino-2-phenylindole (DAPI) which is a nucleic acid stain and Rhodamine-Phalloidin dye, which is a high-affinity probe for F-actin. Fluorescence microscopy was used to visualise the cells in random fields on the gold surface. As shown in **Figure 4.2**, after 24 h more cell attachment was observed on the tmOmpA-ECM peptides/PEG-thiol/gold surfaces than on tmOmpA/PEG-thiol/gold surfaces or PEG-thiol/gold surfaces. After 48 h, on the tmOmpA-ECM peptides/PEG-thiol/gold surfaces, more cells were observed.

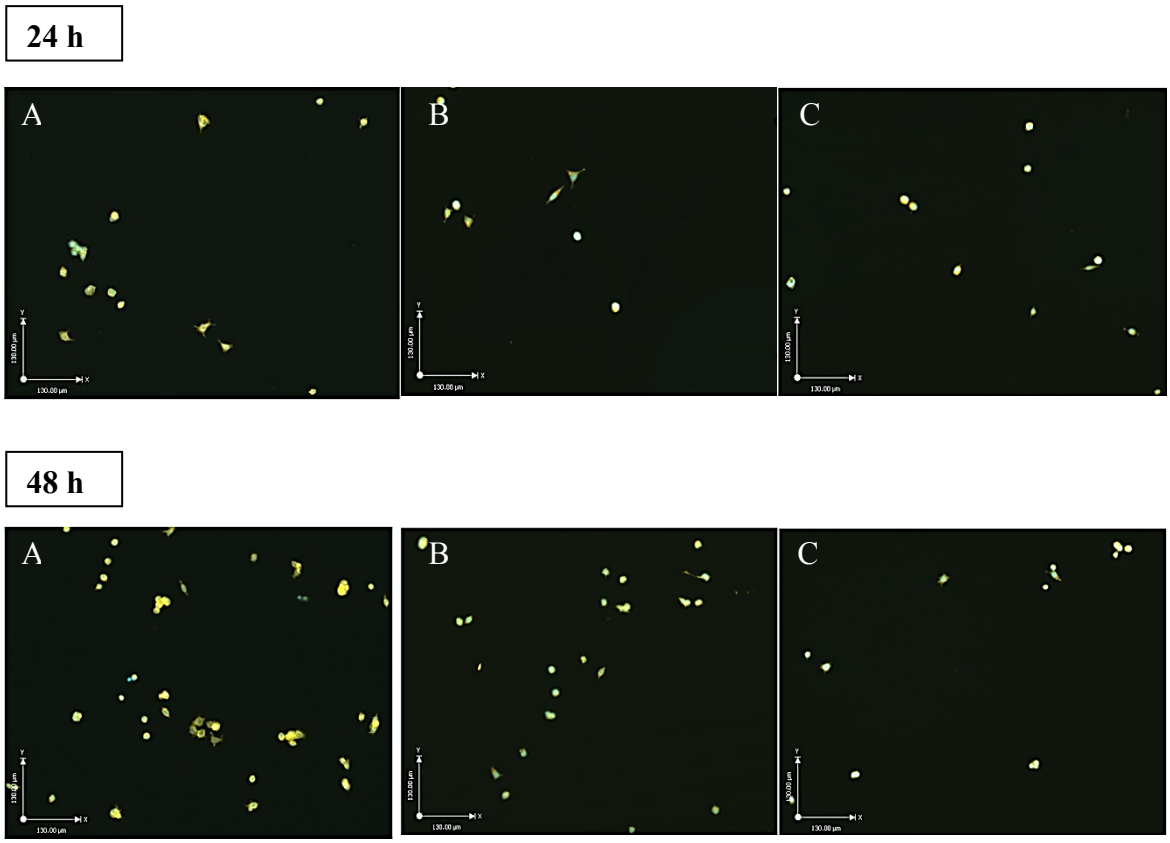

Figure 4.2 - Effect of tmOmpA-ECM peptides on cell attachment and proliferation to the gold surface. PC-12 cells were added on either TmOmpA/PEG-thiol/gold or tmOmpA-ECM peptides/PEG-thiol/gold surfaces and then fixed and stained with DAPI (blue) and Phalloidin (red). The images of fluorescent cells on the surface were collected by fluorescence microscopy at 24 and 48 h. **A** – Cells adhering to tmOmpA-RGDS1/PEG-thiol/gold surfaces. **B** – Cells adhering to tmOmpA-YIGSR/PEG-thiol/gold surfaces. **C** – Cells adhering to tmOmpA/PEG-thiol /gold surfaces (control). Scale bar = 130 μm. Images are representative of three experiments.

The numbers of PC-12 cells adhering to different surfaces coated with tmOmpA-ECM motifs was counted manually after 24 and 48 h. Data represent mean number of cells per field of view (ten randomly selected fields were examined per surface) for three independent experiments (SEM).

As shown in **Figure 4.3**, after 24 h, the number of PC-12 cells adhering to tmOmpA-RGDS2-coated surfaces were significantly more from the number of PC-12 cells adhering to the control surface, OmpA ($P = 0.002$) and Thiol-PEG ($P = 0.001$).

Also the number of PC-12 cells adhering to tmOmpA-MNYYSNS-coated surfaces was significantly more from the number of PC-12 cells adhering to the control surface, OmpA (P = 0.005) and Thiol-PEG (P = 0.003); the number of PC-12 cells adhering to tmOmpA-FHRRIKA-coated surfaces was significantly more from the number of PC-12 cells adhering to the control surface, OmpA (P = 0.001).

Figure 4.3 shows that, after 48 h, the number of PC-12 cells adhering to tmOmpA-RGDS1-coated surfaces was greater than the number of PC-12 cells adhering to the control surface, OmpA (P = 0.025) and Thiol-PEG (P = 0.011). This was also true for tmOmpA-RGDS2 (OmpA (P = 0.011) and Thiol-PEG (P = 0.005)); tmOmpA-MNYYSNS (Thiol-PEG (P = 0.040)); tmOmpA-FHRRIKA (Thiol-PEG (P = 0.036)); tmOmpA-LDVP (OmpA (P = 0.007) and Thiol-PEG (P = 0.003)); tmOmpA-IDAP (OmpA (P = 0.000) and Thiol-PEG (P = 0.000)).

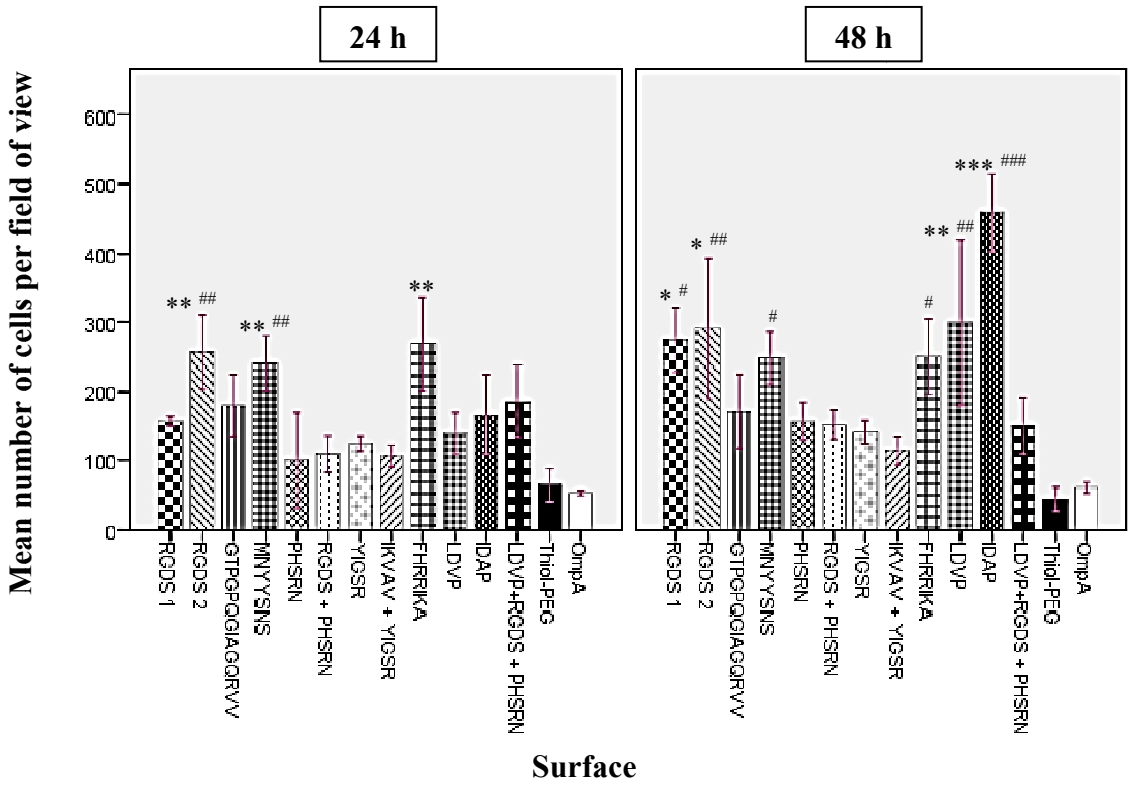

Figure 4.3 – PC-12 cell attachment and proliferation to tmOmpA/PEG-thiol/gold and PEG-thiol/gold (controls) or tmOmpA-ECM peptides/PEG-thiol/gold surfaces. Data representative of three independent experiments; results are mean number of PC-12 cells per field of view ± standard error of the mean (SEM). Ten randomly selected fields were observed per surface. Significance was determined by one way ANOVA analysis with Scheffe post hoc test. (*) $P < 0.05$ compared to OmpA, (**) $P < 0.01$ compared to OmpA and (***) $P < 0.001$ compared to OmpA; ($^{\#}$) $P < 0.05$ compared to Thiol-PEG, ($^{\#\#}$) $P < 0.01$ compared to Thiol-PEG and ($^{\#\#\#}$) $P < 0.001$ compared to Thiol-PEG.

Among the total number of cells that adhered and proliferated on different surfaces (**Figure 4.4**), we verified that a significant number of cells showed either star, oval, round, square, triangle-shapes. PC-12 cells stained with Phalloidin, which binds one of the components of the focal adhesion structures F-actin, showed star-shaped cells containing more than 4 focal adhesions (**Figure 4.4 - A**); oval-shaped cells containing two focal adhesions (**Figure 4.4 - B**); round cells were without visible focal adhesions (**Figure 4.4 - C**); square shaped-cells containing four focal adhesions (**Figure 4.4 - D**) and triangle shaped-cells containing three focal adhesions (**Figure 4.4 - E**).

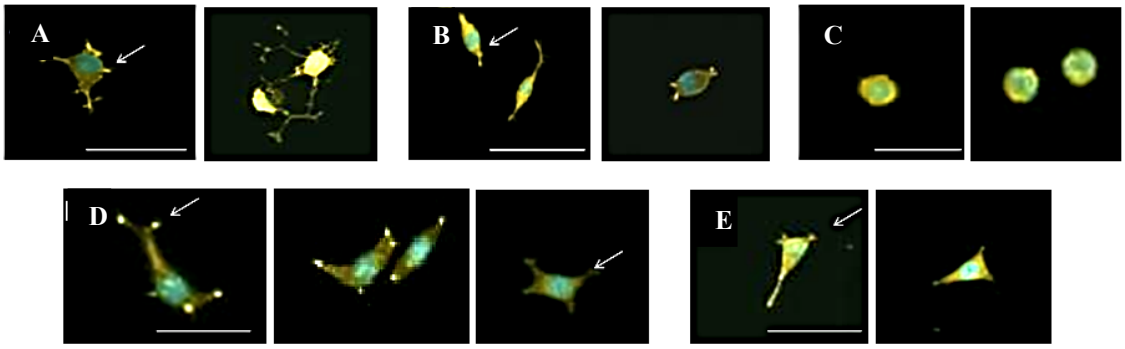

Figure 4.4 – Images of PC-12 cell morphology using fluorescence microscopy. Cells were stained with DAPI (blue) and phalloidin (red). White arrows show focal adhesion. Scale bar = 70 μm. **A –** Star-shaped cells adhered to tmOmpA- RGDS peptide/PEG-thiol/gold surfaces. **B –** Oval-shaped cells adhered to tmOmpA-YIGSR peptide/PEG-thiol/gold surfaces. **C –** Round-shaped cells adhered to a tmOmpA/PEG-thiol/gold surfaces (control). **D –** Square-shaped cells on tmOmpA-MNYYSNS peptide/PEG-thiol/gold surfaces. **E –** Triangle-shaped cells adhered to tmOmpA- LDVP + RGDS + PHSRN peptides /PEG-thiol /gold surfaces.

Figure 4.5 shows that, after 24 h, the number of PC-12 cells, with a non-round morphology, adhering to tmOmpA-RGDS2, tmOmpA-MNYYSNS & tmOmpA-FHRRIKA -coated surfaces was significantly greater than the number of PC-12 cells adhering to the control surface. The number of PC-12 cells, with a round morphology, was not significantly different on surfaces coated with other tmOmpA-ECM and the control surfaces. After 48 h, the number of PC-12 cells adhering to tmOmpA-RGDS1, tmOmpA-RGDS2, tmOmpA-FHRRIKA, tmOmpA-LDVP - tmOmpA-IDAP -coated surfaces was significantly more from the number of PC-12 cells adhering to control surfaces. The number of PC-12 cells, with a round morphology, was not significantly different on surfaces coated with other tmOmpA-ECM and the control surfaces.

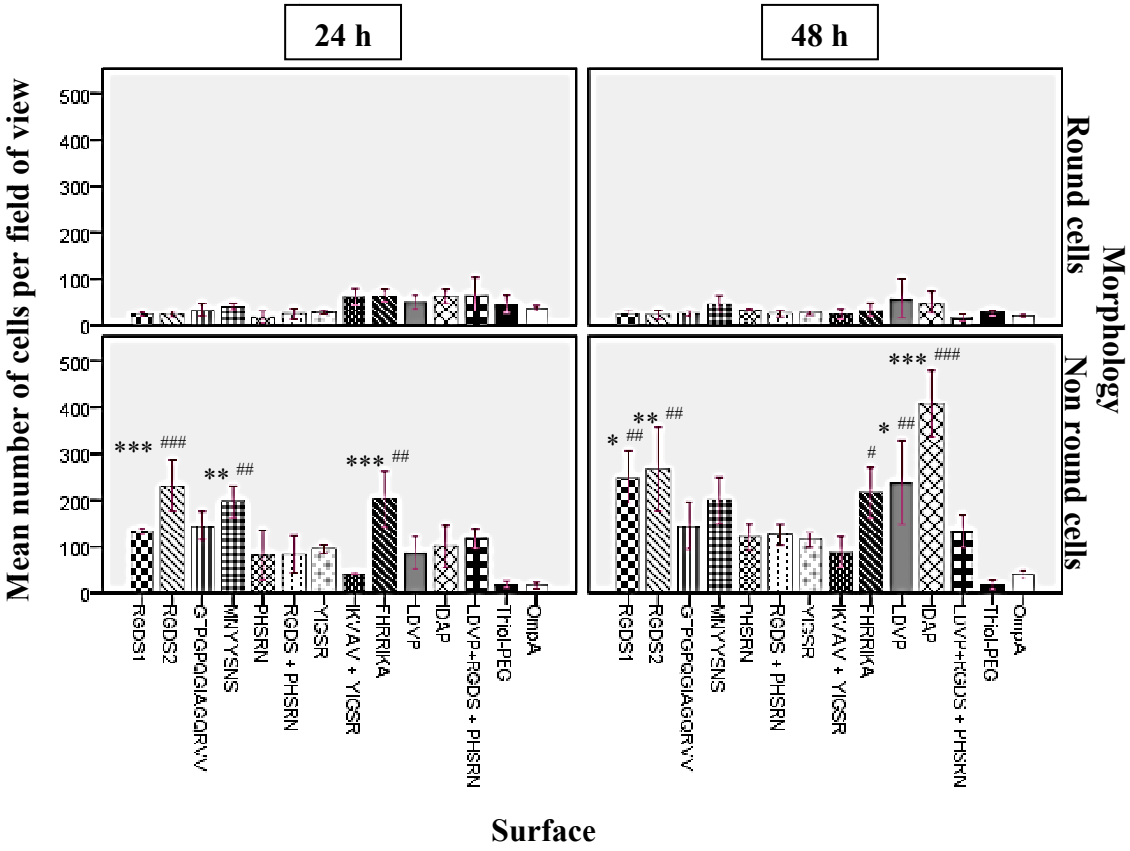

Figure 4.5 – Graph shows the mean number of cells that adhering to different surfaces which presented different shape. Data representative of three independent experiments; results are mean number of PC-12 cells per field of view ± standard error of the mean (SEM). Ten randomly selected fields were observed per surface. Significance was determined by one way ANOVA analysis with Scheffe post hoc test. (*) $P < 0.05$ compared to OmpA, (**) $P < 0.01$ compared to OmpA and (***) $P < 0.001$ compared to OmpA; ($^{\#}$) $P < 0.05$ compared to Thiol-PEG, ($^{\#\#}$) $P < 0.01$ compared to Thiol-PEG and ($^{\#\#\#}$) $P < 0.001$ compared to Thiol-PEG.

The second aim of this initial study was to investigate the effect of different combinations of the tmOmpA-ECM peptides/PEG-thiol/gold surfaces screened before. The results showed above suggested that single tmOmpA-ECM peptides might have some effect on cell behaviour. A study to investigate the effect on PC-12 attachment on gold-coated surfaces containing a combination of two or more peptides using a Press-To-Seal™ silicone isolator with adhesive (24 wells and 2.5 mm diameter) was conducted.

Can the combination of tmOmpA-RGDS peptide and tmOmpA-PHSRN on gold surfaces enhance cell attachment?

Before we began with this study, we tested the Press-To-Seal™ silicone isolator with adhesive using the tmOmpA- FLAG tag (N-DYKDDDDK-C) assembly on gold slides and probed with an anti-FLAG antibody conjugated with alkaline phosphatase. Next we developed the signal using BCIP/NBT alkaline phosphatase substrate solution. The **Figure 4.6** shows individual tmOmpA-FLAG epitope protein spots.

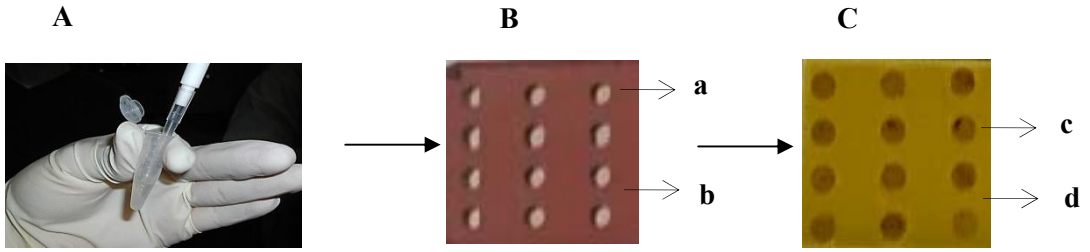

Figure 4.6 – Microspots of tmOmpA-FLAG epitope. A – Five microliters of tmOmpA- FLAG tag (N-DYKDDDDK-C) protein (5 µM) was added to each well; **B -** Press-To-Seal™ silicone isolator with adhesive was adhered to a gold surface, **a -** Gold-coated slide; **b -** Press-To-Seal™ silicone isolator with adhesive (24 wells and 2.5 mm diameter); **C –** After protein assembly on gold surface, the silicone isolator was removed and surface filled in with thiol-PEG molecules for 1 h at room temperature. Anti-FLAG antibody with alkaline phosphatase was incubated for 1 h at RT and BCIP/NBT was added to the surface, **c –** tmOmpA-FLAG epitope protein spots, **d –** Gold-coated slide with PEG-thiol molecules surround the protein.

After we verified that the Press-To-Seal™ silicone isolator adhering to gold-coated surface was suitable for protein immobilization, a study using different concentrations of peptide combinations, tmOmpA-RGDS 2 + tmOmpA-PHSRN was performed. Mixtures of three different concentrations of 0.05, 0.5 and 2.5 µM were applied to the silicone isolator adhered to gold-coated surfaces. Single peptides, at each concentration, were used as controls. PC-12 cells were stained with DAPI and Rhodamine-phalloidin dyes. Number of PC-12 cell adhering to different surfaces was counted manually and data represent mean number of cells per field of view (ten

randomly selected fields were examined per surface) for three independent experiments (SEM).

Figure 4.7 shows that the number of PC-12 cells adhering to surfaces coated with 2.5 µM of tmOmpA-RGDS 2 and 0.5 µM of tmOmpA-PHSRN was significantly more to the tmOmpA at a concentration of 0.05 µM (P = 0.037) and Thiol-PEG (P = 0.020).

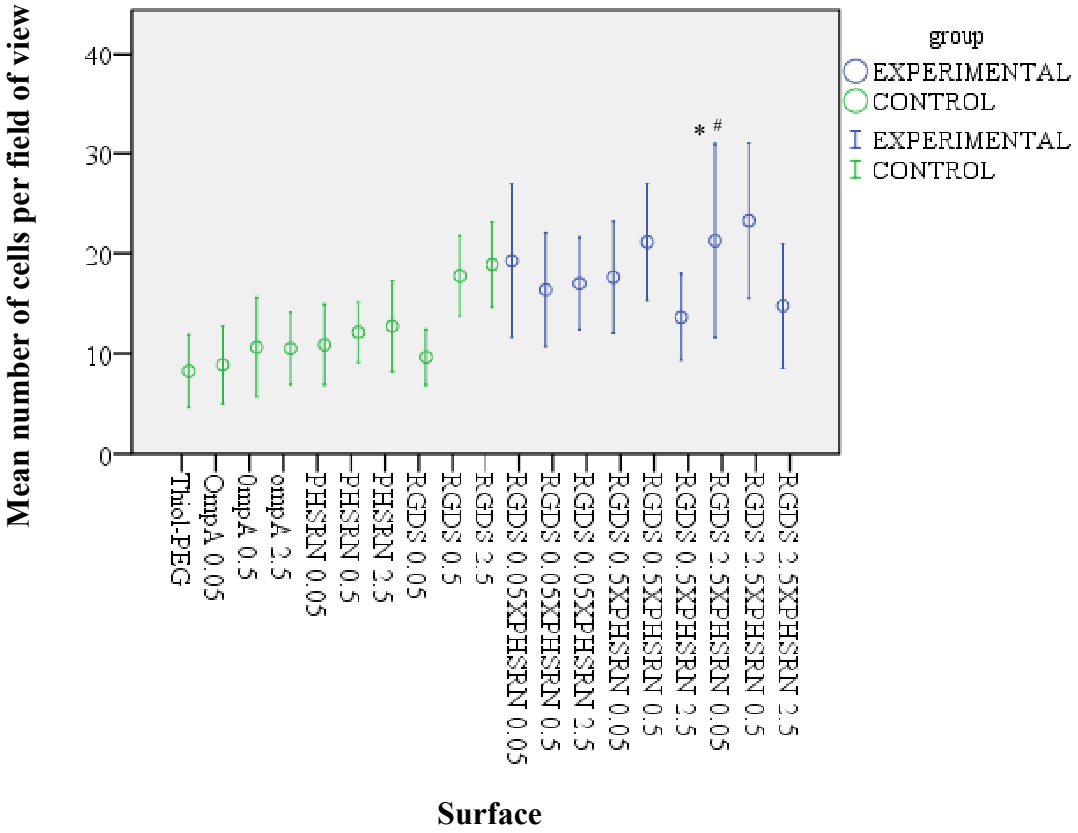

Figure 4.7 – PC-12 cell attachment on different surfaces after 24 h. Data representative of three independent experiments; results are mean number of PC-12 cells per field of view ± standard error of the mean (SEM). Ten randomly selected fields were observed per surface. Significance was determined by one way ANOVA analysis with Bonferroni post hoc test. (*) $P < 0.05$ compared to OmpA at 0.05 µM and ($^{\#}$) $P < 0.05$ compared to Thiol-PEG.

The next study shows an attempt to use Caf1 mutants containing RGDS and RGES for mammalian cell adhesion.

Determination of mammalian cell viability in culture on polystyrene surfaces coated with Caf1 proteins

For this study we used three mammalian cell lines: PC-12; 3T3 Fibroblasts and primary osteoblasts. Each cell line was added to 96-well polystyrene plates (4titude, UK) coated with different proteins including the Caf1 proteins containing the adhesive cell peptide – RGDS, Caf1 proteins containing the non-adhesive cell peptide – RGES and Caf1-WT (without any motif associated). As a positive control, surfaces were coated with fibronectin and collagen IV. As a negative control, surfaces were not coated. Cells were incubated at 37 ºC, 5% CO_2 for 4, 24 and 48 h. The investigation of cell viability; the number of cells adhering to these surfaces; the type of morphology presented and the number of focal contacts formed was conducted.

The **Figures 4.8**, **4.9** and **4.10** show the number of viable cells, of each cell line, adhering to these surfaces after 4, 24 and 48 h of cell culture. The number of viable cells was determined measuring the accumulation of calcein AM, inside the cells.

Figure 4.8 shows that, after 4, 24 and 48 h, the calcein fluorescence in PC-12 cells was similar in surfaces coated with Caf1, fibronectin, surfaces without proteins and the collagen IV control surface.

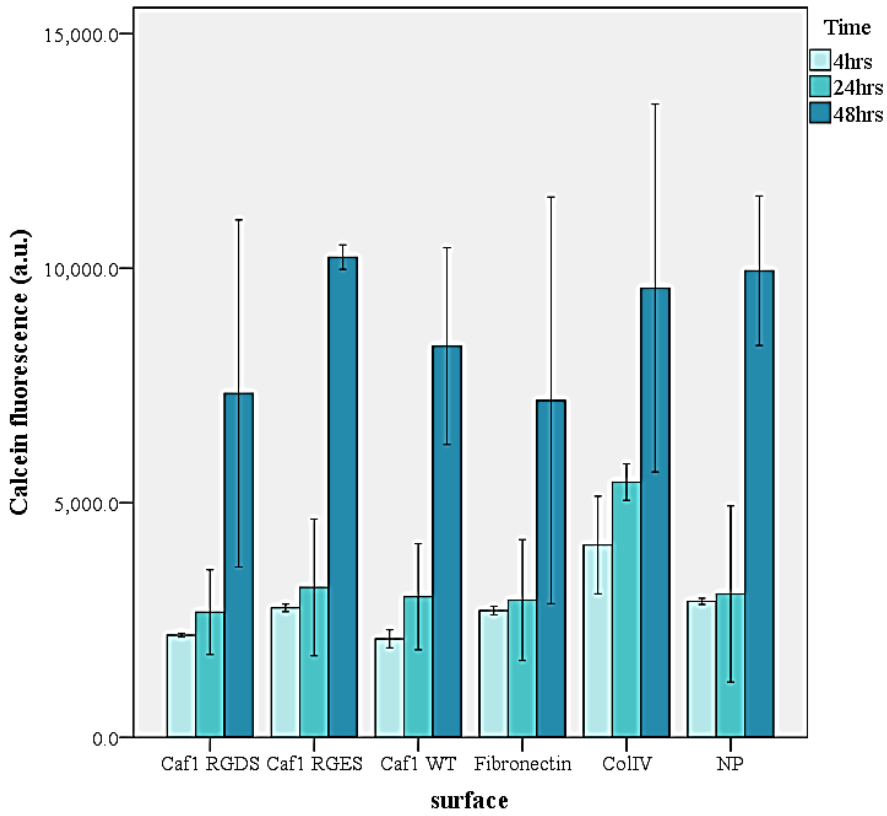

Figure 4.8 – Studies of PC-12 cell viability. Cells were incubated in the presence of 1 μM calcein AM solution in PBS pH 7.4 and the fluorimetric measurements of calcein accumulation in PC-12 cells were determined. Data representative of three independent experiments; values (calcein fluorescence in arbitrary units) represent the mean ± standard error of the mean (SEM). One way ANOVA analysis with Tamhane as a post hoc test was conducted. Legend: ColIV – Collagen IV; NP (Non-protein) – Surface with no protein coating.

Figure 4.9 shows that after 4 and 24 h there was no significant difference in calcein fluorescence levels in 3T3 fibroblast cells adhering to Caf1 proteins-coated surfaces and control surfaces. After 48 h, significant differences were verified comparing the calcein fluorescence levels in 3T3 fibroblast cells adhering to fibronectin control surface with the other protein-coated surfaces: Caf1-RGDS ($P = 0.004$), Caf1-RGES ($P = 0.001$), Caf1-WT ($P = 0.001$) and collagen IV ($P = 0.003$) and also between fibronectin and surface without proteins ($P = 0.001$).

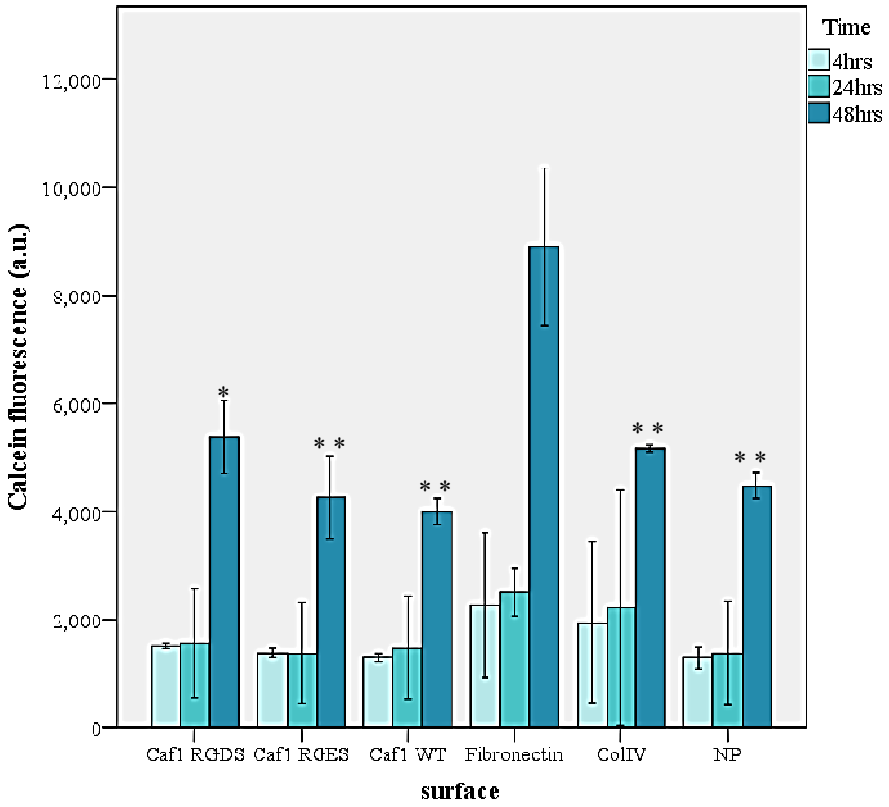

Figure 4.9 – Studies of 3T3 fibroblasts cell viability. Cells were incubated in the presence of 1 µM Calcein AM solution in PBS pH 7.4 and the fluorimetric measurements of Calcein accumulation in 3T3 fibroblasts cells were determined. Data representative of three independent experiments; values (calcein fluorescence in arbitrary units) represent the mean ± standard error of the mean (SEM). Significance was determined by one way ANOVA analysis with Tukey post hoc test. (*) $P < 0.05$ compared to fibronectin, (**) $P < 0.01$ compared to fibronectin. Legend: ColIV – Collagen IV; NP (Non-protein) – Surface with no protein coating.

Figure 4.10 shows that after 4 and 24 h there were no significant differences in calcein fluorescence levels in primary osteoblast cells adhering to Caf1 proteins-coated surfaces and control surfaces. After 48 h, significant differences were verified comparing the calcein fluorescence levels in primary osteoblast cells adhering to fibronectin control surface with the others protein-coated surfaces: Caf1-RGDS (P = 0.033), Caf1-RGES (P = 0.037) and ColIV (P = 0.040).

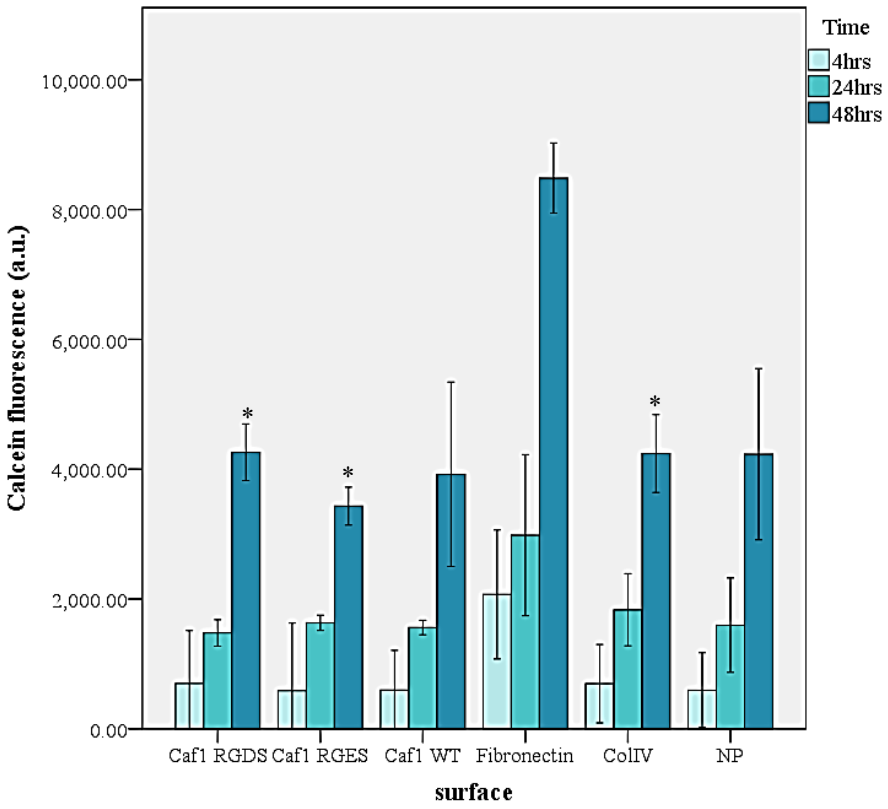

Figure 4.10 – Studies of primary Osteoblasts cell viability. Cells were incubated in the presence of 1 μM Calcein AM solution in PBS pH 7.4 and the fluorimetric measurements of Calcein accumulation in primary osteoblast cells were determined. Data representative of three independent experiments; values (calcein fluorescence in arbitrary units) represent the mean ± standard error of the mean (SEM). Significance was determined by one way ANOVA analysis with Dunnet post hoc test. (*) $P < 0.05$ compared to fibronectin. Legend: ColIV – Collagen IV; NP (Non-protein) – Surface with no protein coating.

Study of mammalian cell adhesion and morphology by Immunofluorescence

After testing the cell viability of the three mammalian cell lines in the study we investigated the adhesion and morphology of these cell lines. For that, we cultured mammalian cells on 96-well polystyrene plates, coated with Caf1 proteins, for 4, 24 and 48 h at 37 ºC. After each incubation period the cells were fixed with 4% of paraformaldehyde and stained with DAPI (fluorescent labelling of nuclei) to count the number of cells adhering to the different surfaces; Rhodamine-conjugated Phalloidin (to stain the actin filaments within cell) to analyse the shape of the cells and the

monoclonal antibody anti-vinculin (specific for the staining of the vinculin focal adhesion protein in cells) followed by the secondary antibody FITC to determine the number of focal contacts in the cells. The 96-well plates, containing the fixed and labelled cells, were taken to the Centre of Excellence in Biopharmaceuticals (CoEBP) at Manchester University to be scanned using the Arrayscan VTI platform (Thermo Scientific) and integrated acquisition system. Some examples of the images obtained (25 fields per well) for each cell line using the DAPI, TRITC, FITC channels are shown in **Figure 4.11, 4.12, 4.13**. All the images obtained were then analysed by Morphology Explorer BioApplication software (Thermo Scientific). Each image was analysed separately by the Morphology Explorer BioApplication software. The cells on the border of each field were disregarded. The final result displayed per well is the average, in pixels, of the cell parameters over the whole 25 images. Analysis of the number of nuclei, shape of the cells and number of focal adhesion are presented below and were conducted at COEBP, Manchester by Dr. Egor Zindy (**Figures 4.14**, **4.18** and **4.22**).

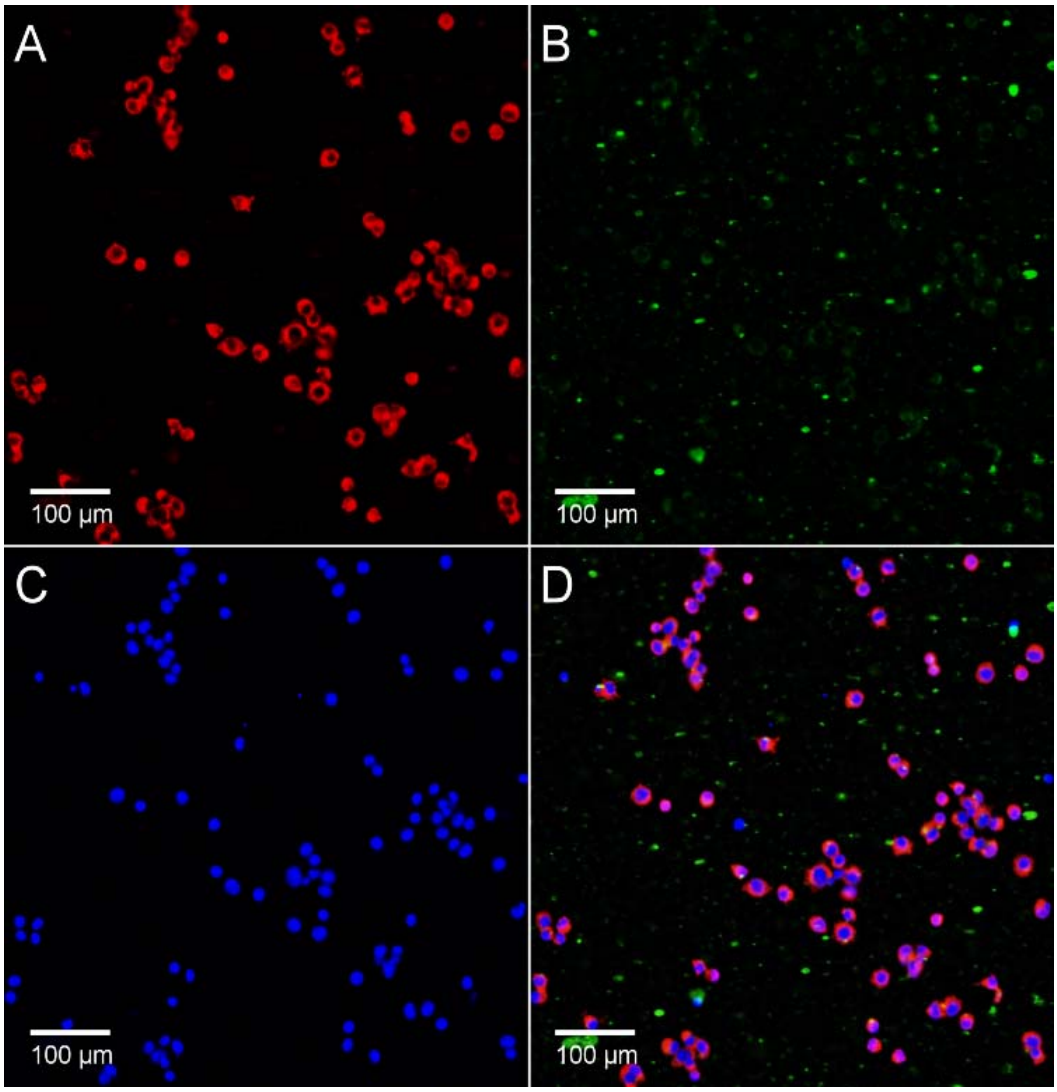

Figure 4.11 – Inverted fluorescence microscopy image of PC-12 cells adhering to surfaces coated with Col IV after 24 h. **(A)** PC-12 cells stained with Rhodamine-conjugated Phalloidin for the detection of F-actin **(B)** PC-12 cells stained with anti-vinculin monoclonal antibody followed by FITC secondary antibody to reveal the focal contacts **(C)** PC-12 cells stained with DAPI to reveal the nuclei **(D)** monochrome images of Rhodamine-conjugated Phalloidin (A), anti-Vinculin (B) and DAPI (C) were overlaid.

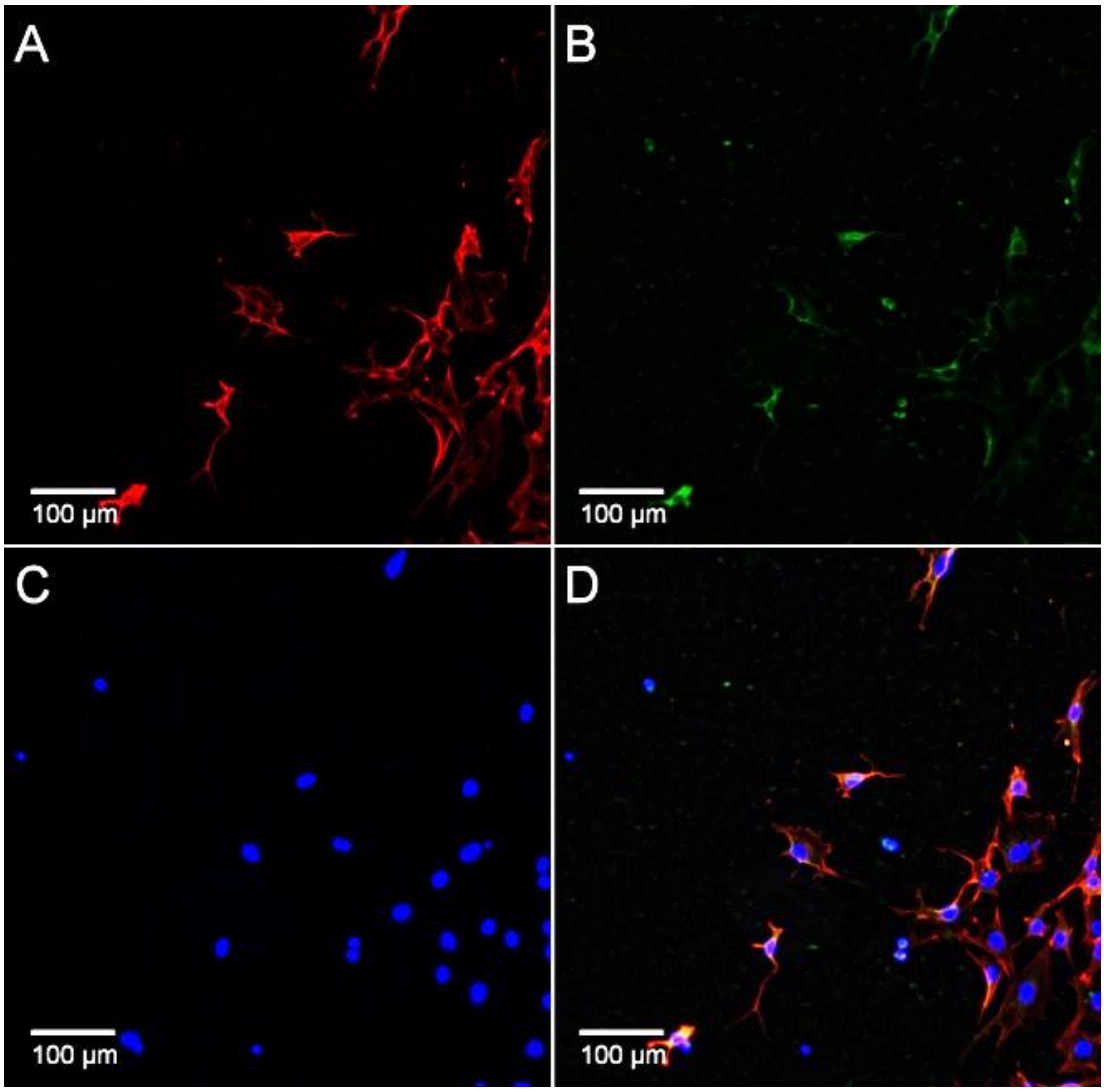

Figure 4.12 – Inverted fluorescence microscopy image of 3T3 fibroblast cells adhering to surfaces coated with fibronectin after 24 h. (A) 3T3 fibroblast stained with Rhodamine-conjugated Phalloidin for the detection of F-actin **(B)** 3T3 fibroblast stained with anti-vinculin monoclonal antibody followed by FITC secondary antibody to reveal the focal contacts **(C)** 3T3 fibroblast stained with DAPI to reveal the nuclei **(D)** monochrome images of Rhodamine-conjugated Phalloidin (A), anti-Vinculin (B) and DAPI (C) were overlaid.

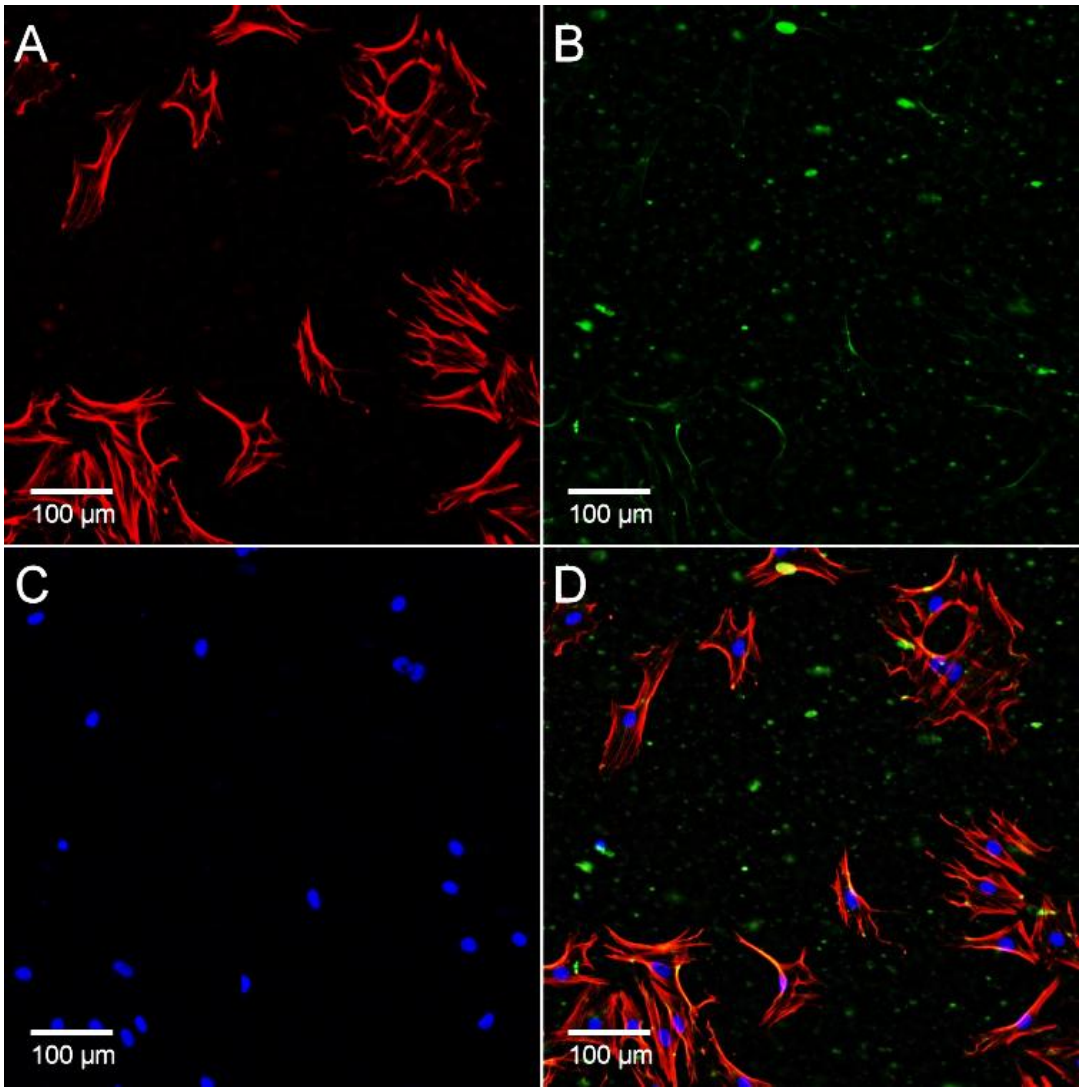

Figure 4.13 – Inverted fluorescence microscopy image of primary osteoblast cells adhering to surfaces coated with fibronectin after 24 h. **(A)** primary osteoblast cells stained with Rhodamine-conjugated Phalloidin for the detection of F-actin **(B)** primary osteoblast cells stained with anti-vinculin monoclonal antibody followed by FITC secondary antibody to reveal the focal contacts **(C)** primary osteoblast cells stained with DAPI to reveal the nuclei **(D)** monochrome images of Rhodamine-conjugated Phalloidin (A), anti-Vinculin (B) and DAPI (C) were overlaid.

A) Study of the number of mammalian cells adhering to the differently coated polystyrene surfaces coated with Caf1 proteins

The analysis of the number of mammalian cells adhering to Caf1 and control surfaces were performed by the counting the number of nuclei using the DAPI channel and measuring the average brightness of the DAPI dye in 25 images which were acquired with the 10x High numerical aperture (NA) magnification objective.

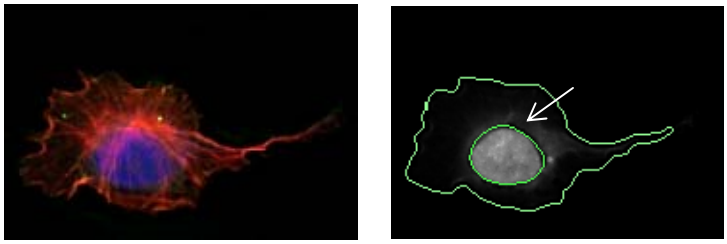

Figure 4.14 – An example of the detection of DAPI-labelled cell nuclei, in 3T3 fibroblast cells adhering to surface coated with Caf1-RGDS after 24 h, with the Morphology Explorer BioApplication. The left panel shows the raw image, and the right panel shows the image containing circles of the identified nuclei. White arrow shows the nucleus. Only objects with 1 nucleus were considered.

The average number of mammalian cells, for each cell line, adhering to Caf1-coated surfaces after 4, 24 and 48 h incubation time for three independent experiments with 2 replicates per incubation time was used to construct the graphs (**Figures 4.15, 4.16** and **4.17)** and performed ANOVA multiple comparisons to compare the surfaces coated with Caf1 proteins with the control surfaces in terms of number of cells adhering to these surfaces.

Additionally, this study was conducted on two groups of cells in suspension, for each cell line. In one of the groups, the cells were incubated with soluble CycloRGDfc peptide at a final concentration of 7 μM for 1 hour. The cyclic peptide containing the RGD can bind with high affinity to αvβ3 integrin receptors and could decrease the number of integrins available to be recognised by the Caf1-RGDS presented on the surfaces, and the other group of cell were not incubated with CycloRGDfc peptide solution.

The **Figure 4.15** shows that **after 4, 24 and 48 h**, no significant differences in the number of PC-12 cells, which were not pre-incubated with soluble CycloRGDfc peptides, adhered to different Caf1 proteins and the control surfaces.

After 4 h, PC-12 cells incubated with soluble CycloRGDfc peptides, adhered to surfaces coated with Caf1-RGDS was significantly less from the surfaces coated with collagen IV ($P = 0.000$). Also significant differences were observed in the number of PC-12 cells adhering to surfaces coated with Caf1-RGES in comparison with the collagen IV-coated surfaces ($P = 0.000$), and also between surfaces coated with Caf1-WT and control surface coated with collagen IV ($P = 0.000$). Between the control surfaces coated with fibronectin and collagen IV ($P = 0.000$) and surfaces without proteins and collagen IV ($P = 0.001$) were also verified significant differences in PC-12 cell adhesion. **After 24 h**, the number of PC-12 cells adhered to surfaces coated with Caf1-RGES was significantly less from the surfaces coated with collagen IV ($P = 0.021$). Also significant differences were observed in the number of PC-12 cells adhering to surfaces coated with fibronectin in comparison with the collagen IV-coated surfaces ($P = 0.011$), and also between surfaces without proteins and control surface coated with collagen IV ($P = 0.025$). **After 48 h** no significant differences were verified between Caf1 proteins-coated surfaces and the control surfaces.

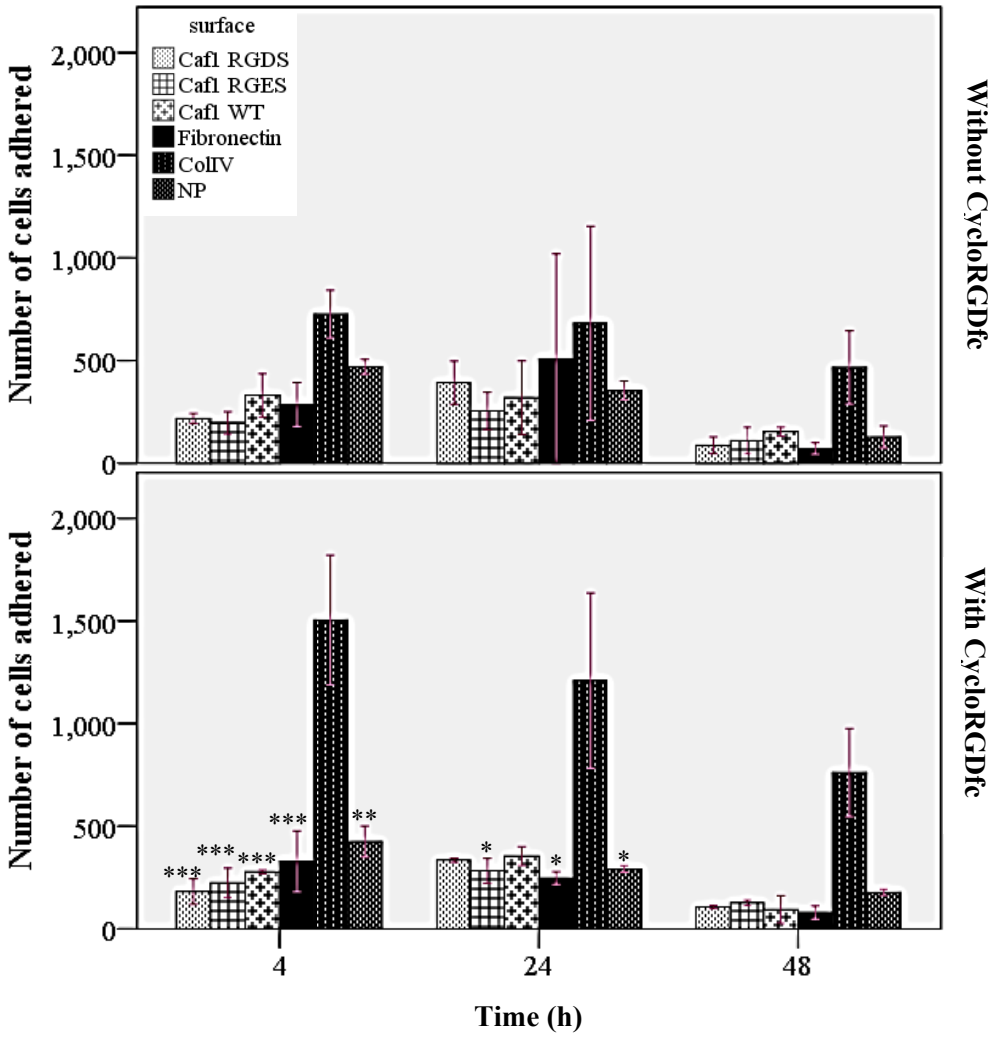

Figure 4.15 – Adhesion of PC-12 cells. Cell adhesion to surfaces coated with different proteins. Data representative of three independent experiments; values (calcein fluorescence in arbitrary units) represent the mean ± standard error of the mean (SEM). Significance was determined by one way ANOVA analysis with Scheffe post hoc test. (*) $P < 0.05$ compared to collagen IV, (**) $P < 0.01$ compared to collagen IV and (***) $P < 0.001$ compared to collagen IV. Legend: ColIV – Collagen IV; NP (Non-protein) – Surface with no protein coating.

The **Figure 4.16** shows that **after 4, 24 and 48 h**, the number of 3T3 fibroblast cells, which were not pre-incubated with soluble CycloRGDfc peptides, adhering to different surfaces were not significant different.

After 4, 24 and 48 h no significant differences in the number of 3T3 fibroblast cells, incubated with soluble CycloRGDfc peptides, adhered to these surfaces were verified.

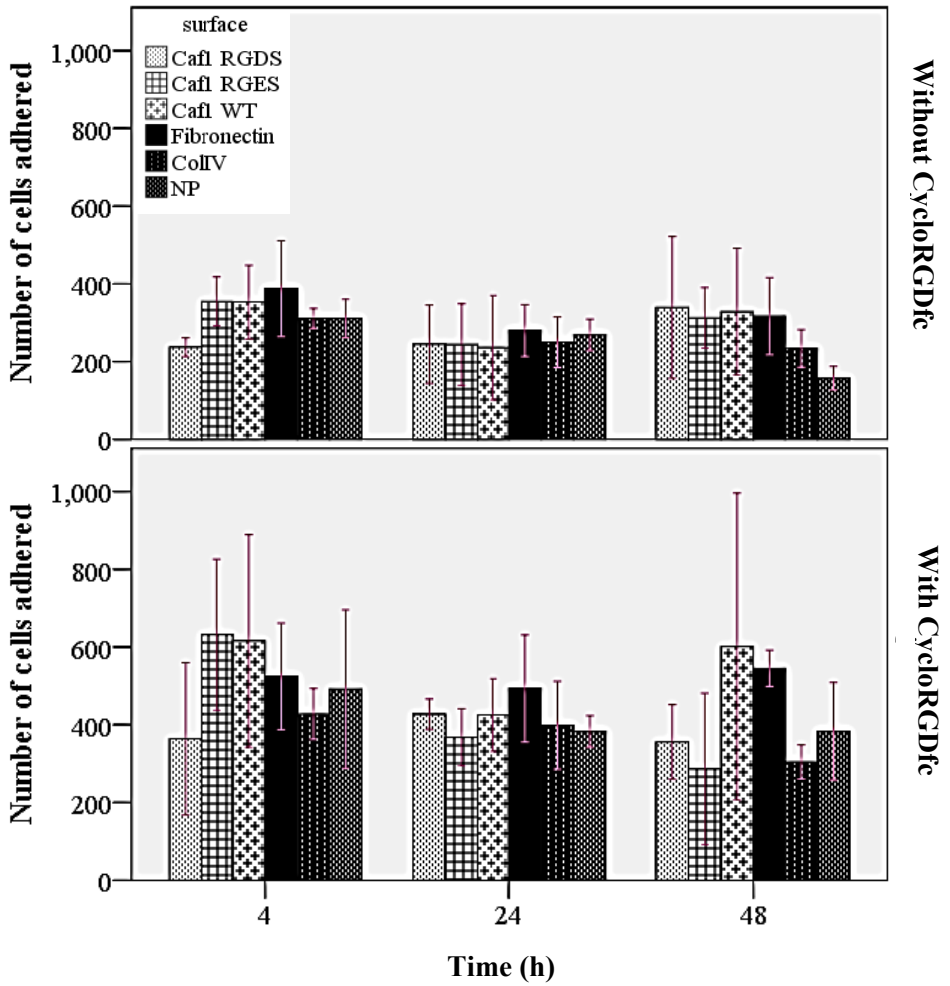

Figure 4.16 – Adhesion of 3T3 fibroblast cells. Cell adhesion to surfaces coated with different proteins. Data representative of three independent experiments; values (calcein fluorescence in arbitrary units) represent the mean ± standard error of the mean (SEM). Significance was determined by one way ANOVA analysis with Scheffe post hoc test. Legend: ColIV – Collagen IV; NP (Non-protein) – Surface with no protein coating.

The **Figure 4.17** shows that **after 4 and 24 h** no significant differences in primary osteoblast cells number were verified between surfaces coated with different Caf1 proteins and between surfaces coated with Caf1 proteins and the control surfaces.

After 48 h, the number of primary osteoblast cells, which were not pre-incubated with soluble CycloRGDfc peptides, adhered to the surface coated with Caf1-RGDS was significantly different from the control surface coated with fibronectin (P = 0.018). A significant difference in primary osteoblast cells number was obtained between surfaces coated with Caf1-RGES and the control surface coated with fibronectin (P = 0.015).

After 4 h, the number of primary osteoblast cells, incubated with soluble CycloRGDfc peptides, adhered to surfaces coated with Caf1-RGDS was significantly different less from the surfaces coated with fibronectin (P = 0.004). **After 24 h**, the number of primary osteoblast cells adhering to surfaces coated with Caf1-RGDS was significantly different less from the surfaces coated with fibronectin (P = 0.000), also a significant difference in primary osteoblast cells number was verified between surfaces coated with Caf1-RGES and surfaces coated with fibronectin (P = 0.000), also for surfaces coated with Caf1-WT and surfaces coated with fibronectin (P = 0.000) and between surfaces without proteins and surfaces coated with fibronectin (P = 0.001). Significant differences in the primary osteoblast cells number were also observed between surfaces coated with Caf1-RGDS and surfaces coated with collagen IV (P = 0.011), and between surfaces coated with Caf1-RGES and fibronectin-coated surfaces (P = 0.040). **After 48 h**, the number of primary osteoblast cells adhering to surfaces coated with Caf1-RGDS was significantly different less from the surfaces coated with fibronectin (P = 0.002), also a significant difference in primary osteoblast cells number was verified between surfaces coated with Caf1-RGES and surfaces coated with fibronectin (P = 0.000), also for surfaces coated with Caf1-WT and surfaces coated with fibronectin (P = 0.001) and between surfaces without proteins and surfaces coated with fibronectin (P = 0.006). Significant differences in the primary osteoblast cells number were also observed between surfaces coated with Caf1-RGDS and surfaces coated with collagen IV (P = 0.028), and between surfaces coated with Caf1-RGES and collagen IV-coated surfaces (P = 0.004) and also between surfaces coated with Caf1-WT and collagen IV-coated surfaces (P = 0.012).

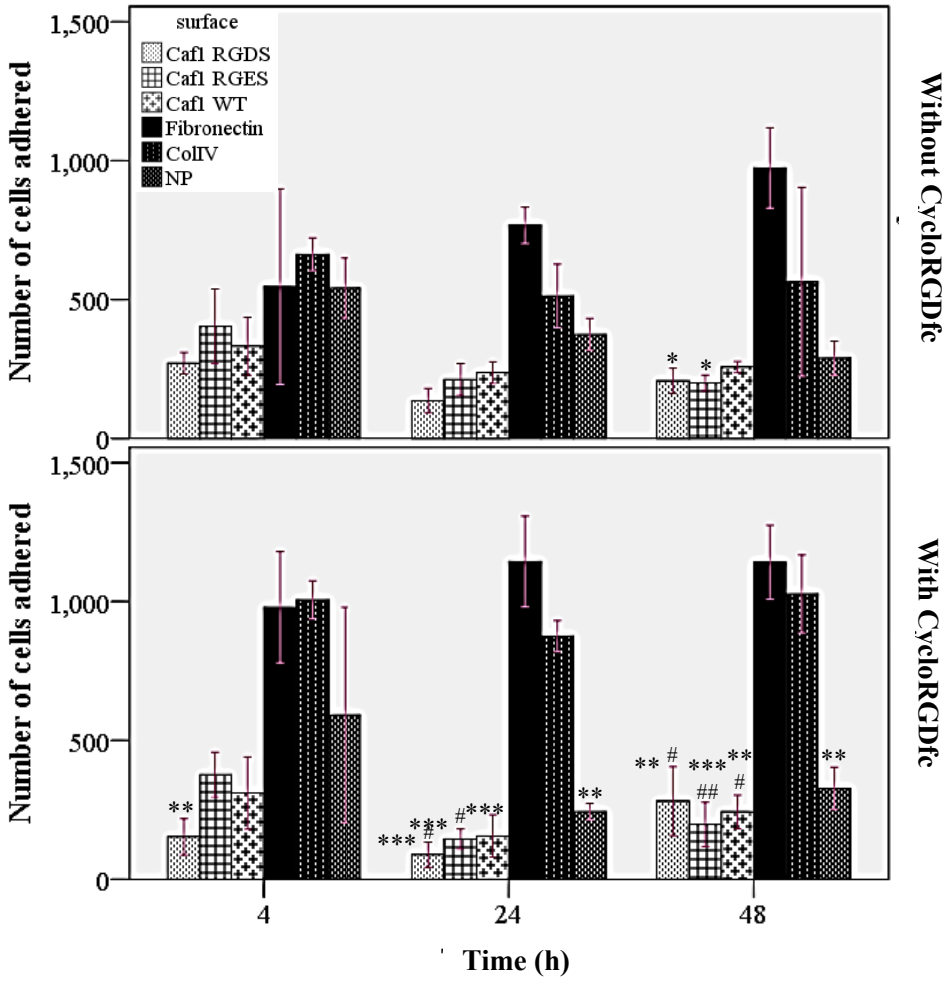

Figure 4.17 – Adhesion of primary osteoblast cells. Cell adhesion to surfaces coated with different proteins. Data representative of three independent experiments; values (calcein fluorescence in arbitrary units) represent the mean ± standard error of the mean (SEM). Significance was determined by one way ANOVA analysis with Scheffe post hoc test. (*) $P < 0.05$ compared to fibronectin, (**) $P < 0.01$ compared to fibronectin and (***) $P < 0.001$ compared to fibronectin; ($^{\#}$) $P < 0.05$ compared to collagen IV, ($^{\#\#}$) $P < 0.01$ compared to collagen IV and ($^{\#\#\#}$) $P < 0.001$ compared to collagen IV. Legend: ColIV – Collagen IV; NP (Non-protein) – Surface with no protein coating.

B) Study of the area of mammalian cells adhering to the different polystyrene surfaces coated with Caf1 proteins

The analysis of the area of mammalian cells adhering to Caf1 and control surfaces were performed by measuring the average brightness of the Rhodamine-Phalloidin dye in 25

images which were acquired with the 10x High numerical aperture (NA) magnification objective.

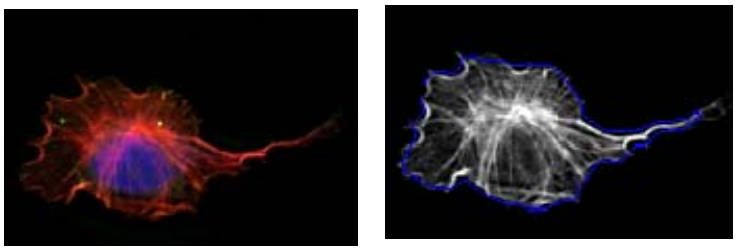

Figure 4.18 – An example of the detection of Rhodamine-Phalloidin labelled F-actin fibres, in 3T3 fibroblast cells adhering to surface coated with Caf1-RGDS after 24 h, with the Morphology Explorer BioApplication. The left panel shows the raw image, and the right panel shows the image of the surrounded cell area. Only objects fully within the image were considered and the border objects were eliminated.

The average area of mammalian cells, for each cell line, adhering to Caf1-coated surfaces after 4, 24 and 48 h incubation time for three independent experiments with 2 replicates per incubation time was used to construct the graphs (**Figures 4.19, 4.20** and **4.21)** and performed ANOVA multiple comparisons to compare the surfaces coated with Caf1 proteins with the control surfaces in terms of cell shape (i.e. the extended of cell spreading) adhered to these surfaces.

Additionally, this study was conducted on two groups of cells in suspension, for each cell line as mention in **section A**.

The **Figure 4.19** reveals that **after 4, 24 and 48 h,** the area of PC-12 cells adhered on all surfaces were similar.

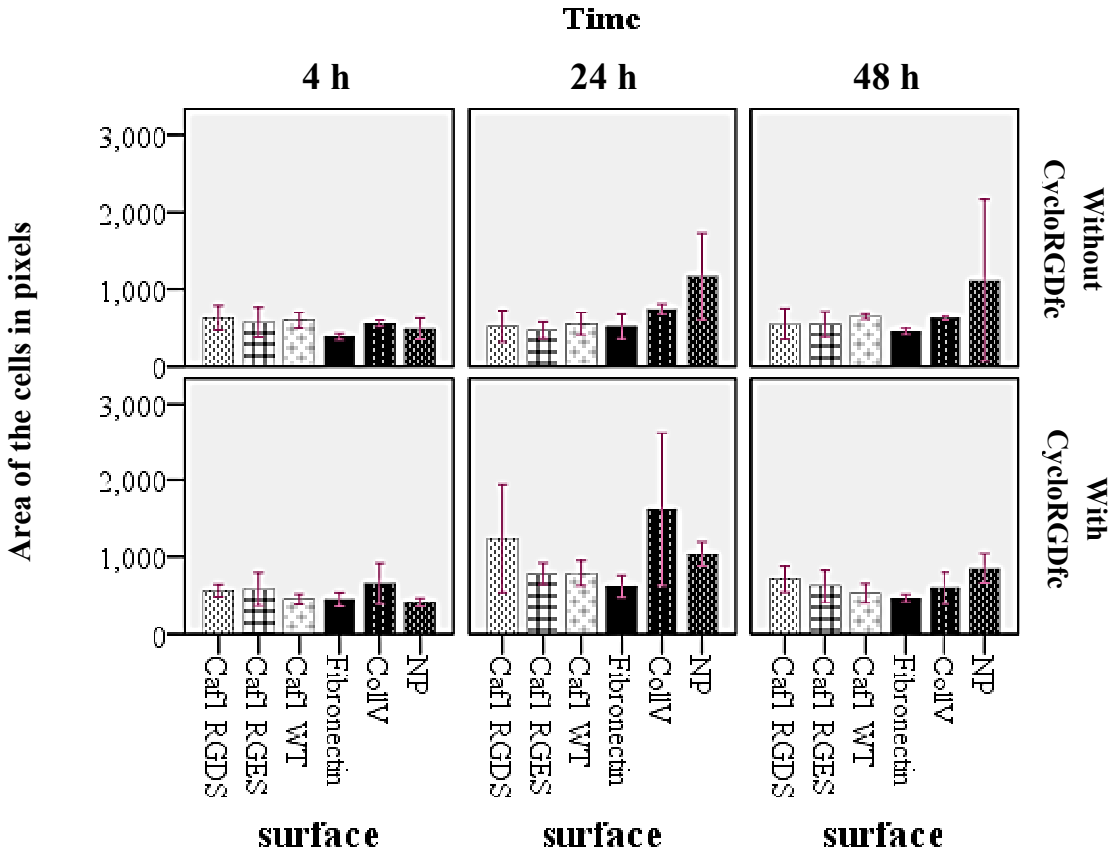

Figure 4.19 – Area of PC-12 cells. Cell adhesion to surfaces coated with different proteins. Data representative of three independent experiments; values (calcein fluorescence in arbitrary units) represent the mean ± standard error of the mean (SEM). Significance was determined by one way ANOVA analysis with Tukey post hoc test. Legend: ColIV – Collagen IV; NP (Non-protein) – Surface with no protein coating

The **Figure 4.20** shows that **after 4, 24 and 48 h**, the area of the 3T3 fibroblast cells, which were not pre-incubated with soluble CycloRGDfc peptides, was not significantly different between all surfaces analysed.

After 4 h, the area of the 3T3 fibroblast cells, incubated with soluble CycloRGDfc peptides, adhered to surfaces coated with Caf1-RGES were significantly different more in comparison with the surfaces without proteins (P = 0.001).

After 24 and 48 h, the area of 3T3 fibroblast cells adhering to all these surfaces analysed was not significantly different.

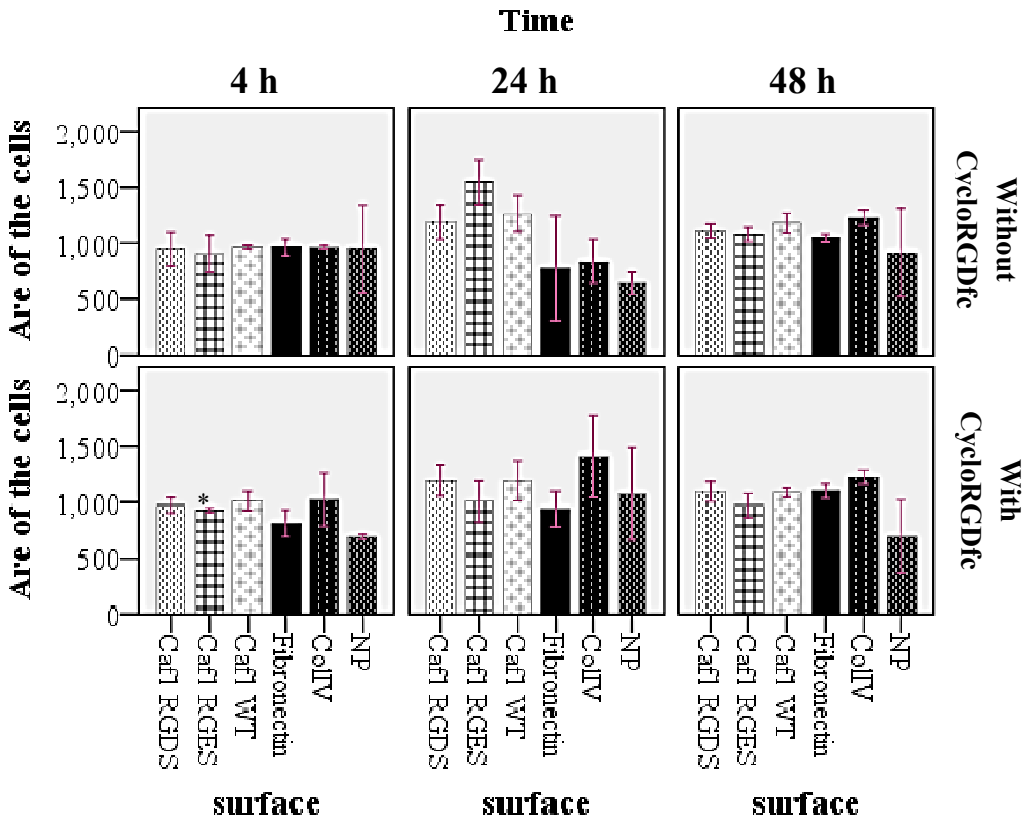

Figure 4.20 – Area of 3T3 fibroblast cells. Cell adhesion to surfaces coated with different proteins. Data representative of three independent experiments; values (calcein fluorescence in arbitrary units) represent the mean ± standard error of the mean (SEM). Significance was determined by one way ANOVA analysis with Tukey post hoc test. (*) $P < 0.05$ compared to surfaces without protein. Legend: ColIV – Collagen IV; NP (Non-protein) – Surface with no protein coating.

The **Figure 4.21** shows that **after 4 h**, the area of the primary osteoblast cells, which were not pre-incubated with soluble CycloRGDfc peptides, adhering to surfaces coated with Caf1-RGDS was significantly less to surfaces coated with collagen IV (P = 0.017). Significant differences in the area of primary osteoblast cells were also verified between surfaces coated with Caf1-RGES and collagen IV-coated surfaces (P = 0.031) and also between the surfaces coated with Caf1-WT and collagen IV-coated surfaces (P = 0.045). **After 24 h**, the area of the primary osteoblasts was significantly less on surfaces coated with Caf1-RGDS and fibronectin-coated surfaces (P = 0.001). Significant differences in osteoblast area were verified for surfaces coated with Caf1-RGDS and collagen IV-coated surfaces (P = 0.031), and also between surfaces coated with Caf1-RGES and fibronectin-coated surfaces (P = 0.002), and between surfaces coated with

Caf1-WT and fibronectin-coated surfaces (P = 0.001). **After 48 h**, no significant differences in the area of primary osteoblasts adhering to different surfaces were observed.

After 4 and 24 h, there were no significant differences in the area of the osteoblasts adhered to all surfaces analysed. **After 48 h**, the area of primary osteoblast cells, incubated with soluble CycloRGDfc peptides, adhered to surfaces coated with Caf1-RGDS show significant differences in comparison with the surfaces coated with Caf1-RGES (P = 0.011). Significant differences in osteoblasts area was observed on surfaces coated with Caf1-RGES and fibronectin-coated surfaces (P = 0.034).

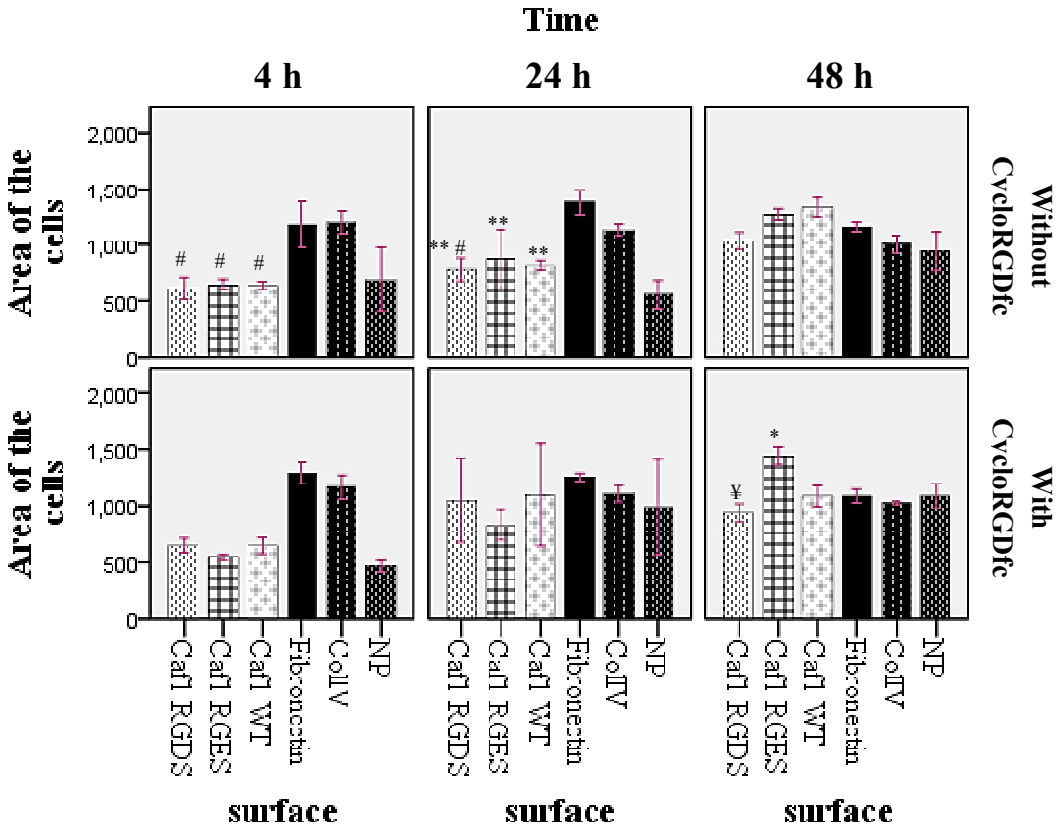

Figure 4.21 – Area of primary osteoblast cells. Cell adhesion to surfaces coated with different proteins. Data representative of three independent experiments; values (calcein fluorescence in arbitrary units) represent the mean ± standard error of the mean (SEM). Significance was determined by one way ANOVA analysis with Tukey post hoc test. (*) $P < 0.05$ compared to fibronectin, (**) $P < 0.01$ compared to fibronectin; ($^{\#}$) $P < 0.05$ compared to collagen IV; (¥) $P < 0.01$ compared to RGES. Legend: ColIV – Collagen IV; NP (Non-protein) – Surface with no protein coating.

C) Study of the mammalian cells focal adhesions adhering to the different polystyrene surfaces coated with Caf1 proteins

The analysis of the number of focal adhesion in cells adhering to Caf1 and control surfaces were performed by the counting the number of focal adhesion using the FITC channel and measuring the average brightness of the FITC (it was used as secondary antibody to bind to the anti-vinculin primary antibody) in 25 images which were acquired with the 10x High numerical aperture (NA) magnification objective.

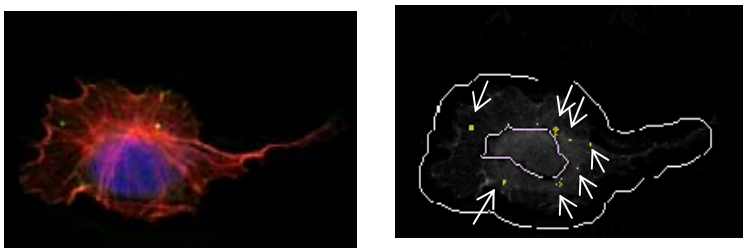

Figure 4.22 – An example of the detection of FITC-anti-vinculin labelled vinculin protein present in the focal adhesions, in 3T3 fibroblast cells adhering to surface coated with Caf1-RGDS after 24 h, with the Morphology Explorer BioApplication. The left panel shows the raw image, and the right panel shows the image with the focal adhesion highlighted (white arrows show the focal adhesions). Due to the high background obtained in some images stained with anti-vinculin antibody/FITC we noticed that some non-specific spots were outside the cell, thus a ring mask was created showed in purple to isolate more specific spots (focal adhesions) inside the cells. (An average brightness > 150 was considered a positive result).

Analysis of the **Tables 4.1-4.3** by ANOVA multiple comparisons allowed us to compare the number of focal contacts in the cells which adhered to different surfaces. Additionally, this study was conducted on two groups of cells in suspension, for each cell line. In one of the groups, the cells were incubated with CycloRGDfc protein solution before adding the cells to the surface and the other group of cells were not incubated with CycloRGDfc peptide solution.

Table 4.1 shows that the number of focal adhesions in PC-12 cells adhered to all these surfaces were not significantly different.

Table 4.1 – Mean number of focal contacts in PC-12 cells. The mean of the number of focal contacts in PC-12 cells which adhered to surfaces coated with different proteins and as a control a non-coated surface was used. All data are reported as mean ± standard error of the mean (n=3).

Surfaces	**Mean number of focal contacts in PC-12 cells (Mean ± S.E.M)**					
	Without CycloRGDfc			**With CycloRGDfc**		
	Time (h)			**Time (h)**		
	4	**24**	**48**	**4**	**24**	**48**
RGDS	13.3 ± 5.6	5 ± 1	6 ± 1	5.9 ± 1.3	13 ± 3	14 ± 4
RGES	4.0 ± 0.9	5 ± 2	7 ± 2	8.8 ± 4.7	28 ± 18	6 ± 0
WT	5.2 ± 1.5	9 ± 4	15 ± 8	3.6 ± 0.3	9 ± 3	10 ± 2
FN	3.4 ± 0.6	6 ± 2	6 ± 0	2.3 ± 0.2	7 ± 2	6 ± 1
ColIV*	3.7 ± 1.0	11 ± 3	8 ± 2	8.1 ± 3.0	17 ± 11	11 ± 5
NP+	3.8 ± 0.8	14 ± 7	70 ± 57	5.5 ± 2.1	5 ± 2	12 ± 3

Legend: (*) ColIV – Collagen IV; (+) NP – surfaces non-coated

Table 4.2 shows that the number of focal adhesions in 3T3 fibroblast cells adhered to these surfaces were not significantly different.

Table 4.2 – Mean number of focal contacts in 3T3 fibroblast cells. The mean of the number of focal contacts in PC-12 cell line which adhered to surfaces coated with different proteins and as a control non-coated surface was used. All data are reported as mean ± standard error of the mean (n=3).

Surfaces	**Mean number of focal contacts in 3T3 fibroblast cells (Mean ± S.E.M)**					
	Without CycloRGDfc			**With CycloRGDfc**		
	Time (h)			**Time (h)**		
	4	**24**	**48**	**4**	**24**	**48**
RGDS	13 ± 2.6	8 ± 1.5	8 ± 0.9	8 ± 0.6	9 ± 1.5	7 ± 0.7
RGES	8 ± 0.8	8 ± 1.6	8 ± 1.7	6 ± 0.8	6 ± 1.7	7 ± 1.4
WT	8 ± 2.5	7 ± 0.9	9 ± 1.5	12 ± 3.5	9 ± 1.9	7 ± 1.4
FN	7 ± 1.1	13 ± 0.7	9 ± 1.8	5 ± 0.7	14 ± 5.7	7 ± 0.9
ColIV	5 ± 0.7	12 ± 1.8	4 ± 0.4	4 ± 0.3	77 ± 45	4 ± 0.2
NP	32 ± 27	9 ± 1.7	9 ± 0.7	6 ± 1.4	5 ± 1.4	8 ± 1.5

Legend: (*) ColIV – Collagen IV; (+) NP – surfaces non-coated

Table 4.3 showed that the number of focal adhesions in primary osteoblast cells adhered to these surfaces was not significantly different.

Table 4.3 – Mean number of focal contacts in primary osteoblast cells. The mean of the number of focal contacts in primary osteoblast cell line which adhered to surfaces coated with different proteins and as a control non-coated surface was used. All data are reported as mean ± standard error of the mean (n=3).

Surfaces	Mean number of focal contacts in primary Osteoblasts cells (Mean ± S.E.M)					
	Without CycloRGDfc			With CycloRGDfc		
	Time (h)			Time (h)		
	4	24	48	4	24	48
RGDS	8 ± 0.6	10 ± 4.6	10 ± 3	10 ± 1.9	13 ± 2.1	11 ± 2.6
RGES	14 ± 3.5	7 ± 0.4	11 ± 2.5	9 ± 1.6	10 ± 0.3	13 ± 1.5
WT	8 ± 0.3	7 ± 0.7	13 ± 2.5	10 ± 1.7	13 ± 3.2	13 ± 2.3
FN	6 ± 0.6	6 ± 0.4	9 ± 0.8	5 ± 0.2	6 ± 0.5	8 ± 0.8
ColIV	5 ± 0.7	5 ± 0.1	7 ± 1.2	4 ± 0.8	4 ± 0.02	5 ± 0.4
NP	5 ± 0.5	13 ± 3.2	18 ± 11	6 ± 1.4	9 ± 2.4	14 ± 6

Legend: (*) ColIV – Collagen IV; (+) NP – surfaces non-coated

Study of mammalian cell adhesion and morphology by Scanning Electron Microscopy (SEM)

Each cell line was added to the different surfaces and incubated for 24 h. A study of the percentage of cell adhesion and cell morphology was performed by SEM. The number of cells adhered, on the different surfaces, was determined applying two criteria: first, consider the clusters as a single cell adhering to the surface and second, count only the cells in contact with the surface.

A) Cell adhesion on Caf1 proteins-coated on glass surfaces

The **Figures 4.23-4.25** were obtained by Scanning Electron Microscopy. Ten images, of each cell line were examined and the percentage of cell adhesion was determined (**Table 4.4**).

The **Figure 4.23** shows the PC-12 cells adhering to different surfaces.

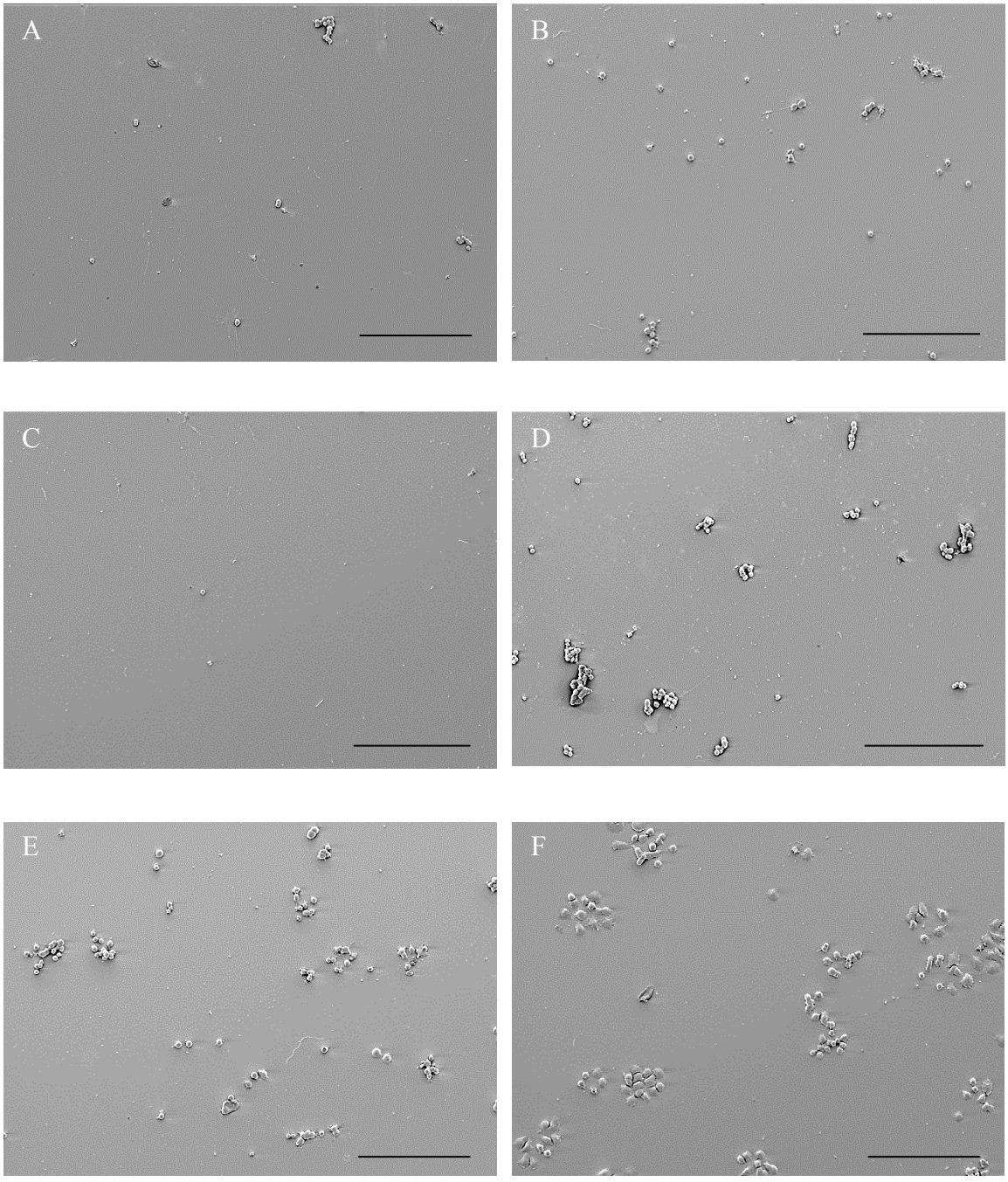

Figure 4.23 – Scanning electron micrograph of PC-12 cells adhering to glass surfaces coated with different proteins after 24 h. A – Glass surface coated with fibronectin; B – Glass surface coated with CAF1-RGDS; C – Glass surface coated with CAF1-WT; D – Glass surface coated with CAF1-RGES; E – Glass surface; F – Glass surface coated with collagen IV. Scale bar: 200 μm.

The **Figure 4.24** shows the 3T3 fibroblast cells adhering to different surfaces.

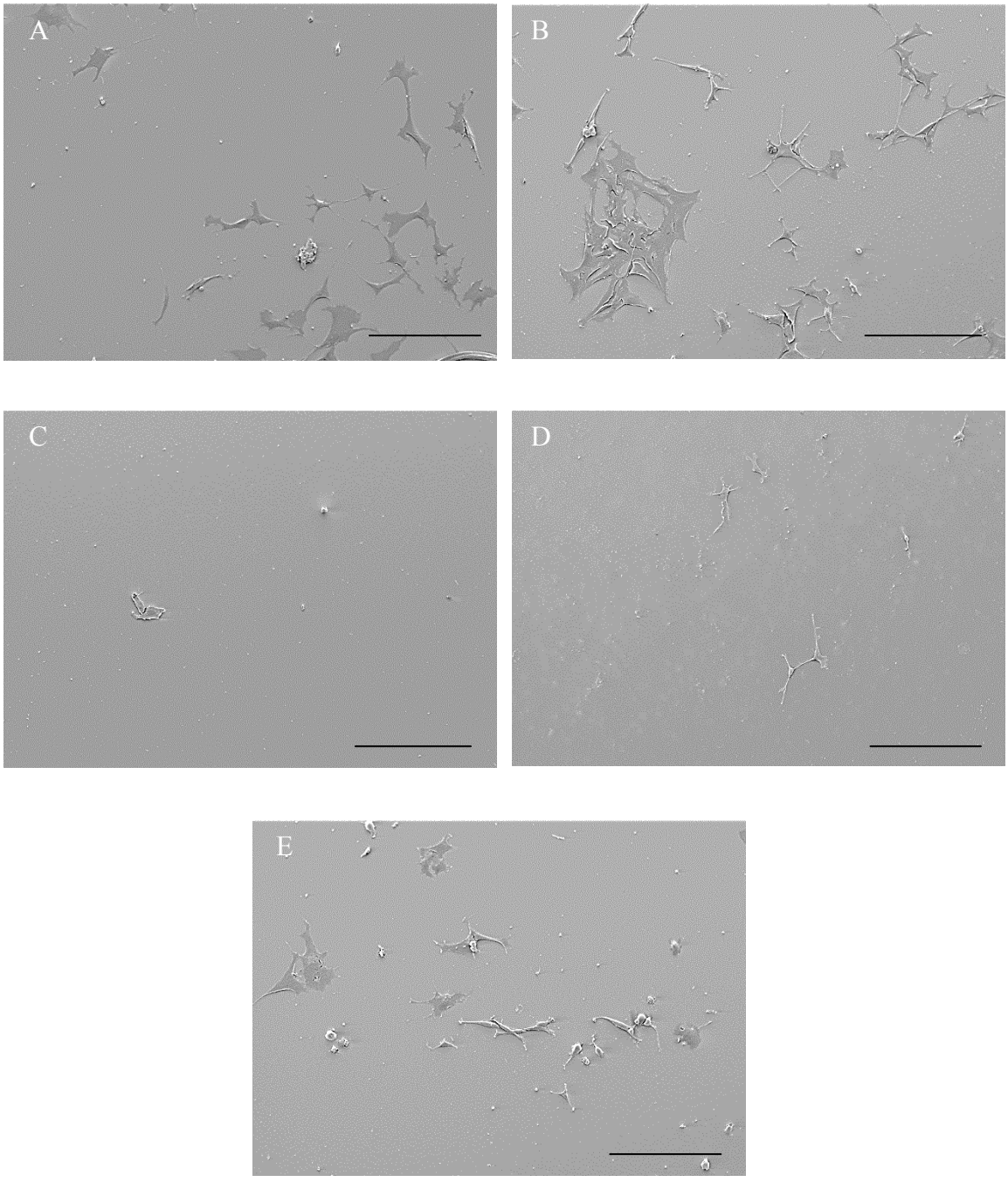

Figure 4.24 – Scanning electron micrograph of mouse 3T3 fibroblast adhering to glass surfaces coated with different proteins after 24 h. A – Glass surface coated with fibronectin; B – Glass surface coated with CAF1-RGDS; C – Glass surface coated with CAF1-WT; D – Glass surface coated with CAF1-RGES; E – Glass surface. Scale bar: 200 μm.

The **Figure 4.25** shows the primary osteoblast cells adhering to different surfaces.

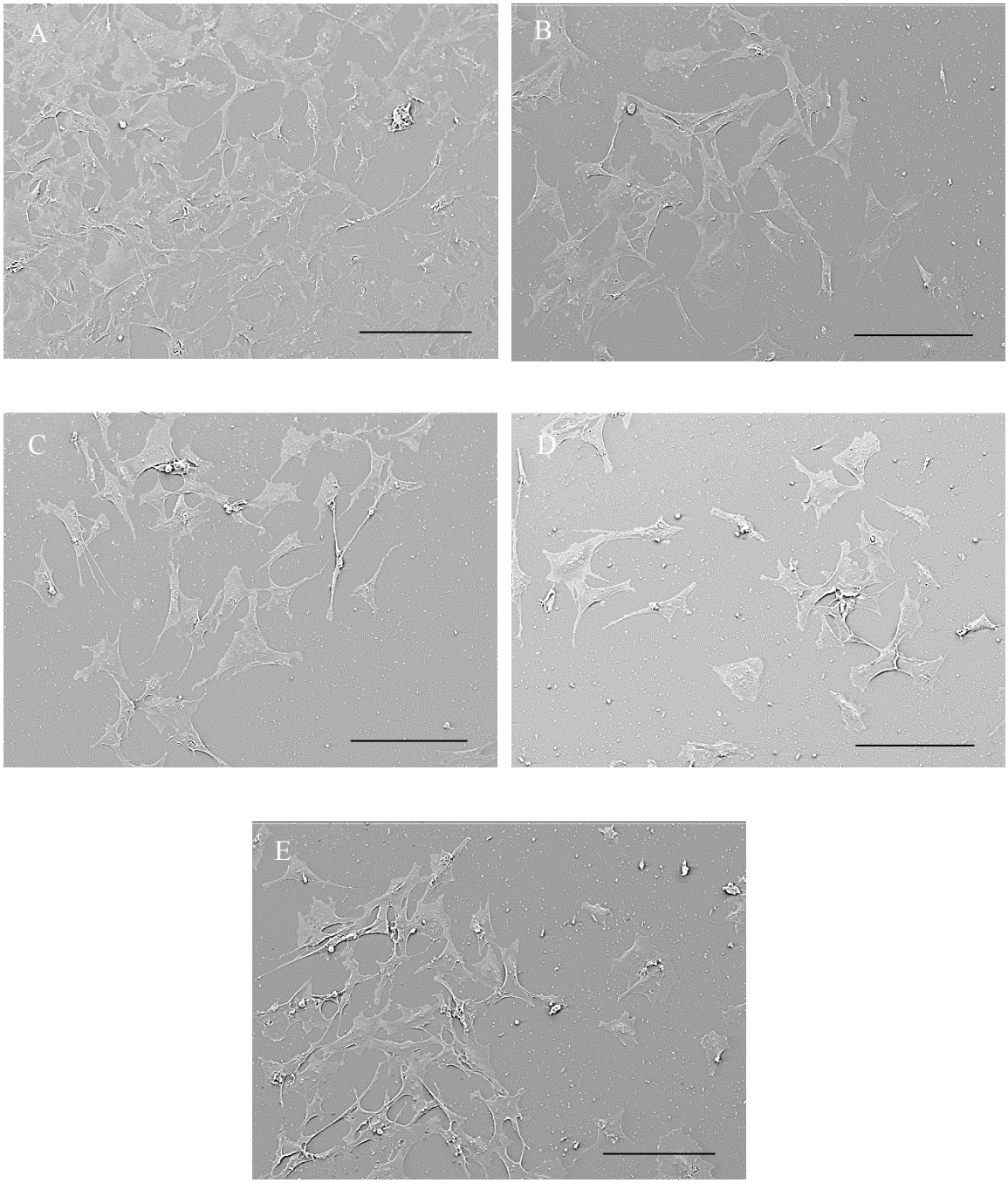

Figure 4.25 – Scanning electron micrograph of rat primary calvarial osteoblasts cells adhering to glass surfaces coated with different proteins after 24 h. A – Glass surface coated with fibronectin; B – Glass surface coated with CAF1-RGDS; C – Glass surface coated with CAF1-WT; D – Glass surface coated with CAF1-RGES; E – Glass surface. Scale bar: 200 μm.

Table 4.4 shows that the percentage of PC-12 cell adhesion was higher on the control glass coated with collagen IV (93%) than on the other surfaces. The percentage of 3T3 fibroblasts was higher on the glass coated with fibronectin (85.5%) than on the other surfaces. The percentage of primary osteoblast cells was higher on glass coated with fibronectin (95%) than on the other surfaces. Both for PC-12 and 3T3 fibroblast cells very low number of cells adhered to glass coated with Caf1-WT, 8% and 3%, respectively.

Table 4.4 – Mammalian cell adhesion (% of initial number of cells) after 24 h. The mean of the number of different mammalian cell lines which adhered to glass surfaces coated with different proteins and as a control only glass surface was used. All data are reported as mean of three independent experiments ± standard error of the mean (S.E.M).

Surface	% of Adherent cells on the surface (Mean ± S.E.M)		
	PC-12	**3T3 Fibroblasts**	**Primary Osteoblasts**
Glass coated with fibronectin	39.0 (78 ± 0.33)	85.5 (171 ± 0.33)	95.0 (190 ± 0.57)
Glass coated with Caf1-RGDS	51.0 (102 ± 0.33)	81.5 (163 ± 0.33)	63.0 (126 ± 0.33)
Glass coated with CAF1-WT	8.0 (16 ± 0.33)	3.0 (6 ± 0.57)	55.5 (111 ± 0.33)
Glass coated with CAF1-RGES	43.5 (87 ± 0.33)	18.0 (36 ± 0.33)	48.5 (97 ± 0.33)
Glass	66.0 (132 ± 0.66)	72.5 (157 ± 0.33)	69.0 (138 ± 0.33)
Glass coated with collagen IV	93.0 (186 ± 0.33)	-	-

B) Cell morphology on Caf1 proteins-coated on glass surfaces.

The **Figures 4.26, 4.28 and 4.30** were obtained by Scanning Electron Microscopy. The morphology, of ten images, of each cell line was examined.

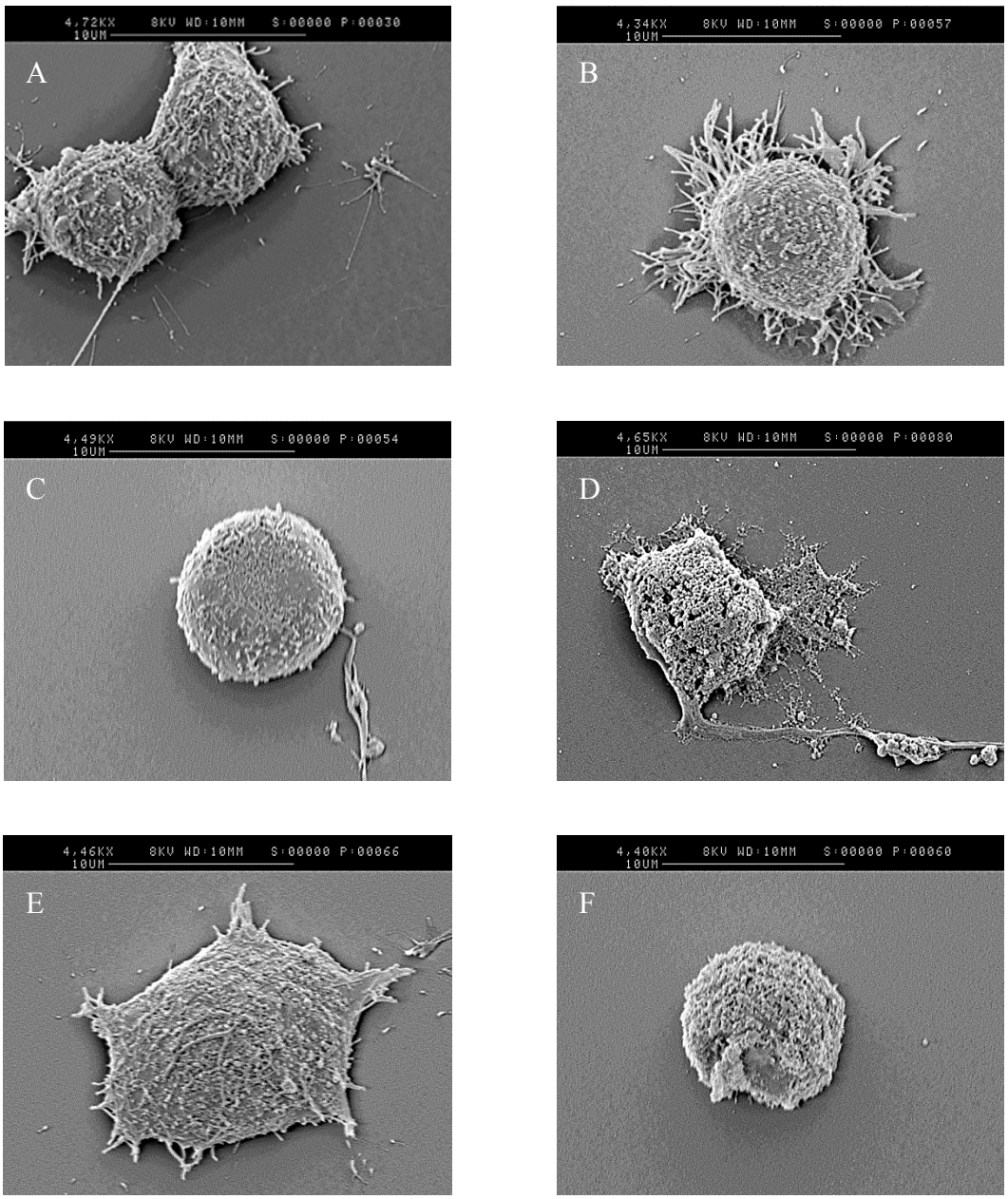

Figure 4.26 – Scanning electron micrograph of PC-12 cells adhering to glass surfaces coated with different proteins after 24 h. A – Glass surface coated with fibronectin; B – Glass surface coated with CAF1-RGDS; C – Glass surface coated with CAF1-WT; D – Glass surface coated with CAF1-RGES; E – Glass surface coated with collagen IV; F – Glass surface. Scale bar: 200 μm.

SEM of PC-12 adhering to the different surfaces (**Figure 4.26**) were analysed to determine the number of PC-12 cells with a round and non-round morphology.

Figure 4.27 shows that, after 24 h, the number of PC-12 cells, with a round morphology, adhered to glass surfaces coated with collagen IV was significantly less from Caf1-RGDS (P = 0.000), Caf1-RGES (P = 0.000), Caf1-WT (P = 0.000), fibronectin (P = 0.000) and also from surfaces without proteins (P = 0.000). The number of PC-12 cells, with a non-round morphology, adhered onto collagen IV surfaces was significantly more from the PC-12 cells adhered on surfaces coated with Caf1-RGDS (P = 0.000), Caf1-RGES (P = 0.000), Caf1-WT (P = 0.000), fibronectin (P = 0.000) and also from surfaces without proteins (P = 0.000).

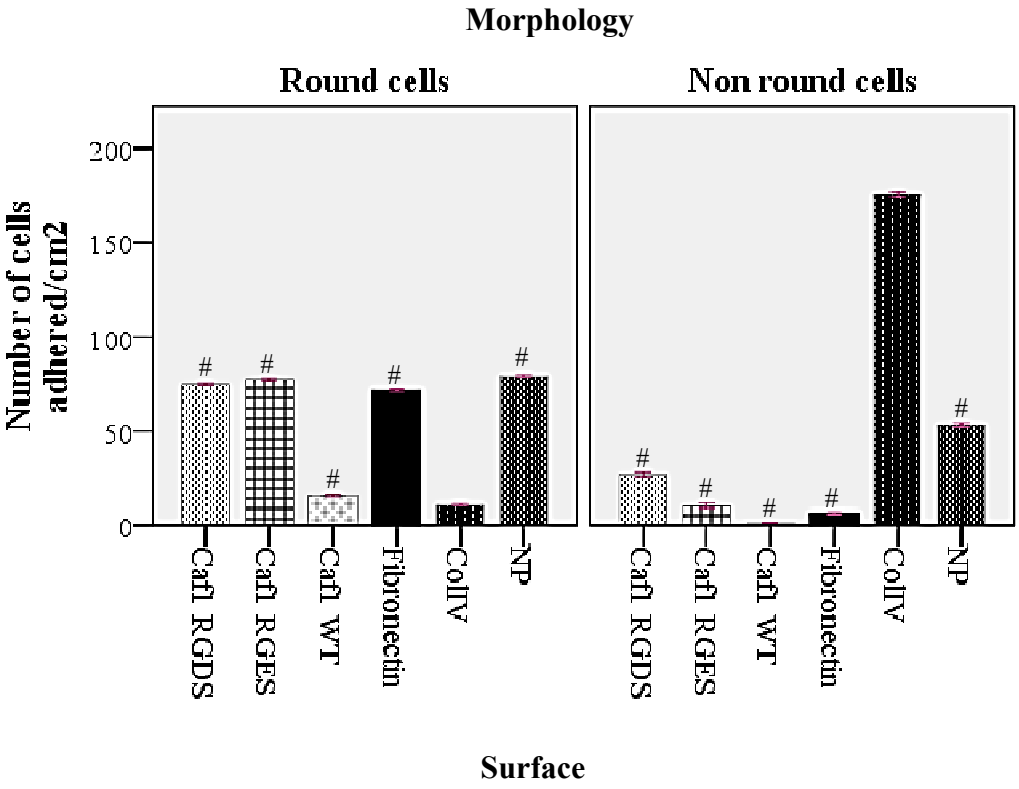

Figure 4.27 – Analysis of PC-12 cell morphology by SEM after 24 h. The number of cells adhered per cm^2 with a round morphology and cells with a non-round morphology. Data represent the mean of three experiments ± standard error of the mean (S.E.M). Significance was determined by one way ANOVA analysis with Scheffe as a post hoc test was conducted. ($^{\#}$) $P < 0.001$ compared to collagen IV. Legend: ColIV – Collagen IV; NP (Non-protein) – Surface with no protein coating.

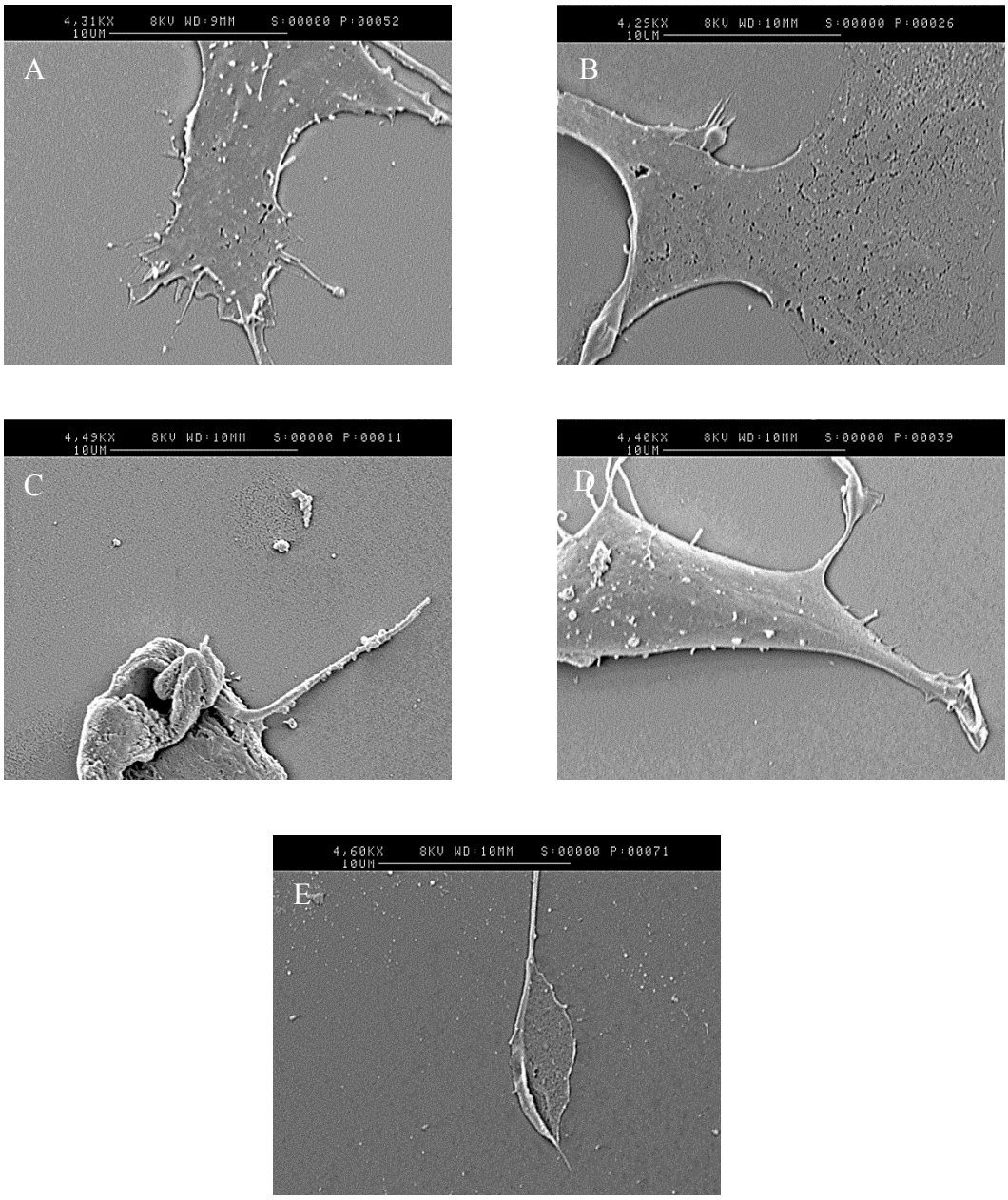

Figure 4.28 – Scanning electron micrograph of mouse 3T3 Fibroblast adhering to glass surfaces coated with different proteins. A – Glass surface coated with fibronectin; B – Glass surface coated with Caf1-RGDS; C – Glass surface coated with Caf1-WT; D – Glass surface coated with Caf1-RGES; E – Glass surface. Scale bar: 10 μm.

Scanning electron micrographs of 3T3 fibroblast adhering to the different surfaces (**Figure 4.28**) were analysed to determine the number of 3T3 fibroblast cells with a round and non-round morphology.

Figure 4.29 shows that, **after 24 h**, the number of 3T3 fibroblast cells, with a round morphology, adhered to glass surfaces coated with fibronectin was significantly less from Caf1-RGES (P = 0.000), Caf1-WT (P = 0.000) and surfaces without proteins (P = 0.000). The number of 3T3 fibroblast cells, with a non-round morphology, adhering to surfaces coated with Caf1-RGES was significant more to number of 3T3 fibroblasts presenting similar morphology adhered to fibronectin (P = 0.001). Significant differences between number of non-rounded 3T3 fibroblasts adhering to Caf1-WT and fibronectin (P = 0.000).

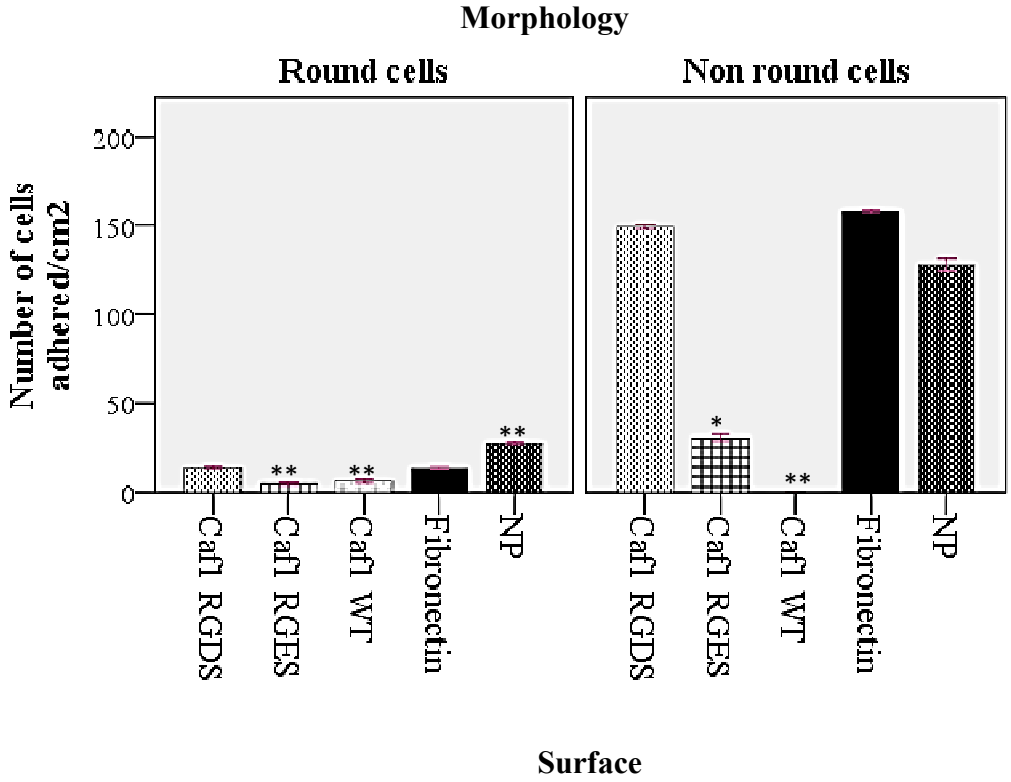

Figure 4.29 – Analysis of 3T3 fibroblast cell morphology by SEM after 24 h. The number of cells adhered per cm^2 with a round morphology and cells with a non-round morphology. Data represent the mean of three experiments ± standard error of the mean (S.E.M). Significance was determined by one way ANOVA analysis with Scheffe as a post hoc test was conducted. (*) $P < 0.01$ compared to fibronectin, (**) $P < 0.001$ compared to fibronectin. Legend: ColIV – Collagen IV; NP (Non-protein) – Surface with no protein coating.

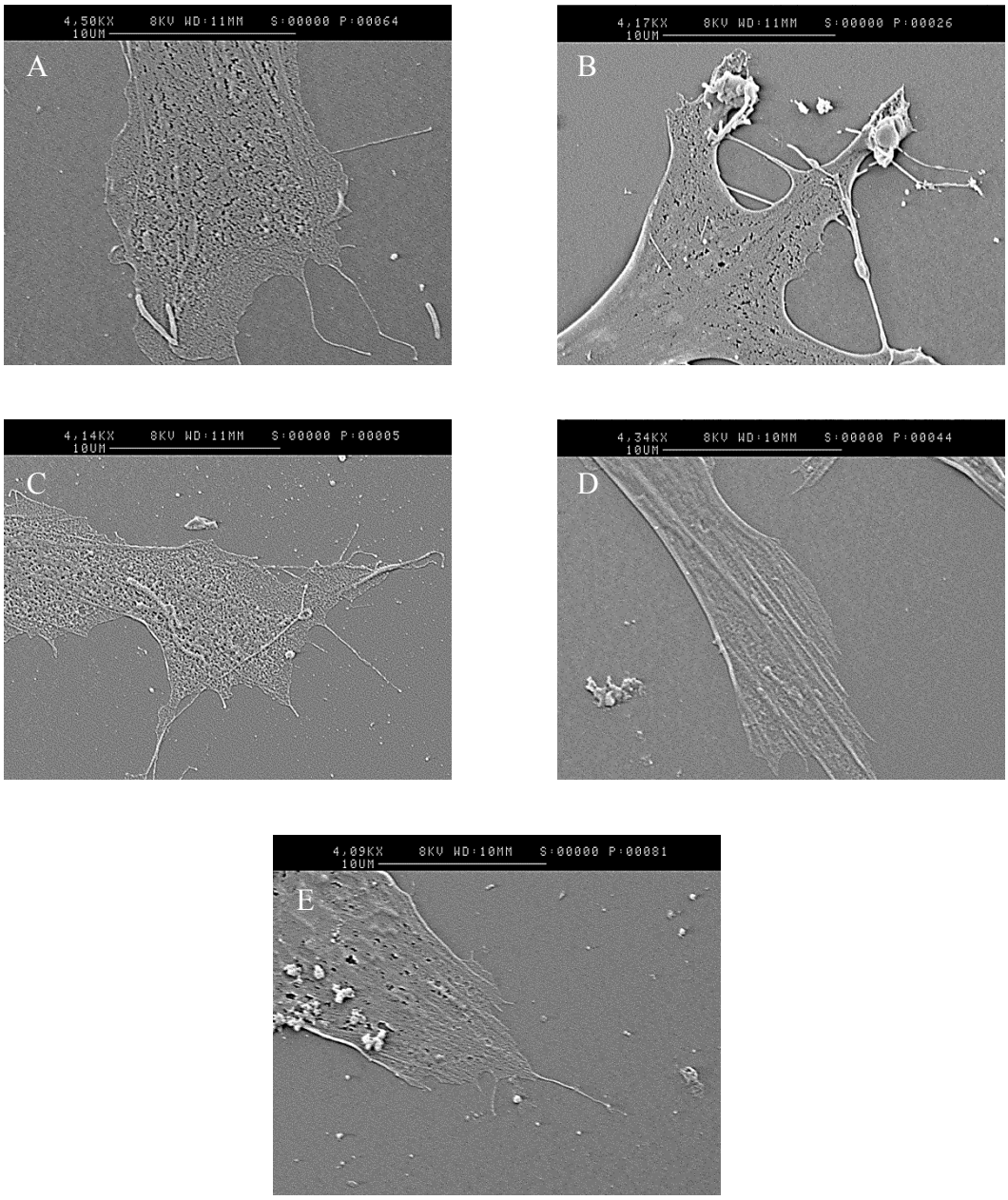

Figure 4.30 – Scanning electron micrographs of primary osteoblasts cells adhering to glass surfaces coated with different proteins. A – Glass surface coated with fibronectin; B – Glass surface coated with CAF1-RGDS; C – Glass surface coated with CAF1-WT; D – Glass surface coated with CAF1-RGES; E – Glass surface. Scale bar: 200 μm.

Scanning electron micrographs of primary osteoblast cells adhering to the different surfaces (**Figure 4.30**) were analysed to determine the number of primary osteoblast cells with a round and non-round morphology, i.e. presenting one or more filopodia (cytoplasmic projections).

Figure 4.31 shows that, after 24 h, the number of primary osteoblast cells, with a round morphology, adhered to glass surfaces coated with fibronectin was significantly less from Caf1-RGES (P = 0.000), Caf1-WT (P = 0.000) and surfaces without proteins (P = 0.000).

The number of primary osteoblast cells, with a non-round morphology, adhered to glass surfaces coated with fibronectin was significantly more from Caf1-RGDS (P = 0.000), Caf1-RGES (P = 0.000), Caf1-WT (P = 0.000) and surfaces without proteins (P = 0.000).

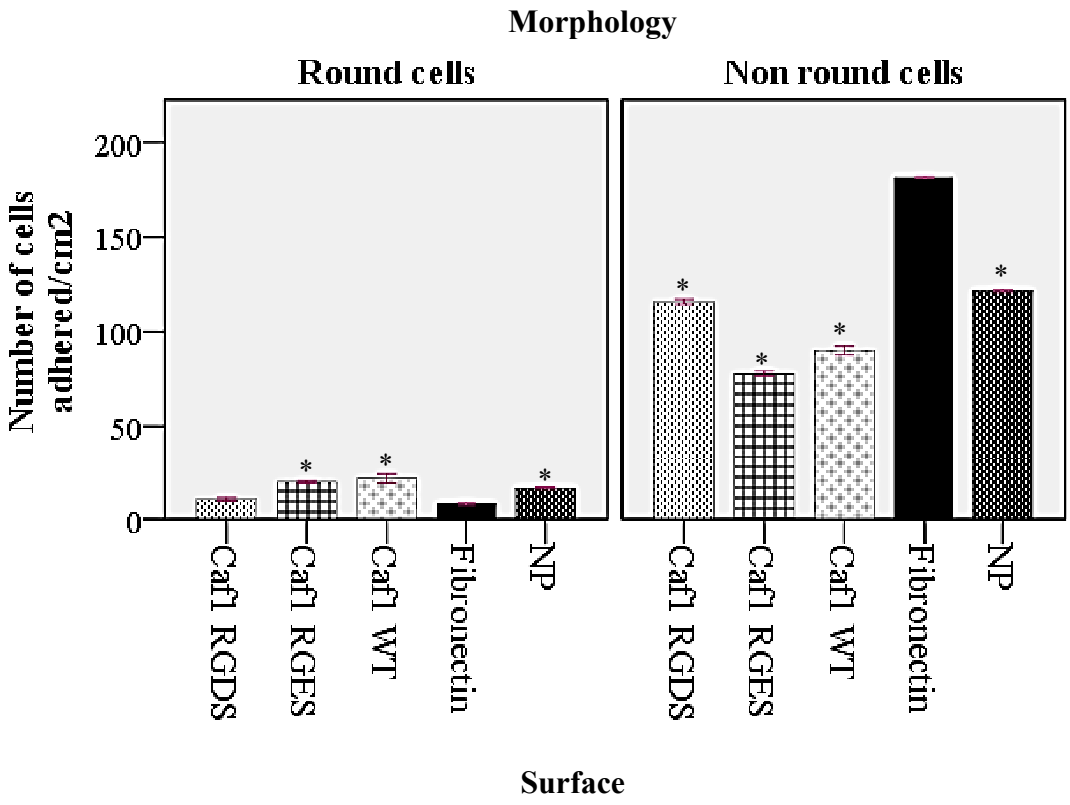

Figure 4.31 – Analysis of primary osteoblast cell morphology. The number of cells adhered per cm^2 with a round morphology and cells with a non-round morphology. Data represent the mean of three experiments ± Standard error of the mean (S.E.M). Significance was determined by one way ANOVA analysis with Scheff as a post hoc test was conducted. (*) $P < 0.001$ compared to fibronectin. Legend: ColIV – Collagen IV; NP (Non-protein) – Surface with no protein coating.

4.3. Discussion

tmOmpA ECM mutants promote cell adhesion and proliferation

In agreement with earlier work (Chaffey *et al.*, 2008; Cooke *et al.*, 2008), our data showed that PC-12 cells adhered poorly to tmOmpA and PEG-thiol surfaces. In contrast, tmOmpA-ECM namely RGDS (from fibronectin), MNYYSNS (from collagen IV), FHRRIKA (heparin) significantly increased the cell adhesion and spreading after 24 h, whilst LDVP and IDAP (both peptides from fibronectin) showed this effect after 48 h. These results were also supported by a variety of adherent cell morphologies that were categorized into four types: round-shaped oval (with one or two focal contact points), triangular (with three focal points) and star-shaped (with four focal contact points) (**Figure 4.4**). The differences in cell morphologies are associated to the ligand-integrin interaction which leads to signal transduction and therefore changes in the cytoskeleton (Chen *et al.*, 2003).

In addition, this study contributed to a better understanding as to which peptides from the whole extracellular matrix proteins, such as fibronectin, laminin and collagen, have higher affinity for integrin binding and thus, could enhance PC-12 cell adherence, proliferation and differentiation.

It is well known that PC-12 attach poorly to plastic (Tomaselli *et al.*, 1987 ; Schwarz *et al.*, 1990) and therefore, in order for PC-12 cells to adhere in large numbers to surfaces, cell culture flasks need to be coated with ECM proteins, namely collagen, fibronectin and laminin (Levi *et al.*, 1983).

Most importantly for this study, cell receptors (mainly integrins) recognised ligands (in this case small ECM peptides) present on OmpA loops and bound to them. The interaction between receptors and ligands provides cell anchor points, known as focal adhesions, which are critical for cell adhesion and morphogenetic changes (Chen *et al.*, 2003).

Cooke *et al*., 2008 have already shown that some of these ECM peptides can mimic the effect of whole ECM molecules and here we extended this data and investigated mixtures (Cooke *et al.*, 2008).

Using this technology, we investigated if tmOmpA-PHSRN alone supports cell attachment and also if the combination of the tmOmpA-RGDS peptide and tmOmpA-PHSRN at different concentrations enhances cell attachment. Our data shows that

tmOmpA-PHSRN peptide alone can promote cell attachment. However, a higher number of PC-12 cells adhered to surfaces coated with both peptides, tmOmpA-RGDS and tmOmpA-PHSRN, thus tmOmpA-RGDS+PHSRN can enhance cell attachment in comparison with the controls: tmOmpA-PHSRN and tmOmpA-RGDS peptides alone. The capacity of tmOmpA-PHSRN peptides alone to promote PC-12 cell adhesion was also reported by Cooke et al. (2008).

Nevertheless, the role of PHSRN is not completely understood. Studies with PHSRN were conducted following the discovery of RGD cell-adhesion peptide, which is present in the 10th type III domain of fibronectin (Pierschbacher and Ruoslahti, 1984). PHSRN peptide, located in the 9th type III domain of fibronectin, was first identified by Yamada and co-workers when they studied the attachment and spreading of baby hamster kidney cells to either RGD or RGD and PHSRN-coated plates and found that more cells adhered and spread on surfaces containing both peptides than only RGD. However surfaces coated with only PHSRN did not show cell attachment (Humphries *et al.*, 1987).

Later Feng and Mrksich (2004) examined the role of PHSRN in cell adhesion using self-assembled monolayers presenting in a orientated way oligo(ethylene glycol) groups and RGD and PHSRN ligands, together and separately. The glycol groups prevented the non-specific adsorption of protein. Two cell lines, baby hamster kidney fibroblasts and 3T3 Fibroblast were added to the monolayers and were able to attach on surfaces presenting the two peptides. To investigate if the cells could attach to surfaces containing SAMs with PHSRN they performed inhibition studies using soluble peptides and showed that both peptides compete for the same binding site of the integrin receptors, however the RGD ligand binds with higher affinity than does PHSRN and also using scrambled peptide sequences they reported that the RGD and PHSRN ligands can bind in a highly specific way to the integrin receptors. These findings showed that both PHSRN and RGD peptides can bind competitively to the same integrin receptors. PHSRN was identified as the synergistic ligand, i.e. it can enhance the spreading of cells adhered to RGD-coated substrates (Feng and Mrksich, 2004). However in this study it was demonstrated that PHSRN could also mediate alone the cell adhesion by the recognition and binding to integrins (Feng and Mrksich, 2004).

To study the effects of Caf1 protein on mammalian cell adhesion, we used black 96-well plates tissue culture treated (see in the material and methods) with a 150 μm

polystyrene clear bottom suitable for fluorescent assays. These are the type usually used at CoEBP and tissue-culture treated polystyrene is usually used in cell culture to allow cell attachment in a more natural manner. On the other hand, the untreated polystyrene would have been more suitable for protein adsorption since it has a more hydrophobic surface. Thus it was not clear if the binding of Caf1 to these surfaces was reliable. In our work on hydrophobic polystyrene we have seen visible reductions in surface hydrophobicity after incubation with Caf1 and other proteins but this verification was not possible in the CoeBP experiments.

The Caf1 proteins (at a concentration of 50 μg/ml) applied to the polystyrene surfaces were Caf1-RGDS, Caf1-RGES and Caf1-WT. RGDS was incorporated into Caf1 loop 5, by site-directed mutagenesis, because it is the main adhesive peptide of fibronectin leading to integrin binding and cell adhesion. RGDS peptides can alter either integrin binding, according to their affinity for certain class of integrins, or properties of the surface, introducing charged functional groups which change for example the surface hydrophilicity (Lin *et al.*, 1992).

In order to ensure that the cell adhesion was only due to integrin binding, it is necessary to have a negative control. Since integrin binding is very sensitive to minor changes in the RGD sequence (Hersel *et al.*, 2003), we substituted the aspartic acid in the RGDS sequence by a glutamic acid, through site-directed mutagenesis, generating the RGES, which is similar to RGDS but it is not recognised by integrins (Hersel *et al*., 2003).

The Caf1-WT was used as a negative control for integrin binding since does not contain integrin binding sites or any bio-active site and thus no modification was performed in these proteins. It was reported that the affinity of RGE and other RGDS-similar peptides for integrins is about 2 to 4 orders of magnitudes lower when compared with RGD sequence (Pierschbacher and Ruoslahti, 1984).

Entire fibronectin (at a concentration of 50 μg/ml), is usually used as a positive control for 3T3 fibroblast and primary osteoblast cells while collagen IV is used for coating tissue culture flasks for PC-12 cell adhesion.

Another control was uncoated polystyrene surfaces of the 96-well plates.

Proteins were incubated in the 96-well plates at 4 ºC, for 16 h with slow shaking to avoid agglomeration of proteins in some areas of the wells.

The mammalian cells were selected based on their ability to adhere on RGDS-coated surfaces. Both, mouse 3T3 fibroblasts and rat primary osteoblasts express

integrins such as α5β1 which recognise and bind to RGD ligands. Neuronal cell line, PC12 also included in this study, express high levels of β1 integrins which are implicated in PC-12 cell attachment namely on surfaces coated with laminin and collagen IV and poorly on fibronectin- or RGDS-coated surfaces.

Cell adhesion was studied for 4 h, the minimum time of cell incubation (Massia and Hubbell, 1991), for 24 h and 48 h, maximum time of cell culture (Cooke *et al.*, 2008 ; Cooke *et al.*, 2010).

The three mammalian cell lines are viable on surfaces coated with Caf1 proteins.

In the present study, cell viability was assayed via calcein uptake. The results obtained for PC-12 cells revealed that this cell line, when added to surfaces coated with Caf1 proteins: Caf1-RGDS, Caf1-RGES and Caf1-WT, can survive after 4, 24 and 48 h. The fluorescence intensity of the PC-12 adhering to Caf1 protein-coated surfaces at all-time points was similar to the fluorescence intensity of the control surfaces: collagen IV and fibronectin. In addition, the fluorescence intensity increased considerably after 48 h on all surfaces. At approximately this time point PC-12 cells divided leading to an increase in cell number which might increase the calcein AM uptake and thus raise the fluorescence intensity (**Figure 4.8**).

The results obtained for 3T3 fibroblasts (**Figure 4.9**) and primary osteoblasts (**Figure 4.10**) showed that the initial levels of fluorescence in these two cell lines adhering to Caf1 protein-coated surfaces were similar to the control surfaces at 4 and 24 h. After 48 h we observed significantly greater calcein AM uptake by both 3T3 fibroblasts and primary osteoblasts cultured on control fibronectin-coated surfaces compared to the same cell lines cultured on Caf1 protein-coated surfaces and on the other control surfaces (collagen IV-coated surfaces and non-coated surfaces).

Caf1 proteins-coated surfaces did not enhance PC-12, primary osteoblasts and 3T3 Fibroblasts cell adhesion.

Following cell viability studies, we examined the number of cells adhered to the polystyrene surfaces coated with Caf1 proteins, fibronectin (the positive control for 3T3 fibroblasts and osteoblasts) and collagen IV (the positive control for PC-12 cells). Polystyrene surfaces without protein were used as a negative control.

Each cell line was divided into two groups: cells were incubated with CycloRGDfc peptides at concentration of 7 μM for 1 h at 37 ºC (Jeschke *et al.*, 2002) before being added to the surfaces and control which were not. Cyclic RGD peptide contains a cysteine to eventually bind it to gold surfaces presents a high affinity for αvβ3 integrins; therefore it can promote cell adhesion when immobilised on a surface. In this study, cycloRGDfc peptides were added to a solution containing cells in suspension to bind to the αvβ3-cell receptors. These cells were then added to the different surfaces to test for specific RGD-integrin interactions.

After cell culture for 4, 24 and 48 h, the cells were fixed in 4% paraformaldehyde and stained for the nuclei with DAPI. The numbers of PC-12 cells that adhered to polystyrene surfaces coated with Caf1 proteins, fibronectin and surfaces without proteins were similar. As expected, a higher number of PC-12 cells was obtained on surfaces coated with collagen IV than on the other surfaces. Studies using integrin alpha subunit-specific antibodies revealed that PC-12 express high levels of α1 β1 which alone mediated responses to collagen types I and IV (Tomaselli *et al.*, 1990). Nevertheless, no significant differences were obtained by multi-comparison analysis of variance of surfaces coated with Caf1 proteins and the control surfaces: collagen IV (for PC-12 cells) (**Figure 4.15**).

Unexpectedly, after 4 h the incubation of PC-12 cells with cycloRGDfc peptides seemed to enhance PC-12 cell adhesion to collagen IV-coated surfaces and did not have a great effect on their adhesion to fibronectin-coated surfaces. In addition, PC-12 cells adhered poorly to Caf1 proteins-coated polystyrene surfaces and polystyrene surfaces without proteins. Interestingly, after 24 h, the differences between PC-12 cell adhesion to collagen IV-coated surfaces and the Caf1 proteins-coated surfaces was less significant and after 48 h, no significant differences in the PC-12 cells adhesion was observed between these two groups of surfaces.

One possible reason for these inconclusive results could be due to the low concentration of collagen IV (50 μg/ml) on the surface which leads to lower number of PC-12 cells adhered on the collagen IV-coated surface. The addition of cycloRGDfc to PC-12 might have stimulated PC-12 to express other class of integrins which could enhance cell adhesion when cells were added to the collagen-coated surfaces. Other possible reason could be the low concentration of collagen IV adsorbed on the well

plates and a possible the excess of cycloRGDfc peptides could contribute to promote more cell adhesion.

In order to optimise the competitive assay we can test several concentrations of soluble cyclic RGD peptides until saturating integrin receptors on the cell surface. Jeschke *et al*., (2002) reported that adhesion of chondrocytes to immobilized cyclic-RGD peptides containing a thiol anchor to bind to the surfaces (used for surface coating) was inhibited with increasing amounts (0.01 to 1000 μM) of soluble cyclic RGDfk peptide without the thiol anchor (used for competition assays) and their results might indicate that binding of the cells to adhesion peptide coated surfaces was specific to the RGD-coated plate (Jeschke *et al*., 2002).

Analysis of the 3T3 Fibroblasts cell adhesion showed that this cell line can adhere in a similar number to all surfaces used in this study (**Figure 4.16**). The fibroblasts particularly express high levels of a variety of integrins, namely α5β1 the main receptor for the RGD ligand from fibronectin, and also synthesise ECM proteins which allow them to attached on different surfaces (Gailit and Clark, 1996).

The results obtained for primary osteoblast cells in the absence of cycloRGDfc peptides revealed that after 4 and 24 h the number of primary osteoblast cells was very similar in all the surfaces, however after 48 h the number of primary osteoblasts adhered to fibronectin-coated surfaces was slightly higher than to Caf1-RGDS- and Caf1-WT-coated surfaces (**Figure 4.17**). The possible reason for the lower osteoblast cell adhesion to Caf1-WT is due to the absence of cell adhesion binding sites in this protein. In the case of Caf1-RGDS-coated surfaces, the lower osteoblast cell adhesion is more difficult to explain since this protein contains the RGD responsible for cell binding.

In this study it was not possible to determine the concentration of Caf1-RGDS adsorbed to the surface. A method to immobilise the protein could allow the determination of the quantity of Caf1-RGDS present on the surface and the correct immobilisation of the protein in order to insure the proper accessibility of the motifs. On the other hand the Caf1 is very long polymer formed by many Caf1 monomer engineered with RGDS. The necessary quantity of these ligands for cell adhesion depends among other aspects on cell type. For these reasons will be difficult to understand only with this study if Caf1-RGDS can support cell adhesion, namely in the cases of fibroblasts and osteoblasts which express high levels of α5β1 that mediates the cell adhesion.

Differences in cell adhesion could be due to differences in the concentration of peptide on the surface. Several cell adhesion studies indicated that there may be an optimal ligand concentration for adhesion and migration. Burgess *et al*. examined the adhesion and migration of osteoblasts on RGDS and RDGS grafted surfaces and found that with a low cell adhesion ligand density on the surface, more cells adhere and migrate.

Moreover, Caf1-RGDS proteins might not be sufficient to support cell adhesion. The binding of α5β1 requires both the PHSRN sequence in the 9th type III repeat and RGD motif in the 10th type III repeat of fibronectin (Aota *et al.*, 1994). The RGD and PHSRN peptides synergistically bind to α5β1 integrins and can provide a stable adhesion (Garcia *et al.*, 2002).

In general, and surprisingly, the incubation of cycloRGDfc with the cells seemed to promote some cell adhesion on collagen IV and fibronectin surfaces. In one previous study it was described that PC-12 cells can adhere in greater number to surfaces coated with laminin than to fibronectin. When the synthetic peptide, cyclic RGD peptide at a concentration of 0.5 mM, was added to surfaces coated with laminin it did not reduce the number of PC-12 cells however the addition of RGD peptides to surfaces coated with fibronectin reduced the number of PC-12 cells by 70% (Dai *et al.*, 1994).

A possible reason for the unexpected results using the cycloRGDfc could be due to the excess of cycloRGDfc which did not bind to the cell receptors and remained in solution. When the cells incubated with cycloRGDfc were added to the surfaces, these cycloRGDfk peptides might coat possible gaps on the surface, enhancing cell adhesion.

The cyclic RGD peptide used in our studies binds with high affinity to the αvβ3 integrin, but it was reported that can also bind to a lesser degree to α5β1, αvβ1 and αvβ5 (Gurrath *et al.*, 1992; Friedlander *et al.*, 1995).

We also investigated the cell spreading at COEBP on the different surfaces. After cell seeding for 4, 24 and 48 h, the cells were stained for F-actin using rhodamine-phalloidin. Each cell line was divided into two groups: cells incubated with CycloRGDfc proteins during 1 h and cells which were not incubated with CycloRGDfc proteins before added to the surfaces. Analysis of the area of the cells adhered on different surfaces could allow us to understand cell spreading and proliferation.

The area of the PC-12 cells non- and treated with CycloRGDfc was similar in all surfaces after 4, 24 and 48 h. This observation could be explained by absence of growth

factors such as Nerve Growth Factor (NGF) which are responsible for the formation and elongation of neurites (Li *et al*., 1998). Without NGF the shape and area of the PC-12 cells do not undergo considerable changes over the cell culture time. A similar result was obtained for 3T3 fibroblasts. Primary osteoblasts did not spread on surfaces coated with Caf1-proteins compared to surfaces coated with collagen IV and fibronectin. PHSRN may also enhance cell spreading (García *et al.*, 2002).

The results from scanning electron microscopy analysis of the number of PC-12, 3T3 fibroblast and primary osteoblast cells adhered on Caf1 protein-coated glass surfaces, to collagen IV- and fibronectin-coated glass surfaces and to glass without proteins have shown that the 93% of the PC-12 adhered to collagen IV, 85.5% of the 3T3 fibroblasts adhered to fibronectin-coated surfaces and 95% of the primary osteoblasts adhered to fibronectin-coated surfaces. The percentage of cells adhering to Caf1-RGDS-coated surfaces was similar to fibronectin-coated surfaces, whereas Caf1-WT coated surfaces inhibited cell attachment below the levels seen on glass alone. The number of primary osteoblast on Caf1-WT-coated surface was slightly less than on Caf1-RGDS surfaces. Thus this analysis provides evidence that the addition of RGDS to Caf1 allows it to mimic fibronectin. Furthermore it also shows that wild type Caf1 has the ability to prevent cell adhesion by an unknown mechanism.

PC-12, 3T3 Fibroblasts and primary osteoblast cells can form focal adhesions on Caf1 protein-coated surfaces.

The number of focal adhesions, in the three mammalian cell lines mentioned above, was examined by immunofluorescence using the anti-vinculin antibody. All the cell lines were able to form focal contacts with the different surfaces however no significant differences were observed between the numbers of focal adhesions in the cells adhered on the surfaces in this study. The high background fluorescence observed in the FITC channel due to the non-specific binding of anti-vinculin antibody made it difficult to determine the number of focal adhesions in the cells.

The formation of focal adhesion on surfaces coated with Caf1-WT can be explain by the capacity of cells after a certain time to start to secrete their own ECM proteins which allows them to adhere to the different surfaces. This has been reported in other studies, for example using BSA which does not contain bio-functional sites for cell adhesion.

Ponik and Pavalko found that osteoblasts cultured on BSA-coated surfaces inhibited the formation of focal adhesions after 2 h of culture. Nevertheless, after 5 h of stationary culture or fluid shear stress, osteoblasts were able to overcome this inhibition and synthesised fibronectin forming focal adhesions (Ponik and Pavalko, 2004).

Caf1 engineered with RGDS motifs small quantities of protein adsorbed to the substrate make it difficult to assess these events. The low cell adhesion cannot be rigorously assumed to be evidence that the ligand is not active for attachment.

5. Chapter Five: Advanced Use of Caf1 Polymer

5.1. Introduction

Scaffolds incorporating bio-adhesive motifs derived from extracellular matrices have been developed as surface modification strategies for tissue-engineering and regenerative medicine. Although considerable advances have been achieved with short peptides such as RGD, engineered bio-adhesive scaffolds should incorporate additional characteristics present in extracellular matrices (Lutolf *et al.*, 2003).

A rational design of biomaterials allows the introduction of specific cell-cell and cell-matrix interactions involved in a particular biological process such as for example, adhesion or proliferation (Banwell *et al.*, 2009).

In addition to biochemical signals, mechanical interactions between cells and biomaterials are important to promote or inhibit a variety of signalling pathways in cells (Cross and Claesson-Welsh, 2001).

Hydrogels are three-dimensional highly hydrated polymeric networks prepared by physical and chemical cross-linking in aqueous solution without dissolving in it, forming pores and void spaces between the polymer chains (Lee and Mooney, 2001). Due to their structure, hydrogels have the advantages over solid scaffolds of (1) enhancing the diffusion of nutrients and oxygen for the cells due to their high porosity; (2) providing space for cell proliferation and expansion due to their pore interconnectivity (3) retaining a high percentage of water similar to some tissues and extracellular matrices (Huang *et al.*, 2011).

Previously, in Chapter 3, we have described the design, production and characterization of a new functional protein scaffold, Caf1-RGDS for cell culture. The applicability of this new system was investigated in Chapter 4 using mammalian cells. In this chapter we report the advanced use of this system. One possible application is the formation of a hydrogel suitable for cell culture. For that, Caf1 WT was covalently cross-linked with three cross-linkers containing different spacer arm length (i.e. the distances between conjugated molecules) and different numbers of the same functional group, *N*-hydroxysuccinimide (NHS) at the end.

The NHS-ester reacts with primary amines to form covalent amide bonds. The reaction is usually performed in phosphate buffer at pH 7.2-8.0 for 0.5 h at room

temperature. Primary amine buffers such as Tris-buffered saline are not compatible because they compete for reaction; however, in some procedures, it is useful to add Tris or glycine buffer at the end of a conjugation procedure to quench (stop) the reaction. The reaction releases *N*-hydroxysuccinimide (M.W. 115), which can be removed easily by dialysis or desalting (Kalkhof and Sinz, 2008).

A brief description of each cross-linker is provided below.

The **Linear homobifunctional, short spacer arm,** DTSSP (Sulfo-DSP) (3,3´-Dithiobis[sulfosuccinimidylpropionate]) (**Figure 5.1**) with molecular weight of 608.51 and a spacer arm with approximately of 12.0 Å. DTSSP is water-soluble and thiol-cleavable (Paine-Saunders *et al.*, 2002).

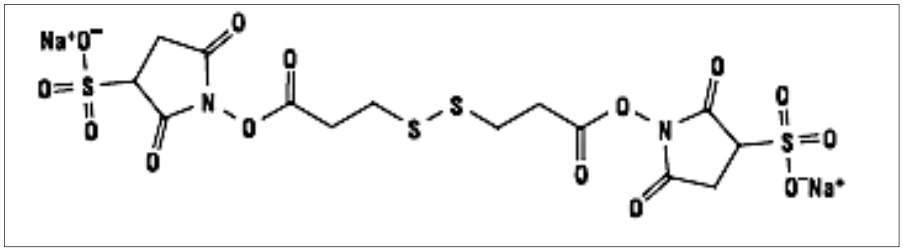

Figure 5.1 – DTSSP cross-linker structure (Bennett *et al.*, 2000)

One of the most studied and widely used hydrogels is poly(ethylene glycol) (PEG). PEG is a chemical compound composed of repeating ethylene glycol units and has been explored as a cell scaffold as well as in drug delivery devices and stabilisation of therapeutic proteins. However, PEG by itself is non-reactive, non-toxic, non-immunogenic, soluble and highly flexible. To create insoluble networks, it requires end-functionalization with cross-linking groups (Roberts *et al.*, 2002).

A number of chemistries have been developed for the functionalization of PEG including the addition of acrylate, thiol, amine, maleimide or vinyl sulfone reactive groups. As cross-linked networks, these materials are non-biodegradable under physiological conditions (Bryant *et al.*, 2005).

Polyethylene glycol spacer arms have a defined structure and molecular weight which ensures reproducible protein-modification effects. Moreover, it provides high stability, reduced tendency toward aggregation and immunogenicity even at high molecular weights (Roberts *et al.*, 2002).

The **Linear homobifunctional, long spacer arm,** NHS-PEG-NHS (O,O´-Bis[2-(N-Succinimidyl-succinylamino)ethyl]polyethylene glycol) (**Figure 5.2**) has a molecular weight of 10000 and a spacer arm of approximately 197 Å (Veronese, 2001).

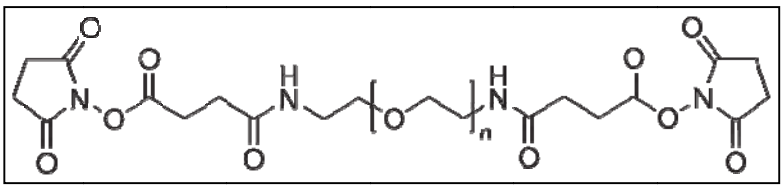

Figure 5.2 – NHS-PEG-NHS cross-linker structure (Roberts *et al.*, 2002)

The **Multi-arm, long spacer arm,** 4-Arm NHS-PEG (4-Arm PEG-Succinimidyl Carboxy Methyl ester) (**Figure 5.3**) has a molecular weight of 20000 and a spacer length of approximately 394 Å (Tan *et al.*, 2010).

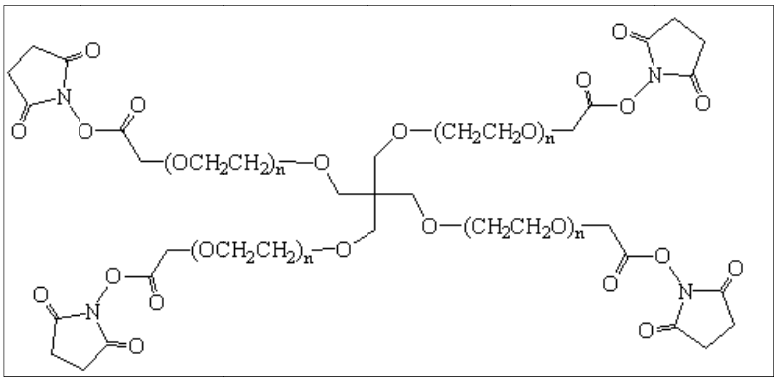

Figure 5.3 – 4-Arm NHS-PEG cross-linker structure (Zhu, 2010)

A description of the techniques and assays used in this study is provided below.

The viability/cytotoxicity assay (Promega) is used to assess cell viability and cytotoxicity of the materials used. The first part of the assay simultaneously measures

two protease activities; one is a marker of cell viability, and the other is a marker of cytotoxicity. The live-cell protease activity is restricted to intact viable cells and is measured using a fluorogenic, cell-permeant, peptide substrate (glycylphenylalanyl-aminofluorocoumarin; GF-AFC). The substrate enters intact cells and is cleaved by the live-cell protease to generate a fluorescent signal proportional to the number of living cells. This live-cell protease becomes inactive upon loss of cell membrane integrity and leakage into the surrounding culture medium. A second, fluorogenic cell-impermeant peptide substrate (bis-alanylalanyl-phenylalanyl-rhodamine 110; bis-AAF-R110) is used to measure dead-cell protease activity, which is released from cells that have lost membrane integrity. Because bis-AAF-R110 is not cell-permeant, essentially no signal from this substrate is generated by intact, viable cells (Prasad *et al.*, 2012).

The traditional scanning electron microscopy procedure was described in chapter 4. In this study, we analysed Caf1 hydrogels by traditional SEM, after gelation, after gelation followed by freeze drying, and also by Environmental scanning electron microscopy (ESEM). The ESEM methodology is a variant of SEM which works in a low vacuum and has the ability to keep the sample in a hydrated state due to the control of the water vapour pressure within the chamber. This is achieved by maintaining a constant sample temperature using a Peltier stage. The pressure can be controlled by a valve which introduces water vapour into the chamber. The rate of condensation and evaporation of the water is dependent on the nature of the sample which means that it can be sometimes more difficult to control the hydration of the sample surface. Thus the thermal conductivity is a critical aspect (Demanuele and Gilpin, 1996).

The ESEM was designed to allow the analysis of biological samples without the complex drying procedures that are necessary for high-vacuum microscopes and it has special features such as specialized electron detectors and differential pumping systems to allow for the transfer of the electron beam from the high vacuum in the gun area to the relatively high pressures attainable in the specimen chamber. Moreover, the sample can be prepared without coating with carbon or gold unlike high-vacuum SEM applications that require the coating of the sample to avoid charge build-up. In 1995, Gilpin and Sigee demonstrated that biological samples can be visualised in the ESEM in wet or partially hydrated states with a minimum of changes in sample morphology (Gilpin and Sigee, 1995).

Another possible application studied in this chapter was the design and synthesis of a second generation of scaffolds for cell culture, e.g. the same scaffold containing several different ECM motifs to enhance cell adhesion, for example the PHSRN from fibronectin (and not only one cell adhesive motif as in Caf1-RGDS) or even to promote other biological processes such as differentiation with the inclusion of growth factors. Also the incorporation of specific protease cleavable sites which can be recognised and cleaved by, for example, metalloproteinases secreted by the cells at specific time points of the cellular development including migration. This new generation of scaffolds, containing more than one motif from ECM proteins, have been desgined to more closely mimic the ECM *in vivo* environment.

Previously, Zaviolov et al. (2001) demonstrated the Caf1 secretion pathway was capable of facilitating the secretion of full-length heterologous proteins fused the C-terminus of Caf1 signal peptide and the N-terminus of structure Caf1 protein, for example, human interleukin-1beta (Holmgren *et al.*, 1992; Zavialov *et al.*, 2001).

In this system, genes encoding chimeric proteins were created in which the human interleukin-1beta was incorporated between the Caf1 signal peptide and the mature Caf1 subunit, leaving the C-terminus of the Caf1 subunit free to interact with the chaperone.

Here we report an approach to secrete Caf1 mutants interspersed with the Caf1 wild type through the chaperone/usher system. The simultaneous expression of two different genes is designated co-expression and is generally achieved with two or more plasmids, each carrying the gene of one subunit and a different selection marker and the plasmids should have different compatible replicons (Scheich *et al.*, 2007).

The pAH34L plasmid (Miller *et al.*, 1998) encodes the *caf* operon and the compatible pBAD33 plasmid encodes only the *caf1* gene. The *caf1* gene expression on pAH34L is temperature-regulated and maximally expressed at 37 °C. Below this temperature the levels of *caf1* gene expression decrease. The plasmid pBAD33 (Guzman *et al.*, 1995) is a low copy chloramphenicol resistant plasmid, containing the P_{BAD} promoter of the araBAD (arabinose) operon and the gene encoding the positive and negative regulator of this promoter (araC). The cloning of the *caf1* gene into the pBAD33 was conducted by GeneArt. In our laboratory, in order to improve the levels of *caf1* expression in *E. coli* expression system we introduced the ribosomal binding site in the mRNA – Shine-Dalgarno sequence (AGGAGG), 8 basepairs upstream of the start

codon AUG. The plasmid pAH34L contains the ColE 1 origin of replication and the plasmid pBAD33 contains the pACYC184 origin of replication.

This system has several advantages; including (1) the modulation of *caf1* gene expression and protein production by controlling either the temperature or the concentration of arabinose. The expression of *caf1* encoded by pAH34L can be induced by performing the cell culture growth at 37°C or above and repressed by decreasing the temperature to below 37°C. At 23°C the expression level of the *caf1* gene is very low. The expression levels of *caf1* encoded by pBAD33 can be modulated over a varied range of L-arabinose concentrations, usually from 0.002-2% and reduced to extremely low levels by the presence of glucose, which represses the gene expression; (2) the production of hybrid Caf1 polymers (Caf1 mutants + Caf1 WT).

5.2. Results

Crosslinking of CAF1 WT with different spacer arm lengths

Caf1 protein at a final concentration of 30 mg/ml was cross-linked with DTSSP, NHS-PEG-NHS and 4-arm NHS-PEG solutions at final concentrations of 3, 6, 9 and 15 mg/ml which correspond to ratio of cross-linking (w/w, cross-linkers:Caf1) of 1:10, 1:5, 1:3, 1:2, respectively. The Caf1 hydrogels at these ratios were characterised by their gelation time, swelling, degree of cross-linking analysed by SDS-PAGE gel, Transmission Electron microscopy (TEM), biocompatibility of the Caf1 hydrogels with mammalian cells performing viability/cytotoxicity assay and morphology studied by Scanning Electron microscopy (SEM).

A) Gelation time

The gelation rate of the Caf1 hydrogels was monitored under sealed conditions at room temperature for 30 minutes, stirring every minute. **Table 5.1** shows that increasing the concentration of DTSSP cross-linker did not change the gelation time. After 30 minutes the reaction did not lose its fluidity, e.g. when the tubes were slightly inverted the solution in the tube slid along the walls of the glass test tubes and did not result in a gel, thus the gelation time was not determined. However, increasing the concentration of NHS-PEG-NHS decreased slightly the gelation time. A more visible decrease in the gelation time was observed by the addition of 4-arm PEG-NHS. The gelation rate of the 4-arm PEG-NHS was faster than the 2-arm PEG-NHS. For example the quickest gelation time for 4arm-PEG-NHS and NHS-PEG-NHS was 2 seconds and 24 min, respectively. Nevertheless, based only on these simple observations we noticed that all Caf1 hydrogels cross-linked with the different cross-linkers resulted in a sample viscosity comparable with the viscosity of the corresponding solution of unreacted Caf1.

B) Swelling

The swelling of Caf1 hydrogels cross-linked with DTSSP, NHS-PEG-NHS and 4-arm PEG-NHS at different concentrations was determined by analysis of the change between the initial diameter of a dried spot of material and final diameter after swelling

following the addition of PBS (**Table 5.1**). The swelling increased as the cross-linker concentration decreased. This trend was most pronounced for the Caf1 hydrogel cross-linked with DTSSP with the greatest swelling at w/w ratio of cross-linking of 1:10.

Table 5.1 – Analysis of the gelation time of Caf1 cross-linked with DTSSP, NHS-PEG and 4-arm PEG-NHS hydrogels at room temperature (≤ 30 min) and Caf1 hydrogel swelling in PBS at 37 ºC. All data are reported as mean percentage of three independent experiments ± standard error of the mean (S.E.M).

Protein	**Cross-linker**	**Ratio crosslinker:protein w:w (mol:mol)**	**Gelation time (min)**	**Swelling % Mean ± S.E.M**
Caf1	DTSSP	1:10 (2.7:1)	N.D	61.2 ± 0.17
		1:5 (5.4:1)	N.D	58.1 ± 0.12
		1:3 (9:1)	N.D	54.3 ± 0.11
		1:2 (13.5:1)	N.D	44.4 ± 0.11
	NHS-PEG-NHS	1:10 (1:6.25)	N.D	40.3 ± 0.17
		1:5 (1:3.25)	27 ± 0.58	40.2 ± 0.42
		1:3 (1:1.9)	26 ± 0.33	35.2 ± 0.33
		1:2 (1:1.25)	24 ± 0.33	32.9 ± 0.49
	4-arm PEG-NHS	1:10 (1:12.5)	22 ± 0.33	24.2 ± 0.60
		1:5 (1:6.5)	5 ± 0.17	24.7 ± 0.33
		1:3 (1:3.8)	4 ± 0.33	14.2 ± 0.05
		1:2 (1:2.5)	2 ± 0.17	14.2 ± 0.03

The **Figure 5.4** shows transparent Caf1 hydrogels cross-linked with 4-arm PEG-NHS after 2 min (**Figure 5.4 - A**) and the swelling properties of the Caf1 hydrogels depending on the ratio of cross-linking, higher for the 1:10 and 1:5 than for 1:3 and 1:2 (**Figure 5.4 - B**).

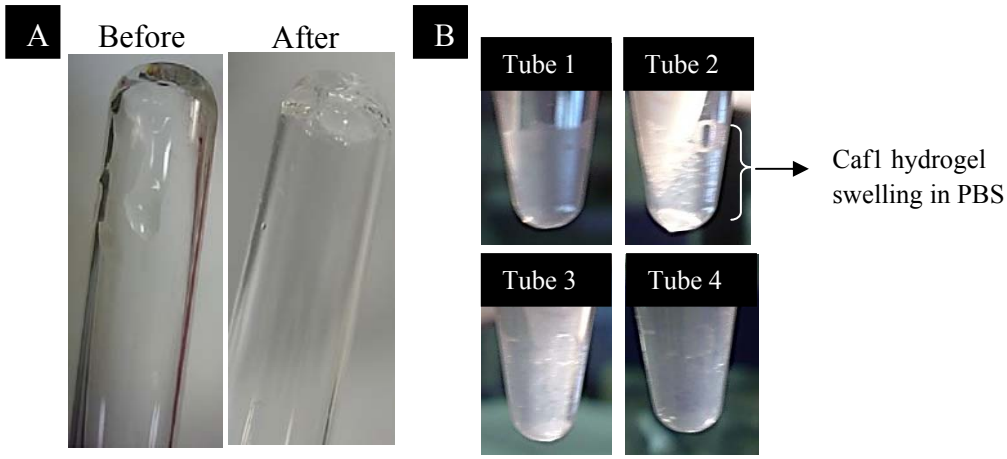

Figure 5.4 – Image of the Caf1 hydrogel cross-linked with 4-arm PEG-NHS. (A) Caf1 hydrogel formed after 2 minutes of reaction (4 arm PEG-NHS: Caf1, ratio of cross-linking of 1:2). **(B)** Swelling of Caf1 hydrogels in polypropylene micro-centrifuge tubes after addition of PBS. Caf1: 4-arm PEG-NHS, ratios of cross-linking (w/w): Tube 1 - 1:10; Tube 2 - 1:5; Tube 3 - 1:3**;** Tube 4 - 1:2.

C) Degree of Cross-linking

Caf1 polymers were treated with the three different cross-linkers each presenting a NHS reactive group on each end of the cross-linker. The NHS group reacts with primary amine groups of lysines at pH 7-8.5 to form stable amide bonds. The reactions were terminated after 30 min. After cross-linking, the samples were incubated in SDS sample buffer at 100 °C for 5 min and the loaded onto a 4-20% gradient polyacrylamide gel for electrophoresis. **Figure 5.5** shows the denatured Caf1 protein samples and revealed the degree of cross-linking. At the bottom of the gel were observed bands of approximately 15 kDa. In the case of Caf1 cross-linked with DTSSP, the bands are resolved between the 25 and 37 kDa protein standard markers (**lanes 1-4**). In the case of Caf1 cross-linked with NHS-PEG-NHS the bands ran approximately with the 37 kDa protein standard markers (**lanes 5-8**). The Caf1 cross-linking with 4-arm PEG-NHS presents a second band which is resolved between 50 and 75 kDa protein standard

markers. The remaining high molecular weight bands could not be assigned by SDS-PAGE gel analysis. However increasing the ratio of cross-linking using different cross-linkers decreased the Caf1 monomeric fraction so this could be used to measure the cross linking efficiency.

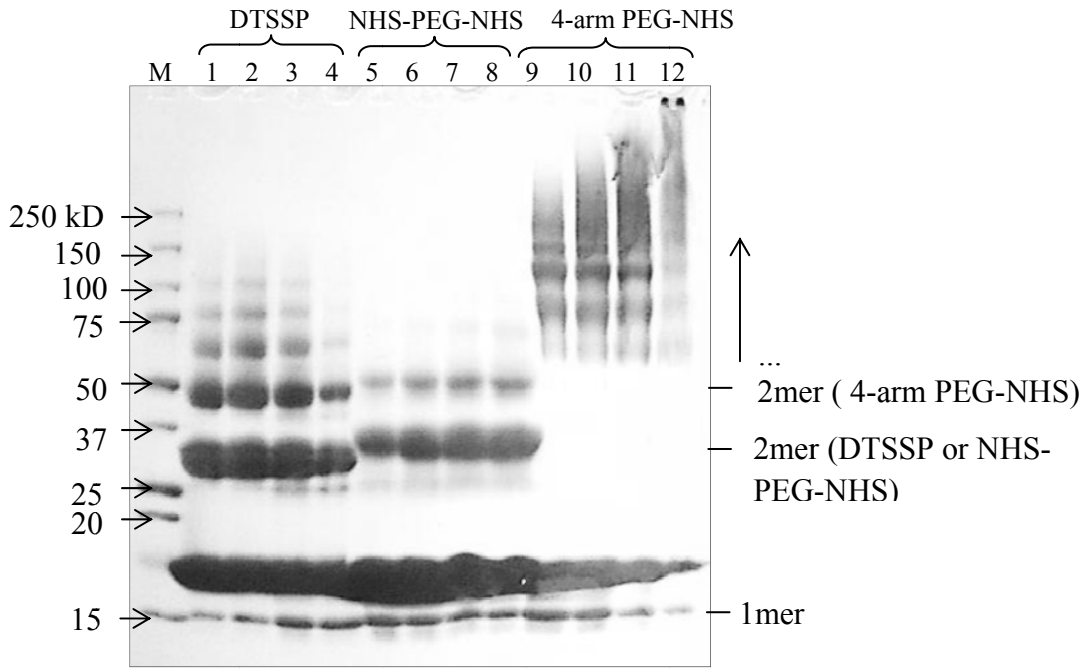

Figure 5.5 – Analysis of Caf1 protein cross-linking using different cross-linkers by 4-20% gradient polyacrylamide gel electrophoresis. Legend: M, molecular weight marker proteins (molecular mass x 10^3 kDa); **lanes 1-4**, Caf1 hydrogel cross-linked with DTSSP; **lanes 5-8**, Caf1 hydrogel cross-linked with NHS-PEG-NHS; **lanes 9-12**, Caf1 hydrogel cross-linked with 4-arm PEG-NHS. The ratios of cross-linking used in this study were: l**ane 1** – 1:10; **lane 2** – 1:5; **lane 3** – 1:3**; lane 4** – 1:2; **lane 5** – 1:10; **lane 6** – 1:5; **lane 7** – 1:3**; lane 8** – 1:2; **lane 9** – 1:10; **lane 10** – 1:5; **lane 11** – 1:3**; lane 12** – 1:2. The gradient polyacrylamide gel was stained with Coomassie Brilliant Blue G-250 stain. Precision Plus Protein standard was used.

The **Table 5.2** shows the values of relative band density obtained by densitometry using ImageJ software. Analysis of the cross-linked fraction and non-cross-linked fraction were performed. The theoretical values for the cross-linked fractions were determined by subtracting the amount of Caf1 protein monomer (in the

presence of cross-linkers) from a Caf1 protein control (in the absence of cross-linker) and then dividing by the latter to get the theoretical crosslinked fraction. The quantity of cross-linked and non crosslinked fractions were taken directly from the gel. Increasing the concentration of the cross-linkers increased the Caf1 cross-linked fraction and decreased the Caf1 non-cross-linked fraction. The exception was for the Caf1 cross-linking with 4-arm PEG-NHS sample at a mass ratio of 1:2 which showed a decrease in the non-cross-linked and in the cross-linked fraction. The theoretical value for the cross-linked fraction was higher than that obtained directly for the cross-linked fraction and it was assumed that this highly cross-linked fraction failed to enter the gel.

Table 5.2 – Relative densitometry for Caf1 non-cross-linked and cross-linked fractions was determined by ImageJ software. All data are reported as mean of three independent experiments ± standard error of the mean (S.E.M).

Cross-linker	**Caf1: Cross-linker (w/w)**	**Non-cross-linked fraction** (Mean ± S.E.M)	**Cross-linked fraction** (Mean ± S.E.M)	**Theoretical values for the cross-linked fraction**
DTSSP	1:10	0.34 ± 0.016	0.55 ± 0.033	0.66
	1:5	0.33 ± 0.0015	0.58 ± 0.08	0.67
	1:3	0.30 ± 0.010	0.63 ± 0.05	0.70
	1:2	0.28 ± 0.0018	0.82 ± 0.06	0.72
NHS-PEG-NHS	1:10	0.87 ± 0.0095	0.11 ± 0.015	0.13
	1:5	0.86 ± 0.068	0.17 ± 0.026	0.14
	1:3	0.72 ± 0.0039	0.20 ± 0.07	0.28
	1:2	0.61 ± 0.0008	0.30 ± 0.04	0.39
4-armNHS-PEG	1:10	0.71 ± 0.013	0.33 ± 0.022	0.30
	1:5	0.33 ± 0.014	0.57 ± 0.04	0.67
	1:3	0.21 ± 0.014	0.62± 0.023	0.79
	1:2	0.16 ± 0.0036	0.28 ± 0.02	0.84

The **Figure 5.6** shows examples of TEM images of Caf1 cross-linked using the short-spacer DTSSP (12.0 Å), the long-spacer NHS-PEG-NHS (~ 197 Å) and the long-spacer with 4-arm PEG-NHS (~ 394 Å) at the same molecular ratio 10:1 (cross-linker: Caf1). The Caf1 hydrogels were prepared as described before, after gelation and swelling in PBS pH 7.4, the Caf1 hydrogels were diluted in nanopure water. The size of hydrogels formed was determined by Jmicrovision version 1.2.5 (Roduit, 2007). Lines along the perimeter of the hydrogel meshes (pieces of hydrogel) were drawn. Graphs were constructed using the SPSS version 19.

TEM images show small pieces of Caf1 hydrogels cross-linked with DTSSP with an average size of 76 nm and a size distribution ranging from 10 to 300 nm. Caf1 hydrogels cross-linked with NHS-PEG-NHS presented an average size of 393 nm and a more disperse size distribution with mesh sizes ranging from 10 to 600 nm. The Caf1 hydrogels cross-linked with 4-arm PEG-NHS showed an average size of 254 nm and an extreme size distribution from around 20 nm to 1500 nm.

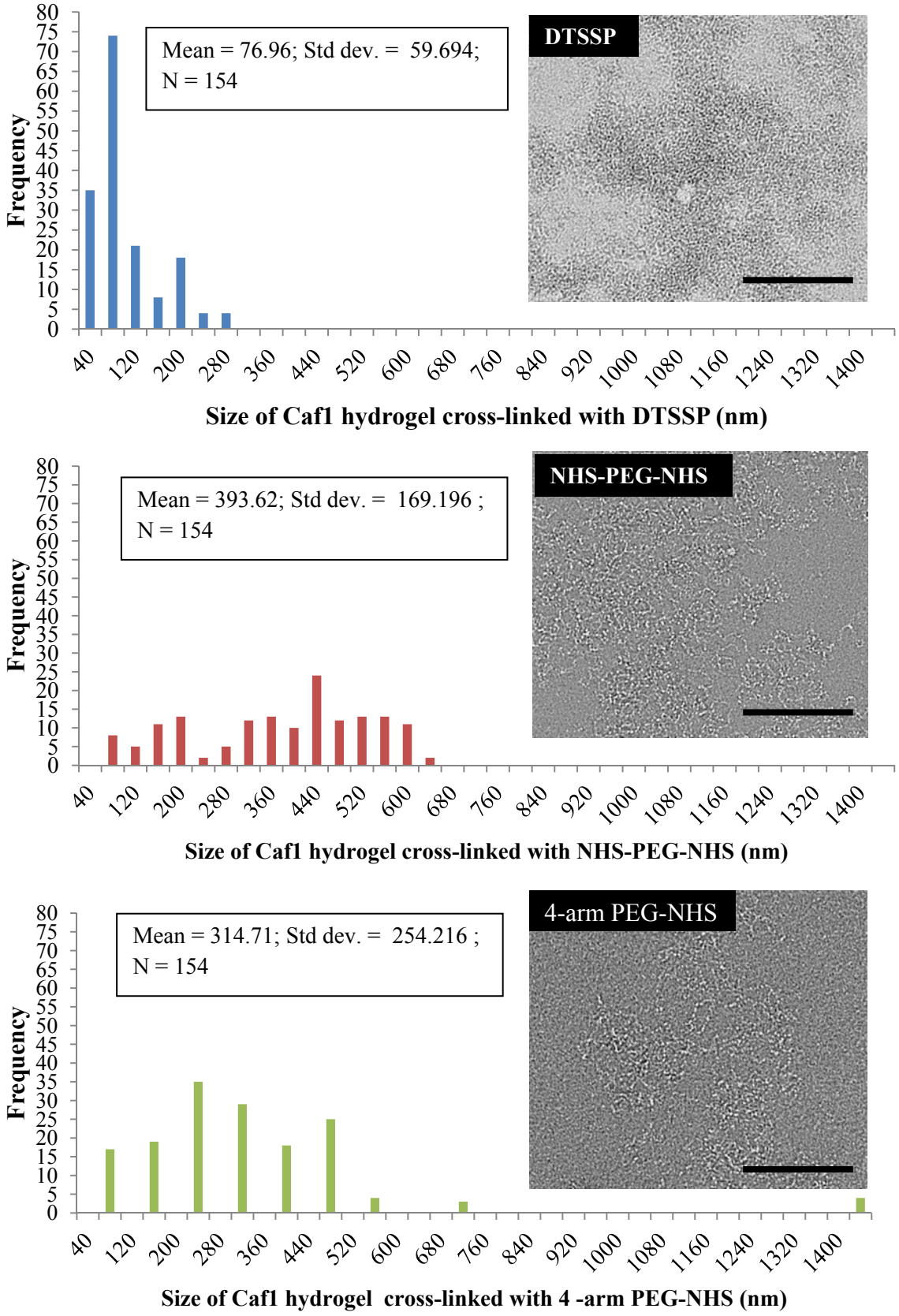

Figure 5.6 – Histograms showing the size of cross-linked Caf1 hydrogel mesh. And TEM image of Caf1 hydrogels cross-linked with different cross-linkers (w/w ratio of 1:10). The scale bar represents 100 nm.

D) Viability and cytotoxicity assay

Rat primary osteoblasts were cultured on the surface of Caf1 hydrogels. After 24 h, viability and membrane integrity were determined by the viability/cytotoxicity assay (Promega), where intact viable-cell protease activity is measured using a fluorogenic, cell-permeant, peptide substrate (glycylphenylalanyl-aminofluorocoumarin; GF-AFC) and dead-cell protease activity is measured by the cell-impermeant peptide substrate (bis-alanylalanyl-phenylalanyl-rhodamine 110; bis-AAF-R110). **Table 5.3** shows the percentage of viability and cytotoxicity for rat primary osteoblasts attached on Caf1 hydrogels and cells tolerated 2D culture on the Caf1 hydrogels shown by 70-80% viability and low percentages for cytoxicity.

Table 5.3 – Percentage of cell viability and cytotoxicity when attached on Caf1 hydrogels cross-linked with different cross-linkers at various ratios.

Hydrogels	Ratio (crosslinker:protein)	Cell viability % (Fluorescence intensity)	Cell cytotoxicity % (Fluorescence intensity)
Caf1: DTSSP	1:10	80% (21004)	20% (5317)
	1:5	76% (21608)	24% (6788)
	1:3	78% (21543)	22% (5964)
	1:2	80% (21310)	20% (5328)
Caf1: NHS-PEG-NHS	1:10	77% (22154)	23% (6441)
	1:5	77% (23214)	23% (6818)
	1:3	76% (23880)	24% (7397)
	1:2	73% (24104)	27% (8805)
Caf1: 4-arm PEG-NHS	1:10	71% (23939)	29% (9563)
	1:5	77% (23365)	23% (7101)
	1:3	75% (24298)	25% (8042)
	1:2	74% (18713)	26% (6605)
Only Caf1	-	61% (15185)	39% (9567)
DME Medium	-	84% (24225)	16% (4730)
15% ethanol	-	7% (1606)	93% (20641)

The ability of Caf1 polymers cross-linked with 4-arm PEG-NHS to form a hydrogel was explored. The **Figure 5.7** shows TEM images of both the monomeric circularly permuted variation of Caf1 (cpCaf1) (Chalton *et al.*, 2006) and Caf1 polymers cross-linked with 4-arm PEG-NHS, only 4-arm PEG-NHS and Caf1 alone.

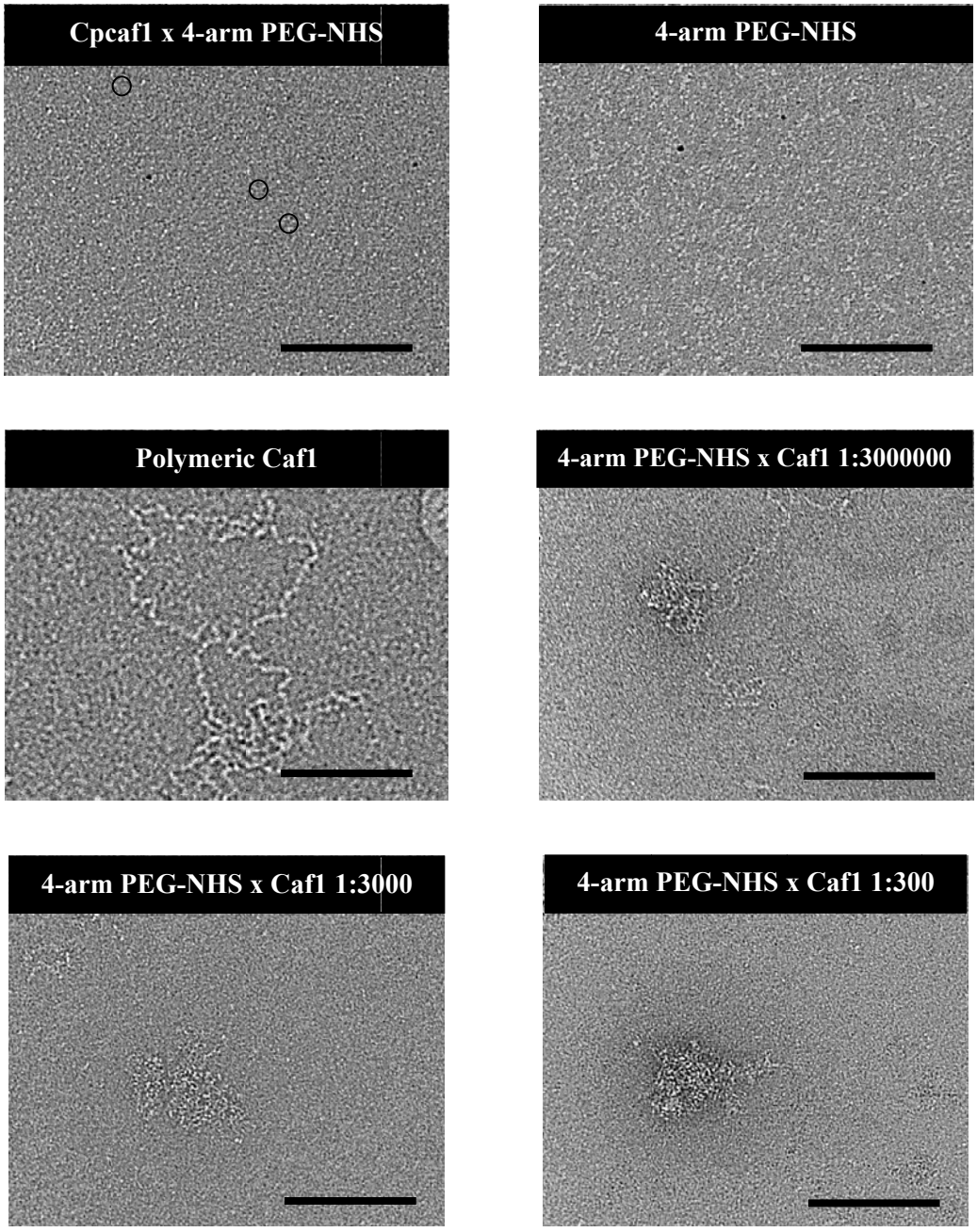

Figure 5.7 – Transmission electron microscopy of Caf1 polymers cross-linked with different concentrations of 4-arm PEG-NHS (w/w ratio of 1: 3000000, 1: 3000, 1:300) and the controls: cpCaf1 (Chalton *et al.*, 2006), 4-arm PEG-NHS and Caf1 polymer. All specimens were negatively stained. The scale bar indicates 100 nm.

The TEM images (**Figure 5.7**) revealed that monomeric circularly permuted variation of Caf1 (cpCaf1) (Chalton *et al*., 2006) cross-linked with 4-arm PEG-NHS did not form visible gel-like structures. We can observe very small structures indicated by the circles. In addition, both the 4-arm PEG-NHS and Caf1 alone did not form large hydrogel networks. Some examples of these hydrogels networks begin to be visible using Caf1 polymers cross-linked with 4-arm PEG-NHS at various ratios of cross-linking (w/w).

The Caf1 polymer cross-linked with 4-arm PEG-NHS at various ratios of cross-linking (w/w, cross-linker: Caf1) samples at 1: 3000000, 1: 300000, 1: 30000, 1: 3000, 1:300, 1:60 and 1:30 after gelation as mentioned before were heated at 100ºC for 5 min in SDS-sample buffer and loaded onto a SDS- PAGE. The gel was scanned and analysed as described above by ImageJ version 1.46. The values corresponding to Caf1 cross-linked fraction either determined by ImageJ the Caf1 non-cross-linked fraction are presented in **Table 5.4**. The Caf1 cross-linked fraction increased with the increase of cross-linker concentration.

Table 5.4 – Relative densitometry for Caf1 non-cross-linked and cross-linked fractions was determined by ImageJ software. All data are reported as mean of three independent experiments ± standard error of the mean (S.E.M).

4-arm PEG-NHS:Caf1 w:w (mol:mol)	**Non-cross-linked fraction** (Mean ± S.E.M)	**Cross-linked fraction** (Mean ± S.E.M)	**Theoretical values for cross-linked fraction**
1: 3000000 (1:3800000)	0.99 ± 0.0034	0.006 ± 0.0014	0.01
1: 300000 (1:380000)	0.99 ± 0.0024	0.0079 ± 0,0015	0.01
1: 30000 (1:38000)	0.98 ± 0.0023	0.043 ± 0.033	0.02
1: 3000 (1:3800)	0.97 ± 0.0022	0.051 ± 0.028	0.03
1: 300 (1:380)	0.89 ± 0.0017	0.14 ± 0.066	0.11
1:60 (1:72)	0.85 ± 0.0016	0.18 ± 0.05	0.15
1:30 (1:38)	0.73 ± 0.0026	0.22 ± 0.07	0.27

The **Figure 5.8** shows TEM images of Caf1 polymers cross-linked with 4-arm PEG-NHS at various ratios of cross-linking (w/w, cross-linker:Caf1).

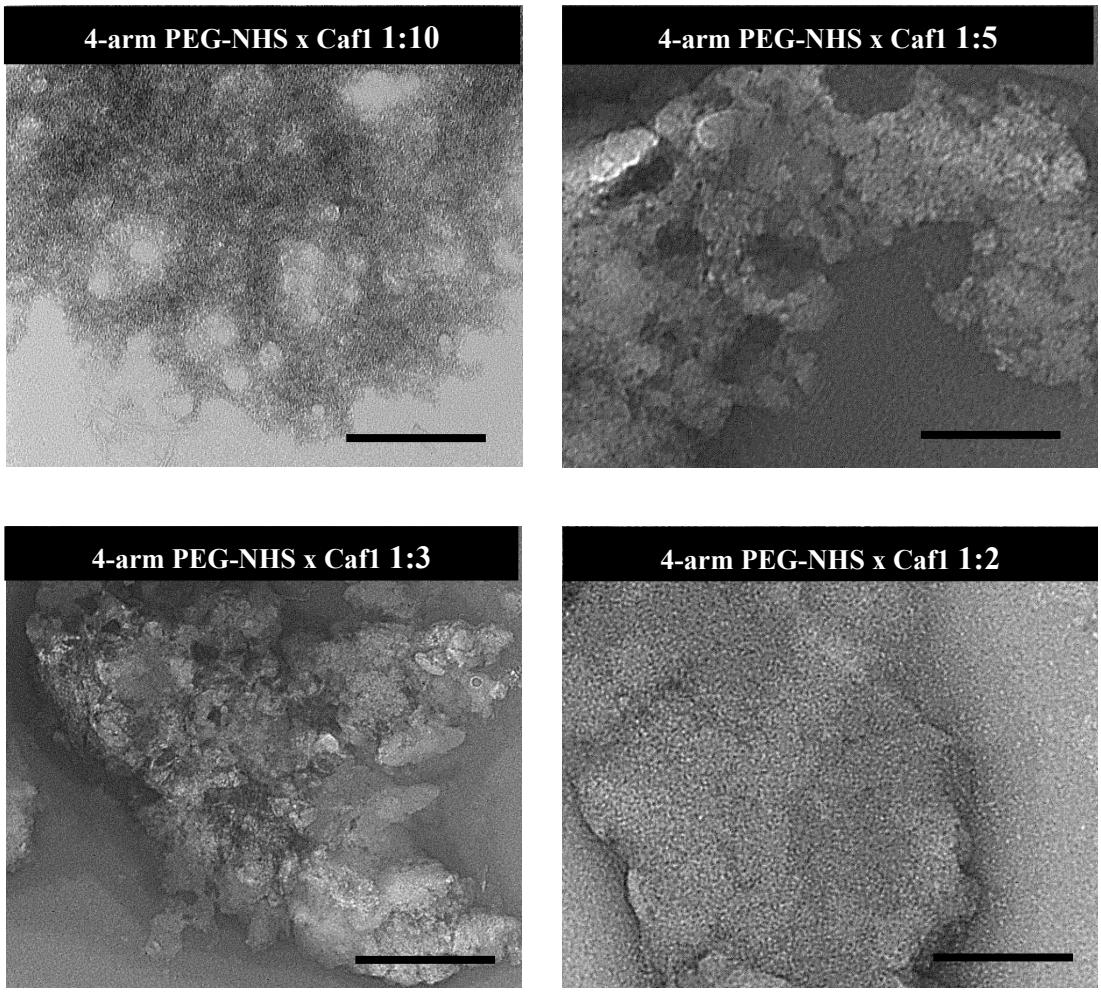

Figure 5.8 – Transmission electron microscopy of Caf1 polymers cross-linked with different concentrations of 4-arm PEG-NHS (w/w ratio of 1: 10, 1: 5, 1:3, and 1:2). As the concentration of 4-arm PEG-NHS crosslinker increases (1:10 to 1:2), the porosity of the Caf1 hydrogel decreases and the Caf1 hydrogel structure becomes more compact. All specimens were negatively stained. The scale bar indicates 100 nm.

The TEM images (**Figure 5.8**) revealed that Caf1 polymers cross-linked with 4-arm PEG-NHS at 1:10 (w/w, cross-linker:Caf1) form a dense hydrogel structure, however the hydrogels formed have a wide distribution of pores with dimensions much smaller than 100 nm. The hydrogel structure becomes more compact with the increase of cross-linker. At ratio of cross-linking of 1:2, the hydrogel presents as an amorphous structure with no visible pores.

Morphology of Caf1 hydrogel by scanning electron microscopy (SEM)

The **Figure 5.9** shows Caf1 hydrogel cross-linked with 4-arm PEG-NHS at a ratio of 1:3.

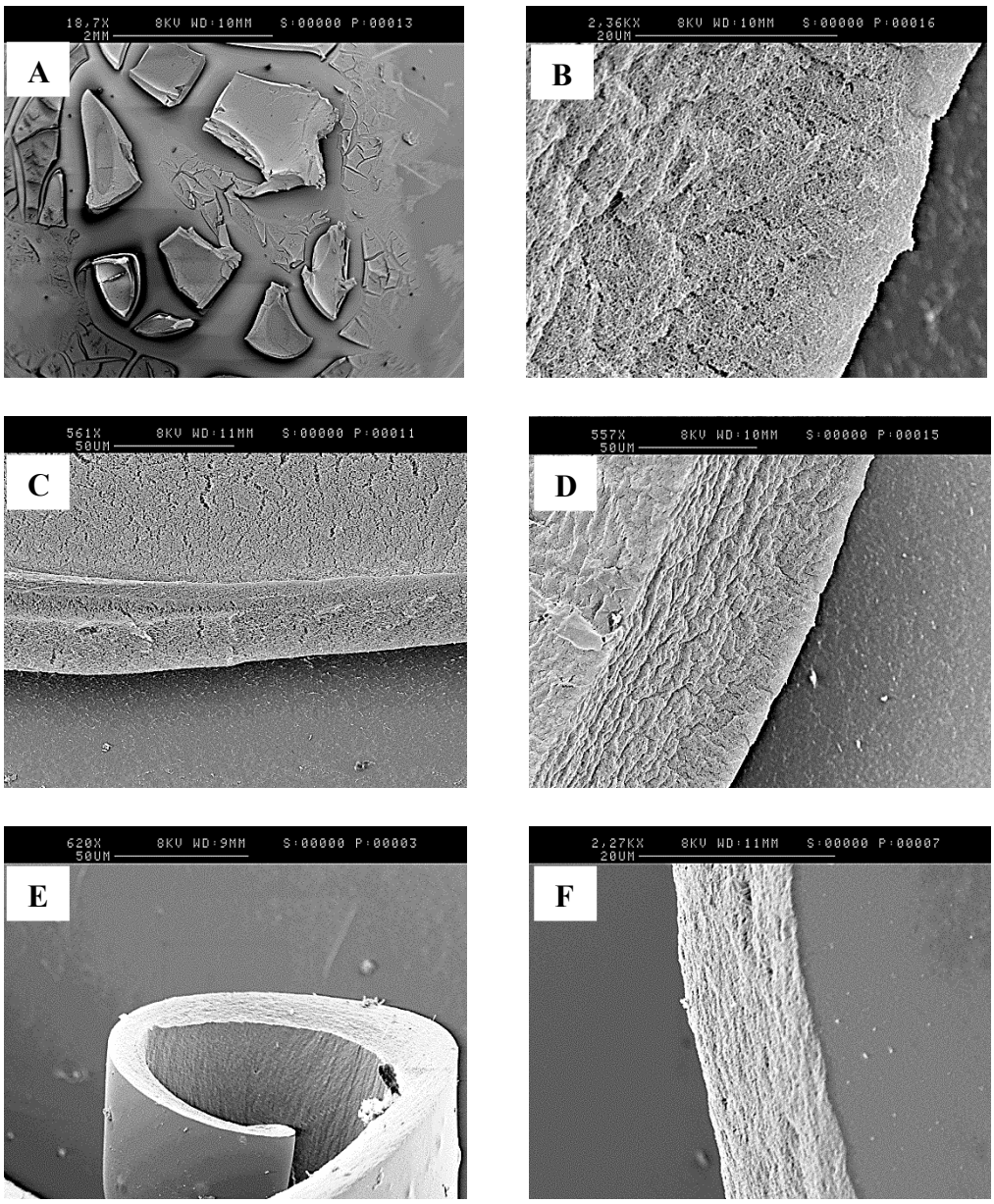

Figure 5.9 – Scanning electron microscopy images of Caf1 hydrogel cross-linked with 4-arm PEG-NHS (w/w ratio 1:3). A – Caf1 hydrogel broken into several pieces. **B, C, D, E and F –** Transverse sections of the Caf1 hydrogel pieces. It has a very compact structure and the diameter of the pores was not determined although they seem to be on an order of nanometres.

The **Figure 5.10** shows Caf1 freeze-dried hydrogel which displays a mesh-like architecture presenting pore diameter ranging from 3 μm to 22 μm with an mean pore diameter of 8 ± 1.9 μm.

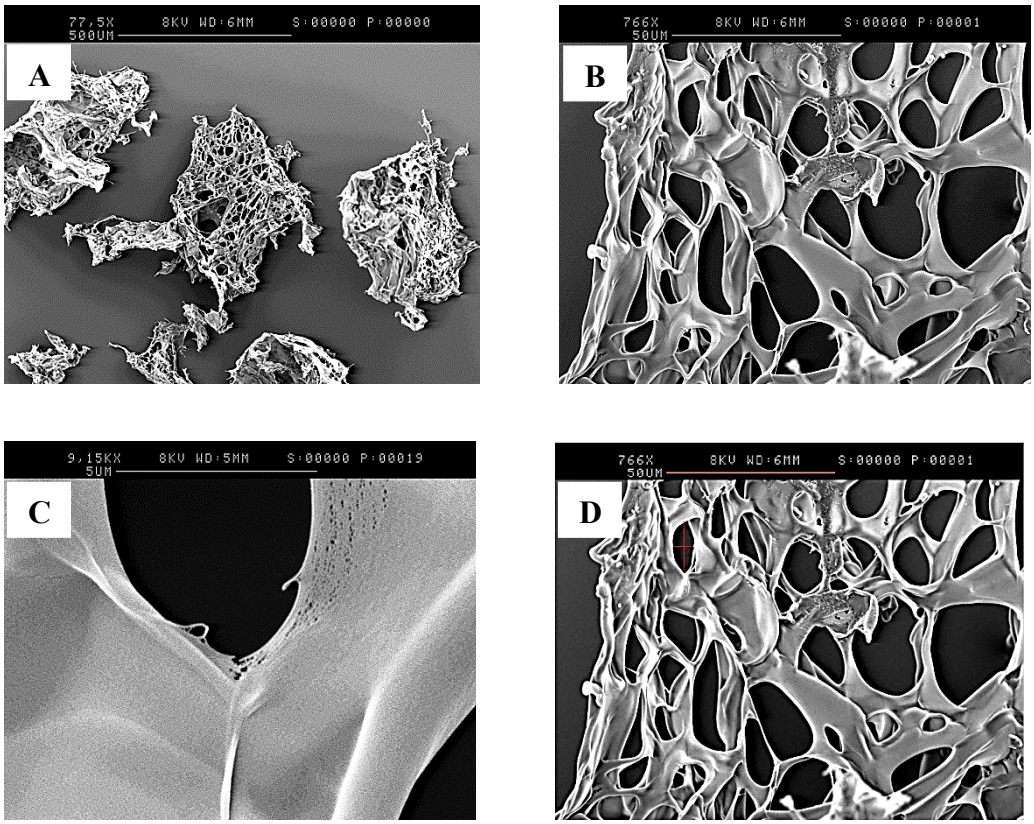

Figure 5.10 – Scanning electron microscopy images of Caf1 hydrogel cross-linked with 4-arm PEG-NHS after freeze-drying (w/w ratio 1:3). A – Fragments of Caf1 hydrogel after freeze-dried process. **B –** Original image of Caf1 hydrogel. **C –** Image of the Caf1 hydrogel pore. **D –** Image processed by Jmicrovision version 1.2.5 (Roduit, 2007). Measurements of pore diameter were conducted by drawing lines, as the red lines represented on the image, across the pore in the hydrogel. The size of the pore was calculated using the equation presented in the Materials and Methods, SEM analysis. This equation was obtained from Soliakov *et al*., 2010.

Unprocessed hydrated Caf1 hydrogels were visualised by ESEM. In ESEM, the hydrogels are exposed to a saturated water vapour environment with minimal drying which allows the study of the pore structure of the hydrogels in the natural hydrated state. The hydrated Caf1 hydrogel exhibited nanopores ranging from 100 nm to 600 nm.

The mean size of the pores was approximately 300 ± 0.3 nm but the size distribution observed seems relatively wide. Here the void spaces of Caf1 protein hydrogel are larger than dehydrated Caf1 hydrogel (**Figure 5.11**).

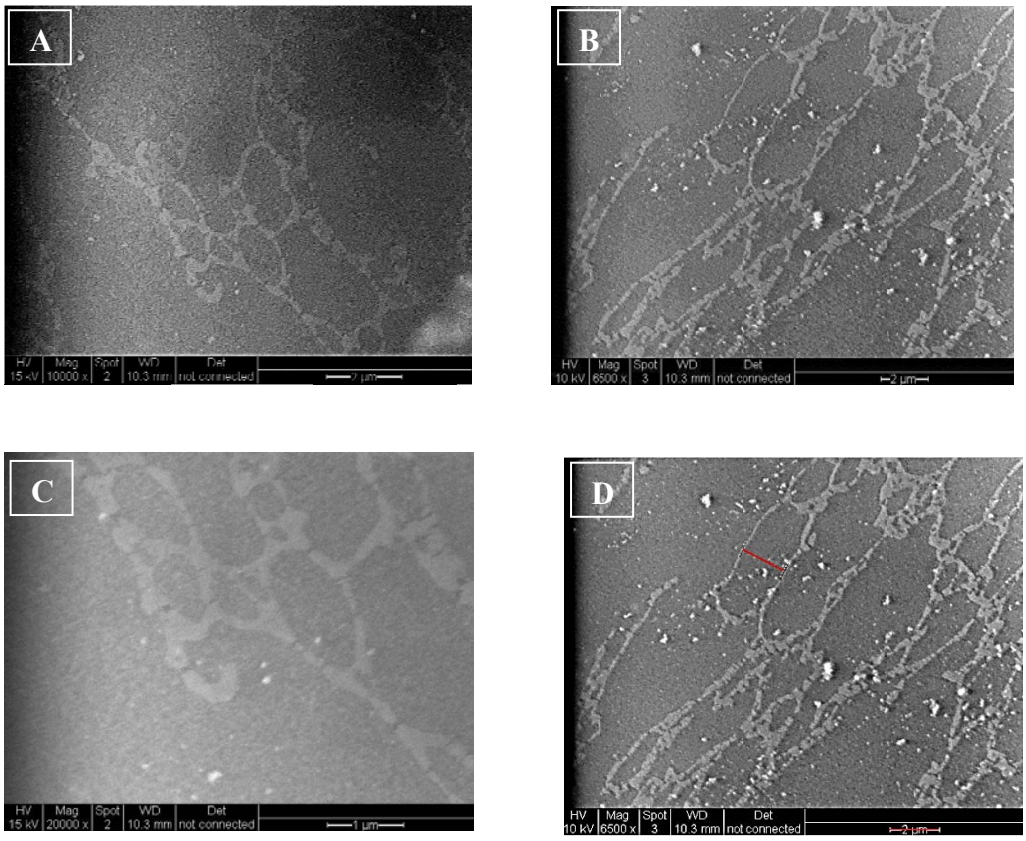

Figure 5.11 – Environmental scanning electron microscopy images of Caf1 hydrogel cross-linked with 4-arm PEG-NHS (w/w ratio 1:3). A – Caf1 hydrogel network with different pore sizes. **B –** Original image of Caf1 hydrogel. **C** – Caf1 hydrogel network showing the pores of the hydrogel at higher magnification. **D –** Image processed by Jmicrovision version 1.2.5 (Roduit, 2007). Measurements of pore diameter were conducted by drawing lines like the red lines shown on the image, across the pore of the hydrogel. The size of the pore was calculated in nanometers using the equation presented in Materials and Methods. This equation was obtained from (Soliakov *et al.*, 2010).

Morphology of mammalian cells on the Caf1 hydrogel by SEM

Mouse 3T3 fibroblasts and rat primary osteoblasts were cultured on the surface of Caf1 hydrogels. After 24 h, cells were fixed with 2% glutaraldehyde, dehydrated and gold coated to be visualised by traditional SEM. In 2D cultures, more fibroblasts

presented elongated morphology than osteoblasts. This result indicates that fibroblasts adhere and spread more on these surfaces coated with Caf1 hydrogels (**Figure 5.12**). The majority of the osteoblasts displayed a rounded morphology and only a few cells showed visible spreading on surfaces coated with Caf1 hydrogels.

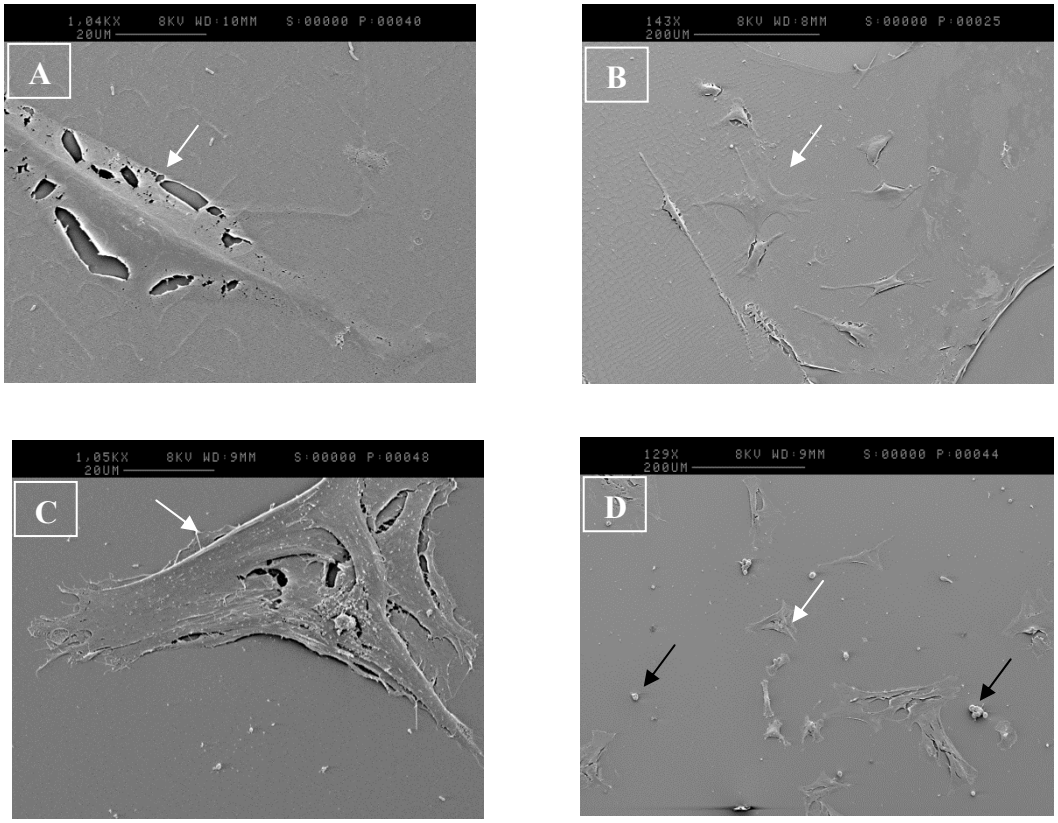

Figure 5.12 – Scanning electron microscopy images of Caf1 hydrogel after 24 h in culture with mammalian cells. (A) Mouse 3T3 Fibroblast at higher magnification. **(B)** Mouse 3T3 Fibroblasts spread on Caf1 hydrogel. **(C)** Rat primary osteoblast at higher magnification. **(D)** Rat primary osteoblasts which spread on Caf1 hydrogel (white arrow) and which did not spread on Caf1 hydrogel (black arrows). The white and black arrows show the mammalian cells on Caf1 polymers cross-linked with 4-arm PEG-NHS (w/w ratio 1:3).

Co-expression of Caf1 WT using two compatible plasmids, the pAH34L and pBAD33

Two groups of three glass test tubes, each containing 5 mL of LB broth media supplemented with 20 μg/mL of chloramphenicol, 100 μg/mL of ampicillin and both 100 μg/mL of ampicillin and 20 μg/mL of chloramphenicol antibiotics were inoculated with single colonies of the transformed *E. coli* TOP10 containing pBAD33_SD_Caf1, pAH34L or both pBAD33_SD_Caf1 + pAH34L, respectively. For each set 0.2% glucose was added to one group of 3 tubes. All the glass test tubes were incubated at 37 ºC in a rotation wheel at 180 rpm. When cultures reached the mid-log phase of growth (optical density of 0.5-0.6 at 600 nm), three concentrations of L-arabinose (0.02, 0.2 and 2 %) was added to separate glass test tubes. After 16 h of further incubation the bacterial cell cultures were transferred to a 15 ml Falcon tube and these were centrifuged at 3000 rpm for 15 minutes at 4 ºC. Photographs of all Falcon tubes were taken. The sizes of the pellet and flocculent layer were immediately measured on the Falcon tube using a ruler (**Figure 5.10**).

The **Figure 5.13** shows some examples of the measurements of the flocculent layer and the cell pellet from cultures in this study. Although the presence of a flocculent layer was observed in all tubes containing either pAH34L or pBAD33_SD_Caf1 + pAH34L, the flocculent layer was thicker in glucose containing tubes than in the tubes where no D-glucose was added. The cell pellet was smaller in cells expressing only pAH34L compared to either pAH34L and pBAD33 or pBAD33 alone. This was true whether D-glucose was added or not. In the tubes containing pBAD33_SD_Caf1 no flocculent layer was observed either in the presence or absence of D-glucose.

Falcon tubes containing 0.2% L-arabinose and no D-glucose

E. coli TOP10/ pAH34L

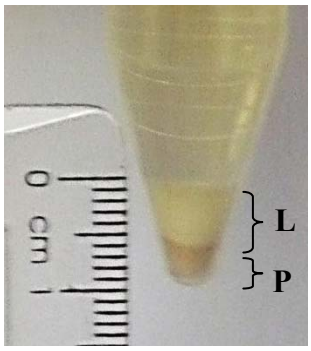

E. coli TOP10/pBAD33_SD_Caf1 + pAH34L

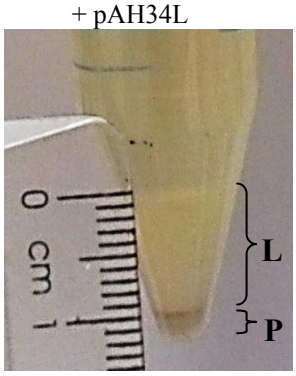

E. coli TOP10/pBAD33_SD_Caf1

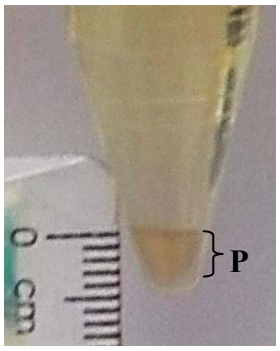

Falcon tubes containing 0.2% L-arabinose and 0.2% D-glucose

E. coli TOP10/ pAH34L

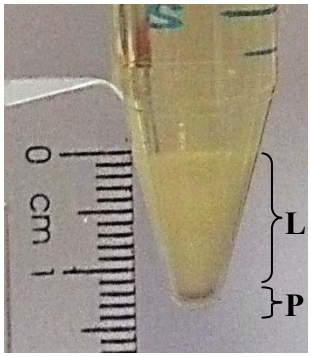

E. coli TOP10/pBAD33_SD_Caf1 + pAH34L

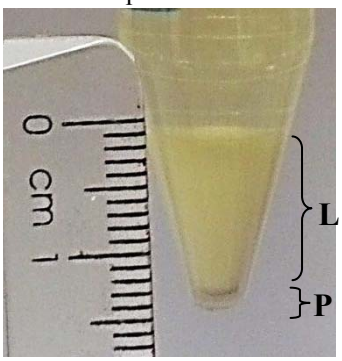

E. coli TOP10/pBAD33_SD_Caf1

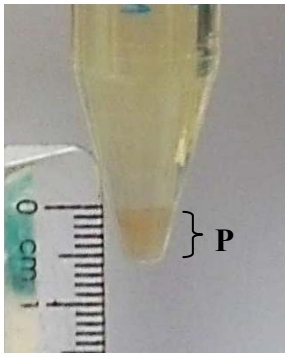

Figure 5.13 – Co-expression of Caf1 WT using the plasmids pAH34L and pBAD33. Represented are the images of the Falcon tubes containing *E. coli* TOP10/pBAD33_SD_Caf1, *E. coli* TOP10/pAH34L and *E. coli* TOP10/pBAD33_SD_Caf1 + pAH34L in the presence of 0.2% of L-arabinose and in the presence or absence of D-glucose. Legend: L – Flocculent layer; P – cell pellet.

The following procedure was applied to the tubes containing the cultures in 0, 0.02 and 0.2% L-arabinose in the presence or absence of D-glucose. Excess LB media, approximately 4 ml, was carefully taken out of each Falcon tube using a pipette. The flocculent layer, with the remaining LB, was carefully separated from the cell pellet using the pipette. Samples of this layer were added to SDS-sample buffer and heated at 100 ºC for 5 minutes and loaded onto 12% SDS-PAGE. One of the gels was stained with Coomassie Brilliant Blue and the other gel was used to perform a western blot. The blot was probed for Caf1 using a monoclonal anti-Caf1 antibody (YPF19) followed by detection of bound antibody using goat anti-mouse IgA-horse-radish peroxidise conjugate. Bound antibody was detected using 4CN (4-chloro-1-naphthol) substrate.

The western blot membrane was scanned and analysed by the ImageJ software to compare the density of the bands on the western blot. The mean of the relative density of the bands and the standard error of the mean were determined. The results obtained for the quantification of the Caf1 present in the flocculent layer and the measured size of the flocculent layer can be seen in **Figure 5.14**.

Figure 5.14 shows the relation between the size of flocculent layer and the quantity of Caf1 protein present in the flocculent layer.

E.coli TOP10 cells transformed with the plasmid pBAD33, encoding only for *caf1* gene (without the chaperone and usher), did not secrete Caf1 into the cell culture medium, thus the quantification of the flocculent layer in this case was nearly zero even after adding different concentrations of the inducer, L-arabinose.

This was true in presence or absence of 0.2% of D-glucose. Cultures of *E. coli* TOP10 competent cells carrying the *caf* operon and *caf1* gene cloned into pAH34L and pBAD33 respectively showed a small flocculent layer and no Caf1 in the absence of either D-glucose or the inducer L-arabinose.

After induction with 0.02, 0.2 and 2% L-arabinose an increased Caf1 level and a corresponding larger flocculent layer was observed. *E.coli* TOP10 competent cells transformed with the plasmid pAH34L (encoding for *caf* operon) showed a level of Caf1 slightly smaller than that observed for cultures containing both plasmids induced with 0.2 and 2% L-arabinose.

The levels of Caf1 obtained for *E. coli* TOP10 competent cells transformed with the plasmid pBAD33 (encoding only *caf1*) were similar in the presence or absence of

D-glucose. For *E. coli* TOP10/pBAD33_SD_Caf1 + pAH34L a high level of Caf1 was detected in the flocculent layer for any concentrations of L-arabinose used. A slightly higher quantity of Caf1 was detected in the culture induced with 2% of L-arabinose and the flocculent layer was similar in all cultures even though they were induced with different concentrations of L-arabinose. For the *E. coli* TOP10 competent cells transformed with the plasmid pAH34L encoding for the *caf* operon the level of Caf1 in the flocculent layer was high.

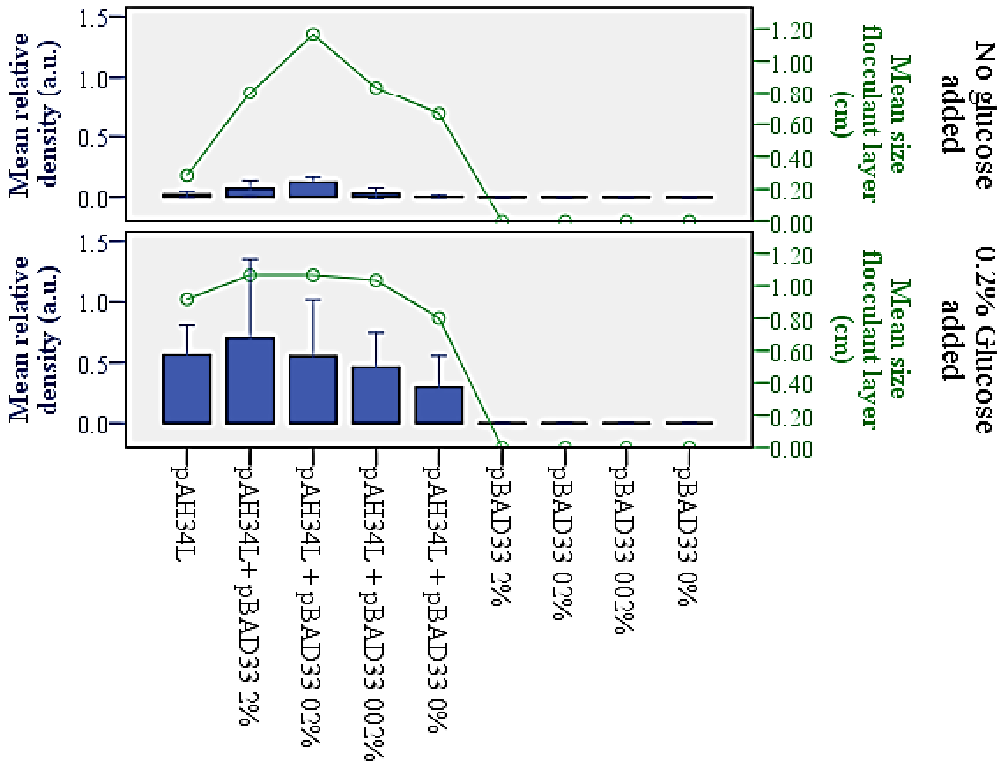

Figure 5.14 – Relation between the size of flocculent layer of Caf1 and the relative density of Caf1 for each preparation.

Expression of heterologous sequences fused to the Caf1 subunit in *Escherichia coli*

The *caf1* gene in pBAD33 was mutated by the insertion of: **(1)** 6-Histidine near its N-terminus (Caf1-6HisNT); **(2)** PHSRN motif which is the RGD synergy sequence in fibronectin (Caf1-PHSRN) in the loop 1 of Caf1 (Caf1-PHSRN Loop1); **(3)** FLAG epitope (DYKDDDDK) in the N-terminus of Caf1 (caf1-FLAG epitope NT); **(4)** Cysteine in the NT-terminus of Caf1 (Caf1-Cys-NT); **(5)** Cysteine in loop 4 of Caf1 (Caf1-G35C Loop4); Cysteine in loop 2 of Caf1 (Caf1-Q106C Loop 2); **(6)** PENFF

cleavage site for metalloproteinase 13 (MMP13) in the N-terminus of Caf1 (Caf1-PENFF-NT); **(7)** 6-Histidine in the N-terminus of Caf1 followed by a spacer linking peptide (GGGGSGGGGS) (Caf1-6His-NT spacer); **(8)** 6-Histidine in the C-terminus of Caf1 (Caf1-6His-CT); **(9)** PHSRN motif in the loop 3 of Caf1 (Caf1-PHSRN Loop3) (**Figure 5.15**). These mutations in the caf1 gene were designed as variants of the *caf1* gene. The variants were synthesised and cloned into pBAD33 vector by GeneArt (Invitrogen Life technologies).

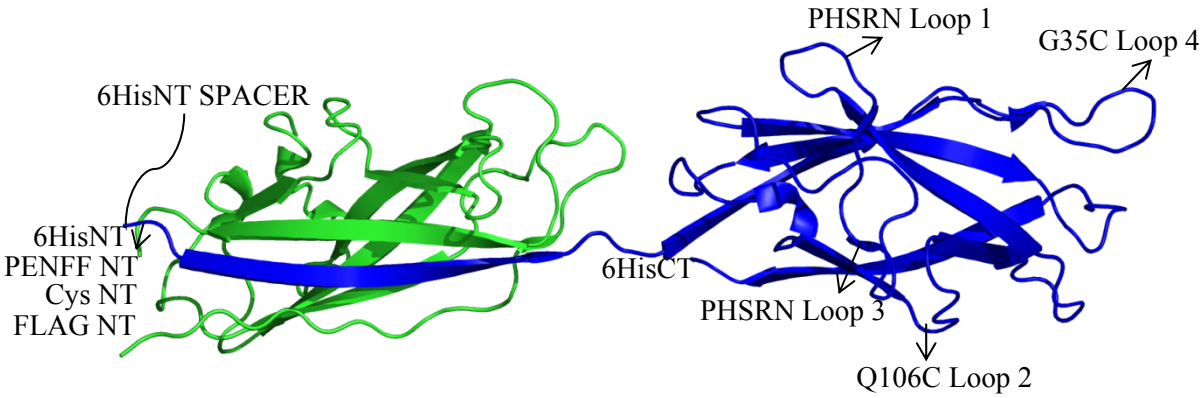

Figure 5.15 – *Caf1n: Caf1*complex (Caf1 dimer) (PDB file: 1P5U). This image was generated using PyMOL software (*http://www.pymol.org*). The full length Caf1 is represented in blue. The mutations were incorporated in loops 1, 2, 3, 4 and in the N- and C-terminal of Caf1.

Plasmid DNA for each pBAD33_SD_Caf1 mutant (For more details about the constructs see Materials and Methods **Table 2.12**) was used to transform *E. coli* TOP10 competent cells either with or without pAH34L. In the positive control only pAH34L plasmid DNA was used to transform *E. coli* TOP10 competent cells. The transformed bacterial cells were grown on L-agar containing the relevant antibiotic(s) mentioned above. Individual colonies from a plate of transformed *E. coli* TOP10 competent cells were grown in glass test tubes with 10 mL of Luria broth medium containing the relevant antibiotic(s) at 37 ºC until they reached an optical density of 0.5-0.6 at 600 nm. Arabinose at a final concentration of 0.2% was added in each glass test tube. The bacterial cell culture was allowed to grow at 37 ºC for 16 h. After this incubation time, the culture was centrifuged at 3000 rpm for 15 minutes at 4 ºC. The flocculent layer and the cell pellet were measured using a ruler (**Table 5.5**).

The **Table 5.5** shows that, after induction with 0.2% of L-arabinose, co-expression of pBAD33 with pAH34L was needed to produce a flocculent layer with pBAD33_SD_caf1-FLAG epitope NT, pBAD33_SD_caf1-G35C Loop 4, pBAD33_SD_caf1-6His-NT spacer, pBAD33_SD_caf1-6His-CT and pBAD33_SD_caf1-PHSRN Loop 3.

In two cultures, pBAD33_SD_caf1-Q106C Loop2 + pAH34L and pBAD33_SD_caf1-PHSRN Loop1 + pAH34L no flocculent layer was detected after induction. In the pBAD33_SD_caf1-PENFF-NT+ pAH34L culture we observed a flocculent layer before induction however we did not observe the flocculent after induction.

The flocculent layer was very thick in the L-arabinose induced cultures of pBAD33_SD_caf1-G35C Loop 4 + pAH34L when compared with the non-induced cultures which could indicate some contribution of the mutant to the polymer. In the case of pBAD33_SD_caf1-FLAG epitope NT+ pAH34L the size of the layer was similar in the induced and non-induced cultures. It was more difficult to understand this result if one only uses the size of the layer as an indication of Caf1 co-expression.

Thus, a western-blot was performed to analyse these samples using the monoclonal anti-caf1 antibody and the monoclonal anti-FLAG epitope antibody (**Figure 5.16**). A test was performed for pBAD33_SD_caf1-6His NT + pAH34L (**Figure 5.17)** and for pBAD33_SD_caf1-6His-NT spacer + pAH34L (**Figure 5.18**). These last two samples were analysed by two western blots probed for Caf1 using a monoclonal anti-Caf1 antibody and for poly-histidine using a monoclonal anti-poly-histidine antibody. An identical analysis was performed in pBAD33_SD_caf1-6His-CT + pAH34L cultures where the flocculent layer observed after induction with 0.2% of L-arabinose was slightly higher than the one observed before induction (**Figure 5.19**).

And also western blots for pBAD33_SD_caf1 PHSRN Loop 1 + pAH34L**,** pBAD33_SD_caf1 Cys-NT + pAH34L, pBAD33_SD_caf1 G35C + pAH34L, pBAD33_SD_caf1 Q106C + pAH34L, pBAD33_SD_caf1 PENFF-NT + pAH34L, pBAD33_SD_caf1 PHSRN Loop 3 + pAH34L were performed using the monoclonal anti-Caf1 antibody (**Figure 5.20**).

Table 5.5 – Measurements of the flocculent layer thickness in *E. coli* TOP10 cells transformed with plasmid pBAD33_SD_caf1 mutants jointly with pAH34L encoding for Caf1 WT. The same measurements were performed in *E. coli* TOP10 transformed with plasmid pAH34L and with plasmid pBAD33_SD_caf1 mutants in separately. All data are reported as mean of three independent experiments ± standard error of the mean (S.E.M).

Plasmids	Flocculent layer (cm) (Mean ± S.E.M) n=3	
	No L-arabinose	0.2% L-arabinose
pBAD33_SD_caf1-6His NT + pAH34L	0.2 ± 0.005	0.2 ± 0.005
pBAD33_SD_caf1-PHSRN Loop1 + pAH34L	-	-
pBAD33_SD_caf1-FLAG epitope NT+ pAH34L	0.2 ± 0.003	0.2 ± 0.005
pBAD33_SD_caf1-Cys-NT+ pAH34L	0.1 ± 0.003	-
pBAD33_SD_caf1-G35C Loop 4 + pAH34L	0.3 ± 0.006	1 ± 0.044
pBAD33_SD_caf1-Q106C Loop2 + pAH34L	-	-
pBAD33_SD_caf1-PENFF-NT+ pAH34L	0.2 ± 0.003	-
pBAD33_SD_caf1-6His-NT spacer + pAH34L	0.3 ± 0.008	0.3 ± 0.008
pBAD33_SD_caf1-6His-CT + pAH34L	0.1 ± 0.003	0.2 ± 0.005
pBAD33_SD_caf1-PHSRN Loop 3 + pAH34L	0.2 ± 0.003	0.3 ± 0.005
pBAD33_SD_caf1-6His NT	-	-
pBAD33_SD_caf1-PHSRN Loop1	-	-
pBAD33_SD_caf1-FLAG epitope NT	-	-
pBAD33_SD_caf1-Cys-NT	-	-
pBAD33_SD_caf1-G35C Loop 4	-	-
pBAD33_SD_caf1-Q106C Loop2	-	-
pBAD33_SD_caf1-PENFF-NT	-	-
pBAD33_SD_caf1-6His-NT spacer	-	-
pBAD33_SD_caf1-6His-CT + pAH34L	-	-
pBAD33_SD_caf1-PHSRN Loop 3	-	-
pAH34L	0.1± 0.003	0.1± 0.005

The **Figure 5.16** shows that the pBAD33_SD_ caf1-FLAG epitope NT + pAH34L sample contains Caf1protein detected by the anti-Caf1 antibody and it is in the polymeric form. Caf1 polymers were observed after heating the sample for 45 seconds at 100ºC (**western blot A-lane 2**). A different result was obtained for the pBAD33_SD_ caf1-FLAG epitope NT only sample in which no Caf1 was detected. In the pAH34L samples Caf1 in a polymeric form was detected (**western blot A-lane 8**). The western blot performed for the same samples but using the anti-FLAG epitope revealed the presence of Caf1-FLAG epitope NT in a polymeric form (**western blot B-lane 2**). The pAH34L which did not encode for Caf1-FLAG epitope NT we did not observe bands (**western blot B-lanes 7-9**). In the sample containing pBAD33_SD_ caf1-FLAG epitope N some weak bands were detected corresponding to the FLAG epitope in the monomer form only (**western blot B-lanes 5 and 6**).

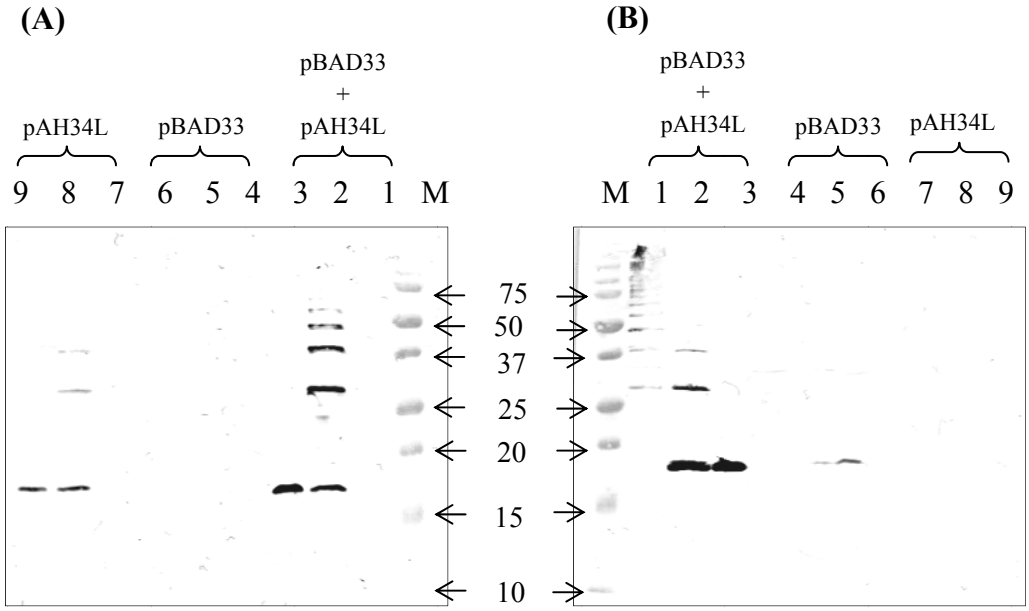

Figure 5.16 – Western blots of Caf1-FLAG epitope NT protein expression. Heterologous Caf1 protein samples from the supernatant were heated in 2x SDS-sample buffer, at 100ºC for 45 seconds or 5 minutes. Non-heated samples in 2x SDS-sample buffer were also loaded onto SDS-PAGE gel (**A)** pBAD33_SD_caf1 NT-FLAG + pAH34L probed for Caf1 with the monoclonal anti-Caf1 antibody**. (B)** pBAD33_SD_caf1 NT-FLAG + pAH34L probed for FLAG epitope with anti-flag epitope antibody. **M,** molecular weight marker proteins (molecular mass kDa); **lane 1**, pBAD33_SD_caf1 NT-FLAG + pAH34L sample non-heated; **lane 2,** pBAD33_SD_caf1 NT-FLAG + pAH34L sample heated at 95 ºC for 45 seconds; **lane 3,** pBAD33_SD_caf1 NT-FLAG + pAH34L sample heated at 95 ºC for 5 minutes; **lane 4**, pBAD33_SD_caf1 NT-FLAG sample non heated; **lane 5**, pBAD33_SD_caf1 NT-FLAG sample heated at 95 ºC for 45 seconds; **lane 6** , pBAD33_SD_caf1 NT-FLAG sample heated at 95 ºC for 5 minutes; **lane 7,** pAH34L sample non-heated; **lane 8**, pAH34L sample heated at 95 ºC for 45 seconds; **lane 9,** pAH34L sample heated at 95 ºC for 5 minutes**.**

The **Figure 5.17** shows that the pBAD33_SD_Caf1-6His-NT + pAH34L sample contains Caf1 protein detected by the anti-Caf1 antibody and it is in the polymeric form. Caf1 polymers were observed after heating the sample for 45 seconds at 100ºC (**western blot A-lane 2**). No Caf1 was detected in the pBAD33_SD_Caf1-6His-NT

sample. The pAH34L samples contained Caf1 in a polymeric form (**western blot A-lane 8**). The western blot performed for the same samples but using the anti-poly-histidine revealed the presence of a very small quantity of monomeric Caf1-6His-NT and in a monomeric form (**western blot B-lane 1-3**). The pAH34L did not encode for Caf1-6His-NT and no band was detected (**western blot B-lanes 7-9**). In the sample containing pBAD33_SD_caf1-6His-NT was detected some non-specific bands (**western blot B-lanes 4-6**).

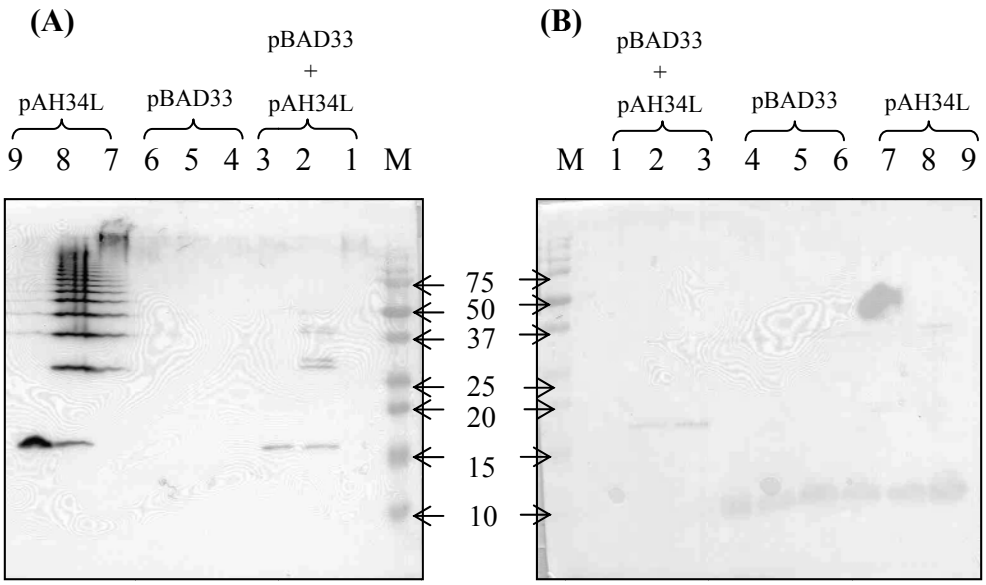

Figure 5.17 – Western blots of Caf1-6His-NT protein expression. Heterologous Caf1 protein samples from the supernatant were heated in 2x SDS-sample buffer, at 100ºC for 45 seconds and 5 minutes. Non-heated samples in 2x SDS-sample buffer were also loaded onto SDS-PAGE (**A)** pBAD33_SD_caf1-6His-NT + pAH34L probed for Caf1 with the monoclonal anti-Caf1 antibody**. (B)** pBAD33_SD_caf1 6His-NT + pAH34L probed with anti-polyhistidine antibody. **M,** molecular weight marker proteins (molecular mass kDa); **lane 1**, pBAD33_SD_caf1-6His-NT + pAH34L sample non-heated; **lane 2,** pBAD33_SD_caf1-6His-NT + pAH34L sample heated at 95 ºC for 45 seconds; **lane 3,** pBAD33_SD_caf1-6His-NT + pAH34L sample heated at 95 ºC for 5 minutes; **lane 4**, pBAD33_SD_caf1-6His-NT sample non heated; **lane 5**, pBAD33_SD_caf1-6His-NT sample heated at 95 ºC for 45 seconds; **lane 6** , pBAD33_SD_caf1-6His-NT sample heated at 95 ºC for 5 minutes; **lane 7,** pAH34L sample non-heated; **lane 8**, pAH34L sample heated at 95 ºC for 45 seconds; **lane 9,** pAH34L sample heated at 95 ºC for 5 minutes.

The **Figure 5.18** shows that the pBAD33_SD_caf1-6His-NT spacer + pAH34L sample contains Caf1protein detected by the anti-Caf1 antibody and it is in the polymeric form. Caf1 polymers were observed after heating the sample for 45 seconds at 100ºC (**western blot A-lane 2**). No Caf1 was detected in pBAD33_SD_ caf1-6His-NT spacer sample. In the pAH34L samples Caf1 was detected in a polymeric form (**western blot A-lane 8**). The western blot performed for the same samples but using anti-poly-histidine revealed the presence of Caf1-6His-NT spacer in a monomeric form and a second band between 37 and 50 kDa (**western blot B-lane 2**). The pAH34L did not encode for caf1-6His-NT spacer and thus no band was detected in the **western blot B-lanes 7-9**. In the sample containing pBAD33_SD_ caf1-6His-NT spacer some non-specific bands were detected (**western blot B-lanes 4-6**).

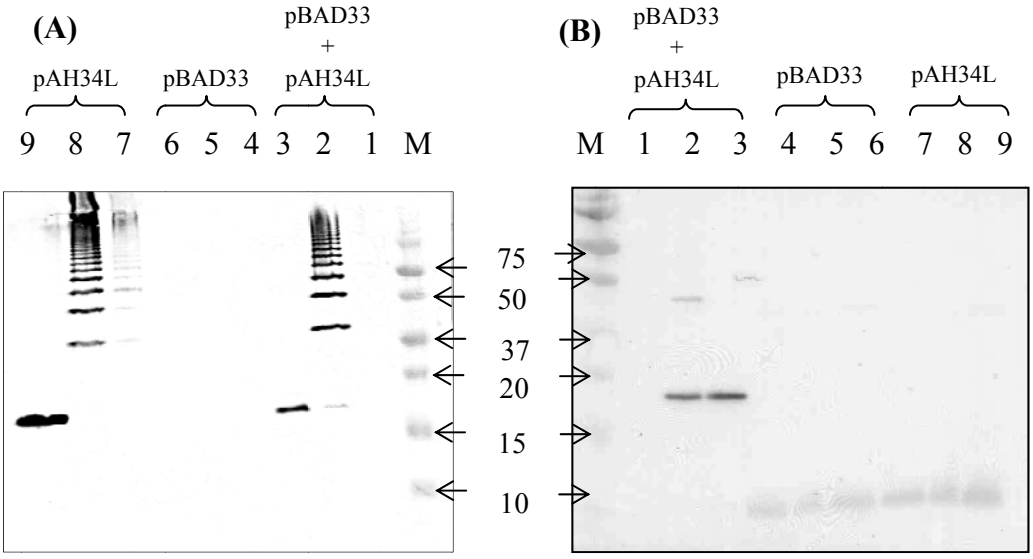

Figure 5.18 – Western blots of Caf1-6His-NT spacer protein expression. Heterologous Caf1 protein samples from the supernatant were heated in 2x SDS-sample buffer, at 100ºC for 45 seconds and 5 minutes. Non-heated samples in 2x SDS-sample buffer were also loaded onto SDS-PAGE gel (**A)** pBAD33_SD_caf1 6His-NT spacer + pAH34L probed for Caf1 with the monoclonal anti-Caf1 antibody**. (B)** pBAD33_SD_caf1-6His-NT spacer + pAH34L probed for polyhistidine with anti-polyhistidine antibody. **M,** molecular weight marker proteins (molecular mass kDa); **lane 1**, pBAD33_SD_ caf1-6His-NT spacer + pAH34L sample non-heated; **lane 2,** pBAD33_SD_caf1-6His-NT spacer +pAH34L sample heated at 95 ºC for 45 seconds; **lane 3,**pBAD33_SD_caf1-6His-NT spacer+pAH34L sample heated at 95 ºC for 5 minutes; **lane 4**, pBAD33_SD_caf1 6His-NT spacer sample non heated; **lane 5**, pBAD33_SD_caf1-6His-NT spacer sample heated at 95 ºC for 45 seconds; **lane 6** , pBAD33_SD_caf1-6His_NT_Spacer sample heated at 95 ºC for 5 minutes; **lane 7,** pAH34L sample non-heated; **lane 8**, pAH34L sample heated at 95 ºC for 45 seconds; **lane 9,** pAH34Lsample heated at 95 ºC for 5 minutes.

The **Figure 5.19** shows that the pBAD33_SD_caf1-6His-CT + pAH34L sample contains Caf1 protein detected by the anti-Caf1 antibody and it is in the polymeric form. Caf1 polymers were observed after heating the sample for 45 seconds at 100ºC (**western blot A-lane 2**). In pBAD33_SD_caf1-6His-CT sample no Caf1 was detected. In the pAH34L samples Caf1 in a polymeric form was detected (**western blot A-lane 8**). The western blot performed for the same samples but using the anti-poly-histidine

did not reveal the presence of Caf1-6His-CT (**western blot B-lane 1-3**). The pAH34L which did not encode for caf1-6His-CT presented a similar result (**western blot B-lanes 7-9**). In the sample containing pBAD33_SD_caf1-6His-CT some non-specific bands were detected (**western blot B-lanes 4-6**).

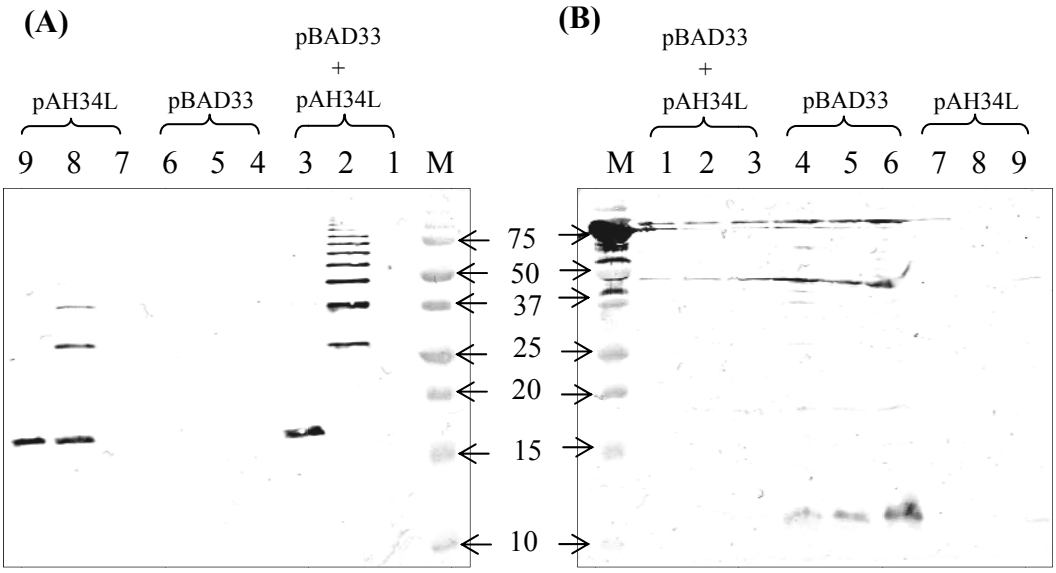

Figure 5.19 – Western blots of Caf1-6His-CT protein expression. Heterologous Caf1 protein samples from the supernatant were heated in 2x SDS-sample buffer, at 100ºC for 45 seconds and 5 minutes. Non-heated samples in 2x SDS-sample buffer were also loaded onto SDS-PAGE gel. (**A)** pBAD33_SD_caf1-6His-CT + pAH34L probed for Caf1 with the monoclonal anti-Caf1 antibody**. (B)** pBAD33_SD_caf1-6His-CT + pAH34L probed for polyhistidine with anti-polyhistidine antibody. **M,** molecular weight marker proteins (molecular mass kDa); **lane 1**, pBAD33_SD_caf1-6His-CT + pAH34L sample non-heated; **lane 2,** pBAD33_SD_caf1-6His-CT + pAH34L sample heated at 95 ºC for 45 seconds; **lane 3,** pBAD33_SD_caf1-6His-CT + pAH34L sample heated at 95 ºC for 5 minutes; **lane 4**, pBAD33_SD_caf1-6His-CT sample non heated; **lane 5**, pBAD33_SD_caf1-6His-CT sample heated at 95 ºC for 45 seconds; **lane 6** , pBAD33_SD_caf1-6His-CT sample heated at 95 ºC for 5 minutes; **lane 7,** pAH34L sample non-heated; **lane 8**, pAH34L sample heated at 95 ºC for 45 seconds; **lane 9,** pAH34L sample heated at 95 ºC for 5 minutes.

The **Figure 5.20** shows that the pBAD33_SD_caf1-PHSRN Loop1 + pAH34L, pBAD33_SD_caf1-Cys-NT+ pAH34L, pBAD33_SD_caf1-G35C Loop 4 + pAH34L,

pBAD33_SD_caf1-PENFF-NT+ pAH34L samples contain polymeric Caf1protein detected by the anti-Caf1 antibody. The purified Caf1 (Avecia) in a polymeric form was detected by the monoclonal anti-Caf1antibody. The pBAD33_SD_caf1-Q106C Loop2 + pAH34L sample was not detected by the monoclonal anti-Caf1 antibody and the pBAD33_SD_caf1-PHSRN Loop 3 + pAH34L sample did not produce a ladder.

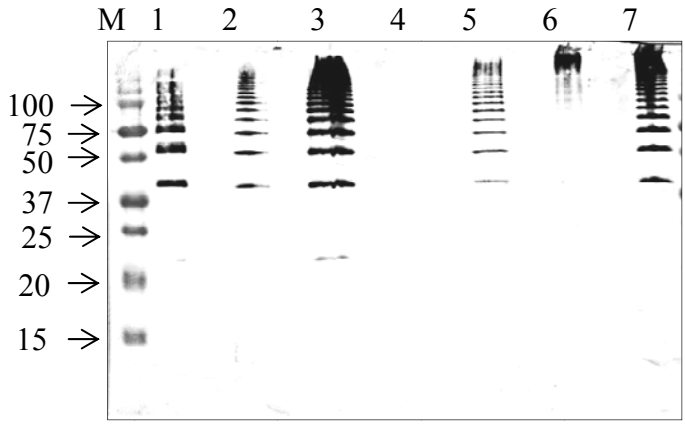

Figure 5.20 – Western blots of heterologous Caf1 protein expression. Heterologous Caf1 protein samples from the supernatant were heated in 2x SDS-sample buffer, at 100ºC for 45 seconds. **M,** molecular weight marker proteins (molecular mass kDa); **lane 1**, pBAD33_SD_caf1-PHSRN Loop1 + pAH34L; **lane 2,** pBAD33_SD_caf1-Cys-NT+ pAH34L; **lane 3,** pBAD33_SD_caf1-G35C Loop 4 + pAH34L; **lane 4**, pBAD33_SD_caf1-Q106C Loop2 + pAH34L; **lane 5**, pBAD33_SD_caf1-PENFF-NT+ pAH34L; **lane 6**, pBAD33_SD_caf1-PHSRN Loop 3 + pAH34L; **lane 7,** Caf1 (Avecia).

5.3. Discussion

Caf1 protein cross-linked with 4-arm PEG-NHS formed a gel-like material.

In this study the Caf1 hydrogels were tested at room temperature using the tube-inversion method. The gelation time was visually estimated to be within 24 to 27 min for NHS-PEG-NHS and 2 to 22 min for 4-arm PEG-NHS, depending on the concentration of the cross-linker. The higher the concentration of these two cross-linkers the quicker the gelation time. The reaction of Caf1 with different concentrations of DTSSP did not allow the visual estimation of the gelation time since a solid gel was not observed (**Table 5.1**).

Thus, the gelation rate was significantly quicker with 4-arm PEG-NHS than the NHS-PEG-NHS and the DTSSP. The increase in gelation rate of 4-arm PEG-NHS could be due to the structure of 4-arm PEG which influences its ability to react with the primary amine groups of Caf1 (Tan *et al.*, 2010).

In another study, Tan and colleagues examined the gelation time and morphology of 4-arm and 8-arm amino-terminated poly(ethylene glycol) (PEG) hydrogels cross-linked with genipin, which is an excellent natural and non-toxic cross-linker for proteins such as for example gelatin and collagen, and showed that the 8-arm PEG demonstrated a much slower gelation time compared to the 4-arm PEG. They proposed that the structural differences of the 4-arm and 8-arm PEG influenced the ability of genipin to react with the amine groups. They also showed that the 4-arm PEG hydrogels can promote human adipose-derived stem cell adhesion whilst the same result was not observed for the 8-arm PEG hydrogels (Tan *et al*., 2010).

Previous studies conducted by Butler et al., using different proteins for cross-linking revealed the importance of protein secondary and tertiary structure in determining the accessibility of protein sites for cross-linking with other cross-linkers molecules over the number of primary amines (Butler *et al.*, 2003). Studies to investigate the relation between PEG-architecture and the gelation time were performed by, for example, Lee and co-workers. They reported that the gelation time of 4-arm PEG amine was quicker that the linear bis-amine PEG (Lee *et al.*, 2002).

Our results showed that the structure of 4-arm PEG-NHS was important for the formation of a gel within a few minutes. The Caf1 protein cross-linked with 4-arm

PEG-NHS in ratios (w/w) of 1:5, 1:3 and 1:2 formed hydrogels in 5, 4 and 2 min, respectively. Nevertheless, Caf1 protein cross-linked with DTSSP was not a gel-like material even after 30 min using the same protein: cross-linker ratios and under sealed conditions (**Table 5.4**). The cross-linking reaction time of 30 min was determined based on the available literature and as described in the product instructions. The cross-linkers contain N-hydroxysuccinimide *(*NHS*)* ester at the end of the chain which reacts immediately with the primary amines (–NH2) of the proteins, and can be rapidly hydrolysed in aqueous solution.

Caf1 cross-linked with linear PEG-NHS (NHS-PEG-NHS) was less efficient at forming hydrogels in the same ratios and preparation conditions. In this case the gelation time was slower than with 4-arm PEG-NHS. Possibly the reaction between Caf1 and either DTSSP or NHS-PEG requires additional time to form a more compact structure during gelation.

The gelation time reported here is on the order of minutes, which is comparable with other studies using PEG hydrogels, for example Liu *et al*., (2012) examined the combination of PEG diacrylate (PEGDA) and acryloyl-PEG-RGD, and using the photo-initiator with ultraviolet light they formed hydrogels within a few minutes (Liu *et al.*, 2012).

The most precise method to determine gelation time is rheology. Rheology is based on time-dependent changes of the viscoelastic material such as hydrogel storage (G`) and loss (G``) modulli in an oscillatory platform at constant strain and frequency when an oscillatory force (stress) is applied to a material in order to determine the relation of the flow/deformation behaviour of the material and its internal structure such as elongation and orientation of the polymer molecules (Malkin *et al.*, 2006). For that, two viscoelastic parameters are determined: the storage (G`) modulus is used to measure the stored energy in viscoelastic materials which represents their elastic portion and the loss (G``) modulus is used to measure the energy dissipated as heat from the materials, which represents their viscous portion. Thus, with the formation of the hydrogels, the G` modulli increases with the time whereas G`` decreases at a specific time point these two crossover, and that time point is defined as gelation time (Anseth *et al.*, 1996).

Swelling

The hydrogel swelling performance also varied according to the crosslinker used. For example, the diameter change of Caf1 hydrogel cross-linked with DTSSP at ratio of cross-linking of 1:10 is higher (61.2%) than both the diameter change of Caf1 hydrogel cross-linked with NHS-PEG-NHS (40.3%) and 4-arm PEG-NHS (24.2%) using the same ratio of cross-linking (**Table 5.1**). This result could indicate that the hydrogel *swelling* is a function of network *structure* of the cross-linker which is consistent with *previous* research (Zustiak and Leach, 2010).

Caf1 hydrogel cross-linked with 4-arm PEG-NHS shows the highest degree of cross-linking

After Caf1 hydrogel cross-linking for 30 min at room temperature, 10 µl of each hydrogel were heated at 100 ºC for 5 min in the presence of SDS-sample buffer and loaded onto a 4-20% gradient gel as well as the control Caf1 protein without any cross-linker at the same concentration used for the formation of Caf1 hydrogel. The gel was stained with Coomassie Brilliant Blue, scanned and analysed by ImageJ version 1.46 software. The band of approximately 15 kDa corresponding to the Caf1 monomer in the non-cross linked Caf1 sample (control) was used as reference for the subsequent analysis. The relative density of the Caf1 monomer band in Caf1 samples cross-linked with the different cross-linkers at various concentrations was determined. The ratio between the values obtained for each sample and the value obtained for the reference sample allowed the determination of the relative density for each band to be calculated. The calculation using the monomers was more accurate than using relative amounts of dimer, trimer, etc due to the presence of a single band with about 15 kDa corresponding to the Caf1 monomer. Since the calculations of the relative density for the high molecular weight bands were more complex, these were considered a single band and designed as “Caf1 cross-linked fraction”.

At the bottom of the gel the bands with approximately 15 kDa should correspond to the monomers of Caf1 which were not cross-linked. In the case of Caf1 cross-linked with DTSSP, the bands which are resolved between the 25 and 37 kDa protein standard markers could correspond to the Caf1 dimers (35 kDa) linked by one molecule of DTSSP (608.51 Da) (**lanes 1-4**). In the case of Caf1 cross-linked with

NHS-PEG-NHS the bands with approximately 37 kDa protein standard markers might correspond to a Caf1 dimer linked by one molecule of NHS-PEG-NHS (10 kDa) (**lanes 5-8**). The Caf1 cross-linking with 4-arm PEG-NHS presents a second band resolved between 50 and 75 kDa protein standard markers that could correspond to the Caf1 dimer (35 kDa) linked by one molecule of 4-arm PEG-NHS (20 kDa). The remained high molecular weight bands could not be reliably indentified only by SDS-PAGE gel analysis but for the smaller two crosslinkers is presumably progressed as trimers, tetramers etc. Increasing the ratio of cross-linker using different cross-linkers decreased the Caf1 monomeric fraction. A more accurate technique to determine the mass of the complexes formed by Caf1 and cross-linkers could be mass spectrometry, but varying levels of cross-linker attached to monomers would make this difficult.

As the concentration of the cross-linkers increased the Caf1 cross-linked fraction also increased. In the case of the highest concentration of 4-arm PEG-NHS (20000 Da) the high molecular weight of Caf1 cross-linked fraction did not allow it to totally pass through the gradient gel and thus the value for Caf1 cross-linked fraction calculated (0.28) was much less than the theoretical values calculated (0.84).

Caf1 hydrogel cross-linked with DTSSP revealed a highly compact structure however NHS-PEG-NHS and 4-arm PEG-NHS formed porous scaffold. High concentrations of 4-arm PEG-NHS resulted in a more compact structure.

Caf1 polymers cross-linked with a short arm length cross-linker such as DTSSP (12.0 Å) promote a closer contact between the Caf1 fibres and increase the probability of Caf1 self-assembling. Thus, the images obtained by TEM revealed a compact Caf1 hydrogel which reflects the Caf1 fibres proximity (**Figure 5.6-A**).

A different result was obtained for Caf1 polymers cross-linked with a long spacer NHS-PEG-NHS (197 Å), which can better separate the Caf1 fibres. Large Caf1 hydrogel meshes were observed by TEM (**Figure 5.6-B**).

When we used the even longer spacer with four arms containing each of them a functional group – NHS (394 Å), the interactions between Caf1 and the 4-arm PEG-NHS were frequent due to the number of NHS groups and lysines residues on the Caf1 available for the reaction. The structure was more condensed that on NHS-PEG-NHS (**Figure 5.6 - C**).

TEM observations revealed hydrogel meshes (pieces of hydrogel). This could be due to (1) the preparation of hydrogel for TEM analysis; (2) differences in Caf1 polymer length; (3) number of cross-linking sites obtained by the Caf1 and cross-linker reaction (**Figure 5.6**). Possibly large meshes of hydrogel are the result of high stability in the chemical interactions formed between Caf1 polymer and cross-linkers (Seliktar, 2012). It seems that Caf1 hydrogels cross-linked with NHS-PEG-NHS are slightly more stable and flexible than the Caf1 hydrogels cross-linked with 4-arm PEG-NHS which form a stiffer network with more cross-linking sites.

The 4-arm PEG-NHS was further characterised due to the fact that it formed a gel-like network.

The Caf1 hydrogels were only obtained with the Caf1 in the polymeric form (up to 1.5 μm long) seen by Soliakov *et al*., 2010) This is composed of many monomers each of them containing 8 lysines that can interact with NHS functional groups presented in the cross-linkers ends. In the Caf1 monomeric form made by circular permutation, cpCaf1 (Chalton *et al*. 2006) these large networks were not seen, just as in the other control, 4-arm PEG-NHS only (**Figure 5.7**). The small dots indicated by circles might correspond to bead-like structures analysed by Soliakov et al. (2010) as Caf1 monomers.

A highly porous hydrogel (**Figure 5.8**) could be advantageous for swelling and water uptake and also as a scaffold for cell culture that can allow the passage of nutrients, oxygen through the pores. The TEM images confirmed that the formation of the Caf1 hydrogels depends on the cross-linker concentration and structure.

Caf1 hydrogels presented varying pore diameters depending on the technique used

The pore diameters of Caf1 hydrogels were assessed by SEM and ESEM. The samples analysed by SEM were prepared by critical point drying and dehydrated using differential ethanol concentrations which might cause some collapse of the network. The pores diameters obtained by traditional SEM were on the order of nanometers, while freeze-dried hydrogels presented larger pore with a mean pore diameter of 8 ± *1.9* μm (can be seen in Figure 5.10).

Caf1 hydrogels were then analysed by ESEM to avoid the dehydration process. The images revealed a mesh-like network structure with a mean pore diameter of 300 ± 0.3 nm (can be seen in Figure 5.11).

Some published results showed that PEG hydrogel pores are on the order of 23 nm diameter (Nazli *et al.*, 2012). The dehydration process can contribute to the hydrogel collapse and form small pores. The freeze-drying process should be done quickly in order to avoid the formation of ice crystals which could damage or deform the hydrogel structure. We observed some distortion on the hydrogel structure which could explain the large pore diameter (can be seen in **Figure 5.10 - A**). For ESEM the samples are observed in their native state and thus the structure should be more preserved than by SEM. The explanation for the large pore diameter obtained in this study compared to the previous published work could be due to the water content of the sample (Demanuele and Gilpin, 1996).

Caf1 hydrogels are non-toxic for cells but promote low cell adhesion.

Cell hydrogel interactions were examined by measuring the cell viability and spreading on glass coverslips surfaces coated with Caf1 hydrogel cross-linked with 4-arm PEG-NHS (w/w ratio of cross-linking of 1:2). Viable primary osteoblasts seeded onto Caf1 hydrogel displayed few elongated expansions and most of the cells were round. The mouse 3T3 fibroblasts were not tested for viability. Nevertheless, it was visible that more fibroblasts displayed an elongated morphology when seeded onto Caf1 hydrogels. The cell adhesion and spreading could be improved by the addition of cell adhesive peptides (e.g. RGDS) and also incorporation of proteolytic degradation sites such as metalloproteinase cleavage sites.

The Caf1 protein hydrogel morphology indicated a network with micron sized pores, suggesting the need for cell protease secretion to migrate through the hydrogel. As shown by Lutolf and Hubbell (2005) that in tighter gel networks, cells are required to use proteolytic strategies to degrade the surrounding matrix and be able to migrate through the gel (Lutolf and Hubbell, 2005). Hydrogel pore size influences the cell migration through the material. When the pore size of the hydrogels is approximately the same size of the cell, cells utilize the amoeboid migration; e.g. cells can adopt a blebbing or gliding motility (Laemmermann and Sixt, 2009).

In another study, Adelow and co-workers (2008) examined the effect of a four-armed poly(ethylene glycol)-vinyl sulfone (PEG-VS) (reacted with cysteine-containing adhesion peptides for cell attachment (e.g. RGD) and cross-linked with bis-cysteine with matrix metalloproteinase (MMP)- sensitive peptides (e.g. MMP-2) to form a degradable PEG hydrogels) on smooth muscle cell and human mesenchymal stem cells. This showed that these two cell lines cultured in the PEG hydrogels were able to express matrix metalloproteinases to degrade the MMPs specific cleavage sites in the hydrogel and be able to proliferate into it for up to 21 days in culture (the duration of their study). Cells can remain viable in stiffer gels, however they cannot spread and proliferate which is fundamental for obtaining cell-cell contacts and subsequent tissue formation (Chen *et al.*, 2004).

Combining Caf1 hydrogels with the Caf1-RGDS proteins reported in chapter 3 could, in future work; improve the cell adhesion and proliferation.

Co-expression of Caf1 WT was mediated by the two compatible plasmids, pAH34L and pBAD33

This study revealed a system to co-express copies of *caf1* gene using the plasmid pBAD33 which contains: (1) the pBR322-compatible p15A origin of replication from the pACYC184 vector and (2) resistance to chloramphenicol antibiotic, and the *caf* operon using the plasmid pAH34L which has a different origin of replication (ColE 1) and antibiotic resistance (kanamycin) and thus cells can maintain both plasmids if grown on kanamycin/chloramphenicol L-agar plates. Based on the size of the flocculent layer, TOP10 *E.coli* cells transformed by two compatible plasmids and grown in media containing L-arabinose expressed higher levels of *caf1* gene. This was confirmed by western blot using the monoclonal anti-Caf1 antibody.

In other studies *Båga* and co-workers investigated the overproduction of PapA (the major pilin subunit) by electron microscopy and immunoblot analysis of PapA antigen. For that, they constructed a plasmid pPAP267, which overproduces just the PapA pilin subunit and it was introduced into HB101 cells harbouring the pPAP5, which contain the wild-type *pap* operon (composed of 11 genes responsible for the expression of *papA* pilin) and found that the expression of PapA was 10-fold higher in

comparison with Ppap5 alone and also the pili were longer than the wild-type (Båga M, 1987).

In this study, it was possible to modulate the Caf1 expression over a range of L-arabinose concentrations, from 0.02 to 2%. The levels of *caf1* expression increased with the increase of L-arabinose concentration (**Figure 5.13**). In the absence of L-arabinose very low levels of *caf1* expression were achieved. The TOP10 strain (ara^-) can transport L-arabinose but does not metabolise it, which is important for expression studies since the level of L-arabinose is constant inside the cell and does not decrease over time.

However, an efficient repression of Caf1 expression was not achieved in the presence of 0.2% D-glucose. In fact, cells grew better and expressed more protein in some cases with glucose. Guzman et al. (1995) constructed a series of pBAD vectors containing the P_{BAD} promoter of the arabinose operon and its regulatory gene, araC, which can be used for gene cloning and modulate the gene expression using L-arabinose induction and glucose as a repressor (Guzman *et al*., 1995). They proposed that glucose-6-phosphate that can repress the levels of expression more efficiently than glucose. Another option could be D-fucose, the non-metabolisable analog of L-arabinose that antagonises arabinose induction by AraC. Mixtures of D-fucose and L-arabinose could result in low levels of expression from P_{BAD} (Guzman *et al*., 1995).

Caf1-Flag was co-expressed with Caf1 WT

Here, we developed an approach to co-express Caf1 mutants with Caf1 WT using the expression system mentioned above. Analysis of co-expression of Caf1 mutants was performed by western blot using antibodies against the proteins in study. In this study the Caf1-FLAG was detected at the cell surface of *E. coli* (see western blot for FLAG epitope using the monoclonal anti-FLAG epitope antibody, **Figure 5.16**) mediated by the chaperone-usher system. This result shows for the first time the export of Caf1 hybrid polymers.

The western blot performed did not reveal the presence of Caf1-6His-NT (**Figure 5.17**) or Caf1-6His-CT (**Figure 5.19**). Which could indicate that the Caf1-6Hist were not incorporated into the Caf1 fibres and thus the Caf1 detected in the western blot probed with anti-Caf1 antibody was only provide by the expression of Caf1 into the

pAH34L. However, the western blot performed for pBAD33_SD_Caf1-6His-NT + pAH34L sample using anti-poly-histidine revealed the presence of Caf1-6His-NT spacer in a monomeric form and a second band between 37 and 50 kDa, which could correspond to two Caf1 monomers linked together (Caf1 dimer), each of them with a 6-Histidine tag (**Figure 5.18**, **western blot B-lane 2**). Further analysis need to be conducted to confirm this result.

For the other Caf1 mutants: Caf1-PHSRN, Caf1-Cys and Caf1- PENFF it was not totally clear by western blot if mutant proteins were incorporated into the polymers. Other approaches should be conducted to analyse the expression of these mutants. Clearly for the cysteine mutants specific thiol labelling could be attempted. For Caf1-PHSRN cell adhesion and proliferation assays can be performed using the Caf1-RGDS as a positive control. A co-expression using the pGEMcaf1containing the *caf* mutated encoding for Caf1-RGDS and the pBAD33 containing *caf* mutated encoding for Caf1-PHSRN should also be attempted to see if synergy occurs. For Caf1-PENFF enzymatic cleavage using matrix metalloproteinases, namely MMP-13 could be conducted.

6. Conclusion

In this study, we successfully expressed Caf1 mutants in a polymeric form. Previously, the fusion of cytokine proteins with Caf1 or insertion of mutations into the Caf1 subunit did not result in Caf1 polymer being exported to outside of the bacterial cells (Zavialov *et al*., 2003). The successful system was achieved by the subcloning of *caf* operon (around 5 Kb) into a small-size vector appropriate for Quikchange site-directed mutagenesis. Caf1 was expressed and above the centrifuged cell pellet a flocculant layer was observed characterised and reported as containing mainly Caf1 polymeric protein (Miller *et al*., 1998). Since the principal aim of this project was to create a cell culture system, we inserted the smallest peptide known to promote cell adhesion (RGDS) in each of the five loops of Caf1 monomer. The decision to mutate the loops of Caf1 monomer was due to the need to expose the RGDS on the surface in order to be accessible for cell receptor binding. This also serves to retain the core fold of Caf1 and its high stability.

Previous studies demonstrated Caf1 stability and its high resistance to proteases (Soliakov *et al*., 2010). The expression of the Caf1 mutants revealed that when some loops were mutated the level of expression of the Caf1 mutants was reduced and in one case visible expression was not achieved. However, the Caf1 RGDS mutant for which the level of expression was the highest was used as the basis for the next mutations (in that site or in its proximity). Here we characterised these Caf1 mutants for their thermo stability, secondary, tertiary and quaternary structure (e.g. their capability to form high-molecular mass polymers). Thus initial constraints in the productive mutation of the Caf1 gene were discovered. Moreover, expression and purification of Caf1 needed to be improved. Here the use of ammonium sulphate precipitation and size exclusion chromatography was confirmed as the basis for a generic purification system. We obtained 2.37 mg/L of Caf1 WT, 1.3 mg/L of Caf1 RGDS and 0.56 mg/L of Caf1 RGES. Since the main goal of this project was to investigate the applicability of the Caf1 protein scaffold engineered with RGDS motif for mammalian cell responses we decided, also considering the quantity of pure proteins obtained per litre of culture, to coat 96-well plates with these proteins for a cell adhesion assay using three different mammalian cell lines.

Before we performed this experiment some previous work was carried out in order to understand the effect of small peptides when inserted in other protein scaffolds.

We have shown that gold surfaces coated with tmOmpA-ECM show more PC-12 cell attachment and proliferation in comparison to the gold surfaces without ECM motifs as was demonstrated previously by Cooke et al. 2008. Furthermore, this study contributed to a better understanding of the role of the motifs from the whole extracellular matrix proteins (fibronectin, laminin and collagen) in mammalian cells behaviour. We also showed that arrays of specifically engineered cell interaction proteins can be created and used in cell culture. This technique has the advantage that the influence of specific peptides is observable as a spatial distribution in an otherwise controlled cell culture.

We aimed to produce a new scaffold for cell culture and for this we chose Caf1 which presents a low immunogenicity and its structure resembles the structure of fibronectin.

We have shown that mammalian cells are viable when cultured on surfaces coated with Caf1 proteins. Nevertheless, studies of cell adhesion on surfaces containing Caf1 proteins were not conclusive and more improvements need to be performed in order to understand if Caf1 can support cell adhesion, proliferation, and with the incorporation of proper signal peptides, cell differentiation. The investigation by fluorescence microscopy at COEBP of the influence of surface bound proteins on adherence, actin filament formation and the appearance of focal adhesion sites was inconclusive and may be due to poor protein binding. The results from scanning electron microscopy showed a clearer effect of the RGDS mutant in Caf1. In fact wild type Caf1 seems to inhibit cell binding.

These results highlight the complexity associated with cellular interactions with these engineered biomaterials, and the need for rigorous analyses of cell adhesion and signalling on bio-adhesive supports.

In this study we showed that Caf1 system for cell culture can be improved. We presented here some advanced uses of Caf1 polymer, such as the possibility to cross-link the Caf1 polymers and produce a 3D hydrogel for cell culture. Our results showed that we can use a variety of cross-linkers depending on the final structure we would like to obtain. Short-arm cross-linkers can generate a very dense and compact Caf1 hydrogel. On the other hand, long-arm cross-linkers can produce highly porous structures which can benefit the transport of nutrients and oxygen to the cells. The Caf1 protein cross-linked with 4-arm PEG-NHS formed a gel-like material with nano-pores

that resisted cell adhesion, since it did not contain bio-active peptides but importantly was non-toxic for cells.

Another advanced use for Caf1 demonstrated in this study was the co-expression of two genes for Caf1 mediated by two compatible plasmids. With this new expression system we can overcome the limitations of mutagenesis using the large plasmid encoding the *caf* operon. Therefore we can mutate only the *caf1* gene present in the smaller of the plasmids and co-express that with the plasmid containing chaperone/usher mechanism to export the Caf1 hybrid fibres to outside the bacterial cell. New Caf1 mutants can thus be generated by this system for cell differentiation and tissues engineering. This has the advantage that mutations which might inhibit expression can be inserted as a minority component but still at a frequency to influence cell culture. Using this system we were able to produce a new Caf1 mutant-Caf1 containing a FLAG epitope. The other Caf1 mutants containing PHSRN, cysteine and an MMP-cleavage site need further analysis to prove their insertion into the full Caf1 polymer.

Future Perspective

Future experiments should be conducted to improve the efficiency of Caf1 expression and purification. Improved quantification of Caf1 on the surface will be useful as a control in future experiments. Moreover, the formation of a 3D cell hydrogel, with Caf1 mutants such as Caf1-RGDS and MMP degradation sites, and its use in cell culture will be the final test of this new system.

Bibliography

Akiyama, S.K. and Yamada, K.M. (1985) 'Synthetic peptides competitively inhibit both direct binding to fibroblasts and functional biological assays for the purified cell-binding domain of fibronectin', *Journal of Biological Chemistry*, 260(19), pp. 402-405.

Alberts, B., Johnson, A., Lewis, J., Raff, M., Roberts, K. and Walter, P. (2002) *Molecular Biology of the Cell*. 4th edition edn. New York.

Alcantar, N.A., Aydil, E.S. and Israelachvili, J.N. (2000) 'Polyethylene glycol-coated biocompatible surfaces', *Journal of Biomedical Materials Research*, 51(3), pp. 343-351.

Allison, D.D. and Grande-Allen, K.J. (2006) 'Review. Hyaluronan: A powerful tissue engineering tool', *Tissue Engineering*, 12(8), pp. 2131-2140.

Andrews, G.P., Heath, D.G., Anderson, J., Welkos, S.L. and Friedlander, A.M. (1996) 'Fraction 1 Capsular Antigen (F1) Purification from Yersinia pestis CO92 and from an Escherichia coli recombinant strain and efficacy against plague challenge', *Infectious and Immunity*, 64(6), pp. 2180-2187.

Anseth, K., Bowman, C. and Brannon-Peppas, L. (1996) 'Mechanical properties of hydrogels and their experimental determination.', *Biomaterials*, 17(17), pp. 1647-57.

Aota, S., Nomizu, M. and Yamada, K.M. (1994) 'The short amino acid sequence Pro-His-Ser-Arg-Asn in human fibronectin enhances cell-adhesive function', *J Biol Chem*, 269(40), pp. 24756-61.

Ashe, H.L. and Briscoe, J. (2006) 'The interpretation of morphogen gradients', *Development*, 133(3), pp. 385-394.

Athanasiou, K.A., Agrawal, C.M., Barber, F.A. and Burkhart, S.S. (1998) 'Orthopaedic applications for PLA-PGA biodegradable polymers', *Arthroscopy*, 14(7), pp. 726-737.

Athey, D., Shah, D., Phillips, S. and Lakey, J. (2005) 'A manufacturable surface-biology platform for nano applications Cell culture, analyte detection, diagnostics sensors', *Ind Bioetchnol 1:185–189* .

Badylak, S.F., Freytes, D.O. and Gilbert, T.W. (2009) 'Extracellular matrix as a biological scaffold material: Structure and function', *Acta Biomater.*, 5(1), pp. 1-13.

Båga M, N.M., Normark S. (1987) 'Biogenesis of E. coli Pap pili: papH, a minor pilin subunit involved in cell anchoring and length modulation.', *Cell*, 49(2), pp. 241-51.

Bain, C.D., Troughton, E.B., Tao, Y.T., Evall, J., Whitesides, G.M. and Nuzzo, R.G. (1989) 'Formation of Monolayer Films by the Spontaneous Assembly of Organic Thiols from Solution onto Gold', *Journal of the American Chemical Society*, 111(1), pp. 321-335.

Baker, E., Sommer, H., Foster, L., Meyer, E. and Meyer, K. (1952) 'Studies on immunization against plague. I. The isolation and characterization of the soluble antigen of Pasteurella pestis.', *J Immunol.* , 68(2), pp. 131-45.

Banwell, E.F., Abelardo, E.S., Adams, D.J., Birchall, M.A., Corrigan, A., Donald, A.M., Kirkland, M., Serpell, L.C., Butler, M.F. and Woolfson, D.N. (2009) 'Rational design and application of responsive alpha-helical peptide hydrogels', *Nature Materials*, 8(7), pp. 596-600.

Bennett, K.L., Matthiesen, T. and Roepstorff, P. (2000) 'Probing protein surface topology by chemical surface labeling, crosslinking, and mass spectrometry', *Methods in molecular biology (Clifton, N.J.)*, 146, pp. 113-31.

Bhatnagar, R., Gough, C., Qian, J. and Shattuck, M. (1999) 'Fine structure of collagen: Molecular mechanisms of the interactions of collagen', *Journal of Chemical Sciences*, 111(2), pp. 301-317.

Bhattarai, N., Gunn, J. and Zhang, M. (2010) 'Chitosan-based hydrogels for controlled, localized drug delivery', *Advanced Drug Delivery Reviews*, 62(1), pp. 83-99.

Billiet, T., Vandenhaute, M., Schelfhout, J., Van Vlierberghe, S. and Dubruel, P. (2012) 'A review of trends and limitations in hydrogel-rapid prototyping for tissue engineering', *Biomaterials*, 33(26), pp. 6020-6041.

Bodnár, M., Daróczi, L., Batta, G., Bakó, J., Hartmann, J.F. and Borbély, J. (2009) 'Preparation and characterization of cross-linked hyaluronan nanoparticles ', *Colloid & Polymer Science*, 287(8), pp. 991-1000.

Boyle, A.L. and Woolfson, D.N. (2011) 'De novo designed peptides for biological applications', *Chemical Society Reviews*, 40(8), pp. 4295-4306.

Bradham, D.M., Passaniti, A. and Horton, W.E. (1995) 'Mesenchymal cell chondrogenesis is stimulated by basement membrane matrix and inhibited by age-associated factors.', *Matrix Biology*, 14(7), pp. 561-571.

Branco, M.C. and Schneider, J.P. (2009) 'Self-assembling materials for therapeutic delivery', *Acta Biomaterialia*, 5(3), pp. 817-831.

Bresalier, R.S., Schwartz, B., Kim, Y., Duh, Q., Kleinman, H. and Sullam, P. (1995) 'The laminin alpha 1 chain Ile-Lys-Val-Ala-Val (IKVAV)-containing peptide promotes liver colonization by human colon cancer cells', *Cancer Res.*, 55(11), pp. 2476-80.

Brun, A.L., Holt, S., Shah, D., Majkrzak, C. and Lakey, J. (2008) 'Monitoring the assembly of antibody-binding membrane protein arrays using polarised neutron reflection.', *Eur Biophys J.*, 37(5), pp. 639-45.

Brun, A.L., Shah, D., Athey, D., Holt, S. and Lakey, J. (2011) 'Self-assembly of protein monolayers engineered for improved monoclonal immunoglobulin g binding.', *Int J Mol Sci.*, 12(8), pp. 5157-67.

Bryant, S.J., Arthur, J.A. and Anseth, K.S. (2005) 'Incorporation of tissue-specific molecules alters chondrocyte metabolism and gene expression in photocrosslinked hydrogels', *Acta Biomaterialia*, 1(2), pp. 243-252.

Burridge, K. and Connell, L. (1983) 'A new protein of adhesion plaques and ruffling membranes.', *J Cell Biol*, 97(2), pp. 359-67.

Burridge, K. and Feramisco, J. (1980) 'Microinjection and localization of a 130K protein in living fibroblasts: a relationship to actin and fibronectin.', *Cell.*, 19(3), pp. 587-95.

Butler, M.F., Ng, Y.F. and Pudney, P.D.A. (2003) 'Mechanism and kinetics of the crosslinking reaction between biopolymers containing primary amine groups and genipin', *Journal of Polymer Science Part a-Polymer Chemistry*, 41(24), pp. 3941-3953.

Cao, L., Lim, T., Jun, S., Thornburg, T., Avci, R. and Yang, X. (2012) 'Vulnerabilities in Yersinia pestis caf operon are unveiled by a Salmonella vector', *Plos One*, 7(4), pp. e36283-e36283.

Chaffey, B., E, M., MA, B. and JH, L. (2008) 'A generic expression system to produce proteins that co-assemble with alkane thiol SAM', *Int J Nanomedicine*, 3(3), pp. 287-93.

Chalton, D.A., Musson, J.A., Flick-Smith, H., Walker, N., McGregor, A., Lamb, H.K., Williamson, E.D., Miller, J., Robinson, J.H. and Lakey, J.H. (2006) 'Immunogenicity of a Yersinia pestis vaccine antigen monomerized by circular permutation', *Infection and Immunity*, 74(12), pp. 6624-6631.

Chen, C.S., Alonso, J.L., Ostuni, E., Whitesides, G.M. and Ingber, D.E. (2003) 'Cell shape provides global control of focal adhesion assembly', *Biochemical and Biophysical Research Communications*, 307(2), pp. 355-361.

Chen, C.S., Mrksich, M., Huang, S., Whitesides, G.M. and Ingber, D.E. (1997) 'Geometric control of cell life and death', *Science*, 276(5317), pp. 1425-1428.

Chen, C.S., Tan, J. and Tien, J. (2004) 'Mechanotransduction at cell-matrix and cell-cell contacts', *Annual Review of Biomedical Engineering*, 6, pp. 275-302.

Chen, Y., Whetstone, H.C., Youn, A., Nadesan, P., Chow, E.C.Y., Lin, A.C. and Alman, B.A. (2007) 'beta-catenin signaling pathway is crucial for bone morphogenetic protein 2 to induce new bone formation', *Journal of Biological Chemistry*, 282(1), pp. 526-533.

Chenite, A., Chaput, C., Wang, D., Combes, C., Buschmann, M.D., Hoemann, C.D., Leroux, J.C., Atkinson, B.L., Binette, F. and Selmani, A. (2000) 'Novel injectable neutral solutions of chitosan form biodegradable gels in situ', *Biomaterials*, 21(21), pp. 2155-2161.

Cho, J., Heuzey, M., Bégin, A. and Carreau, P. (2005) 'Physical gelation of chitosan in the presence of beta-glycerophosphate: the effect of temperature.', *macromolecules.*, 6(6), pp. 3267-75.

Choh, S.-Y., Cross, D. and Wang, C. (2011) 'Facile Synthesis and Characterization of Disulfide-Cross-Linked Hyaluronic Acid Hydrogels for Protein Delivery and Cell Encapsulation', *Biomacromolecules*, 12(4), pp. 1126-1136.

Choi, B.G., Park, M.H., Cho, S.-H., Joo, M.K., Oh, H.J., Kim, E.H., Park, K., Han, D.K. and Jeong, B. (2010) 'In situ thermal gelling polypeptide for chondrocytes 3D culture', *Biomaterials*, 31(35), pp. 9266-9272.

Choudhury D, T.A., Stojanoff V, Langermann S, Pinkner J, Hultgren SJ, Knight SD. (1999) 'X-ray structure of the FimC-FimH chaperone-adhesin complex from uropathogenic Escherichia coli.', *Science*, 285(5430), pp. 1061-6.

Chung, H.J. and Park, T.G. (2009) 'Self-assembled and nanostructured hydrogels for drug delivery and tissue engineering', *Nano Today*, 4(5), pp. 429-437.

Clements, J.M., Newham, P., Shepherd, M., Gilbert, R., Dudgeon, T., Needham, L., Edwards, R.M., Berry, L., Brass, A. and Humphries, M.J. (1994) 'Identification of a key integrin-binding sequence in VCAM-1 homologous to the LDV active site in fibronectin.', *J Cell Sci*, 107(Pt 8), pp. 2127-35.

Cooke, M.J., Phillips, S.R., Shah, D.S.H., Athey, D., Lakey, J.H. and Przyborski, S.A. (2008) 'Enhanced cell attachment using a novel cell culture surface presenting functional domains from extracellular matrix proteins', *Cytotechnology*, 56(2), pp. 71-9.

Cooke, M.J., Zahir, T., Phillips, S.R., Shah, D.S.H., Athey, D., Lakey, J.H., Shoichet, M.S. and Przyborski, S.A. (2010) 'Neural differentiation regulated by biomimetic surfaces presenting motifs of extracellular matrix proteins', *Journal of Biomedical Materials Research Part A*, 93A(3), pp. 824-832.

Cooper, L.F., Uoshima, K. and Guo, Z.Y. (2000) 'Transcriptional regulation involving the intronic heat shock element of the rat hsp27 gene', *Biochimica Et Biophysica Acta-Gene Structure and Expression*, 1490(3), pp. 348-354.

Corbett, S.A., Wilson, C.L. and Schwarzbauer, J.E. (1996) 'Changes in cell spreading and cytoskeletal organization are induced by adhesion to a fibronectin-fibrin matrix', *Blood*, 88(1), pp. 158-166.

Cornelis, G.R. (2006) 'The type III secretion injectisome', *Nature Reviews Microbiology*, 4(11), pp. 811-825.

Cross, M.J. and Claesson-Welsh, L. (2001) 'FGF and VEGF function in angiogenesis: signalling pathways, biological responses and therapeutic inhibition', *Trends in Pharmacological Sciences*, 22(4), pp. 201-207.

Cukierman, E., Pankov, R., Stevens, D.R. and Yamada, K.M. (2001) 'Taking cell-matrix adhesions to the third dimension', *Science*, 294(5547), pp. 1708-1712.

Dado, D. and Levenberg, S. (2009) 'Cell-scaffold mechanical interplay within engineered tissue.', *Semin Cell Dev Biol*, 20(6), pp. 656-64.

Dai, W.G., Belt, J. and Saltzman, W.M. (1994) 'Cell-binding peptides conjugated to poly(ethylene glycol) promote neural cell aggregation', *Bio-Technology*, 12(8), pp. 797-801.

Dalton, P. and Mey, J. (2009) 'Neural interactions with materials.', (14), pp. 769-95.

Dean, J.A. (1995) *The Analytical Chemistry Handbook*. New York: McGraw Hill, Inc.

DeLong, S.A., Moon, J.J. and West, J.L. (2005) 'Covalently immobilized gradients of bFGF on hydrogel scaffolds for directed cell migration', *Biomaterials*, 26(16), pp. 3227-3234.

Demanuele, A. and Gilpin, C. (1996) 'Applications of the environmental scanning electron microscope to the analysis of pharmaceutical formulations', *Scanning*, 18(7), pp. 522-527.

Derynck, R., Roberts, A.B., Winkler, M.E., Chen, E.Y. and Goeddel, D.V. (1984) 'Human transforming growth factor-alpha: precursor structure and expression in E . coli', *Cell*, 38(1), pp. 287-297.

Du, Y.D., Rosqvist, R. and Forsberg, A. (2002) 'Role of fraction 1 antigen of Yersinia pestis in inhibition of phagocytosis', *Infection and Immunity*, 70(3), pp. 1453-1460.

Dubois, L.H. and Nuzzo, R.G. (1992) 'Synthesis, Structure, and Properties of Model Organic Surfaces. ', *Annual Review of Physical Chemistry*, 43, pp. 437-463.

Dutta, R.C. and Dutta, A.K. (2009) 'Cell-interactive 3D-scaffold; advances and applications', *Biotechnology Advances*, 27(4), pp. 334-339.

Eisenberg, J., Piper, J. and Mrksich, M. (2009) 'Using self-assembled monolayers to model cell adhesion to the 9th and 10th type III domains of fibronectin.', *Langmuir*, 24(25), pp. 13942-51.

Engler, A.J., Sen, S., Sweeney, H.L. and Discher, D.E. (2006) 'Matrix elasticity directs stem cell lineage specification', *Cell*, 126(4), pp. 677-89.

Englesberg, E., Levy, J.B. and Gibor, A. (1954) 'Some enzymatic changes accompanying the shift from anaerobiosis to aerobiosis in Pasteurella pestis', *Journal of Bacteriology*, 68(2), pp. 178-85.

Fasman, G.D. (ed.) (1996) *Circular Dichroism and the Conformational Analysis of Biomolecules*. New York: Plenum.

Felding-Habermann, B. and Cheresh, D.A. (1993) 'Vitronectin and its receptors', *Current Opinion in Cell Biology*, 5(5), pp. 864-868.

Feng, Y. and Mrksich, M. (2004) 'The synergy peptide PHSRN and the adhesion peptide RGD mediate cell adhesion through a common mechanism.', *Biochemistry*, 43(50), pp. 15811-21.

Fields, G.B., Lauer, J.L., Dori, Y., Forns, P., Yu, Y.C. and Tirrell, M. (1998) 'Proteinlike molecular architecture: Biomaterial applications for inducing cellular receptor binding and signal transduction', *Biopolymers*, 47(2), pp. 143-151.

Floquet, N., Pasco, S., Ramont, L., Derreumaux, P., Laronze, J.Y., Nuzillard, J.M., Maquart, F.X., Alix, A.J. and Monboisse, J. (2004) 'The antitumor properties of the alpha3(IV)-(185-203) peptide from the NC1 domain of type IV collagen (tumstatin) are conformation-dependent', *J Biol Chem*, 279(3), pp. 2091-100.

Freytes, D.O., Wan, L.Q. and Vunjak-Novakovic, G. (2009) 'Geometry and force control of cell function', *J Cell Biochem.*, 108(5), pp. 1047-58.

Friedlander, M., Brooks, P.C., Shaffer, R.W., Kincaid, C.M., Varner, J.A. and Cheresh, D.A. (1995) 'Definition of two angiogenic pathways by distinct alpha v integrins.', *Science*, 270(5241), pp. 1500-1502.

Frisch, S.M. and Francis, H. (1994) 'Disruption of epithelial cell-matrix interactions induces apoptosis.', *Journal of Cell Biology*, 124(4), pp. 619-626.

Gailit, J. and Clark, R.A.F. (1996) 'Studies in vitro on the role of alpha v and beta 1 integrins in the adhesion of human dermal fibroblasts to provisional matrix proteins fibronectin, vibronectin, and fibrinogen', *Journal of Investigative Dermatology*, 106(1), pp. 102-108.

Galyov, E.E., Karlishev, A.V., Chernovskaya, T.V., Dolgikh, D.A., Smirnov, O.Y., Volkovoy, K.I., Abramov, V.M. and Zavyalov, V.P. (1991) 'Expression of the Envelope Antigen-F1 of Yersinia-Pestis Is Mediated by the Product of Caf1m-Gene Having Homology with the Chaperone Protein-Papd of Escherichia-Coli', *Febs Letters*, 286(1-2), pp. 79-82.

Galyov, E.E., Smirnov, O., Karlishev, A.V., Volkovoy, K.I., Denesyuk, A.I., Nazimov, I.V., Rubtsov, K.S., Abramov, V.M., Dalvadyanz, S.M. and Zav'yalov, V.P. (1990) 'Nucleotide sequence of the Yersinia pestis gene encoding F1 antigen and the primary structure of the protein. Putative T and B cell epitopes', *FEBS Lett*, 277(1-2), pp. 230-2.

Gandhi, N. and Mancera, R. (2008) 'The structure of glycosaminoglycans and their interactions with proteins.', *Chem Biol Drug Des*, 72(6), pp. 455-82.

Garcia, A.J., Schwarzbauer, J.E. and Boettiger, D. (2002) 'Distinct activation states of alpha 5 beta 1 integrin show differential binding to RGD and synergy domains of fibronectin', *Biochemistry*, 41(29), pp. 9063-9069.

Geiger, B. (1979) 'A 130K protein from chicken gizzard: its localization at the termini of microfilament bundles in cultured chicken cells.', *Cell*, 18(1), pp. 193-205.

Geiger, B., Bershadsky, A., Pankov, R. and Yamada, K.M. (2001) 'Transmembrane extracellular matrix-cytoskeleton crosstalk', *Nature Reviews Molecular Cell Biology*, 2(11), pp. 793-805.

Gelain, F., Bottai, D., Vescovi, A. and Zhang, S. (2006) 'Designer Self-Assembling Peptide Nanofiber Scaffolds for Adult Mouse Neural Stem Cell 3-Dimensional Cultures', *Plos One*, 1(2).

Giancotti, F.G., Comoglio, P.M. and Tarone, G. (1986) 'Fibronectin-plasma membrane interaction in the adhesion of hemopoietic cells.', *J Cell Biol.*, 103(2), pp. 429-37.

Gilpin, C. and Sigee, D.C. (1995) 'X-ray microanalysis with the environmental scanning electron microscope: interpretation of data obtained under different atmospheric conditions', *Journal of Microscopy-Oxford*, 179, pp. 22-28.

Goa, K.L. and Benfield, P. (1994) 'Hyaluronic Acid. A Review of its Pharmacology and Use as a Surgical Aid in. Ophthalmology, and its Therapeutic Potential in Joint Disease and Wound Healing', *Drugs*, 47(3), pp. 536-566.

Goldstein, J., Newbury, D.E., Joy, D.C., Lyman, C.E., Echlin, P., Lifshin, E., Sawyer, L.C. & and Michael, J.R. (2003) *Scanning Electron Microscopy and X-ray Microanalysis*. New York, USA.

Grant, D.S., Tashiro, K.I., Segulreal, B., Yamada, Y., Martin, G.R. and Kleinman, H.K. (1989) 'Two different laminin domains mediate the differentiation of human endothelial cells into capillary-like structures in vitro.', *Cell*, 58(5), pp. 933-943.

Greene, L.A. and Tischler, A.S. (1976) ' Establishment of a noradrenergic clonal line of rat adrenal pheochromocytoma cells which respond to nerve growth factor', *Proceedings of the National Academy of Sciences of the United States of America*, 73(7), pp. 2424-2428.

Greener, A., Callahan, M. and Jerpseth, B. (1997) 'An efficient random mutagenesis technique using an E. coli mutator strain.', *Mol Biotechnol.* , 7(2), pp. 189-95.

Gronthos, S., Simmons, P.J., Graves, S.E. and Robey, P.G. (2001) 'Integrin-mediated interactions between human bone marrow stromal precursor cells and the extracellular matrix', *Bone*, 28(2), pp. 174-181.

Guadamillas, M.C., Cerezo, A. and del Pozo, M.A. (2011) 'Overcoming anoikis - pathways to anchorage-independent growth in cancer', *Journal of Cell Science*, 124(19), pp. 3189-3197.

Gurrath, M., Muller, G., Kessler, H., Aumailley, M. and Timpl, R. (1992) 'Conformation/activity studies of rationally designed potent anti-adhesive RGD peptides.', *European Journal of Biochemistry*, 210(3), pp. 911-921.

Guzman, L., Belin, D., Carson, M. and Beckwith, J. (1995) 'Tight regulation, modulation, and high-level expression by vectors containing the arabinose PBAD promoter.', *J Bacteriol.*, 177(14), pp. 4121-30.

Habig, W., Hudson, B.W., Marshall, J.D., Cavanaug.Dc and Rust, J.H. (1971) 'Evidence for Molecular Heterogeneity of the Specific Antigen (Fraction-1) of Pasteurella pestis.', *Infect Immun.* , 3(3), pp. 498-&.

Haines, L.A., Rajagopal, K., Ozbas, B., Salick, D.A., Pochan, D.J. and Schneider, J.P. (2005) 'Light-activated hydrogel formation via the triggered folding and self-assembly of a designed peptide', *Journal of the American Chemical Society*, 127(48), pp. 17025-17029.

Han, J., Chang, H., Giricz, O., Lee, G., Baehner, F., Gray, J., Bissell, M., Kenny, P. and Parvin, B. (2010) 'Molecular predictors of 3D morphogenesis by breast cancer cell lines in 3D culture', *PLoS Comput Biol*, 6(2), p. e1000684.

Harris, P.J.F. (1997) 'Carbon nanotubes and other graphitic structures as contaminants on evaporated carbon films', *Journal of Microscopy-Oxford*, 186, pp. 88-90.

Hassell, J.R., Robey, P.G., Barrach, H.J., Wilczek, J., Rennard, S.I. and Martin, G.R. (1980) 'Isolation of a heparan sulfate-containing proteoglycan from basement

membrane.', *Proceedings of the National Academy of Sciences of the United States of America-Biological Sciences*, 77(8), pp. 4494-4498.

Haubner, R., Gratias, R., Diefenbach, B., Goodman, S.L., Jonczyk, A. and Kessler, H. (1996) 'Structural and functional aspects of RGD-containing cyclic pentapeptides as highly potent and selective integrin alpha(v)beta(3) antagonists', *Journal of the American Chemical Society*, 118(32), pp. 7461-7472.

Hern, D.L. and Hubbell, J.A. (1998) 'Incorporation of adhesion peptides into nonadhesive hydrogels useful for tissue resurfacing', *Journal of Biomedical Materials Research*, 39(2), pp. 266-276.

Hersel, U., Dahmen, C. and Kessler, H. (2003) 'RGD modified polymers: biomaterials for stimulated cell adhesion and beyond', *Biomaterials*, 24(24), pp. 4385-4415.

Hickman, J.J., Bhatia, S.K., Quong, J.N., Schoen, P., Stenger, D.A., Pike, C.J. and Cotman, C.W. (1994) 'Rational pattern design for in vitro cellular networks using surface photochemistry', *Journal of Vacuum Science & Technology a-Vacuum Surfaces and Films*, 12(3), pp. 607-616.

Holmes, T.C. (2002) 'Novel peptide-based biomaterial scaffolds for tissue engineering', *Trends in Biotechnology*, 20(1), pp. 16-21.

Holmgren, A., Kuehn, M.J., Branden, C.I. and Hultgren, S.J. (1992) 'Conserved immunoglobin-like features in a family of periplasmic pilus chaperones in bacteria', *Embo Journal*, 11(4), pp. 1617-1622.

Holtzman, T., Levy, Y., Marcus, D., Flashner, Y., Mamroud, E., Cohen, S. and Fass, R. (2006) 'Production and purification of high molecular weight oligomers of Yersinia pestis F1 capsular antigen released by high cell density culture of recombinant Escherichia coli cells carrying the caf1 operon', *Microbial Cell Factories* 5 (Supplement I), p. 98.

Honarmandi, P., Lee, H., Lang, M.J. and Kamm, R.D. (2011) 'A microfluidic system with optical laser tweezers to study mechanotransduction and focal adhesion recruitment', *Lab on a Chip*, 11(4), pp. 684-694.

Horton, M.A. (1997) 'The alpha v beta 3 integrin "vitronectin receptor"', *International Journal of Biochemistry & Cell Biology*, 29(5), pp. 721-725.

Huang, T., David, L., Mendoza, V., Yang, Y., Villarreal, M., De, K., Sun, L., Fang, X., López-Casillas, F., Wrana, J. and Hinck, A. (2011) 'TGF-β signalling is mediated by two autonomously functioning TβRI:TβRII pairs.', *EMBO J.* , 30(7), pp. 1263-76.

Hughes, C.S., Postovit, L.M. and Lajoie, G.A. (2010) 'Matrigel: a complex protein mixture required for optimal growth of cell culture', *Proteomics*, 10(9), pp. 1886-90.

Humphries, M., Komoriya, A., Akiyama, S., Olden, K. and Yamada, K. (1987) 'Identification of two distinct regions of the type III connecting segment of human plasma fibronectin that promote cell type-specific adhesion.', *Biol Chem.*, 262(14), pp. 6886-92.

Hung, D.L., Knight, S.D., Woods, R.M., Pinkner, J.S. and Hultgren, S.J. (1996) 'Molecular basis of two subfamilies of immunoglobulin-like chaperones', *Embo Journal*, 15(15), pp. 3792-3805.

Hynes, R. (2002) 'Integrins: bidirectional, allosteric signaling machines.', *Cell*, 110(6), pp. 673-87.

Ibusuki, S., Fujii, Y., Iwamoto, Y. and Matsuda, T. (2003) 'Tissue-engineered cartilage using an injectable and in situ gelable thermoresponsive gelatin: Fabrication and in vitro performance', *Tissue Engineering*, 9(2), pp. 371-384.

Ingber, D.E. (2006) 'Cellular mechanotransduction: putting all the pieces together again.', *FASEB J.*, 20(7), pp. 811-27.

Iwamoto, Y., Robey, F., Graf, J., Sasaki, M., Kleinman, H., Yamada, Y. and Martin, G. (1987) 'YIGSR, a synthetic laminin pentapeptide, inhibits experimental metastasis formation.', *Science*, 238(4830), pp. 1132-4.

Jacob-Dubuisson, F., Striker, R. and Hultgren, S. (1994) 'Chaperone-assisted self-assembly of pili independent of cellular energy.', *Journal of Biological Chemistry*, 269(17), pp. 12447-12455.

Jeschke, B., Meyer, J., Jonczyk, A., Kessler, H., Adamietz, P., Meenen, N.M., Kantlehner, M., Goepfert, C. and Nies, B. (2002) 'RGD-peptides for tissue engineering of articular cartilage', *Biomaterials*, 23(16), pp. 3455-3463.

Jo, Y.S., Rizzi, S.C., Ehrbar, M., Weber, F.E., Hubbel, J.A. and Lutolf, M.P. (2010) 'Biomimetic PEG hydrogels crosslinked with minimal plasmin-sensitive tri-amino acid peptides', *Journal of Biomedical Materials Research Part A*, 93A(3), pp. 870-877.

Kalkhof, S. and Sinz, A. (2008) 'Chances and pitfalls of chemical cross-linking with amine-reactive N-hydroxysuccinimide esters', *Analytical and Bioanalytical Chemistry*, 392(1-2), pp. 305-312.

Karlyshev, A.V., Galyov, E.E., Abramov, V.M. and Zavyalov, V.P. (1992a) 'gene and its role in the regulation of capsule formation of Y. pestis', *Febs Letters*, 305(1), pp. 37-40.

Karlyshev, A.V., Galyov, E.E., Smirnov, O.Y., Guzayev, A.P., Abramov, V.M. and Zavyalov, V.P. (1992b) 'A new gene of the f1 operon of Y. pestis involved in the capsule biogenesis', *Febs Letters*, 297(1-2), pp. 77-80.

Kelly, S.M., Jess, T.J. and Price, N.C. (2005) 'How to study proteins by circular dichroism', *Biochimica Et Biophysica Acta-Proteins and Proteomics*, 1751(2), pp. 119-139.

Kielty, C., Wess, T., Haston, L., Ashworth, J., Sherratt, M. and Shuttleworth, C. (2002) 'Fibrillin-rich microfibrils: elastic biopolymers of the extracellular matrix.', *J Muscle Res Cell Motil.*, 23(5-6), pp. 581-96.

Kim, J.B., Yu, J.H., Ko, E., Lee, K.W., Song, A.K., Park, S.Y., Shin, I., Han, W. and Noh, D.Y. (2010) 'The alkaloid Berberine inhibits the growth of Anoikis-resistant MCF-7 and MDA-MB-231 breast cancer cell lines by inducing cell cycle arrest', *Phytomedicine*, 17(6), pp. 436-440.

Kleinman, H., Luckenbill-Edds, L., Cannon, F. and Sephel, G. (1987) 'Use of extracellular matrix components for cell culture', *Anal Biochem.* , 166(1), pp. 1-13.

Kleinman, H.K. and Martin, G.R. (2005) 'Matrigel: Basement membrane matrix with biological activity', *Seminars in Cancer Biology*, 15(5), pp. 378-386.

Kleinman, H.K., McGarvey, M.L., Hassell, J.R., Star, V.L., Cannon, F.B., Laurie, G.W. and Martin, G.R. (1986a) 'Basement Membrane Complexes with Biological Activity', *Biochemistry*, 25(2), pp. 312-318.

Kleinman, H.K., McGarvey, M.L., Hassell, J.R., Star, V.L., Cannon, F.B., Laurie, G.W. and Martin, G.R. (1986b) 'Basement membrane complexes with biological activity.', *Biochemistry*, 25(2), pp. 312-318.

Kleinman, H.K., McGarvey, M.L., Liotta, L.A., Robey, P.G., Tryggvason, K. and Martin, G.R. (1982) 'Isolation and characterization of type IV procollagen, laminin, and heparan sulfate proteoglycan from the EHS sarcoma.', *Biochemistry*, 21(24), pp. 6188-6193.

Knight, S.D., Berglund, J. and Choudhury, D. (2000) 'Bacterial adhesins: structural studies reveal chaperone function and pilus biogenesis', *Current Opinion in Chemical Biology*, 4(6), pp. 653-660.

Kraehenbuehl, T.P., Zammaretti, P., Van der Vlies, A.J., Schoenmakers, R.G., Lutolf, M.P., Jaconi, M.E. and Hubbell, J.A. (2008) 'Three-dimensional extracellular

matrix-directed cardioprogenitor differentiation: Systematic modulation of a synthetic cell-responsive PEG-hydrogel', *Biomaterials*, 29(18), pp. 2757-2766.

Krause, A., Cowles, E.A. and Gronowicz, G. (2000) 'Integrin-mediated signaling in osteoblasts on titanium implant materials', *Journal of Biomedical Materials Research*, 52(4), pp. 738-747.

Laemmermann, T. and Sixt, M. (2009) 'Mechanical modes of 'amoeboid' cell migration', *Current Opinion in Cell Biology*, 21(5), pp. 636-644.

Laemmli, U.K. (1970) 'Cleavage of structural proteins during the assembly of the head of bacteriophage T4.', *Nature*, 227(5259), p. 680.

Lapcik, L., De Smedt, S., Demeester, J. and Chabrecek, P. (1998) 'Hyaluronan: Preparation, structure, properties, and applications', *Chemical Reviews*, 98(8), pp. 2663-2684.

Laurie, G.W., Bing, J.T., Kleinman, H.K., Hassell, J.R., Aumailley, M., Martin, G.R. and Feldmann, R.J. (1986) 'Localization of binding sites for laminin, heparan sulfate proteoglycan and fibronectin on basement membrane (type IV) collagen.', *Journal of Molecular Biology*, 189(1), pp. 205-216.

Lee, B.P., Dalsin, J.L. and Messersmith, P.B. (2002) 'Synthesis and gelation of DOPA-Modified poly(ethylene glycol) hydrogels', *Biomacromolecules*, 3(5), pp. 1038-1047.

Lee, K.Y. and Mooney, D.J. (2001) 'Hydrogels for tissue engineering', *Chemical Reviews*, 101(7), pp. 1869-1879.

Legate, K., Montañez, E., Kudlacek, O. and Fässler, R. (2006) 'ILK, PINCH and parvin: the tIPP of integrin signalling.', *Nat Rev Mol Cell Biol.*, 7(1), pp. 20-31.

Levi, G., Wilkin, G.P., Ciotti, M.T. and Johnstone, S. (1983) 'Enrichment of differentiated, stellate astrocytes in cerebellar interneuron cultures as studied by

GFAP immunofluorescence and autoradiographic uptake patterns with 3H D-aspartate and 3H GABA', *Brain research*, 312(2), pp. 227-41.

Li, F., B, L., M, W.Q. and H, W.J. (2008) 'Cell shape regulates collagen type I expression in human tendon fibroblasts', *Cell Motil Cytoskeleton*, 65(4), pp. 332-41.

Li, Y., Rodrigues, J. and Tomas, H. (2012) 'Injectable and biodegradable hydrogels: gelation, biodegradation and biomedical applications', *Chemical Society Reviews*, 41(6), pp. 2193-2221.

Lichtenfels, R., Schulz, H., Vogt, A.B. and Martin, R. (1994) 'CARE-LASS (calcein release assay), an improved fluorescence-based test system to measure cytotoxic T lymphocyte activity', *Journal of Cellular Biochemistry Supplement*, 0(18D), pp. 405-405.

Lin, P.S., Ho, K.C., Sung, S.J. and Gladding, J. (1992) 'Effect of tumour necrosis factor, heat, and radiation on the viability and microfilament organization in cultured endothelial cells.', *International Journal of Hyperthermia*, 8(5), pp. 667-677.

Liotta, L.A., Wicha, M.S., Foidart, J.M., Rennard, S.I., Garbisa, S. and Kidwell, W.R. (1979) 'Hormonal requirements for basement membrane collagen deposition by cultured rat mammary epithelium.', *Laboratory Investigation*, 41(6), pp. 511-518.

Liu, Y.-L., Huang, L.-M., Lin, W.-P., Tsai, C.-C., Lin, T.-S., Hu, Y.-a.H., Chen, H.-S., Han, J.-M., Wang, H.-J. and Liu, Y.-T. (2006) 'Secretion of biologically active human epidermal growth factor from Escherichia coli using Yersinia pestis Caf1 signal peptide', *Journal of Microbiology Immunology and Infection*, 30(5), pp. 366-371.

Liu, Y.-L., Jiang, S., Ke, Z.-M., Wu, H.-S., Chi, C.-W. and Guo, Z.-Y. (2009) 'Recombinant expression of a chitosanase and its application in chitosan oligosaccharide production', *Carbohydrate Research*, 344(6), pp. 815-819.

Liu, Z., Xiao, L., Xu, B., Zhang, Y., Mak, A.F.T., Li, Y., Man, W.-y. and Yang, M. (2012) 'Covalently immobilized biomolecule gradient on hydrogel surface using a

gradient generating microfluidic device for a quantitative mesenchymal stem cell study', *Biomicrofluidics*, 6(2).

Lutolf, M.P. and Hubbell, J.A. (2005) 'Synthetic biomaterials as instructive extracellular microenvironments for morphogenesis in tissue engineering', *Nat Biotechnol.*, 23(1), pp. 47-55.

Lutolf, M.P., Lauer-Fields, J.L., Schmoekel, H.G., Metters, A.T., Weber, F.E., Fields, G.B. and Hubbell, J.A. (2003) 'Synthetic matrix metalloproteinase-sensitive hydrogels for the conduction of tissue regeneration: Engineering cell-invasion characteristics', *Proceedings of the National Academy of Sciences of the United States of America*, 100(9), pp. 5413-5418.

Malkin, A.I.A., Malkin, A.Y. and Isayev, A.I. (2006) *Rheology: Concepts, Methods & Applications*. ChemTec Publishing.

Maniatis, T., Fritsch, E.F. and Sambrook, J. (1982) 'Molecular Cloning: A Laboratory Manual '. New York: Cold Spring Harbor Laboratory, p. 202−203.

Mann, B.K., Schmedlen, R.H. and West, J.L. (2001) 'Tethered-TGF-beta increases extracellular matrix production of vascular smooth muscle cells', *Biomaterials*, 22(5), pp. 439-444.

Mao, Y. and Schwarzbauer, J.E. (2005) 'Fibronectin fibrillogenesis, a cell-mediated matrix assembly process', *Matrix Biol*, 24(6), pp. 389-99.

Massia, S.P. and Hubbell, J.A. (1991) 'An RGD spacing of 440 nm is sufficient for integrin alpha V beta 3-mediated fibroblast spreading and 140 nm for focal contact and stress fiber formation.', *Journal of Cell Biology*, 114(5), pp. 1089-1100.

McCann, M., Stacey, N., Wilson, R. and Roberts, K. (1993) 'Orientation of macromolecules in the walls of elongating carrot cells.', *J Cell Sci.*, 106 (Pt 4), pp. 1347-56.

McIntyre, S., Knight, S. and J., F. (2004) *Structure, assembly and applications of the polymeric F1 antigen of Yersinia pestis.* Wymondham: Horizon Press.

Meyer, K.F., Hightower, J.A. and McCrumb, F.R. (1974) 'Plague immunization. VI. Vaccination with the fraction I antigen of Yersinia pestis', *The Journal of infectious diseases*, 129, pp. Suppl:S41-5.

Miller, J., Williamson, E.D., Lakey, J.H., Pearce, M.J., Jones, S.M. and Titball, R.W. (1998) 'Macromolecular organisation of recombinant Yersinia pestis F1 antigen and the effect of structure on immunogenicity', *Fems Immunology and Medical Microbiology*, 21(3), pp. 213-221.

Mitchell, E.A., Chaffey, B.T., McCaskie, A.W., Lakey, J.H. and Birch, M.A. (2010) 'Controlled spatial and conformational display of immobilised bone morphogenetic protein-2 and osteopontin signalling motifs regulates osteoblast adhesion and differentiation in vitro', *Bmc Biology*, 8, p. 57.

Mizuguchi, H., Nakatsuji, M., Fujiwara, S., Takagi, M. and Imanaka, T. (1999) 'Characterization and application to hot start PCR of neutralizing monoclonal antibodies against KOD DNA polymerase', *Journal of Biochemistry*, 126(4), pp. 762-768.

Mould, A.P. and Humphries, M.J. (1991) 'Identification of a novel recognition sequence for the integrin alpha 4 beta 1 in the COOH-terminal heparin-binding domain of fibronectin.', *EMBO J*, 10(13), pp. 4089-95.

Moursi, A.M., Globus, R.K. and Damsky, C.H. (1997) 'Interactions between integrin receptors and fibronectin are required for calvarial osteoblast differentiation in vitro', *Journal of Cell Science*, 110, pp. 2187-2196.

Mrksich, M. (2009) 'Using self-assembled monolayers to model the extracellular matrix', *Acta Biomaterialia*, 5(3), pp. 832-841.

Mrksich, M. and Whitesides, G.M. (1996) 'Using self-assembled monolayers to understand the interactions of man-made surfaces with proteins and cells', *Annual Review of Biophysics and Biomolecular Structure*, 25, pp. 55-78.

Murphy-Ullrich, J.E. (2001) 'The de-adhesive activity of matricellular proteins: is intermediate cell adhesion an adaptive state?', *Journal of Clinical Investigation*, 107(7), pp. 785-790.

Nair, M., Belak, Z.R. and Ovsenek, N. (2011) 'Effects of fluoride on expression of bone-specific genes in developing Xenopus laevis larvae', *Biochemistry and Cell Biology-Biochimie Et Biologie Cellulaire*, 89(4), pp. 377-386.

Nakamura, M., Mie, M., Mihara, H., Nakamura, M. and Kobatake, E. (2008) 'Construction of multi-functional extracellular matrix proteins that promote tube formation of endothelial cells', *Biomaterials*, 29(20), pp. 2977-86.

Nazli, C., Ergenc, T.I., Yar, Y., Acar, H.Y. and Kizilel, S. (2012) 'RGDS-functionalized polyethylene glycol hydrogel-coated magnetic iron oxide nanoparticles enhance specific intracellular uptake by HeLa cells', *International Journal of Nanomedicine*, 7, pp. 1903-1920.

Newham, P. and Humphries, M.J. (1996) 'Integrin adhesion receptors: Structure, function and implications for biomedicine', *Molecular Medicine Today*, 2(7), pp. 304-313.

Nguyen, H., Qian, J.J., Bhatnagar, R.S. and Li, S. (2003) 'Enhanced cell attachment and osteoblastic activity by P-15 peptide-coated matrix in hydrogels', *Biochem Biophys Res Commun*, 311(1), pp. 179-86.

Orwin, E.J. and Hubel, A. (2000) 'In vitro culture characteristics of corneal epithelial, endothelial, and keratocyte cells in a native collagen matrix', *Tissue Engineering*, 6(4), pp. 307-319.

Paine-Saunders, S., Viviano, B.L., Economides, A.N. and Saunders, S. (2002) 'Heparan sulfate proteoglycans retain Noggin at the cell surface - A potential

mechanism for shaping bone morphogenetic protein gradients', *Journal of Biological Chemistry*, 277(3), pp. 2089-2096.

Pariente, J.L., Kim, B.S. and Atala, A. (2002) 'In vitro biocompatibility evaluation of naturally derived and synthetic biomaterials using normal human bladder smooth muscle cells.', *J Urol.*, 167(4), pp. 1867-71.

Parsons, J.T., Horwitz, A.R. and Schwartz, M.A. (2010) 'Cell adhesion: integrating cytoskeletal dynamics and cellular tension', *Nature Reviews Molecular Cell Biology*, 11(9), pp. 633-643.

Pavlin, D., Lichtler, A., Bedalov, A., Kream, B., Harrison, J., Thomas, H., Gronowicz, G., Clark, S., Woody, C. and Rowe, D. (1992) 'Differential utilization of regulatory domains within the alpha 1(I) collagen promoter in osseous and fibroblastic cells', *J Cell Biol.*, 116(1), pp. 227-36.

Peppas, N.A., Keys, K.B., Torres-Lugo, M. and Lowman, A.M. (1999) 'Poly(ethylene glycol)-containing hydrogels in drug delivery', *Journal of Controlled Release*, 62(1-2), pp. 81-87.

Perry, R. and Fetherston, J.D. (2007) *In The Genus Yersinia: from genomics to function*. New York, NY, USA

Pierschbacher, M.D. and Ruoslahti, E. (1984) 'Cell attachment activity of fibronectin can be duplicated by small synthetic fragments of the molecule', *Nature*, 309(5963), pp. 30-3.

Polizzotti, B.D., Fairbanks, B.D. and Anseth, K.S. (2008) 'Three-dimensional biochemical patterning of click-based composite hydrogels via thiolene photopolymerization', *Biomacromolecules*, 9(4), pp. 1084-1087.

Ponik, S.M. and Pavalko, F.M. (2004) 'Formation of focal adhesions on fibronectin promotes fluid shear stress induction of COX-2 and PGE(2) release in MC3T3-E1 osteoblasts', *Journal of Applied Physiology*, 97(1), pp. 135-142.

Prante, O., Einsiedel, J., Haubner, R., Gmeiner, P., Wester, H.-J., Kuwert, T. and Maschauer, S. (2007) '3,4,6-tri-O-acetyl-2-deoxy-2- F-18 fluoroglucopyranosyl phenylthiosulfonate: A thiol-reactive agent for the chemoselective F-18-glycosylation of peptides', *Bioconjugate Chemistry*, 18(1), pp. 254-262.

Prasad, B.R., Mullins, G., Nikolskaya, N., Connolly, D., Smith, T.J., Gerard, V.A., Byrne, S.J., Davies, G.-L., Gun'ko, Y.K. and Rochev, Y. (2012) 'Effects of long-term exposure of gelatinated and non-gelatinated cadmium telluride quantum dots on differentiated PC12 cells', *Journal of Nanobiotechnology*, 10.

Protsenko, O., Anisimov, P., Mozharov, O., Konnov, N. and Popov, I. (1983) 'Detection and characterization of Yersinia pestis plasmids determining pesticin I, fraction 1 antigen and mouse toxin synthesis', *Genetika*, 19, pp. 1081-1090.

Rao, J.Y., Hurst, R.E., Bales, W.D., Jones, P.L., Bass, R.A., Archer, L.T., Bell, P.B. and Hemstreet, G.P. (1990) 'Cellular F-actin levels as a marker for cellular transformation: relationship to cell division and differentiation', *Cancer Research*, 50(8), pp. 2215-2220.

Roberts, J., Marklund, B., Ilver, D., Haslam, D., Kaack, M., Baskin, G., Louis, M., Möllby, R., Winberg, J. and Normark, S. (1994) 'The Gal(alpha 1-4)Gal-specific tip adhesin of Escherichia coli P-fimbriae is needed for pyelonephritis to occur in the normal urinary tract.', *Proc Natl Acad Sci U S A.*, 91(25), pp. 11889-93.

Roberts, M.J., Bentley, M.D. and Harris, J.M. (2002) 'Chemistry for peptide and protein PEGylation', *Advanced Drug Delivery Reviews*, 54(4), pp. 459-476.

Robinson, A.L. (1986) 'Electron Microscope Inventors Share Nobel Physics Prize', *Science*, 234(4778), pp. 821-822.

Roduit, N. (2007) 'JMicroVision: Image analysis toolbox for measuring and quantifying components of high-definition images.

Version 1.2.2 (http://www.jmicrovision.com (accessed 2 July 2012).) [Online].

Ruel-Gariepy, E., Shive, M., Bichara, A., Berrada, M., Le Garrec, D., Chenite, A. and Leroux, J.C. (2004) 'A thermosensitive chitosan-based hydrogel for the local delivery of paclitaxel', *European Journal of Pharmaceutics and Biopharmaceutics*, 57(1), pp. 53-63.

Runco, L.M., Myrczek, S., Bliska, J.B. and Thanassi, D.G. (2008) 'Biogenesis of the fraction 1 capsule and analysis of the ultrastructure of Yersinia pestis', *Journal of Bacteriology*, 190(9), pp. 3381-3385.

Ruska, E. (1987) 'The Development of the Electron and of Electron Microscopy', *Bioscience Reports*, 7(8), pp. 607-629.

Salinas, C.N. and Anseth, K.S. (2008) 'The influence of the RGD peptide motif and its contextual presentation in PEG gels on human mesenchymal stem cell viability', *Journal of Tissue Engineering and Regenerative Medicine*, 2(5), pp. 296-304.

Sastry, S.K. and Burridge, K. (2000) 'Focal adhesions: A nexus for intracellular signaling and cytoskeletal dynamics', *Experimental Cell Research*, 261(1), pp. 25-36.

Sauer, F.G., Barnhart, M., Choudhury, D., Knights, S.D., Waksman, G. and Hultgren, S.J. (2000) 'Chaperone-assisted pilus assembly and bacterial attachment', *Current Opinion in Structural Biology*, 10(5), pp. 548-556.

Sauer, F.G., Remaut, H., Hultgren, S.J. and Waksman, G. (2004) 'Fiber assembly by the chaperone-usher pathway', *Biochim Biophys Acta*, 1694(1-3), pp. 259-267.

Sawyer, A.A., Hennessy, K.M. and Bellis, S.L. (2007) 'The effect of adsorbed serum proteins, RGD and proteoglycan-binding peptides on the adhesion of mesenchymal stem cells to hydroxyapatite', *Biomaterials*, 28(3), pp. 383-92.

Schaegger, H. (2006) 'Tricine-SDS-PAGE', *Nature Protocols*, 1(1), pp. 16-22.

Scheich, C., Kuemmel, D., Soumailakakis, D., Heinemann, U. and Buessow, K. (2007) 'Vectors for co-expression of an unrestricted number of proteins', *Nucleic Acids Research*, 35(6).

Schwarz, M.A., Owaribe, K., Kartenbeck, J. and Franke, W.W. (1990) 'Desmosomes and hemidesmosomes: constitutive molecular components', *Annual Review of Cell Biology*, 6, pp. 461-491.

Shah, D., Thomas, M., Phillips, S., Cisneros, D., Brun, A.L., Holt, S. and Lakey, J. (2007) 'Self-assembling layers created by membrane proteins on gold.', *Biochem Soc Trans.*, 35(Pt 3), pp. 522-6.

Shattil, S., Kim, C. and Ginsberg, M. (2010) 'The final steps of integrin activation: the end game.', *Nat Rev Mol Cell Biol.* , 11(4), pp. 288-300.

Simpson, W., Thomas, R. and Schwan, T. (1990) 'Recombinant capsular antigen (fraction 1) from Yersinia pestis induces a protective antibody response in BALB/c mice', *Am J Trop Med Hyg.* , 43(4), pp. 389-96.

Simpson, W., Thomas, R. and Schwan, T. (1990) 'Recombinant capsular antigen (fraction 1) from Yersinia pestis induces a protective antibody response in BALB/c mice.', *Am J Trop Med Hyg.*, 43(4), pp. 389-96.

Slaughter, B.V., Khurshid, S.S., Fisher, O.Z., Khademhosseini, A. and Peppas, N.A. (2009) 'Hydrogels in Regenerative Medicine', *Advanced Materials*, 21(32-33), pp. 3307-3329.

Smith, B.D., Martin, G.R., Miller, E.J., Dorfman, A. and Swarm, R. (1975) 'Nature of the collagen synthesized by a transplantable rat chondrosarcoma', *Arch. Biochem. Biophys*, 166, pp. 181-186.

Soliakov, A., Harris, J.R., Watkinson, A. and Lakey, J.H. (2010) 'The structure of Yersinia pestis Caf1 polymer in free and adjuvant bound states', *Vaccine*, 28(35), pp. 5746-5754.

Stephansson, S.N., Byers, B.A. and Garcia, A.J. (2002) 'Enhanced expression of the osteoblastic phenotype on substrates that modulate fibronectin conformation and integrin receptor binding', *Biomaterials*, 23(12), pp. 2527-2534.

Straley, S. and Bowmer, W. (1986) 'Virulence genes regulated at the transcriptional level by Ca2+ in Yersinia pestis include structural genes for outer membrane proteins.', *Infect Immun.* , 51(2), pp. 445-54.

Sugawara, E. and Nikaido, H. (1992) 'Pore-forming activity of OmpA protein of Escherichia coli.', *Journal of Biological Chemistry*, 267(4), pp. 2507-2511.

Tamm, L.K., Arora, A. and Kleinschmidt, J.H. (2001) 'Structure and assembly of beta-barrel membrane proteins', *Journal of Biological Chemistry*, 276(35), pp. 32399-32402.

Tan, H., DeFail, A.J., Rubin, J.P., Chu, C.R. and Marra, K.G. (2010) 'Novel multiarm PEG-based hydrogels for tissue engineering', *Journal of Biomedical Materials Research Part A*, 92A(3), pp. 979-987.

Tan, H., Wu, J., Lao, L. and Gao, C. (2009) 'Gelatin/chitosan/hyaluronan scaffold integrated with PLGA microspheres for cartilage tissue engineering', *Acta Biomaterialia*, 5(1), pp. 328-337.

Terrettaz, S., Ulrich, W.-P., Vogel, H., Hong, Q., Dover, L.G. and Lakey, J.H. (2002) 'Stable self-assembly of a protein engineering scaffold on gold surfaces', *Protein Science*, 11(8), pp. 1917-1925.

Thanassi, D.G., Saulino, E.T., Lombardo, M.J., Roth, R., Heuser, J. and Hultgren, S.J. (1998) 'The PapC usher forms an oligomeric channel: Implications for pilus biogenesis across the outer membrane', *Proceedings of the National Academy of Sciences of the United States of America*, 95(6), pp. 3146-3151.

Tibbitt, M.W. and Anseth, K.S. (2009) 'Hydrogels as extracellular matrix mimics for 3D cell culture.', *Biotechnol Bioeng.*, 103(4), pp. 655-63.

Timpl, R., Rohde, H., Robey, P.G., Rennard, S.I., Foidart, J.M. and Martin, G.R. (1979) 'Laminin--a glycoprotein from basement membranes.', *Journal of Biological Chemistry*, 254(19), pp. 9933-9937.

Titball, R.W. and Williamson, E.D. (2001) 'Vaccination against bubonic and pneumonic plague', *Vaccine*, 19(30), pp. 4175-4184.

Todaro, G.J. and Green, H. (1963) 'Quantitative studies of the growth of mouse embryo cells in culture and their development into established lines', *The Journal of cell biology*, 17, pp. 299-313.

Tomaselli, K.J., Damsky, C.H. and Reichardt, L.F. (1987) 'Interactions of a neuronal cell line (PC12) with laminin, collagen IV, and fibronectin: identification of integrin-related glycoproteins involved in attachment and process outgrowth', *J Cell Biol.* , 105(5), pp. 2347-58.

Tomaselli, K.J., Hall, D.E., Flier, L.A., Gehlsen, K.R., Turner, D.C., Carbonetto, S. and Reichardt, L.F. (1990) 'A neuronal cell line (PC12) expresses two beta 1-class integrins-alpha 1 beta 1 and alpha 3 beta 1-that recognize different neurite outgrowth-promoting domains in laminin.', *Neuron*, 5(5), pp. 651-662.

Toole, B.P., Munaim, S.I., Welles, S. and Knudson, C.B. (1989) 'Hyaluronate-cell interactions and growth factor regulation of hyaluronate synthesis during limb development.', *Ciba Foundation Symposia*, 143, pp. 138-149.

Vernon-Parry, K.D. (2000) 'Scanning electron microscopy: an introduction', *Analysis* 13(4), pp. 40-44.

Veronese, F.M. (2001) 'Peptide and protein PEGylation: a review of problems and solutions', *Biomaterials*, 22(5), pp. 405-417.

Vogel, V. and Baneyx, G. (2003) 'The tissue engineering puzzle: A molecular perspective', *Annual Review of Biomedical Engineering*, 5, pp. 441-463.

Vukicevic, S., Kleinman, H.K., Luyten, F.P., Roberts, A.B., Roche, N.S. and Reddi, A.H. (1992) 'Identification of multiple active growth factors in basement membrane Matrigel suggests caution in interpretation of cellular activity related to extracellular matrix components.', *Experimental Cell Research*, 202(1), pp. 1-8.

Wang, J.M., Sherry, B., Fivash, M.J., Kelvin, D.J. and Oppenheim, J.J. (1993) 'Human recombinant macrophage inflammatory protein-1 alpha and -beta and monocyte chemotactic and activating factor utilize common and unique receptors on human monocytes.', *Journal of Immunology*, 150(7), pp. 3022-3029.

Wang, S., Nath, N., Minden, A. and Chellappan, S. (1999) 'Regulation of Rb and E2F by signal transduction cascades: divergent effects of JNK1 and p38 kinases', *Embo Journal*, 18(6), pp. 1559-1570.

Wang, X., Terasaki, P., Rankin, G.J., Chia, D., Zhong, H. and Hardy, S. (1993) 'A new microcellular cytotoxicity test based on calcein AM release.', *Hum Immunol.*, 37(4), pp. 264-70.

Welz, M.M. and Ofner, C.M. (1992) 'Examination of self-crosslinked gelatin as a hydrogel for controlled release.', *Journal of Pharmaceutical Sciences*, 81(1), pp. 85-90.

West, J.L. and Hubbell, J.A. (1999) 'Polymeric biomaterials with degradation sites for proteases involved in cell migration', *Macromolecules*, 32(1), pp. 241-244.

Whitesides, G.M., Ostuni, E., Takayama, S., Jiang, X.Y. and Ingber, D.E. (2001) 'Soft lithography in biology and biochemistry', *Annual Review of Biomedical Engineering*, 3, pp. 335-373.

Wierzbicka-Patynowski and Schwarzbauer, J. (2003) 'The ins and outs of fibronectin matrix assembly ', *J Cell Sci.* , 116(Pt 16), pp. 3269-76.

Williams, S.T., M. Shameemullah, E.T. Watson and C.I. Mayfield (1972) 'Studies on the ecology of the Actinomycetes in soil, VI: The influence of moisture tension on growth and survival', *Soil Biol. Biochem.*, 4, pp. 215-225.

Wright, K.J., Seed, P.C. and Hultgren, S.J. (2007) 'Development of intracellular bacterial communities of uropathogenic Escherichia coli depends on type 1 pili', *Cellular Microbiology*, 9(9), pp. 2230-2241.

www.thermoscientific.com *Cellomics ArrayScan VTI reader*

Xiao, R.Z., Zeng, Z.W., Zhou, G.L., Wang, J.J., Li, F.Z. and Wang, A.M. (2010) 'Recent advances in PEG-PLA block copolymer nanoparticles', *International Journal of Nanomedicine*, 5, pp. 1057-1065.

Xu, C.H., Inokuma, M.S., Denham, J., Golds, K., Kundu, P., Gold, J.D. and Carpenter, M.K. (2001) 'Feeder-free growth of undifferentiated human embryonic stem cells', *Nature Biotechnology*, 19(10), pp. 971-974.

Yang, X., Hinnebusch, B.J., Trunkle, T., Bosio, C.M., Suo, Z., Tighe, M., Harmsen, A., Becker, T., Crist, K., Walters, N., Avci, R. and Pascual, D.W. (2007) 'Oral vaccination with Salmonella simultaneously expressing Yersinia pestis F1 and V antigens protects against bubonic and pneumonic plague', *Journal of Immunology*, 178(2), pp. 1059-1067.

Yang, Z.M., Gu, H.W., Fu, D.G., Gao, P., Lam, J.K. and Xu, B. (2004) 'Enzymatic formation of supramolecular hydrogels', *Advanced Materials*, 16(16), pp. 1440-+.

Youssoufian H, M.M., Kwiatkowski DJ (1990) 'Cloning and chromosomal localization of the human cytoskeletal alpha-actinin gene reveals linkage to the beta-spectrin gene.', *Am J Hum Genet.*, 47(1), pp. 62-72.

Yu, D.X., Fooks, L.J., Moslehi-Mohebi, E., Tischenko, V.M., Askarieh, G., Knight, S.D., MacIntyre, S. and Zavialov, A.V. (2012) 'Large Is Fast, Small Is Tight: Determinants of Speed and Affinity in Subunit Capture by a Periplasmic Chaperone', *Journal of Molecular Biology*, 417(4), pp. 294-308.

Zaidel-Bar, R., Milo, R., Kam, Z. and Geiger, B. (2007) 'A paxillin tyrosine phosphorylation switch regulates the assembly and form of cell-matrix adhesions', *Journal of Cell Science*, 120(1), pp. 137-148.

Zamir, E., Katz, M., Posen, Y., Erez, N., Yamada, K.M., Katz, B.Z., Lin, S., Lin, D.C., Bershadsky, A., Kam, Z. and Geiger, B. (2000) 'Dynamics and segregation of cell-matrix adhesions in cultured fibroblasts', *Nature Cell Biology*, 2(4), pp. 191-196.

Zavialov, A.V., Batchikova, N.V., Korpela, T., Petrovskaya, L.E., Korobko, V.G., Kersley, J., MacIntyre, S. and Zav'yalov, V.P. (2001) 'Secretion of recombinant proteins via the chaperone/usher pathway in Escherichia coli', *Applied and Environmental Microbiology*, 67(4), pp. 1805-1814.

Zavialov, A.V., Berglund, J., Pudney, A.F., Fooks, L.J., Ibrahim, T.M., MacIntyre, S. and Knight, S.D. (2003) 'Structure and biogenesis of the capsular F1 antigen from Yersinia pestis: Preserved folding energy drives fiber formation', *Cell*, 113(5), pp. 587-596.

Zavialov, A.V., Kersley, J., Korpela, T., Zav'yalov, V.P., MacIntyre, S. and Knight, S.D. (2002) 'Donor strand complementation mechanism in the biogenesis of non-pilus systems', *Molecular Microbiology*, 45(4), pp. 983-995.

Zavialov, A.V., Tischenko, V.M., Fooks, L.J., Brandsdal, B.O., Aqvist, J., Zav'Yalov, V.P., MacIntyre, S. and Knight, S.D. (2005) 'Resolving the energy paradox of chaperone/usher-mediated fibre assembly', *Biochemical Journal*, 389, pp. 685-694.

Zavialvo, A.V., Tischenko, V.M., Fooks, L.J., Brandsdal, B.O., Aqvist, J., Zav'Yalov, V.P., MacIntyre, S. and Knight, S.D. (2005) 'Resolving the energy paradox of chaperone/usher-mediated fibre assembly', *Biochemical Journal*, 389, pp. 685-694.

Zavyalov, V.P., Chernovskaya, T.V., Chapman, D.A.G., Karlyshev, A.V., MacIntyre, S., Zavialov, A.V., Vasiliev, A.M., Denesyuk, A.I., ZavYalova, G.A., Dudich, I.V., Korpela, T. and Abramov, V.M. (1997) 'Influence of the conserved disulfide bond, exposed to the putative binding pocket, on the structure and function of the immunoglobulin-like molecular chaperone Caf1M of Yersinia pestis', *Biochemical Journal*, 324, pp. 571-578.

Zhang, G.J., Sleiman, S.F., Tseng, R.J., Rajakumar, V., Wang, X.D. and Chamberlin, H.M. (2005a) 'Alteration of the DNA binding domain disrupts distinct functions of

the C-elegans Pax protein EGL-38', *Mechanisms of Development*, 122(7-8), pp. 887-899.

Zhang, S.G., Gelain, F. and Zhao, X.J. (2005b) 'Designer self-assembling peptide nanofiber scaffolds for 3D tissue cell cultures', *Seminars in Cancer Biology*, 15(5), pp. 413-420.

Zhang, S.G., Holmes, T., Lockshin, C. and Rich, A. (1993) 'Spontaneous assembly of a self-complementary oligopeptide to form a stable macroscopic membrane', *Proceedings of the National Academy of Sciences of the United States of America*, 90(8), pp. 3334-3338.

Zhang, S.G., Holmes, T.C., Dipersio, C.M., Hynes, R.O., Su, X. and Rich, A. (1995) 'Self-complementary oligopeptide matrices support mammalian cell attachment.', *Biomaterials*, 16(18), pp. 1385-1393.

Zhang, S.G., Lockshin, C., Cook, R. and Rich, A. (1994) 'Unusually stable beta-sheet formation in an ionic self-complementary oligopeptide', *Biopolymers*, 34(5), pp. 663-672.

Zhao, J., Chai, J., Song, H., Zhang, J., Xu, M. and Liang, Y. (2012) 'Influence of hyaluronic acid on wound healing using composite porcine acellular dermal matrix grafts and autologous skin in rabbits.', *Int Wound J.* , 9(4), pp. 349–459.

Zhu, J. (2010) 'Bioactive modification of poly(ethylene glycol) hydrogels for tissue engineering.', *Biomaterials*, 31(17), pp. 4639-56.

Zustiak, S.P. and Leach, J.B. (2010) 'Hydrolytically Degradable Poly(Ethylene Glycol) Hydrogel Scaffolds with Tunable Degradation and Mechanical Properties', *Biomacromolecules*, 11(5), pp. 1348-1357.